University of Strathclyde

Department of Mechanical & Aerospace Engineering

"Design by analysis of fixed tube sheet heat exchanger subject to a in-phase proportional loading"

Khosrow Behseta

Thesis submitted for degree of Doctoral of Philosophy in Mechanical Engineering

March 25/2014

This thesis is the result of the author's original research. It has been composed by the author and has not been previously submitted for examination which has led to the award of degree. The copy right of this thesis belongs to the author under the terms of the United Kingdom Copy Right Acts as qualified by University of Strathclyde Regulations 3.5, Due acknowledgement always be made of the use of any material contains in, or derived from, this thesis.

Signed: K. Behseta

Date: March 25, 2014

Acknowledgement

I would like to acknowledge Professor Donald Mackenzie and Doctor Robert Hamilton for their continuous support of this work; the present thesis could not have come to existence without their efforts and contributions.

My appreciation also goes to Professor Zeman of Vienna Technical University for his advice on various issues related to limit analysis, and fatigue. I would also like to thank my colleagues in Foster Wheeler company specially Dr Demon Hill, Mr Simon Wesson and Dr Peter Lane for their support of obtaining project initial founding and Dr Derik Hill for his assistance on various issues related to the material post yielding behaviour.

My gratitude to Mr Piroz Ashraf, Mr Mohammad Maleki of EIED Company and Mr Naser Sharifie of NIPC Company for their valuable advice on operating modes of fixed tubesheet exchangers in general and on C2 Hydrogenation reactor in particular.

Abstract

The integrity of the tubesheet to shell junction zone of a fixed tubesheet reactor subject to in phase proportional pressure and temperature loading, and under reduced thickness, has been investigated by applying various failure theories and in accordance to design by analysis rules through considering various material hardening parameters.

Results of an elastic FE analysis for reduced tubesheet and shell thicknesses at the junction of the shell to tubesheet indicates that the junction zone is subject to large stresses. It is shown that, junction stresses are formed as a result of combined action of channel side shell bending and tubesheet rotation at its rim. Additionally, it is discussed that linearization of a stress path at the vicinity of the junction zone categorize a large portion of calculated stresses as a peak stress and that not all of stresses classified as peak are entirely peak stress.

It is further shown that, lower tubesheet thickness can be obtained by identifying the exchanger plastic load. Exchanger plastic load has been calculated through inelastic analysis and in accordance with the twice elastic slope (TES), tangent intersection (TI) and curvature of plastic work (PWC) methods. In contrast to TES and TI methods, which are graphical methods, it is shown that PWC method being a mathematical one produces more accurate plastic load.

Failure mode associated with progressive plastic deformation is investigated for various material hardening models. It is shown that exchanger shakes down to cyclic plasticity after showing some initial ratcheting behaviour under multilinear kinematic model. Under this material model, magnitude of plastic strains are small and are confined within surrounding elastic media, this has been proved by existence of elastic core. It is also shown that, ASME elastic- perfectly plastic material model incorrectly predicted ratcheting behaviour.

Fatigue analysis for both welded and unwelded region of tubesheet and shell junction at the groove location has been carried out, this has been done to demonstrate that under full load cycles of start-up and shutdown, and under upsets conditions the number of life cycles for this reactor is much larger than the number of operating cycles anticipated to occur during the reactor life. This has been

proved by usage of stress method, local strain method and in accordance with experimentally determined equations. Additionally, it is shown that for cases subject to loads of low-cycle in nature, non-cyclic stress-strain material diagram produces higher plastic strains in comparison to the cyclic one and therefore its usage has been advised on similar applications.

Table of Contents

1. Introduction 1

2. Design of Reactor Tubesheets 4

2.1 Tubesheet Design by Formula 7

2.2 Tubesheet Design by Analysis 21

3. Design by Analysis 25

3.1 Elastic Route 25

3.1.1 Stress Linearization 30

3.2 Inelastic or Direct Route 32

3.2.1 Ductile Failure under Static Load 32

3.2.2 Ductile Failure under Repeated or Cyclic Load 39

3.2.3 Fatigue Failure 55

4. Code DBA Procedures 76

4.1 Ductile Failure under Static Load 76

4.1.1 Alternative Definitions of Plastic Load 80

4.2 Incremental Ductile Failure under Repeated Load 83

4.2.1 ASME Methods of Shakedown and Ratcheting Assessment 84

4.3 Fatigue 87

4.3.1 Brief Review of Standard S-N Curves and Fatigue Weld Class 88

4.3.2 Fatigue Life Assessment Methods 94

5. Design of Hydrogenation Reactor Tubesheets 100

5.1 Load Definitions 101

5.2 Reactor Geometry, Material Parameters and Reactor Data Sheet 103

5.3 Finite Element Modeling 105

5.4 Material Model 110

5.4.1 Material Hardening Models 111

5.4.2 Isotropic Hardening 112

5.4.3 Linear Kinematic Hardening Rule....113
5.4.4 Multilinear Kinematic Rule....114
5.4.5 Non-linear Kinematic Rules....116
5.5 Critical Locations....119
6. Static Ductile Failure....123
6.1 Small Deformation Analysis....124
6.1.1 Linear Isotropic Hardening....126
6.1.2 Multilinear Isotropic Hardening....132
6.1.3 Bilinear Kinematic Hardening....140
6.1.4 Multilinear Kinematic Hardening....143
6.2 Large deformation....147
6.2.1 Bilinear Isotropic Material Hardening....147
6.2.2 Multilinear Isotropic Material Hardening....152
6.2.3 Non-linear Isotropic Material Hardening....155
6.2.4 Bilinear Kinematic Material Hardening....159
6.2.5 Multilinear Kinematic Material Hardening....162
6.3 Results....163
6.3.1 Small Deformation....163
6.3.2 Large Deformation....165
6.4 Discussion of Results....166
7. Progressive Plastic Deformation....170
7.1 Extension to ASME Method of Ratcheting Assessment....170
7.2 Reactor Design Parameters....171
7.3 Elastic Finite Element Analysis and Stress Classifications....175
7.4 Cyclic analysis- Elastic Perfect Plastic....194
7.5 Cyclic analysis- Liner, Multilinear Isotropic and Linear Kinematic Hardening....197

7.7 Cyclic Analysis- Multilinear Kinematic Hardening 201
7.7 Elastic Core Calculations 203
7.8 Results 205
7.9 Conclusion 206
8. Fatigue Failure 208
8.1 Exchanger Operating Modes 208
8.2 Estimation of Number of Operating Cycles 211
8.3 Stress Life Evaluation 212
8.4 Reservoir Cycle Counting 217
8.5 Allowable Number of Cycles According to Structural Stress Method 218
8.5.1 Base Metal and Weldment Nodes 218
8.5.2 Weld between Tubesheet and Upper Shell 218
8.5.3 Allowable Cycles for Cyclic Set-1 Operating Mode 219
8.5.3.1 Base Metal 219
8.6 Number of Allowable Cycles for Cyclic Operation Set-2 223
8.6.1 Stress Ranges 223
8.6.2 Stress range values for LC-5 and LC-6 224
8.6.3 Allowable Number of Cycles for Cyclic Set-2 225
8.7 Fatigue Damage Accumulation 226
8.8 Inelastic Fatigue Calculation According to the Local Strain Approach 227
8.8.1 Strain Range Calculation Using Inelastic Material Model 228
8.9 Strain range calculation using experimentally determinate coefficients (experimentally determined strain versus fatigue life curve) 236
8.9.1 Strain Based Approach 236
8.9.2 Stress based approach 237
8.10 Results 239
8.11 Discussion of Results 241

9. Conclusions 242
10. Recommendations and Future Work 245
References 246
Appendix 1 254
A.1 Correction Factors for Base Metal 254
A.2 Correction Factors for Weld 258
A.2.1 Stress Range 258
A.3 Reservoir Counting 262

Nomenclature

a	radius of tube sheet
e	clamped edge plate thickness
E	Modulus of Elasticity
D	modulus of rigidity
D^*	modified flexural rigidity of tube sheet
E^*	effective tube sheet modulus of elasticity
f_t	temperature correction factor
f_s	surface correction factor
f_e	thickness correction factor
f_m	mean stress correction factor
M_T	bending moment of the tube
M_r	radial bending moment in tube sheet
N	number of tube holes
$P_{\text{lim}it}$	limit load
p_a	allowable load
$\dot{P}$	accumulated plastic strain
I_T	moment of inertia of tube
l	baffle spacing
θ	rotation of tube at tube sheet junction
F_n	factor relating effect of baffles on tube-end bending moment

F_m coefficient for clamped edge tube sheet from Gardner curve

q uniformly distributed load

W maximum deflection

Δr radius increment

ν Poisson's ratio

ν^* effective Poisson's ratio

σ_b bending primary stress

σ_m membrane primary stress

σ_R maximum stress range

$D(\dot{\varepsilon}_{i,j})$ rate of dissipation of internal energy

$\dot{\varepsilon}_i$ principal strain rates $(i = 1,2,3)$

$\varepsilon_{ii,TH}$ isotropic thermal strain

σ_{nom} nominal stress

$\sigma_{e\max}$ unaveraged nodal stress

$[\sigma_{i,j}]_{Res}$ residual stress field

$[\sigma_{i,j}]_{Unb}$ unbounded elastic stress field

σ_{eff} stress intensity limited by design criteria

σ_Y first yield

σ_a allowable stress range

σ_u ultimate strength

σ_{fb} true fracture strength

σ_{mean} mean stress

σ_{peak} Peak stress

σ_{total} total stress

S_{PS} ASME allowable limit on primary plus secondary stress range

X_a ratio of the axial stiffness of the tube bundle to the bending rigidity of the perforated plate

S allowable stress of tube sheet material

τ average shear stress in the tube sheet

K_t elastic stress concentration factor

K_{eff} effective stress concentration factor

1. Introduction

The safe and economic performance of chemical, petrochemical, refinery and power plant depend on proper and reliable operation of various types of mechanical equipment. This equipment may be classified as being of the fixed or rotating type. Fixed type equipment may be further subdivided into fired and unfired categories. The most common type of unfired equipment is the pressure vessel, which is designed to contain fluid under pressure. Pressure vessel geometry is mostly based on a cylindrical form. This pressure may arise from an external source, by the direct or indirect application of heat or any combination thereof Ref. [1, 2]. Heat exchangers are a specific form of pressure vessel designed to exchange heat between different pressurised streams subject to specific process requirements. Several types of heat exchangers are available but the most commonly used type is the shell and tube design. Shell and tube heat exchangers are constructed with various configurations; the chosen configuration depends on unit heat and mass balance requirements, the intended service and other process considerations. Shell and tube heat exchangers are further classified according to their configuration and their geometry.

Heat exchanger tube sheets are a significant expense in power and process plants, where large numbers of heat exchangers may be used. The cost of a tube sheet is dependent on the basic thickness required to satisfy safety and functional considerations, not only in terms of material cost but also the added manufacturing costs associated with machining, drilling, welding and NDT. These costs rise greatly as tube sheet thickness increases. It is therefore financially advantageous to minimize the required tube sheet thickness at the design stage.

Tube sheets can be designed based on two pressure vessel design methodologies: Design By Formula (DBF) and Design By Analysis (DBA). In DBF, the major vessel dimension and loads are specified and the corresponding safe vessel wall thickness is calculated by applying a design procedure based on formula, charts, etc. In DBA, the vessel geometry and dimensions are fully defined and the allowable vessel load is calculated by performing detailed structural analysis and applying design criteria. DBA can also be used to establish acceptable wall thicknesses etc. for a required design load through an iterative design approach.

DBF is widely used in pressure vessel design and many pressure vessel design Codes are concerned with this approach. These procedures are relatively straightforward and have been used for many years in various applications. The formulas, rules and tables used have evolved over many decades and represent, where applicable, a safe and conservative approach to pressure vessel design. Most of the formulas and rules are based on linear elastic analysis, with significant safety factors introduced to ensure that the components are safe against all failure modes which can occur under operating conditions. These failure modes include *inter alia* gross plastic deformation, progressive plastic deformation (ratcheting), and buckling.

The design of tube sheets according to DBF rules is based on the classical theory of elastic thin plate bending. This approach has a long history, starting with Poisson's study of plane plates of simple geometry, which determined the extension of inner and outer fibres of the plate in term of the radius of curvature for the purpose of arriving at bending equations.Tube sheet DBF rules take account of the perforations in the plate and the classical equations for bending and shear stresses are modified by addition of coefficients determined by theoretical calculations and verified through experiments.

In pressure vessel DBF procedures such as ASME VIII Div. 2 and Div. 1 [1, 2], design factors are applied to the solid plate model to account for the exchanger type, the tubes and tube pitch and other geometrical details. This conventional approach is safe and functionally effective but may lead to over-conservative designs in which the plate thickness is larger than that required to safely contain the pressurized fluids under the equipment operating conditions. This conservatism can be reduced by basing the design on a more detailed stress analysis of the component through application of DBA procedures. Codes such as ASME VIII Div. 2 [1], ASME III [3], and EN13445 [4] provide DBA approaches based on both elastic and inelastic analysis.

In DBA, the maximum allowable load for design is determined by performing a detailed stress analysis and checking against specific design criteria. In the early days of DBA, the analysis methods used were focused on linear elastic analysis. The elastic DBA procedures were developed with the assumption that Shell Discontinuity analysis would be used to calculate *membrane* and *bending* stresses, subject to Code specified limiting values. Elastic Finite Element Analysis is now the most popular approach in elastic DBA

practice. This allows more accurate stress evaluation for complex, thick components but gives rise to problems when interpreting shell-theory based stress limits when 2D and 3D solid elements are used.

In the inelastic DBA methodology, referred to in EN13445 as the *direct route,* the analysis performed directly addresses specific failure mechanisms. These are:

1. Excessive deformation
2. Gross plastic deformation
3. Incremental plastic collapse
4. High cycle fatigue
5. Large strain – low cycle fatigue
6. Creep deformation
7. Brittle fracture
8. Stress corrosion
9. Corrosion fatigue.

Tube sheet design can be extended to an advanced level by addressing several of the postulated failure using analysis that simulates the post yield plastic deformation of the vessel. This approach may lead to a considerable reduction in the required thickness of vessel components. However, this approach is not currently widely used in industry due to the complexity of the required analysis.

Tube sheets are a major factor in the cost of heat exchangers. Significant reduction in cost of these units can be obtained by minimizing their thickness within safe design limits, which in turn avoids unnecessarily thick adjacent shells. This thesis investigates safe minimisation of tube sheet thickness through application of advanced analysis methods in DBA. Inelastic analysis methods are used to determine the safe plastic load and shakedown load, with accompanying checks on fatigue failure.

Tube sheet DBF procedures are introduced in Chapter 2, details in regard to Design by analysis approach and code DBA are provided in chapters 3 and 4. Chapter 5 gives data and FE model of hydrogenation reactor tubesheet. Chapters 6, 7 and 8 deal with static ductile, progressive plastic and fatigue failure modes. Conclusions of this thesis are provided in chapter 9.

2. Design of Reactor Tubesheets

Heat exchangers are used to heat or cool process streams in power and process plants. Fixed tube sheet heat exchangers are specifically employed to prevent leakage of fluid from one side to the other side. Leakage can contaminate the media and therefore could cause plant shutdown or result in loss of expensive fluid. In fixed tubesheet exchangers, the tubes are welded to the tubesheet, after passing through the tube holes they are attached to tubesheet by a seal and strength weld. In this type of heat exchanger, the tubesheets themselves are welded to the shell. This configuration, although being suitable for process requirements, is mechanically a very stiff construction and, this stiffness can result in various stress problems at the junction zones, and also to thermal stress problems in the tubes, including buckling.

Figures 2.1 – 2.3 show a C2 hydrogenation chemical reactor and its tubesheet. C2 hydrogenation is a fixed tube sheet heat exchanger, exchanging heat between hot and cold methanol. This chemical reactor, with 3200 tubes, is the largest and heaviest heat exchanger in an Olefin plant. Olefin plants provide ethylene as a feed to other units and are among the largest plants in a petrochemical complex.

Fig (2.1): Reactor during assembly.

Fig (2.2): Assembled tubesheet.

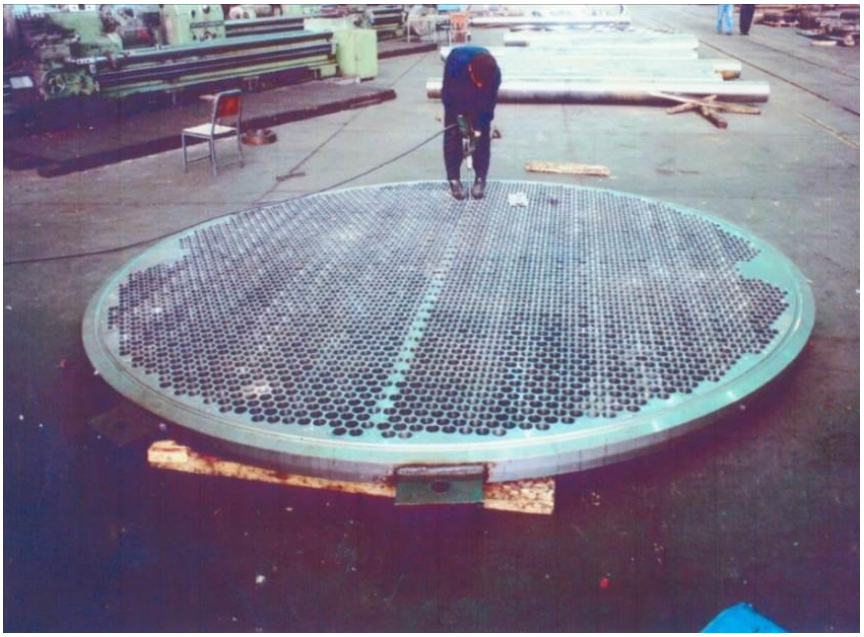

Fig (2.3): Perforated tubesheet

The majority of fixed tubesheet exchangers are subject to steady- state steady flow parameters during their normal operation. They also are subject to load variations due to the scheduled start-up to full shut-down, emergency shut-downs, and process upsets or process fluctuations. Due to steaming out or regeneration requirement or other reasons, equipment operators will occasionally adjust the flow parameters in a way that these

items will experience shift condition, i.e., different pressure/ temperature to the defined values in equipment mechanical data sheet. These shift operations are scheduled, with slow changes in operating parameters. The equipment is not subject to non-proportional loading, i.e., superposition of time dependent thermal gradients on the existing pressure load (as is the case with nuclear reactors). Possible fluctuations in operating pressure and operating temperature from steady-state condition is defined in equipment data sheet and is considered as fatigue loading in this thesis.

The reactors and thus the tubesheet are protected against excessive fluctuations and large variations in pressure and temperature from normal operating conditions by continuous monitoring of the flow parameters both on the shell and on the tube side. Shutdown logic is activated if pre-set parameters are exceeded. This means the tubesheets will not be subject to loads beyond their protected ranges.

In practice, reactor and tubesheet design is performed according to the requirements of a specific design Code or Standard. Two basic design approaches are available: Design by Formula (DBF) and Design by Analysis (DBA).

In DBF, the designer follows a systematic procedure based on explicit formula, charts, etc. to determine the required wall thickness of vessel components. DBF is restricted to specific, standard pressure vessel configurations and often lack comprehensive treatment of intersecting geometries. DBF has strict restrictions with regard to the change of validity of the formula, and strict dependency to the relevant material, manufacturing, and testing requirements. If, for example, specified manufacturing tolerances, which are usually based on workmanship concepts, are exceeded, the DBF approach cannot be used without additional proof of admissibility. The DBF approach is also limited with regard to the load cases for which formula are provided. In the determination of the nominal design stress, the DBF employs only a safety factor for normal operating load cases and one for testing load cases. This approach lacks the flexibility to adjust safety margins according to combinations of actions, the consequences of failure and the uncertainty of the analysis.

In DBA, the designer performs detailed structural analysis of the vessel to determine the allowable loading. In contrast to DBF, the inelastic DBA design procedures are very flexible. They allow any combination of loads, any geometries and geometrical details, directly address the design requirements and is restricted only by material and NDT

testing requirements. These flexibilities are very attractive and the procedures can be used to address the situations in which DBF gives unrealistic solutions or simply fails to predict the results.

2.1 Tubesheet Design by Formula

Classical plate theory has a long history starting with the study of plane structures bent into a simple geometry; this study goes back to Poisson, who determined the extension of inner and outer fibres of a circular plate in term of the radius of curvature for the purpose of arriving at bending equations. His work has been extended by many others to cover elastic plates of various shapes subject to different loads with different edge supports. Results of these efforts for circular solid flat plate with various edge conditions were presented among others by Timoshenko [5].

Timoshenko formulated the deflection equation by studying bending of a flat plate due to distributed loadings. He considered equilibrium, compatibility and elasticity equations for this purpose. The result of his equation for the deflection of a solid flat circular plate made of linear elastic material uniformly loaded and with clamped edge is:

$$W = \frac{qa^4}{64D} \qquad (2.1)$$

Where *W* is the maximum deflection, *q* the uniformly distributed load, *a* is the plate radius, e is the plate thickness and *D* is the plate flexural rigidity according to the relation below.

$$D = \frac{Ee^3}{12(1-\nu^2)}$$

With regard to the application of this equation to a fixed tubesheet heat exchanger, some factors require specific attention:

(1) The effect of plate perforation.

(2) The effect of an imperforated rim with pressure loading as it interacts with the perforated part of the plate.

(3) The effect of the staying action of the tubes specifically those close to the rim.

(4) The effect of differential thermal expansion due to different temperatures and/or different materials of tubes, tube sheets, shells, etc.

These considerations have been the subject of extensive studies by many researchers. The effect of perforation on flat plate deflection and resulting stresses has been the subject of analytical and experimental work in the early 1960's.

Gardner [7-9] proposed to replace the perforated plates with a solid plate with elastic constants appropriately adjusted. A review of the research including an extensive literature survey is given in [10], with the milestone papers [11-14] included in full.

Gardner originally neglected the Poisson effect and also did not assess the actual edge fixity of the tube sheet. Extension of his earlier work was presented in his 1960 publication [9]; in his 1960 paper he provided the interaction between the tube and the tubesheet (i.e. staying actions of tubes) for U-tube heat exchangers. According to his formulation, the interaction between tube and tubesheet can be presented by Fig. (2.4) and therefore the bending in the tubes and radial bending moment in the tubesheet were formulated according to the following equations (2.2-3).

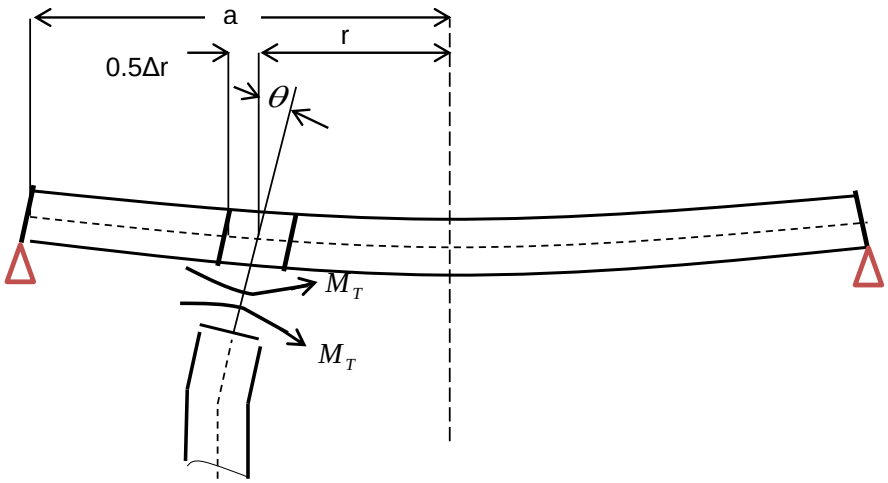

Fig. (2.4): Tube bending at junction with tubesheet

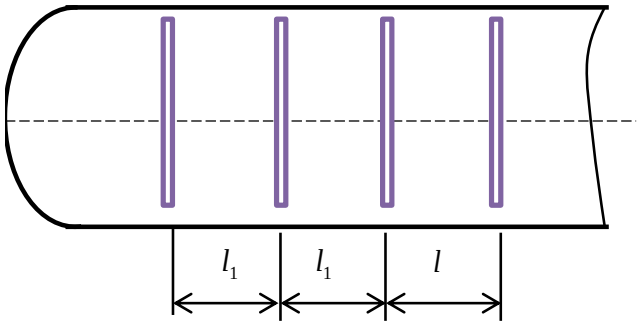

Fig (2.5): Baffle spacing

$$M_T = -F_n \frac{E_T I_T}{l} \theta \qquad (2.2)$$

$$M_r = \frac{N E_T I_T F_n \Delta_r}{\pi a^2 l} \theta \qquad (2.3)$$

where,

M_T = bending moment of the tube

M_r = radial bending moment in tubesheet

E_T = modulus of elasticity of tubes

I_T = moment of area of tube

l = baffle spacing (fig. 2.5)

θ = rotation of tube at tubesheet junction

F_n = factor relating effect of baffles on tube-end bending moment given by fig. (2.5)

N = number of tube holes

Δr = radius increment as shown in fig. (2.4)

a = radius of tubesheet

A table accounting for value of F_n in term of number of tube holes and spacing ratio (Fig. 2.5) was also provided by Gardner. Additionally, the ratio (ξ) was defined to relate the flexural rigidity of the tubesheet to number of tubes:

$$\xi = \left(\frac{NE_T I_T F_n}{\pi a^2 l D^*} \right)^{\frac{1}{2}} \qquad (2.4)$$

where,

$D^* = \frac{E^* T^3}{12\left(1-\mu^{*2}\right)}$ is the modified flexural rigidity of the tubesheet, *N* is the total number of tubes, *T* is tubesheet thickness.

By accounting for the above, the classical differential equation of the bending of the plates under uniform loading for U- tube heat exchanger took a new format as provided below [9,49].

$$\frac{d}{dr}\left[\frac{1}{r}\frac{d}{dr}\left(r\frac{dw}{dr}\right)\right] = \frac{Q}{D^*} + \xi^2 \frac{dw}{dr} \qquad (2.5)$$

Solution of the above equation for obtaining deflection w will require the evaluation of a constant of integration, which is in terms of Bessel functions. Once the deflection is known, M_T, M_r and Q (shear force) can be calculated. The maximum values of M_r and M_T take the following form:

$$\left(M_r\right)_{\max} = pa^2 F_m \qquad (2.6)$$

$$\left(M_T\right)_{\max} = \frac{t^2 P}{6}\left(\frac{\pi d a^3}{2NI_T}\right) U_a^2 F_\theta \qquad (2.7)$$

Curves indicating F_m and F_θ factors as a function of (ξa) were provided by Gardner in his 1960 paper. The maximum bending stress is given by,

$$\sigma = \frac{6F_m P}{\eta}\left(\frac{a}{T}\right)^2 \qquad (2.8)$$

where,

$$\eta = \frac{p - d}{p} \qquad (2.9)$$

η is ligament efficiency of perforated tubesheet in bending, p is tube pitch, d is tube diameter.

The calculation of stresses in perforated plates received considerable attention from 1960 to 1970 as a result of the widespread use of various types of heat exchangers. O'Donnell, *et al.* [11] described a method for calculating stresses and deflections in perforated plates with triangular penetration pattern; the method is based partly on theory and partly on experiment. Average ligament stresses were obtained from purely theoretical considerations but effective elastic constants and peak stresses are derived from strain measurements and photo-elastic tests. Acceptable limits for pressure stresses and thermal stresses in heat exchanger tubesheets were also proposed.

The base for his analytical approach was the same as Gardner proposal and relied on the concept of an equivalent solid plate: stresses and deflections of a solid plate having the effective elastic properties of the perforated material were evaluated in his paper. In another method (not followed by O'Donnell), the equivalent solid plate has the same dimensions as the actual plate but its flexural rigidity is reduced by a factor called its *deflection efficiency*.

O'Donnell derived expressions for the average ligament stress intensities for biaxial condition of the stress field in the equivalent solid plate and for any ligament orientation in the stress field. The accuracy of simplifying assumptions used in the analysis was examined using photo elastic test results.

In the concept of an equivalent solid plate, stresses and deflections of a solid plate having the effective elastic properties of the perforated material are evaluated. To evaluate these values (stresses and deflections); he stated that there is a unique state of stress within a body, having a given set of elastic properties and subject to a particular load. Therefore, the stress field in an equivalent solid plate is the same as the stress field in the perforated plate on the same macroscopic scale for which the effective elastic constants were evaluated. Hence, the resultant load carried by ligaments (at any arbitrary depth in the tube sheet) at any location must be equal to the resultant of load carried by the equivalent solid plate.

O'Donnell stated that in perforated plates such as tube sheets, the perforations and ligaments are quite small relative to the over-all dimensions of the plate itself. As a result, the rate of change of the tangential and radial stresses with radial position in the equivalent solid plate (given by classical circular-plate theory) is small relative to the perforation. Hence, one can assume that there exists only a negligible variation of load from any ligament to its adjacent parallel ligaments. Under these conditions, there are no sides ways bending moments in the minimum ligament sections. This can be seen by considering the equilibrium of an arbitrary cut at the surface, or at any arbitrary depth of the plate, as shown below.

The stress field in the equivalent solid plate is given by σ_r and σ_θ, where the radial and tangential directions are principal directions in the equivalent solid plate. This stress field must be carried by the minimum ligament sections (Fig. 2.6). Since there is no variation of stress from hole to hole, no net moment is supported by the cut section. Hence, the moments in the minimum ligament sections, *M* must be zero. Since the orientation of the cut is arbitrary, it is apparent that the sideway moments *M* is zero in all minimum ligament sections.

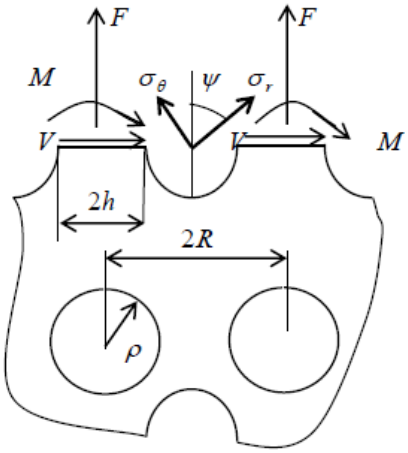

Fig (2.6): Loads acting on a typical section, Ref [11]

The load carried by the ligaments, as shown above are then given by,

$$F = 2(\sigma_r \cos\psi)R\cos\psi + 2\left[\sigma_\theta \cos(\psi - \frac{\pi}{2})\right]R\cos(\psi - \frac{\pi}{2}) \qquad (2.10)$$

$$V = 2(\sigma_r \sin\psi + 2\left[\sigma_\theta \sin(\psi - \frac{\pi}{2})\right]R\cos(\psi - \frac{\pi}{2}) \qquad (2.11)$$

Hence, the average stresses in a ligament at any arbitrary angle ψ with the principal directions of the equivalent solid plate stresses σ_r and σ_θ as shown in Fig. (2.7) are given by:

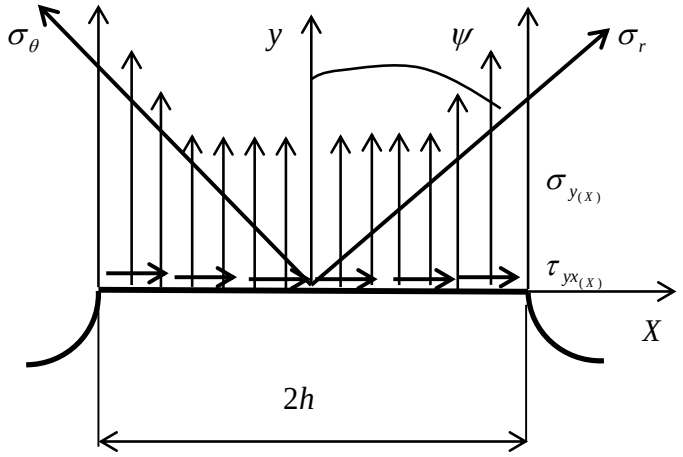

Fig (2.7): Stresses in a typical ligament, Ref [11]

$$(\sigma_y)_{avg} = \frac{1}{2h}\int_{-h}^{h} \sigma_y dx = \frac{R}{h}\left[\sigma_r \cos^2\psi + \sigma_\theta \sin^2\psi\right] \qquad (2.12)$$

$$(\tau_{yx})_{avg} = \frac{1}{2h}\int_{-h}^{h} \tau_{xy} dx = \frac{R}{h}\left[(\sigma_r - \sigma_\theta)\sin\psi\cos\psi\right] \qquad (2.13)$$

The comparable expression for the stress intensity (twice the maximum shear stress) in the minimum ligament section is given by:

$$\sigma_{eff} = \frac{R}{h}\left[\sigma_r^2 \cos^4\psi + \sigma_\theta^2 \sin^4\psi + (\sigma_r^2 - \frac{3}{2}\sigma_r\sigma_\theta + \sigma_\theta^2)\sin^2 2\psi\right]^{\frac{1}{2}} \qquad (2.14)$$

σ_{eff} is the stress intensity limited by the design criterion. It is based on the average stress across any particular minimum ligament section for any ligament orientation ψ at either surface of plate. The major assumption in deriving the above equation is zero transverse stress at the minimum ligament section. The assumption of zero transverse stress reduces the analysis to the case of plane stress. This assumption is valid, as the transverse stress must be zero at the edges of the minimum ligament section and is usually small even at the centre of the ligament section Ref [5].

Yielding would tend to produce a uniform distribution of stress across the minimum ligament sections. Hence, in his analysis a three-dimensional element, subject to the average shear and tensile stress in the minimum ligament section, was analysed in order to evaluate the average stress intensities which are limited by the purposed design criterion.

In early 1980's, the Gardner curves were extended to lower thickness ranges with inclusion of more general features, such as various pitch and tube patterns. His method appeared in Appendix AA-1 of ASME VIII Division 1 for the first time in 1982. The method was improved in 1990 by ASME based on works of Solar [50,51].

A modified version of the above equations to account for stress intensity across the ligament of a perforated plate for various pitch geometry was presented in Article 4-9 of ASME Sec. VIII Div.2, 2001. At that time, ASME Sec. VIII Div. I had a non-mandatory appendix (AA) on design of tubesheet and Div. 2 did not cover tubesheet design apart from article 4-9. A comprehensive procedure for design of heat exchangers and a method of calculation for tubesheets is provided in article (4.18 of Div. II) and in Annex 5.E of ASME section 8, 2007. Annex 5.E, design method for perforated plates based on elastic stress analysis (normative), is a modified version of this article, based on Fig. (2.8) and the stresses and stress intensity multipliers of Article 4-9. Article 4-9 covers the issue of stress intensity through thickness and across ligament with some limitations (i.e., staying action of tubes not considered, etc.).

Basically, the details are:

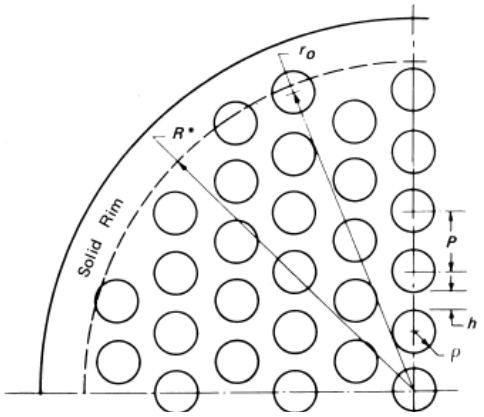

Fig (2.8): Perforated plate Ref. [1]

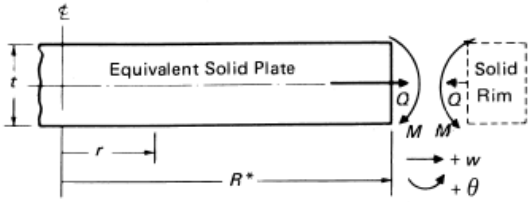

Fig (2.9): Radial force and moment at the edge of the plate Ref [1]

$$\sigma_r = \sigma_\theta = \frac{Q}{t} \pm \frac{6M}{t^2} \qquad (2.15)$$

In equation (2.15), *Q* and *M* are force and moment at the edge of the plate. Under uniformly distributed pressure load and for typical ligaments (in uniform pattern) stress intensity for a circular plate is,

$$S = \frac{P}{h}\left[\left(\frac{\Delta P R^*}{t} + \frac{W}{\pi t R^*}\right)^2 + \left(\bar{\sigma}_r\right)^2\right]^{0.5} \qquad (2.16)$$

In equation (2.16), *S* is stress intensity based on stress averaged across the minimum ligament and through thickness of the plate; this is general primary stress and is limited by S_m. Only the positive root of the equation is used.

The first term under the radical reflects the effect of transverse shear stress due to mechanical and pressure load. It is maximum in the ligament of the outer most radius of the perforated region. $\overline{\sigma_r}$ is the stress resulting from applied in-plane loading averaged through the thickness of the equivalent solid plate. It includes the stress due to pressure in the tubes or perforations; no bending stresses are included.

The stress intensity, based on stresses averaged across the minimum ligament width but not through the thickness of the plate, is limited to 1.5 S_m, i.e. ($\sigma_m + \sigma_b \leq 1.5 S_m$) and should be evaluated according to,

$$S = K \frac{P}{h} \sigma_{ave} \qquad (2.16)$$

In the above equation *K* is stress multiplier provided in the Code.

Details and procedures for design of heat exchanger tubesheet are now available in the 2007 version of ASME Div. 1 and 2 (and in Annex 5.E, design method for perforated plates based on elastic stress analysis (normative)). The Div. I and Div. 2 procedures are similar.

Before the 2007 edition of ASME Div. 2, most heat exchangers tubesheets were designed to satisfy TEMA [60]. In the TEMA standard, the thickness required to resist shear depends on the ligament efficiency of the perforations, but the thickness required to resist bending is independent of ligament efficiency. This does not mean that bending stress is not affected by ligament efficiency; it does mean, however, that all tube sheets designed to TEMA standards are designed to be safe with the minimum ligament efficiency of 20 per cent specified in 1959 TEMA. This is now 25 per cent in RCB-2.5, ninth edition, 2007, Ref [67]. The relevant statement is: Tubes shall be spaced with min. centre-to-centre distance of 1.25 times the outside diameter of the tubes.

The stress analysis of fixed tubesheets in heat exchangers is very complex due to the large number of variables that affect the analysis; such as differences in tube and shell strain, the ratio of shell and tubesheet stiffness, effective applied pressure, and the

relative thermal expansion of shell and tubes. It is noted that the development of simplified (TEMA) design equations which have been used for many years for determining fixed tubesheet thickness is based partly on the theoretical work of Gardner.

ASME, Div. 1, 1992 Appendix AA-2 for fixed tubesheets dealt with fixed tubesheet design for the first time; the method was validated by performing a benchmark of 10 industrial heat exchangers with comparison to TEMA and to CODAP Ref.[75].rules which have been used in France since 1980.

The design method is based on the same stress analysis as described for U- tube tubesheet. However, the tube bundle is considered as an elastic foundation, which adds considerable complications. Figs (2.10) and (2.11) show the details, Ref. [50, 51].

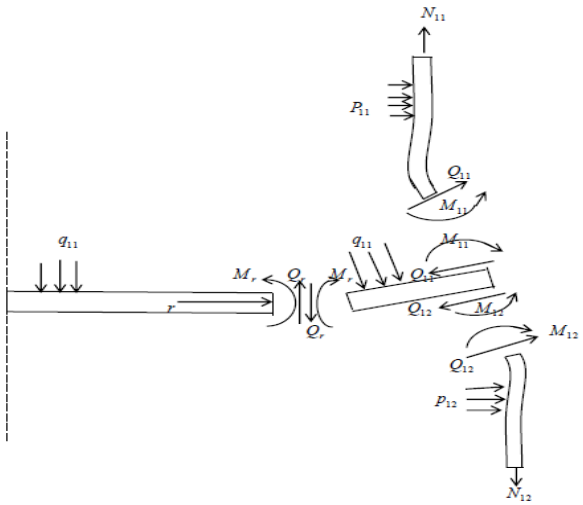

Fig (2.10): Free body of a fixed tube sheet, Ref [51]

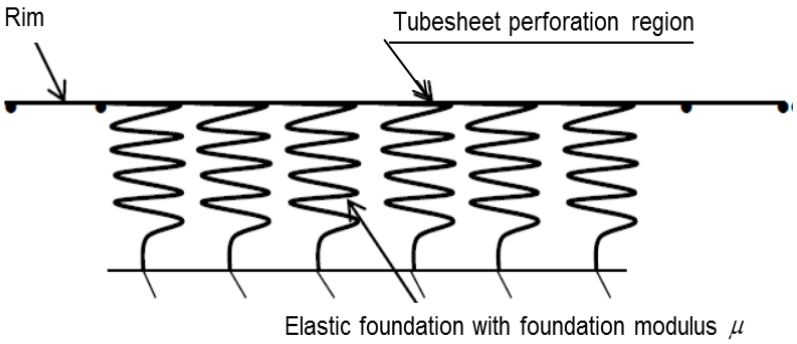

Fig. (2.11): Presentation of tubes effect (elastic foundation), Ref.[51]

The procedure to calculate the deflection (the lateral deflection of the plate with respect to outer edge of the imperforated rim) is governed by the classical elastic plate solution, given in the present context, by Solar [50,51] amongs others in the form

$$D\nabla^4 W = K * Q \qquad (2.17)$$

where *D* is the perforated plate effective stiffness, *K* is an elastic foundation parameter reflecting the staying effect of the tube bundle, and *Q* is the imposed loading or any other action that acts like an imposed loading.

The solution of equation (2.17) involves Bessel (Ber and Bei) functions and a parameter X_a, which represent the ratio of the axial stiffness of the tube bundle to the bending rigidity of the perforated plate, having the form:

$$(X_a)^4 = 24(1-\nu^{*^2})(n.E(d-t)t)((a/h)^3/(E^* L^* a)) \qquad (2.18)$$

where ***E**** and ***ν**** are the effective tubesheet modulus of elasticity and Poisson's ratio, *L* is the tube free length between tube sheet inside faces, *n* is the number of tubes, *E* is the tube modulus of elasticity, *d* and *t* are the tube outer diameter and the tube thickness respectively and *h* is the tube sheet thickness and a radius of the perforated region.

A manual computation is possible with the aid of a series of charts from which values of the Bessel functions versus X_a can be obtained. The design of the heat exchanger

tubesheet is significantly affected by the stiffness ratio X_a, this factor actually accounts for the support provided to the tubesheet by the tube bundle which strengthens the tubesheet and for the perforation which weakens it. The F_m factor has strong dependency on X_a, this fact is not reflected on TEMA as a constant value (F_m=0.8) is chosen for fixed tubesheet.

The staying action of the tubes has been considered by replacing the tubes by an equivalent elastic foundation modulus. This linear elastic approach is employed in many codes and standards, including ASME Sec. 8, Div. I and EN13445-3 (clause 13). A different approach is used in Annex J of EN 13445-3[14X], which is based on limit analysis concepts.

Presently, ASME Sec.8, Div.1 and Div. 2 have a common appendix on design of tube sheets. Part UHX of these standards deals with rules for shell and plate heat exchangers. The adapted approach and method for calculation of tube sheets still use the concept of the equivalent plate. In this respect, the perforated plate is replaced by a solid plate that is geometrically identical to the perforated plate but has modified values of the elastic constants, modulus of elasticity and Poisson's ratio.

The tubesheet rules of ASME Sec. VIII, Div. I Section UHX are intended to generally follow the stress classification of section VIII, Div. 2 for primary and primary plus secondary stresses. The scope of Part UHX does not include any consideration of peak stresses or any requirements for fatigue.

UHX aims to calculate the bending and shear stresses; this is so as bending stress resulting from a pressure loading in a flat plate is a primary (bending) stress. Any yielding of the plate material results in a permanent deformation, and the deformation may continue to occur until the plate fails (or the deformation is so large that the plate cannot perform its intended function).

The stress calculation for a fixed tubesheet exchanger should cover intersection zone between shell/channel tubesheet, tubesheet at the vicinity of the junction and shell/channel away from intersection.

The stresses in the shell and channel are somewhat more complex to categorize. The axial membrane stresses (the averaged stress across thickness) in the shell and

channel remote from the tube sheet resulting from pressure loadings are primary. The bending stress at the shell-to-tubesheet juncture and the channel-to-tubesheet juncture result from restrained differential movement at these junctures. As such, these bending stresses have the basic characteristic of a secondary stress. However, according to note 2 of Table (5.6) of ASME, Div. 2, the bending stress at a shell to flat plate juncture may be defined as secondary unless the discontinuity bending moment at the edge of a flat plate is required to maintain the bending stress elsewhere in the plate within its allowable stress. In this instance, the shell/channel bending stress is classified as primary bending and should be limited to the primary bending stress limit.

When an elastic stress analysis includes the rotation stiffness of the shell and channel in determining the tubesheet stress under primary loading, the discontinuity bending stress should be categorized as primary bending stress and be limited accordingly.

However, if the full strengthening effect of the shell/ channel is not considered for the tubesheet analysis, the shell and channel bending stresses could be correctly categorized as secondary and be limited according to the secondary stress considerations.

The stresses resulting from the temperature differential are secondary, in that they are self-limiting. The code limits on secondary stress are derived to accomplish shakedown to elastic action. The Part UHX rules consider the tubesheet, shell, channel, and the tube stresses to be secondary stresses under the action of thermal load.

The ASME Sec. VIII Code suggests that large discontinuity stresses may exist at the channel-to-tube sheet and/or shell-to-tube sheet joints. To alleviate this condition, a decision may be made to change the geometries of the shell or the tube sheet in order to meet all stress limits. Stress limits for fixed tube sheet exchangers are given in UHX-13. The stress limits are given in UHX – 13.5.8 and UHX- 13.5.11, these stress limits are limits on tube sheet shear and bending stresses and tubes in the outermost tube row:

$$|\sigma| \leq 1.5S \qquad (2.19)$$

$$|\tau| \leq 0.8S \qquad (2.20)$$

where, σ is the bending stress in the tubesheet, *T* is the average shear stress in the tubesheet at the outer edge of the perforated region and *S* is the allowable stress of the tubesheet material.

In certain cases, when the tubesheet stress level is below the limit but either or both of the shell and channel membrane and membrane plus bending stress exceeds their limits, an additional "elastic-plastic" solution step may be taken. This permits an adjustment of the shell and /or channel modulus of elasticity, which in turn affects the rotation of the joint. Adjustment of the modulus of elasticity reflects the anticipated load shift resulting from the plastic action at the joint.

Clause 13 and Annex J of EN 13445-3 provide rules for the design of the fixed tubesheet heat exchangers. The relations provided in Clause 13 are based on the classical elastic theory of thin plates and shells with the assumption of tubesheet staying on an elastic foundation created by the tubes, similar to the ASME approach. Annex J provides an alternative method based on limit analysis. This annex assumes constant shell thickness at the junction. The basic equations are still derived by classical plate theory with account for various stresses defined within classical plate theory. The created stress fields are then simply compared with allowable limits that are based on limit analysis theory. The procedure tabulated in Appendix J for the calculation of the staying effect of the tubes is structurally indeterminate for fixed tubesheets. This fact requires the calculation being performed for various values: minimum, maximum, and possibly intermediate values. The Code recommends that by making a series of assumptions, the most favourable final result should be used. This can affect the final conclusion.

2.2 Tubesheet Design by Analysis

DBA procedures may be used as an alternative to DBF, even in cases covered by DBF of ASME VIII, Div. 2. DBA can be based on either elastic or inelastic analysis. Elastic analysis is simpler to perform but the design procedure itself is complex, as the analysis does not model post yield stress redistribution. Inelastic analysis is more complex to perform but simulates the post yield stress redistribution associated with the static and incremental plastic collapse mechanisms, giving greater insight into the behavior of components and their safety margins.

The specific failure modes addressed in DBA are:

1. Excessive elastic deformation
2. Gross plastic deformation
3. Incremental plastic collapse
4. High cycle fatigue
5. Large strain – low cycle fatigue
6. Creep deformation
7. Brittle fracture
8. Stress corrosion
9. Corrosion fatigue.

A brief description of these failure modes is given below.

- **Excessive elastic deformation.**

Elastic deformation occurs when a loaded structure experiences stress that does not exceed the material yield strength. If the elastic deformation becomes excessive, the structure fails to perform its intended function.

- **Gross plastic deformation.**

Plastic deformation occurs when a loaded structure experiences stress that exceeds the material yield strength under application of static load. If the elastic deformation becomes excessive, the structure may fail to perform its intended function, extensive gross plastic deformation will cause failure to be by global plastic collapse or local plastic instability of the material.

- **Incremental plastic collapse**

If the plastic strain increments in each load cycle are of the same sign then, after a sufficient number of cycles, the total strains (and therefore displacements) become so large that the body departs from its original form and becomes unserviceable. This phenomenon is called incremental collapse or ratcheting.

- **High cycle fatigue**

A common cause of fracture is fatigue, which is failure due to repeated loading. In general, one or more cracks start in the material, and these grow until complete failure. Historically, most attention has been focused on situations that require more than 10^4 cycles to failure where stress is low and deformation is primarily elastic.

In high-cycle fatigue situations, materials performance is commonly characterized by an *S-N* curve, also known as a Wohler curve. This is a graph of the magnitude of a cyclic stress (*S*) against the logarithmic scale of cycles to failure (*N*).

- **Low cycle high strain fatigue**

Where stresses are high enough for plastic deformation to occur, the account in term of stress is less useful, the strain in material offers a simpler description. Low cycle fatigue is usually characterized by the Coffin- Manson relation.

- **Creep failure**

Creep is the tendency of a solid material to move slowly or deform permanently under the influence of stresses. It occurs as a long term exposure to high levels of stress below the yield strength of the material. Creep is more severe in materials that are subject to heat for long periods, and near melting point. Creep always increases with temperature. The rate of deformation is a function of the material properties, exposure time, exposure temperature and applied structural load. Depending on the magnitude of the applied stress and its duration, the deformation may become so large that a component can no longer perform its function. Unlike brittle fracture, creep deformation does not occur suddenly upon the application of stress. Instead, strain accumulates as a result of long-term stress. Creep is a time dependent deformation.

- **Ductile failure.**

Structures of ductile materials that are subjected to mechanical and/or thermal actions will deform elastically or plastically to accommodate the load. Yielding occurs when the material's yield strength is exceeded and the structure can no longer return to its original shape and size. Ductile or plastic collapse occurs when the structure can no longer carry the applied load.

- **Brittle fracture.**

Brittle fracture is a rapid run of cracks through a stressed material; the cracks usually travel very fast. There is very little plastic deformation before failure occurs. Brittle fracture depends on fracture toughness. Fracture toughness is a property which describes the ability of a material containing a crack to resist fracture, and is one of the most important properties of any material for many design applications.

- **Stress corrosion cracking (SCC)**

Stress corrosion cracking is a process involving the initiation of cracks and their propagation, possibly up to complete failure of a component, due to the combined action of tension stresses and a corrosive medium. The tension stress could be due to mechanical or thermal action.

- **Corrosion fatigue**

Corrosion fatigue differs from SCC by the fact that the applied actions and thus the resulting stresses are no longer static but cyclic. In the case of steels, the conventional fatigue limit determined from *S-N* curves does not exist for tests performed in a corrosive medium.

This thesis is specifically concerned with three failure modes and associated criteria:

- The gross plastic deformation design check and limit or plastic load criteria.
- The progressive plastic deformation design check and shakedown criteria.
- The cyclic fatigue design checks and fatigue life criteria.

Elastic and inelastic DBA procedures that can be used to design against these types of failure are discussed in Chapter 3.

2.3 Summary

Design by analysis gives detail information about tube sheet design and provides various means to arrive to the safe and optimized thickness. Optimized tube sheet thickness considerably reduces cost of the exchanger.

3. Design by Analysis

Design by analysis requires detailed analysis of the vessel and assessment with respect to Code-specified criteria to determine allowable loads to ensure safety with respect to the postulated failure mechanisms. The Codes provide alternative rules for design based on elastic analysis and several forms of inelastic analysis.

3.1 Elastic Route

The elastic design procedures use a stress categorization methodology to guard against failure due to gross plastic deformation, incremental plastic deformation (ratcheting) and fatigue. The stress categories considered are:

- **Primary stress**

A primary stress is a stress produced by mechanical loading only; it is of normal or shear stress type and develops by imposed loading which is necessary to satisfy the simple laws of equilibrium of external and internal forces and moments [1]. Primary stresses which considerably exceed the yield strength will result in failure or at least in gross distortion.

Primary stresses are subdivided into general primary membrane (P_m), local primary membrane, (P_L) and primary bending stress, (P_b). A general primary membrane stress is one that is distributed in the structure such that no redistribution of load occurs as a result of yielding. Local primary membrane stress arises from situations in which the membrane stresses produced by pressure or other mechanical loading also acts at a discontinuity in structure. Although this kind of stress is local, it could still produce excessive distortion in the transfer of load to other portion of the structure. Conservatism requires that such a stress be classified as a primary local membrane stress even though it has some characteristics of secondary stress.

- **Secondary stress**

Secondary stresses are in form of normal or shear stresses produced by constraint due to geometric discontinuities, by the use of materials with different material properties or by constraints due to differential thermal expansion. The basic characteristic of a secondary stress is that it is self-limiting. Local yielding and minor distortions can satisfy

the conditions that cause the stress to occur and failure from one application of the stress is not to be expected. Examples of secondary stress are a general thermal stress and the bending stress at a gross structural discontinuity.

- **Peak stress**

Peak stress is that increment of stress which is additive to the primary- plus- secondary stresses by reason of local discontinuities (small fillet radii, small attachments partial penetration welds, etc.) or local thermal stress including the effects of stress concentration. Peak stresses do not cause any noticeable distortion and are only important to fatigue in conjunction with primary and secondary stresses.

The magnitude of the allowable values assigned to the various stress categories reflects the nature of their associated failure mechanisms. It is therefore essential that stress partitioning and categorization is performed correctly. Once stresses in the various categories are known, their assessments are made according to details provided in Ref. [2, 3].

To prevent failure against static plastic collapse, ASME requires the limitation of primary membrane (general and local) and primary bending stresses.

The primary stress limits are derived from limit load analysis of a simple beam under combined membrane and bending action, representing a segment cut from the wall of a pressure vessel component. Limit load theory is based on two assumptions about the material and structural response;

- The material is assumed to display perfect plasticity, post yield stress redistribution occurs without strain hardening or strain softening, as shown in Fig (3.1)
- The structure exhibits small deformations when loaded. This means that changes in geometry of the structure at limit load are negligible and that geometric description of structure remains unchanged during the deformation at the limit load.

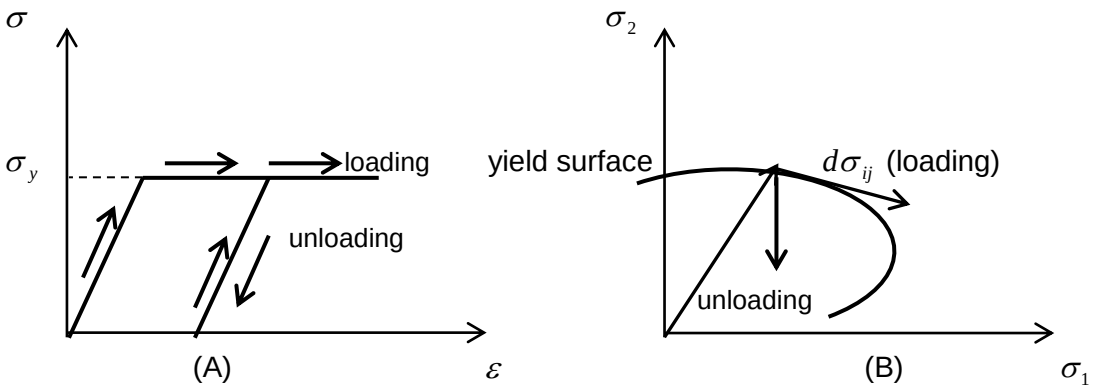

Fig. (3.1): An elastic-perfectly plastic material model, (A) Uniaxial stress- strain, (B) Geometric representation of yield surface and criteria of loading and unloading.

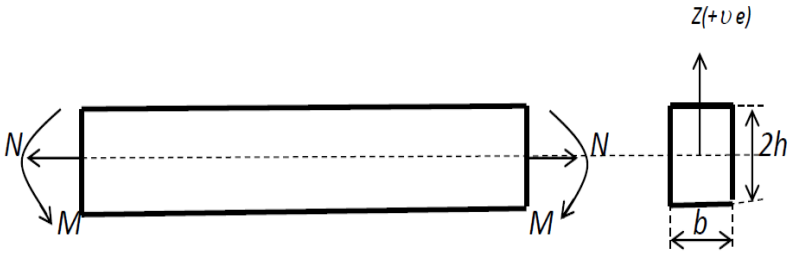

Fig (3.2): Beam loads

Considering the beam defined in Fig (3.2), and assuming the material has yield stress σ_y, it can be shown that first yield occurs when

$$\frac{N}{2bh}+\frac{3}{2}\frac{M}{bh^2}=\sigma_y \qquad (3.1)$$

The limit load of the beam under combined loading can be shown to be:

$$\frac{M}{bh^2\sigma_Y}+\left(\frac{N}{2bh\sigma_Y}\right)^2=1 \qquad (3.2)$$

Defining the primary membrane stress σ_m as:

$$\sigma_m=\frac{N}{2bh} \qquad (3.3)$$

and primary bending stress σ_b at the *outer fibre* of the beam as:

$$\sigma_b = \frac{3}{2}\frac{M}{bh^2} \qquad (3.4)$$

The yield condition may be expressed as:

$$\frac{\sigma_m + \sigma_b}{\sigma_y} = 1 \qquad (3.5)$$

And the limit condition as:

$$\frac{2}{3}\left(\frac{\sigma_b}{\sigma_Y}\right) + \left(\frac{\sigma_m}{\sigma_Y}\right)^2 = 1 \qquad (3.6)$$

The yield and limit conditions can be represented on an interaction diagram, as shown in Fig (3.3).

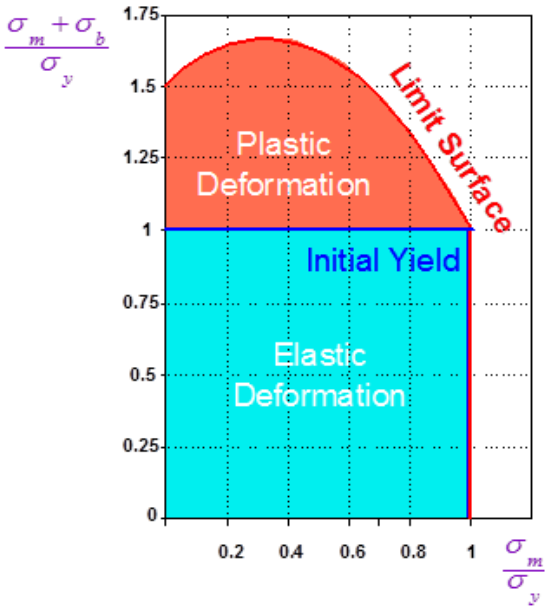

Fig (3.3): Yield and limit conditions

To provide a suitable margin against *limit collapse*, the primary membrane and bending stress limits are defined as:

$$P_m \leq S \qquad (3.7)$$

$$P_l \leq 1.5S \qquad (3.8)$$

$$P_l + P_b \leq 1.5S \qquad (3.9)$$

This margin is not constant but it is proven to be appropriate for the design.

To prevent failure against *incremental plastic collapse*, the Codes requires that the magnitude of primary plus secondary stress must be limited to ensure that the structure exhibits shakedown under repeated loading. The primary plus secondary stress limit is derived from *elastic shakedown* analysis of a simple prismatic bar model of an element of vessel wall subject to cyclic thermal strain [15], as shown in Figure (3.4).

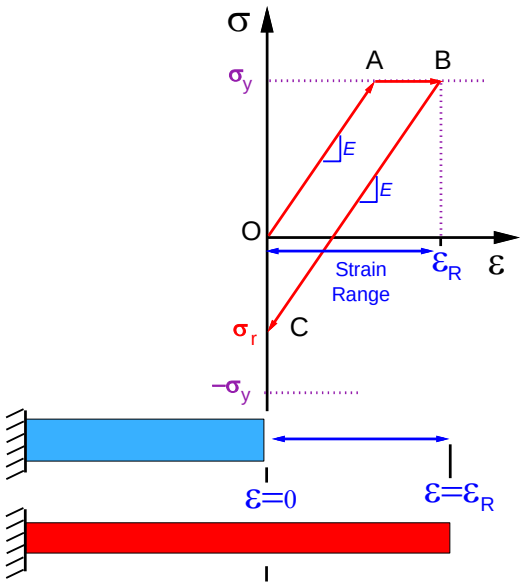

Fig (3.4): Beam subject to thermal strain

The load is applied as a cyclic thermal axial strain, to produce strain from $\varepsilon = 0$ to $\varepsilon = \varepsilon_R$ and back to $\varepsilon = 0$.

Elastic shakedown is assured if the strain range does not cause plastic strain during the unloading part of the load cycle. The maximum strain range meeting this condition, ε_R, is given by the equation:

$$\varepsilon_R = 2\sigma_y / E \qquad (3.10)$$

where E is the material elastic modulus and σ_y is the material yield strength. In pressure vessel design, $E\varepsilon_R$ is treated as an elastically calculated maximum stress range, σ_R. It can thus be stated that shakedown will occur if the elastic stress range σ_R is limited to twice the yield stress of the material**:**

$$\sigma_R \leq 2\sigma_Y \qquad (3.11)$$

The ASME allowable stress S tabulated in the Code for a given material and given design or operating temperature has a value of approximately $S = (\frac{2}{3}\sigma_y)$ for most pressure vessel steels. The shakedown criterion, equation (3.11), can therefore be expressed as

$$\sigma_R \leq 3S \qquad (3.12)$$

When the design by analysis procedure was introduced, the most popular analysis technique in pressure vessel design was thin shell discontinuity analysis. This is reflected in the definitions of stress categories given in the codes, which are based on the assumption of shell theory and stress distributions in form of membrane and bending stresses. It is therefore difficult to evaluate the calculated stresses and the stress categories unless the design is based on shell analysis. It should be noted that the local stress concentration cannot be captured through use of shell elements. In such cases, the normal procedure is to apply stress concentration factors calculated experimentally or derived, otherwise through use of analytical tools. Extrapolation of stresses away from stress risers to risers locations also has been advised: some details are provided in Ref. [4,36].

3.1.1 Stress Linearization

In practice, 3D Finite Element Analysis is often employed to calculate the elastic stress field. If continuum elements are used, the *stress linearization* procedure provides a means to separate the stresses into membrane, bending and local stresses for design

assessment. Use of shell elements would not require the linearization procedure as their output is directly in terms of bending and membrane stresses.

A procedure for linearizing stress was suggested by Kroenke [16, 17] and has been adopted by ANSYS [18]. In this procedure, a stress classification line (or plane) or supporting line segment is chosen and stresses are linearized along this line. The supporting line segment or classification line is the shortest segment joining the two sides of the wall where the stress is linearized. Away from structural discontinuity regions, the stress classification line is normal to the wall mean surface (its length is equal to the wall thickness).

One objection to linearization comes from the point that the linearization must be performed at the stresses component level (and not derived principal values), this means that shear stresses are also included in the procedure. Apart from linear portion of shear stress distributions that result in torsion of the stress classification line (out-of-plane shear stress in the normal-hoop plane), shear stresses should not be linearized. The bending stress is the component which needs to be linearized as code recognizes existence of a non-linear bending stress.

Elastic DBA can result in a less conservative design than DBF but it does not lead to the most effective use of material.

ASME [1], Table 5.6 gives Examples of Stress Classification. Cautious use of this table is advised as the load, geometry and other details must be identical, otherwise the category of each stress should be investigated in detail.

ASME VIII Div. 2 [1], 5.2.1.4 states “The structural evaluation procedures based on elastic stress analysis provide an approximation of the protection against plastic collapse. A more accurate estimate of the protection against plastic collapse of a component can be obtained using elastic-plastic stress analysis to develop limit and plastic collapse loads.” The EN13445 *direct route* and ASME inelastic design rules provide procedures for design based on inelastic analysis.

3.2 Inelastic or Direct Route

In the DBA inelastic route, specific types of analyses are used to directly assess specific failure modes. This approach is sometimes referred to as the DBA *Direct Route*.

The failures modes of pressure vessel structures are not restricted to fracture or collapse, they also include excessive changes in shape, loss of material or changes of mechanical properties. A structure has failed when it becomes unsuitable to carry out the function that it was originally intended or designed to perform. Environmental conditions and operating loads are often the primary causes leading to structural failure: corrosive and high temperature environments are examples of aggressive environments that commonly induce failure. Stress due to various loads, impact, and frictional loading are examples of operating conditions that frequently cause structural failure. Combinations of harsh environments and mechanical loads often lead to more rapid material wear and failure.

The inelastic route of DBA deals directly with design against ductile failure under static loading, ductile failure under repeated or cyclic loading and fatigue failure under repeated or cyclic loading.

3.2.1 Ductile Failure under Static Load

The general expression static ductile failure can be used to describe two forms of failure:

1. Structural or global failure of the vessel due to formation of a global plastic collapse mechanism, resulting in either *gross plastic deformation* or *plastic instability*.
2. Local failure due to material instability.

The global plastic failure load can be defined in DBA using two general approaches:

- Limit analysis.
- Inelastic analysis, selectively incorporating strain hardening and large deformation effects.

The principles of limit analysis as described below are related to the definition of primary stresses defined in Chapter 3.1. Limit analysis can also be used to directly assess the static ductile collapse failure mechanism; this is usually done by calculating:

- A lower bound on the limit load through application of the lower bound limit load theorem.
- The limit load corresponding to violation of structural equilibrium in an incremental or step-by-step inelastic analysis assuming perfect plasticity and small deformation theory.

Analytical limit loads have been evaluated for a restricted number of simple structural configurations, such as beam structures, thick spheres and thick cylinders only. In pressure vessel design, solutions to more complex problems have usually been obtained by performing analysis based on limit load bound theorems, in particular the lower bound limit load theorem. The small deformation theory assumption of limit analysis allows the use of the virtual work principle, which is the key to proving limit load theorems.

The virtual work equation deals with two separate and unrelated sets, the equilibrium and the compatible sets. These sets are brought together, side by side but independently, in the equation of virtual work .Based on figure (3.5), the virtual work equation has the form specified in (3.13),

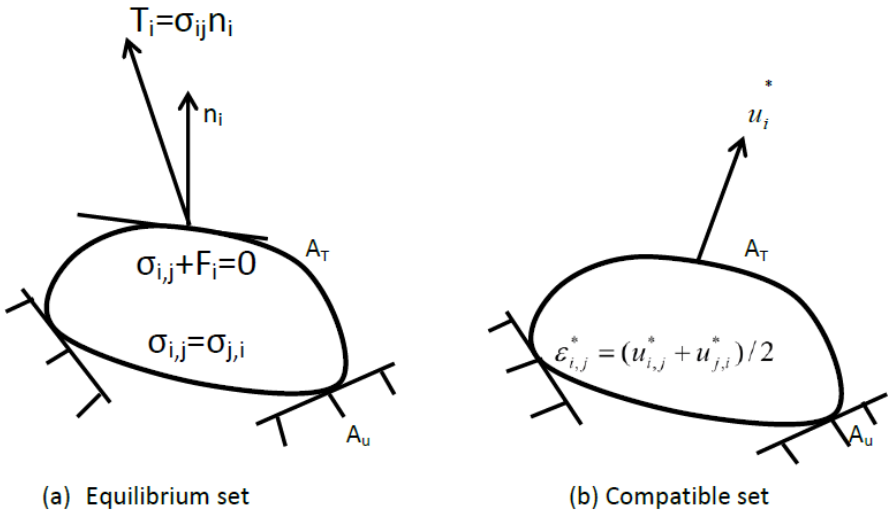

Fig (3.5): Equilibrium and compatible set presentation

compatible set

$$\int_A T_i u_i^* dA + \int_V F_i u_i^* dV = \int_V \sigma_{i,j} \varepsilon_{i,j}^* dV \qquad (3.13)$$

equilibrium set

In the above equation the integration is performed over the whole area, *A* and over volume, *V*, of the body. T_i is surface traction force acting on surface area A_T and that where surface displacements $\bar{u}_i$ are prescribed is denoted by A_u**.** F_i is body force; the stress field $\sigma_{i,j}$ is any set of stresses (real or imaginary) in equilibrium with body forces

F_i within the body (3.14) and with surface forces T_i (3.15) on the surface where the forces T_i are prescribed.

$$\sigma_{i,j} + F_i = 0 \qquad \text{in V} \qquad (3.14)$$

$$\sigma_{i,j} n_j = T_i \qquad \text{at } A_T \qquad (3.15)$$

Similarly, the strain field ε_{ij}^* represent any set of strains or deformations compatible with (real or imagined (virtual)) displacement u_i^* of the points of application of external forces T_i and F_i (3.16) and (3.17).

$$\varepsilon_{i,j} = \frac{1}{2}(u_{i,j} + u_{j,i}) \qquad \text{in V} \qquad (3.16)$$

$$u_i = \bar{u}_i \qquad \text{at } A_u \qquad (3.17)$$

It is important to note that neither the equilibrium set T_i **,** F_i **,** and $\sigma_{i,j}$ nor the compatible set u_i^* and ε_{ij}^* need be the actual state, nor need the equilibrium and compatible sets be related in any way to each other. In equation (3.13), the (*) is used for the compatible set to emphasize the point that these sets are completely independent. When the actual or real states (which satisfy both equilibrium and compatibility) are substituted in (3.13), the asterisk is omitted.

The lower bound limit load theorem then states: if a stress field $\sigma_{i,j}^e$ can be found in equilibrium with the body force F_i in V and the applied loads T_i on the stress boundary A_T and which is everywhere below yield, $f(\sigma_{i,j}^e) \le \sigma_y$, then the structure will not collapse under the loads T_i **,** F_i **.** The lower bound theorem expresses the ability of the ideal body to adjust itself to carry the applied loads if possible.

The upper bound limit load theorem is included here as some stress analysis methods are based on its principle. The upper bound limit load theorem can be stated as *If a path*

of failure exists, the ideal body will collapse. This is formulated by showing that the rate of internal work down on the system through dissipation of internal energy less than the rate of external work. The rate of external and internal work is:

$$W_{ext} = \int_{A_T} T_i (\dot{u}_i)^{P^*} dA + \int_V F_i (\dot{u}_i)^{P^*} dV \qquad (3.18)$$

$$W_{\text{int}} = \int D(\dot{\varepsilon}_{i,j})^{P^*} dV = \int_V (\sigma_{i,j})^{P^*} (\dot{\varepsilon})^{P^*} dV \qquad (3.19)$$

The rate of dissipation of internal energy *D* for Tresca and Mises yield functions are given by,

$$D = \sigma_y (\dot{\varepsilon})_{\max} \qquad (3.20)$$

$$D = \sigma_y \sqrt{(2/3)(\dot{\varepsilon}_1^2 + \dot{\varepsilon}_2^2 + \dot{\varepsilon}_3^2)} \qquad (3.21)$$

where $\dot{\varepsilon}_i$ are principal strains rates (*i*= 1,2,3).

Several procedures such as Gloss r- node method Ref [43], Elastic Compensation Method and Linear Matching Method for evaluating lower and upper bound limit loads based on repeated elastic finite element analysis have been proposed [23]. These methods use simple algorithms to generate stress, strain and displacement fields, through which limit load bounds can be evaluated.

The Elastic Compensation Method was developed from a reduced modulus stress categorization method of Marriot [68], in which the effects of material inelasticity are simulated by repeated elastic analysis. The method is a generalization of the Marriot technique for estimating lower bound limit loads for pressure vessel applications.

The object of the Elastic Compensation Method is to establish a stress field suitable for substitution into the lower-bound theorem by systematically modifying the local elastic modulus in a finite element model so as to cause the stress to redistribute. The procedure involves calculating a series of elastic equilibrium stress fields where the

stress is redistributed by altering the elastic modulus of each element based upon the maximum unaveraged nodal stress from previous iteration:

$$E_i = E_{(i-1)}\left(\frac{\sigma_{nom}}{\sigma_{e\max}}\right) \qquad (3.22)$$

where *E* is the elastic modulus, *I* the iteration number; σ_{nom} is some nominal value, and $\sigma_{e\,max}$ the maximum unaveraged nodal stress in that element from the previous solution. The resulting redistributed stress fields are equilibrium stress fields. By definition, if the equivalent stresses anywhere in the equilibrium stress field does not exceed the yield stress of the material, then that stress field relates to a lower bound on the limit load.

Therefore, scaling the applied loads by the amount given by maximum stress in the redistributed stress field to the yield stress of the material will give the limit load, i.e.:

$$P_L = P_1\left(\frac{\sigma_y}{\sigma_{\max}}\right) \qquad (3.23)$$

Where, P_L is the limit load, P_1 is the applied load, σ_y is the yield strength of the material and σ_{max} is the maximum (unaveraged) nodal stress.

In the Generalized Local Stress Strain (Gloss) r-node method, statically determinate stresses at locations referred to as r-nodes are identified by iterative elastic analysis in which regions of high stress have their modulus reduced, while regions of low stress have theirs increased. The stresses at the r-node locations are insensitive to the assumed material model and considered to be reference stresses similar to creep reference stresses.

The Linear Matching Method involves the matching of the non-linear material behavior to a linear material and forms the basis for an upper bound programing method that may be applied to a significant class of direct methods, Ref [23]. The procedure is based on the Elastic Compensation method. The Linear Matching Method is a non-linear programing method where the local gradient of the upper bound functional and the potential energy of the linear problem are matched at a current strain rate or during a strain rate history.

Limit analysis can also be performed by incremental or step-by-step inelastic FEA, assuming an elastic-perfectly plastic material and small deformation theory. The limit load is the load that causes overall structural instability. This is indicated by the inability to achieve an equilibrium solution for a small increase in load (i.e. the solution will not converge). In limit analysis, the internal stresses and applied forces are related by the usual equations of equilibrium which ignore changes in geometry due to deformations.

The plastic instability failure mechanism is related to the plastic collapse state of a structure when strain hardening and large deformation effects are included. This type of analysis requires a complete solution of the governing equations of the structure and is most commonly performed by incremental FEA. Strain hardening materials can support stresses greater than yield, increasing the static load carrying capacity of a structure. Changes in vessel geometry with increasing load may lead to increased or decreased load carrying capacity of the structure, referred to as geometric strengthening and geometric weakening respectively.

Determination of the plastic collapse load of the structure and the relevant requirements of the Gross Plastic Deformation design check are outlined in EN 13445 Annex B sub clause B.8.2 and in ASME Sec. 8, Div. 2, APP. 5. This check can be performed by evaluation of structural plastic load or it can be approximated by calculation of structural limit load. Numerically, the limit load is calculated by incorporating the elastic-perfectly – plastic material model and small displacement theory in an FEA model. The limit load is then the load that causes overall structural collapse. This point is indicated by the inability to achieve an equilibrium solution for a small increase in load (i.e. the solution will not converge).

The calculation of plastic load requires modelling that accounts for material hardening, flow rule and consistency equation. The limit load approximation to plastic load requires a much simpler formulation, i.e., linear elastic ideal-plastic constitute law, with yield condition and with associated flow rule: Mises' yield condition in ASME VIII and Tresca's in EN. Proportional increase of loads, stress free initial state and limitation of the maximum value of principal structural strains are other requirements.

3.2.2 Ductile Failure under Repeated or Cyclic Load

If the yield stress is exceeded in the first load cycle, this will result in a change in the nature of the stress due to establishment of a residual stress field. The subsequent cyclic behaviour can result into one of three responses:

- Elastic shakedown
- Plastic shakedown
- Ratcheting (incremental collapse)

Under cyclic loading, the structural failure mode corresponding to elastic shakedown is high cycle fatigue failure. This type of mechanism can initiate and propagate a crack mechanism at localized stress concentrated zones, e.g. the weld between a tube sheet and upper shell. Elastic shakedown take place if,

$$\dot{\varepsilon}_{i,j}^{p} = 0 \qquad (3.24)$$

where $(\dot{\varepsilon})_{i.j}^{P}$ is the rate of plastic strains at the component level.

In plastic shakedown, plastic straining occurs with every cycle but the net strain over a full cycle is zero, due to reversal in the sign from one half cycle to the other [19].

This is also known as alternative or reverse plasticity. The failure mode associated with this response is low cycle, high strain fatigue. The condition for plastic shakedown to alternative plasticity after stabilization of the plastic strain cycles is identified by:

$$\int \dot{\varepsilon}_{i,j}^{P}(\tau) dT = 0 \qquad (3.25)$$

Incremental plasticity can also occur under specific cyclic conditions. This is defined as net growth in plastic strain with each load cycle. Over a number of cycles, the accumulated plastic strain increments will cause gross plastic deformation and final plastic collapse of the structure. This failure mode is called incremental plastic collapse or ratcheting.

In DBA, the structure is required to demonstrate either elastic or plastic shakedown. This is usually done by:

- Calculating a lower bound on the shakedown load through application of the lower bound shakedown load theorem.

- Demonstrating the structure exhibits elastic or plastic shakedown under the prescribed conditions through incremental or step-by-step inelastic analysis assuming an elastic-perfectly plastic material model.

Analytical shakedown solutions are more restricted than limit load solutions. In practice, the lower bound shakedown load theorem has been used extensively to obtain solutions for use in pressure vessel design.

Shakedown theory relies on lower and upper bound limit theorems; the theory has been developed based on the two statements, static and kinematic. The static statement or first theorem is Melan's shakedown statement; this statement is a lower bound theorem and relies on the elastic perfectly plastic material model and deals with magnitude of a stress field.

Melan's statement requires identification of an admissible stress field for proof of shakedown to full elastic action. This admissible stress field is obtained by superposition of a residual stress field (to be identified by cycling between operating case and full shutdown condition) and an unbounded elastic stress field calculated for specific operating conditions. Fulfilment of the statement is proved by showing that the superposed stress field remains below the material's yield strength at every location within the model. Further descriptions related to the application of shakedown theory to tubesheets are provided in section (3.2.2.1).

3.2.2.1 Identifying Shakedown and Ratcheting Conditions in Tubesheet Analysis

Heat exchangers and reactors are subject to combination of cyclic thermal and pressure loads arising from process plant demands. These loads are, in principal: scheduled start up and shut down conditions, emergency shut downs, fluctuating or shifting on flow parameters, etc. The resulting stress state at points inside the structure in general and at the tubesheet to shell junction in particular includes primary and secondary stresses. As discussed earlier in this chapter, primary stresses have load control mechanisms while secondary stresses are of the deformation controlled type.

Secondary stresses can exceed the yield limit of the material without causing immediate plastic failure (collapse); however, cyclically recurring loads (transients) that exceed the yield limit of the material can cause deformations which accumulate with each cyclic load application. i.e., ratcheting. Ratcheting (incremental collapse), can result in failure and therefore must be considered in design. Ref. [1, 4] provide stress limits for this purpose.

The classical shakedown theory consists of Melan's lower bound theorem and Koiter's [53] upper bound theorems. By defining suitable stress or displacement fields, the bounds converge to a unique value at which shakedown is established for a specific load system. The classical theorems aim at a state in which the structure is eventually elastic everywhere.

The Melan theorem is suitable for design purposes because its application guarantees a lower bound on the shakedown load. Stresses calculated according to Melan's theorem are elastic everywhere. However, from a practical point of view, Melan's theorem is not satisfactory as a design limit because all structures contain points of stress concentrations, where the yield stress is often exceeded locally. These points are assessed in design for the intended cyclic operation by fatigue analysis, and pose no problem otherwise.

Cyclic plastic deformation is not a concern if the plastic action remains confined to a local region in the structure, as bulk plasticity is required for the continued deformation of the structure. Local stress concentrations may produce local plasticity and may initiate a fatigue crack but it will not lead to a failure by ratcheting. A plastic mechanism is necessary for a ratcheting failure, just like a plastic mechanism is required for non-cyclic plastic collapse under primary loads. Refs [1, 4] recognize the irrelevance of local plasticity for shakedown by imposing limits on the linearized stress range.

Few methods are available to define a load level at which ratcheting starts to occur in a structure. In this thesis, the method used is cyclic elastic-plastic analysis. However, for completeness, overviews of alternative methods are included.

To correctly judge the results of an elastic plastic analysis of a structure, some definitions need to be made. These are: definition of system of loads, shakedown, modes of failure associated with cyclic loading, and modelling of material behaviour.

A) System of loads.

A system of loads consists of primary loads (like pressure), secondary loads (like temperature) and externally applied displacement (anchor motions). Anchor point displacement is not a concern in tubesheet design and is therefore not considered further.

The response of the structure to the primary and secondary loads is divided into three possible types, namely: shakedown, ratcheting or plastic collapse. The details related to plastic collapse mechanism and plastic load have been provided in Section 3.2.1. In this thesis, it is assumed that plastic cycling in the form of reverse plasticity by itself can be dealt with by performing elastic-plastic fatigue analysis (chapter 8).

B) Shakedown.

Ref. [1] provides a definition of shakedown as a system response caused by cyclic loads or cyclic temperature distributions which produce plastic deformations in some regions of the component when the loading or temperature distribution is applied. But upon removal of the loading or temperature distribution, only elastic primary and secondary stresses are developed in the component, except in small areas associated with local stress (strain) concentrations. These small areas shall exhibit a stable hysteresis loop, with no indication of progressive deformation. Further loading and unloading, or applications and removals of the temperature distribution shall produce only elastic primary and secondary stresses. Shakedown is therefore defined as the absence of continuing, accumulation deformation (ratcheting).

C) Modes of failure associated with cyclic loading.

The primary stress evaluation ensures that a pressure vessel does not experience any excessive plastic deformation under a single load application. The fatigue analysis considers the effect of cyclic stress that may lead to cracking, crack growth and eventually to a failure.

However, it should be noted that according to Ref. [1], fatigue analysis by itself can not address the failure due to cyclic loads sufficiently and a separate failure mechanism needs to be additionally investigated. This separate failure mode is ratcheting, which deals with accumulation of plastic deformation with each load cycle. This can lead to formation of a gross plastic deformation failure mode similar to limit collapse but with a

different underlying mechanism, i.e., formation of through thickness plasticization by virtue of strain accumulation.

Demonstrating shakedown means that the cumulative deformation will end at some point, and a purely reversed strain cycling will occur from this point onward. However, some amount of permanent deformation will be incurred before the onset of stable cycling. The accompanying plastic strains build up the residual stress field in the structure that is responsible for causing shakedown.

D) Modeling of material.

Material modelling to represent the material response to general cyclic loading is very complex. The response includes directional hardening (kinematic), cyclic hardening (isotropic) and deformation of the yield surface: all of which may depend on the non-proportionality of the loading. However, a full description of ratcheting is not required for a design limit, only a conservative description of the shakedown boundary is needed. In this way, Ref. [1] suggest the use of elastic-perfectly plastic material. The advantage of elastic-perfect plastic material is that it is consistent with limit analysis, i.e. for Mises yield model the identification of yield stress is sufficient.

The value of the yield stress itself is important as it is not strictly correct to use the yield that is obtained from a unidirectional tension test. This is because after being subjected to plastic cycling, most materials tend to harden or soften compared to their initial values. Materials that are initially soft tend to harden while initially strong material tends to soften. To use the initial yield stress for materials that exhibit cyclic hardening is conservative. On the other hand, experiments with softening materials have shown that these materials can shakedown initially and start ratcheting after undergoing number of stable cycles Ref [36]. Carbon steels used in construction of this heat exchanger are classified as materials which harden post initial yielding. Moreover, ASME implies $1.5S_m$ is the cyclic yield stress and therefore its use is authorized in relevant cyclic calculations.

Use of an elastic-perfectly plastic material model may therefore not correctly predict the response of the heat exchanger considered in this thesis to cyclic loads. If the material model suggested by ASME is used in design, this may result in a conservative value in terms of tube sheet thickness.

E) Shakedown Theorems.

For assessments that involve a steady cycle, the stresses and elastic strain rates of the elastic-plastic material are also periodic. The following relationship for the plastic energy per cycle can be established [36], Ref. [19]:

$$\int_0^T [\int_V (\sigma_{i,j} - \sigma^e_{i,j}) \dot{\varepsilon}^P_{i,j} dV] dt = 0 \qquad (3.26)$$

This relation holds for the steady cyclic condition, regardless of whether it is elastic shakedown, plastic shakedown or ratcheting. In this formulation both the elastic-plastic and purely elastic stress fields are in equilibrium with the same external loads, so that their difference is in equilibrium with zero external loads. In other words, it is a residual stress field.

The strain energy calculated from any residual stress field and a kinematically admissible strain rate is zero because the work put into the structure by the (zero) external loads acting on the corresponding displacement field is zero.

For elastic shakedown, an upper and lower bound theorems are available, the lower bound theorem (Melan) is described in the subsequent paragraphs.

Melan's statement requires identification of an admissible stress field for proof of shakedown to full elastic action. This admissible stress field is obtained by superposition of a residual stress field (to be identified by cycling between operating case and full shutdown condition) and an unbounded elastic stress field calculated for operating conditions. Fulfilment of the statement is proved by showing that the superposed stress field remains below the material's yield strength at every location within the model.

The numerical procedure and various requirements are addressed in Ref [1, 4]. Comprehensive details and examples are provided in ref. [35]. In short, the procedure is outlined by:

$$[\sigma_{i,j}]_{\mathrm{Res}} + [\sigma_{i,j}]_{Unb} \leq \sigma_y \qquad (3.27)$$

Where $[\sigma_{i,j}]_{\mathrm{Res}}$ is residual stress field, $[\sigma_{i,j}]_{Unb}$ is unbounded elastic stress field and σ_y is material yield stress. The residual stress term can be replaced by any self-equilibrating stress field and can be calculated by various methods.

Melan's lower bound theorem requires identification of a stable cyclic solution that satisfies the yield criterion. Any solution meeting this condition gives a conservative estimate of the shakedown load. The practical difficulty is the finding of an efficient residual stress field that avoids an over-conservative assessment.

Several simplified finite element base methods for shakedown analysis based on bounding theorems have been proposed in literature and applied to pressure vessel problems [20-26]. These methods however, allow direct evaluation of shakedown loads without recourse to extensive inelastic finite element analysis (FEA).

When performed in conjunction with actual (total) stress field in the component, Melan's theorem can result in a very conservative assessment of the shakedown limits. Even in the most optimistic case, the stress range anywhere in the structure is limited to $(2\sigma_y)$. This includes any local structural discontinuities, a very restrictive criterion, which also makes some common finite element modelling simplifications impossible (e.g. modelling fillets as sharp corners). Therefore, the global use of Melan's theorem does not result in an optimum design criterion.

Melon's theorem requires the linearized stress for every wall section of the structure. Zeman [27] proposed the use of "structural" stresses and strains instead of linearized ones. This puts the method approximately on the same level of conservatism as the ASME Code elastic $(3S_m)$ criterion. The ASME $(3S_m)$ method also has practical shortcomings: the significant effect of constant primary load is neglected (Melan's theorem will capture this), the method allows any time-independent stress state to be added to the cyclic stress but in reality only a residual stress state is acceptable (this also can be calculated through Melan's theorem). As the use of Melan's theorem requires the linearized stress for every wall section of the structure, the method is convenient for beam and shell models.

Generally, Melan's theorem is provided for elastic shakedown and therefore it cannot be used to assess plastic shakedown, as it was noted earlier elastic shakedown uses a

constant residual stress field. However, the mechanism responsible for plastic shakedown requires capturing the varying part of a residual stress field. This varying part changes from one cycle to the next one until it stabilizes, i.e., a constant strain range (reverse plasticity) is achieved.

Secondary stresses themselves have a similar property to a residual stress, in that they are self-equilibrating. Therefore, a secondary stress that is constant throughout the cycle has no effect - only cyclic secondary stresses make a contribution. The same is not true for the primary stresses, since a residual stress cannot equilibrate a constant primary stress. A purely reversed loading results in stable plastic cycling. Therefore, it is often the constant primary stress that induces ratcheting.

For plastic shakedown, Melan's theorem must be supplemented with a time-varying residual stress field that ensures that the elastic-plastic stresses do not fall outside the yield surface. Polizotto proposed a restriction on the time variant residual stress term that might lead to an extension of the lower bound theorem to the plastic shakedown regime, Ref. [28].

The upper bound shakedown theorem (Koiter [53]) uses an expression for the plastic energy per cycle similar to equation (3.26). For the plastic strain rate, however, now any field $\left(\dot{\varepsilon}_{i,j}^{P}\right)_O$ may be used for which the accumulated strain over a cycle, $\left(\Delta\varepsilon_{i,j}^{P}\right)$, is kinematically admissible, i.e. associated to a kinematically admissible displacement field through,

$$\Delta\varepsilon_{i,j}^{P} = \int_0^T \dot{\varepsilon}_{i,j}^{P} dt \qquad (3.28)$$

$\Delta\varepsilon_{i,j}^{P}$ is required to be kinematically compatible such that:

$$\Delta\varepsilon_{i,j}^{P} = \frac{1}{2}\left[\frac{\partial}{\partial x_j}(\Delta u_i) + \frac{\partial}{\partial x_i}(\Delta u_j)\right] \quad \text{in V} \qquad (3.29)$$

Note that a kinematically admissible field means $\left(\Delta\varepsilon_{i,j}^{P}\right)_0$ satisfies the compatibility conditions, while the corresponding displacement field satisfies zero condition on the surface A_u**:** for A_u and V see figure (3.5). Moreover, the plastic strain rate need not be

kinematically admissible throughout the cycle, just its integral over the whole cycle. The condition (3.29) means that the plastic strains must be periodic for the considered cycle (the thermal stresses are a load and therefore periodic by the definition of a load cycle). The integral

$$\int_0^T \left(\int_V \left[\left(\sigma_{i,j} \right)_O - \sigma_{i,j}^e \right] \left(\dot{\varepsilon}_{i,j}^P \right)_O dV \right) dt \geq 0 \qquad (3.30)$$

is then greater or equal to zero for any admissible strain rate $\left(\dot{\varepsilon}_{i,j}^P \right)_O$ if the structure shakes down. In the integral, $\left(\sigma_{i,j} \right)_O$ is the stress on the yield surface that is associated with the strain rate $\left(\dot{\varepsilon}_{i,j}^P \right)_O$.

The specific property exists between the integral of (3.30) and equation (3.29); that is, the integral is invariant if an arbitrary residual stress field, $\left(\bar{\sigma}_{i,j} \right)_R$, that is constant over the cycle, is to be added to the stress difference $\left[\left(\sigma_{i,j} \right)_O - \sigma_{i,j}^e \right]$. That means, if a residual stress can be found such that the elastic stress path is completely within the yield surface, then the integral (3.30) is positive for any pair $\left(\sigma_{i,j} \right)_O, \left(\dot{\varepsilon}_{i,j}^P \right)_O$ by Drucker's principle.

For an arbitrary admissible plastic strain rate field, the upper bound to the elastic shakedown load can be obtained by increasing the loads on the structure until the integral (3.30) becomes zero. It should be noted that when the elastic stress cycle lies partly outside the yield surface no matter what constant residual stress is added, the integral (3.30) will be less than zero for some strain rate fields.

F) Methods of shakedown analysis

The main objective in shakedown analysis is to determine the steady (stabilized) cycle. If strains are periodic in the structure shakedown occurs, if not the structure ratchets under the applied loads. The methods of calculation can be classified into those that perform a transient cyclic plastic analysis and those that do not.

The methods that rely on the transient cyclic analysis simulate the actual path towards the steady cycle that structure would take; other methods use a different iterative

scheme to establish steady cycle. Cyclic and elastic core methods are examples of transient cyclic plastic method, while the Melan's and Ponter [55] methods represent the other class. These methods are described below,

- Elastic method

ASME Sec.8. Div. II provides two different methods for ratcheting assessment, i.e., the elastic "$3S_m$" method and the elastic-plastic method. Article 5.5.6 of the Code deals with the elastic method. This section of the Code uses the range of primary and secondary stress to assess shakedown, which, for linear stress distributions can be expressed as,

$$f\left(\Delta\sigma_{i,j}^{e}\right) \leq S_{PS} \qquad (3.31)$$

Where $\Delta\sigma_{i,j}^{e}$ the difference between any two is points of the elastically calculated stress history, is the cyclic yield stress, limit of $\Delta\sigma_{i,j}^{e}$ is given by (Fig. 5.1), and Art. (5.5.6.1.d) of Ref. [1], the (S_{ps}) value is larger of $3S_m$ where S_m is $(2/3)\sigma_y$ or $2\sigma_y$. The Code makes no distinction between primary and secondary stress, as only the combined range is used in equation (3.31).

It is known that a constant primary stress can contribute to ratcheting, as has been demonstrated by Bree. Equation (3.31) is the requirement that purely elastic stress path must fit inside the yield surface, this means that code requires elastic shakedown.

Fitting the yield surface around the stress path can be regarded as an effective method of finding the optimum time invariant stress state which, when added to the elastically calculated stress, causes elastic shakedown. The method cannot assure that the additive constant stress state is a residual stress state as demanded by Melan's theorem for elastic shakedown in a perfectly plastic material. Therefore, it is consistent with the linear kinematic material model, not with the perfectly plastic one. In other words, it is assumed that there is no restriction on the transition of the stress path when trying to fit it into yield surface.

If the stress distribution in a component (e.g. the junction between a tube sheet and shell) is nonlinear through thickness, only linearized stresses need be evaluated. This reflects the idea that ratcheting requires a cyclic plastic mechanism in the structure in a

similar way as plastic collapse requires a sufficient number of plastic hinges in the structure.

Localized plasticity at a notch does not cause collapse, and in the same way it does not cause ratcheting in the steady state sense. In other words, ratcheting only happens if, during the steady cycle, each element of an entire section of the structure plasticises at some point in time. The section never plasticises entirely (that would be plastic collapse), but at different parts at different times during the cycle.

Stress linearization works well for through- thickness effects, but not for local “hot spots” on shells, which are frequently encountered, particularly when 3D analysis is required.

- Bree method

The Bree method can be classified as an inelastic method since his material model is elastic-perfectly plastic. Bree applied an analytical method to investigate the presence of ratcheting and hysteresis loop due to cyclic temperature under sustained pressurized loading in the axial as well as the hoop directions in a cylinder. In his investigations he considered modes of failure associated with gross distortion due to ratcheting or incremental collapse and creep fatigue failure. Bree approached the problem by means of uniaxial and biaxial stress models. The uniaxial stress model has formed the basis of the assessment route in Appendix T of Code Case N47 of Ref. [3]. Fig (3.6) shows the Bree [31] diagram for the uniaxial stress model.

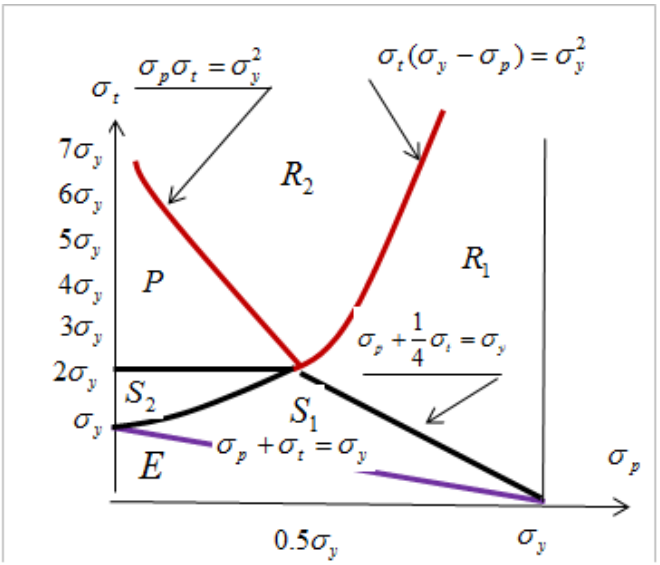

Fig (3.6): Bree load diagram for the uniaxial stress model

Bree's method applies to pipes and vessels with linear through-wall temperature gradients and pressure loading. The Bree problem was investigated numerically using the FE method by Nadarajah and Ng [58]. They investigated the phenomenon of ratcheting and cyclic stress-strain hysteresis loop behaviour in a thin-walled cylinder subject to cyclic thermal stress and sustained internal pressure. Their FE model was a rather simple model as their interest was to observe effect of various load cases on the Bree model geometry. They used an elastic-perfectly plastic material model in line with the Bree assumption.

Their comparison between analytical and F.E calculations shows that ratcheting to shakedown boundaries based on these models are in close agreement with limits predicted by Bree. Moreover, they showed that the hoop ratcheting rates predicted by the uniaxial model enveloped the FE and biaxial models, while for the axial ratcheting rates, the F.E. results are upper bound.

One variation of the Bree classical problem is the case where both the fluctuating moment and the constant axial force are primary loads (Bree primary problem- Fig 3.8) . There is a ratcheting region in this case, which supports the notion that a combination of stress fields with different time dependence is the crucial elements that cause ratcheting. Kalnins [32] has investigated this case and has concluded that a structure that is subject only to primary loading below the code design limit will shakedown.

The case of a structure subject to a constant primary moment and a fluctuating secondary membrane load (inverse Bree problem) has also been the subject of investigation Fig. (3.7). Certain thermally loaded tubesheet are classified according to this loading.

Recalling the example of a beam Fig. (3.7), when the thermal membrane stress fluctuates with amplitude of $2\sigma_y$ or more, it will obviously cause plasticity throughout the beam at every cycle, and the beam will not be able to support any additional moment. Conversely, if the moment reaches the limit moment of the beam, the beam will be at incipient collapse and will not sustain any thermal cycling. It has been shown that the shakedown boundary for Inverse Bree problem is a straight line between the described extremes.

$$\Delta\sigma_{SM} = 2\sigma_Y - \frac{4}{3}|\sigma_{PB}|$$

$\Delta\sigma_{SM}$ is the elastically calculated thermal membrane stress range and σ_{PB} is the elastically calculated bending stress.

Reinhardt [28] looked into the Bree problem numerically and presented the following graphs, the material model in his calculations is elastic-perfectly plastic and the selected geometry is a beam fixed at one end with a guided support at the other end. His model geometry and loading matches the original Bree model. He noted that, unlike the classical Bree problem, the inverse Bree problem does not converge to the cyclic solution within the first cycle. Figures (3.7 to 3.8) depict the above descriptions; these figures also contain details of the loads variation. One of his models is classical Bree models which is subject to an axial force and a through thickness temperature gradient, Fig (3.9).

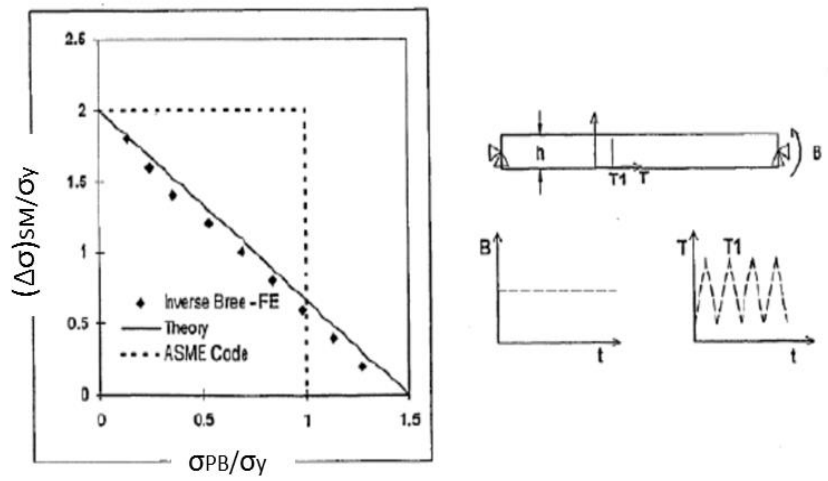

Fig (3.7): Shakedown boundary of the inverse Bree problem (constant primary bending and cyclic secondary axial load). FE results were obtained after 25 cyclic load applications , Ref. [28]

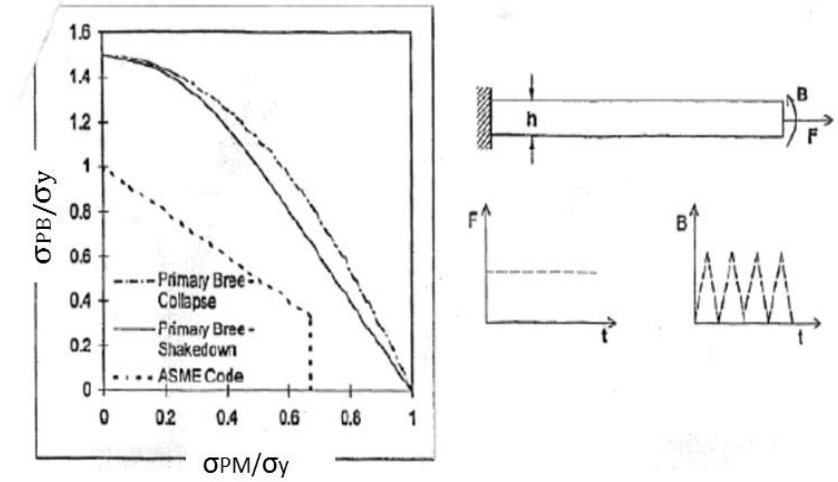

Fig (3.8): Shakedown boundary of the primary Bree problem (constant primary axial and cyclic primary bending load). , Ref. [28]

Fig. (3.9) present shakedown of the classical Bree problem (beam with constant primary axial load and cyclic secondary bending) shows that ASME "$3S_m$" criterion is not a conservative representation of the shakedown boundary if the constant primary stress exceed $\frac{2}{3}S_m(=0.5\sigma_y)$. However, design stress criteria would limit the primary stress to $S_m=\frac{2}{3}\sigma_y$.

The potentially unconservative region would therefore be fairly small. Furthermore, the vessel design pressure is not considered as non-fluctuating. The case where the membrane stress is almost entirely caused by a fluctuating pressure is the realistic case and must be investigated.

The state of stresses in the region of a heat exchanger junction is complex and their separation and categorization is problematic in nature. This means that the procedure and conclusions reported in the above references cannot be applied directly to fixed tubesheet exchangers. Other approaches and details are required to properly address the shakedown load and ratcheting limits of fixed tubesheet exchangers.

- Cyclic method

The simplest way to obtain the steady cyclic solution is to integrate over time. Once the solution has converged sufficiently, the absence of incremental collapse can be proved through observing the existence of a steady cycle of strains. Referring to Fig.(3.9), the investigation of Ref.[28] showed that the Bree problem converges after the first cycle, and after a few cycles for inverse Bree problem. These observations are somewhat misleading for the problem of a fixed tubesheet exchanger. This is investigated in detail for a fixed tubesheet heat exchanger in Chapter 7.

The cyclic method relies on determination of stabilized cycle. By definition, a stabilized cycle is a strain cycle in which its magnitude (amplitude) does not change from one cycle to the next one. The Japan Pressure Vessel Research Council (JPVRC) Ref. (73) has proposed to define the shakedown when the equivalent plastic strain increment over the previous cycle reaches an increment of less than (10^{-4}), while the history of all plastic strain increments indicates a decreasing trend. Ref.[3] in code case N-47-28, Appendix

T, section T-1310 defines permanent strain of 1% as the limit on accumulated inelastic strain averaged through the thickness.

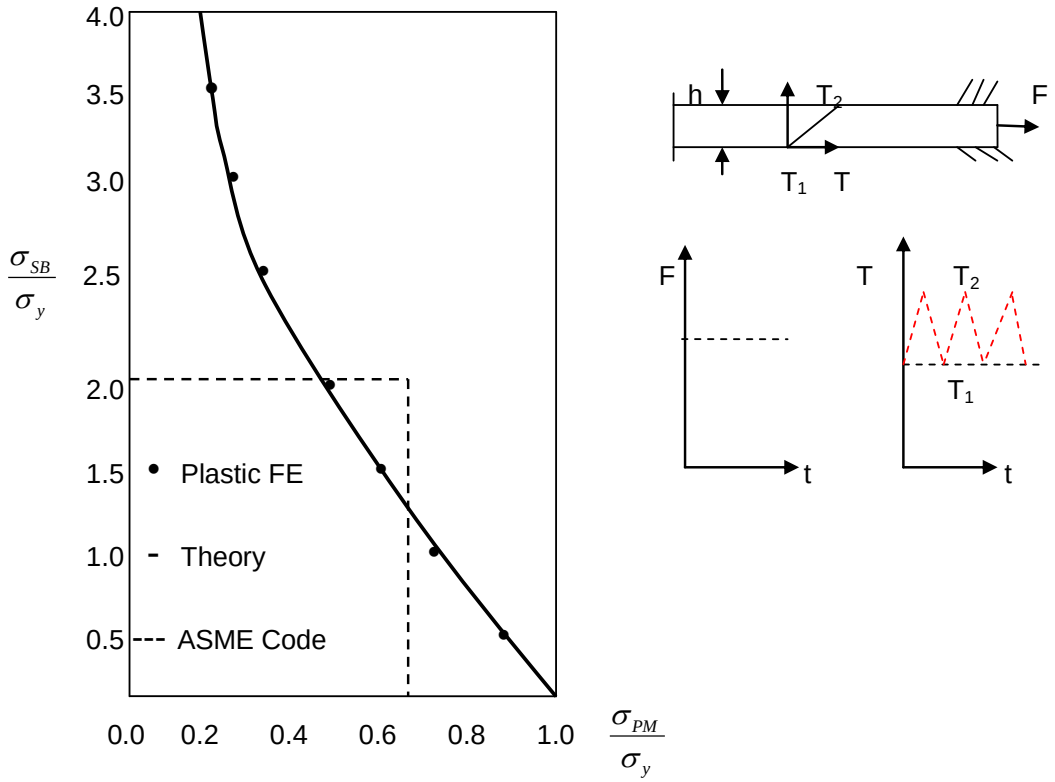

Fig (3.9): Shakedown boundary of the classical Bree problem (beam with constant primary axial load and variable linear temperature gradient through thickness).

- Elastic Core

Kalnins [32] suggested that the elastic core method could be a simple way to assess shakedown. The procedure is that a structure cannot experience incremental collapse as long as a continuous elastic core in the structure that exists throughout the load cycle supports the applied loads.

Some points need clarification in regard to this procedure; that is, for non-incremental plastic collapse, the structure collapses when regions of the structure plastify completely and thus form a through-thickness plastic hinge. For an elastic-plastic structure, on the other hand, it is possible for plastic hinges to form successively. The structure does not

necessarily collapse when the first hinge forms. Therefore, through-thickness plasticity (i.e. the absence of an elastic core) in one location doesn't necessarily signify the onset of collapse or incremental collapse.

- Ponter Method

Ponter [74] used an extended upper bound formulation "in excess of shakedown" to devise a method that yields the shakedown boundary of the elastic or plastic shakedown problem. The problem is decomposed into two separate parts, which are solved with a linear matching technique that matches the response of a linear material to that of the elastic-plastic material. Iterations must be performed to arrive at the steady periodic solution, but is not based on a simple integration of the cyclic solution in time. The problems needs to be run to convergence because this is an upper bound method, at the end of this solution the shakedown boundary is known, not just some steady periodic solution inside or outside of it. The Ponter method is the only way to determine the shakedown boundary directly [55].

3.2.3 Fatigue Failure

Fatigue failure occurs in structures that are subject to cyclic loads. It involves progressive localized damage. Damage will occur as a result of crack initiation, crack growth and the propagation of micro cracks.

Cracks may initiate in originally undamaged areas and propagate afterwards. Existing cracks and crack-like defects can also propagate due to the cyclic actions. The process eventually leads to the reduction of cross sectional area to such an extent that rupture occurs. Since cyclic fatigue eventually leads to failure of the structure, it is to be considered in the design as a failure mode related to cyclic actions.

Fatigue analysis may be performed using several approaches. The most widely used are:

A. Stress Approach (High cycle Fatigue)

B. Local Strain Approach (Low Cycle fatigue)

The stress approach is based on the calculation of various elastic stresses for use in fatigue curves (*S-N curves*). Elastic stresses have been defined differently in various standards but as a general rule and in accordance with definition provided in the relevant standard (Ref 4, 69) any of the following paths can be taken, Niemi [33],

- Nominal stresses
- Structural stresses
- Notch stresses

Definitions of the above stresses are different from each other and each type serves a special purpose. The nominal stresses are beam type stresses with combination of axial and bending stresses with all the assumptions underlying classical beam theory. They should be calculated for solid sections away from discontinuities. Calculated nominal stresses must be then multiplied by stress concentration factors determined experimentally before their further use.

Structural stress definition is somewhat different between Ref [4] and Ref [34]. In Ref [4] the structural stresses are the ones associated with a model accounting for major discontinuities. Stresses are calculated close to the discontinuity and then extrapolated to the desire locations in the discontinuity to capture the nonlinear part: this is peak stress and its value is required for use of the S-N curve. In Ref. [34] they are defined as stresses associated with classical shell and plate theory away from structural discontinuities. To convert these remote stresses to peak stresses, they must be multiplied by an appropriate stress concentration factor.

The results of either reference should be the same provided the stresses calculated according to Ref [4] are based on FEA with the elastic linear shell elements, since output of elastic shell elements are directly in term of bending and membrane stresses with total stress as their summation.

As shell elements are incapable of capturing stress concentrations, i.e. the nonlinear part of total stress distribution at a hot spot, the FEA result based on their use must be multiplied with appropriate factors before use in an *S-N* curve. Ref [34] extensively concentrates on the above stresses and provides guide lines on FEA and other related items.

Notch stresses are the nonlinear part of stress distributions close to or at the discontinuity. They can be calculated through use of solid elements and can be estimated through their separation from membrane and from bending stresses. This is normally performed in FEA modeling by stress linearization.

Traditionally the fatigue criteria have been dealt with through use of standard curves (*S-N* curves). In this regard the curves are entered with calculated elastic total (peak) stress ranges for purpose of identifying allowable number of cycles.

Standard curves have been prepared for standard specimens through push-pull and through standard bending tests. The number of cycles to failure is recorded and through applying safety factors the S-N curve is prepared. The curves can be used directly for checking base material; the number of extracted cycles from an *S-N* curve must be corrected through a few correction factors.

As noted above, methodologies for calculation of stress range and for mean stress for base metal and for weld–hot spots can be based on the elastic approach as well as local strain evaluation, these are discussed below.

In the elastic Base Metal-Hot Spot approach, the stress range on the component level is calculated by considering the value of individual stresses at periods of (T_1) and (T_2),i.e.:

$$\Delta\sigma_{i,j} = \sigma_{i,j}(T_1) - \sigma_{i,j}(T_2), \qquad i, j = 1,2,3 \tag{3.32}$$

$$\Delta\sigma_{eq}(T) = \sqrt{[(\Delta\sigma_{11} - \Delta\sigma_{22})^2 + (\Delta\sigma_{11} - \Delta\sigma_{33})^2 + (\Delta\sigma_{22} - \Delta\sigma_{33})^2 + 6(\Delta\sigma_{11}^2 + \Delta\sigma_{22}^2 + \Delta\sigma_{33}^2)^2]} \tag{3.33}$$

$$\overline{\sigma}_{i,j} = (\overline{\sigma}_{ij,\max} + \overline{\sigma}_{ij,\min})/2 \tag{3.34}$$

$$\overline{\sigma}_{eq} = \overline{\sigma}_{11} + \overline{\sigma}_{22} + \overline{\sigma}_{33} \tag{3.35}$$

Where $\overline{\sigma}_{i,j}$ is mean stress at component level and $\overline{\sigma}_{eq}$ is equivalent mean stress.

Weldment due to the welding process has different features in comparison with the base metal. For example, the existence of the molten weld pool and its subsequent cooling creates questions in regard to the applicability of isotropic material properties for

welds. Ref. [35] suggest the use of σ_1, the largest of principal stresses if ($\sigma_1 > \sigma_2 > \sigma_3$), instead of Mises equivalent stress. Here (3.36) has been used, based on principal stress:

$$\sigma_m(T) = [\sqrt{(\Delta\sigma_{11} - \Delta\sigma_{22})^2 + (\Delta\sigma_{11} - \Delta\sigma_{33})^2 + (\Delta\sigma_{22} - \Delta\sigma_{33})^2}]/2 \qquad (3.36)$$

Weld details of various nature have been tested and results are given in Ref.[2,4] as fatigue class.

Elastic fatigue calculations require number of correction factors. These correction factors are provided by Ref. [4] in detail. They are formulated to correct calculated stress ranges in a way that *S-N* curves can be used. The *S-N* curves have been prepared according to unbounded linear elastic stress-strain relation for short, polished specimens under push-pull tests at an ambient temperature for base metal and for various weld details. The basic correction factors to be applied to base metal and welds are:

Base Metal

- temperature
- surface roughness
- thickness
- mean stress
- plasticity
- stress concentration factor.

Welds

- temperature
- thickness
- plasticity

In the designing of fatigue curves for welds, the influence of the stress concentration due to the surface irregularities, material inhomogeneity of the welds themselves, welding

residual stresses, mean stress resulting from applied actions, thickness up to 25 mm have been accounted for. Not taken into account in the design model or in the fatigue damage calculation procedure are the influences of alternating plasticity, temperature, and section thickness of larger than 25 mm. Specimens for evaluating the fatigue resistance of material have 25 mm thickness and are designed to fit the test apparatus.

In the local strain approach, the strains are calculated using a kinematic material model and are converted to stresses afterward. The conversion is done through elastic relation for their use in S-N curves. A multilinear kinematic material model with true stress-strain data according to Ref [1] can be used.

The methodology is to extract elastic, plastic and thermal strains calculated with multilinear hardening from FEA output, and then convert these strains to stress using a linear elastic law.

The reactor investigated in this thesis experiences shifts from its standard anticipated operation mode. It is therefore necessary to consider the effect of various cycles arising from these shifts. To account for multi amplitude cycles, a counting method is required. In this thesis, the *reservoir counting* method has been employed, based on the following.

The design fatigue curves provide the allowable number of cycles for a relevant stress range of *single-amplitude* cycles. The various operation modes of the reactor, on the other hand, generally produces periodic *variable-amplitude* stress ranges (functions of time). In Chapter 8, various operating modes are identified for the reactor. Most of these modes are non-periodic and are random in nature. The task therefore is to deduce from this (multi-amplitude) stress history a sequence of single-amplitude stress cycles that if applied separately without interaction, result in the same fatigue damage (index) as the original stress history.

Figures (3.10-11) show a typical non- periodic stress cycles and non-periodic stress history based on combination of various operating modes according to the reservoir cycle counting method. This cycle counting method uses graphical representation of the stress ranges: the maxima and minima of the relevant stress history are plotted versus time and connected by straight lines.

The profile from one maximum to the next is visualized as reservoir walls, with peaks and troughs, and the reservoir between the two maximum peaks filled with water. The

largest depth of the whole reservoir between the highest peak and the lowest trough corresponds to the first stress range; to be listed as the stress range of one cycle. The reservoir is then considered to be drained at the lowest trough, leaving the water that cannot escape trapped in troughs, if there is more than one lowest point the drainage may be from any of them, Fig (3.12).

The whole procedure is then repeated again with the next respective lowest trough, the next minimum, until all water is drained out. The procedure results in a list of individual stress ranges, if necessary conveniently ordered in descending order afterwards.

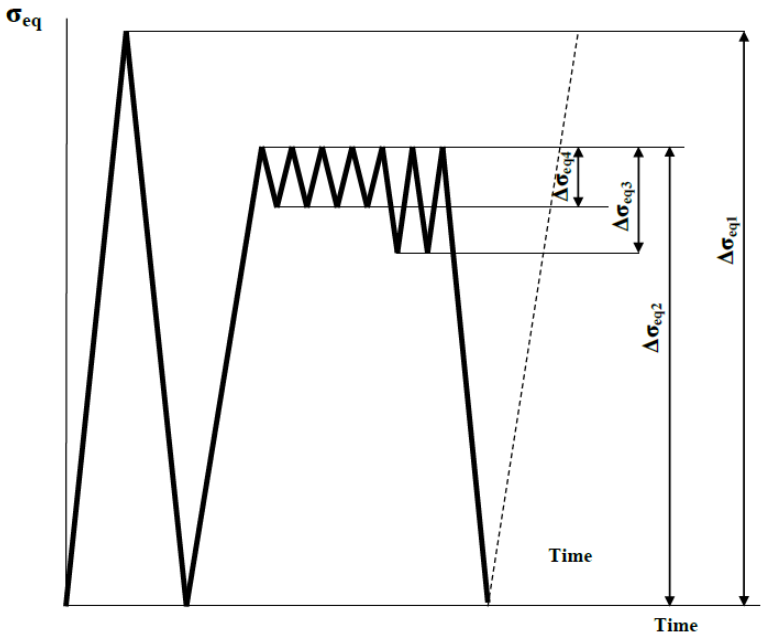

Fig. (3.10): Reservoir cycle counting method for non-periodic stress history

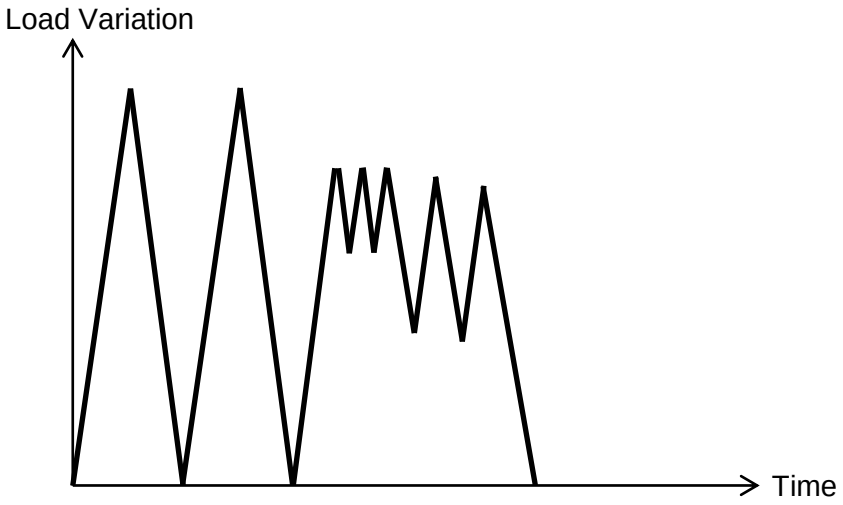

Fig (3.11): Non-periodic cycles

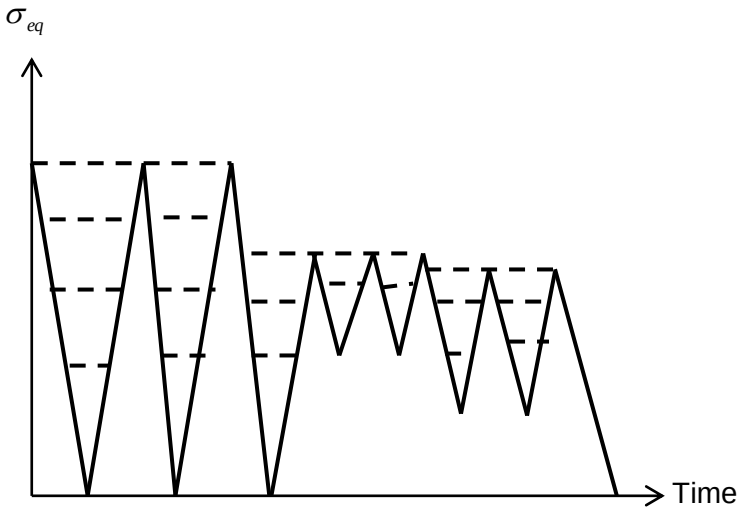

Fig (3.12): Non-periodic stress history

3.2.3.1 S-N curves

Mechanical failures due to fatigue have been the subject of engineering studies for more than 150 years. One early study was that of W. Albert, who tested mine hoist chains under cyclic loading in Germany around 1820. The term fatigue for first time was used

by J. Poncelet of France on his book on mechanics in 1839, the term minted to explain the process of damage and failure due to cyclic loading.

Fatigue was further discussed and studied in the mid -1800s by a number of individuals in several countries in respond to failures of components such as railway axels, shafts, gears, beams and bridge girders. The work of August Wohler, a German engineer, which was motivated by railway axe failure in 1850's, is of specific importance. He began the development of design strategies for avoiding fatigue failure, and he tested irons, steels, and other materials under bending, torsion and axial loads.

Wohler also demonstrated that failure was affected not only by cyclic stresses, but also by the accompanying steady (mean) stresses. Following Wohler work, among others, Gerber and Goodman performed more detailed studies on effect of mean stresses. The early work on fatigue and subsequent efforts up to 1950's are reviewed in a paper by Mann (1958).

The basis of the stress-life method is the Wohler S-N diagram, shown schematically for two materials in Fig. (3.13). The S-N diagram plots nominal stress amplitude (range) versus cycles to failure. There are numerous testing procedures to generate the required data for a proper S-N diagram. S-N data are usually displayed on a log-log plot, with the actual S-N line representing the mean data from several tests.

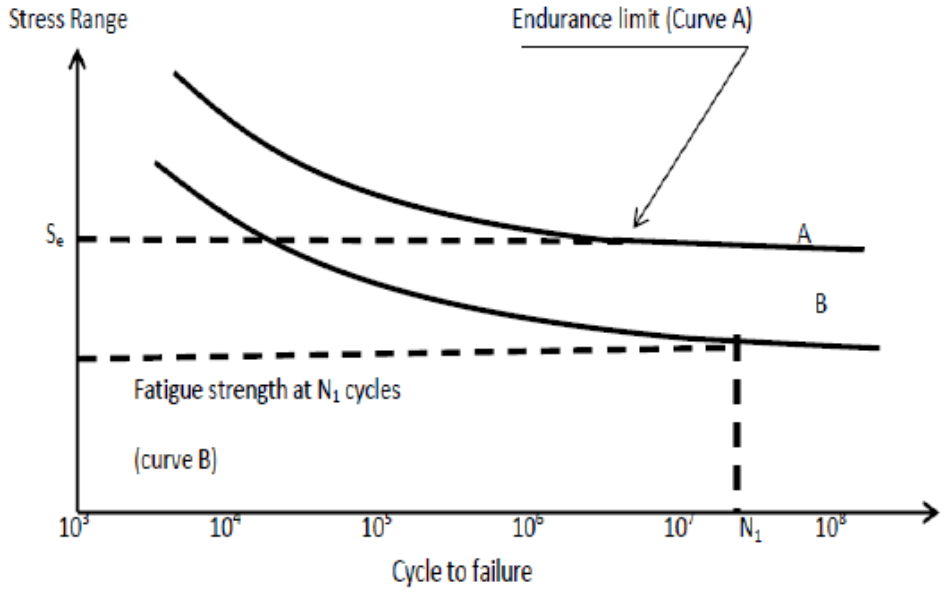

Fig (3.13): Typical S-N curves

In Fig (3.13), an additional parameter has also been shown: the endurance limit. The endurance limit represents a stress level below which the material model does not fail and can be cycled almost infinitely. The endurance limit is also marked by change of slope in the S-N curve; change of slope occurs at approximately 10^7 cycles for carbon steel and stainless steel materials.

The endurance limit is an important parameter in the fatigue life of components and its magnitude is one of the limiting factors on determination of allowable number of cycles.

As can be observed from Fig (3.13), the number of cycles to failure changes rapidly with stress range. For this reason, cycle numbers are usually plotted on a logarithmic scale. The reason for this is that on a linear plot, the cycle numbers for shorter lives cannot be read accurately. Fig. (3.14-15) presented for a typical alloy steel demonstrate this point.

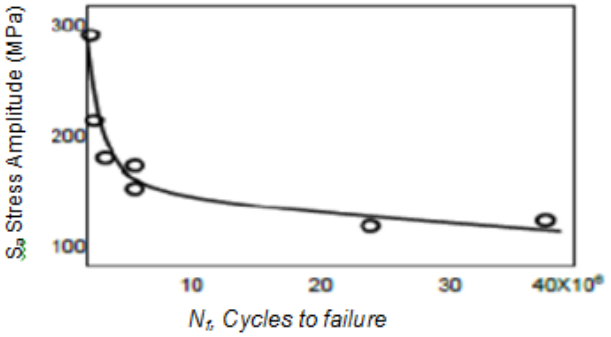

Fig (3.14): Typical S-N curve for an alloy material, linear scale, σ_m=0, K_t=1

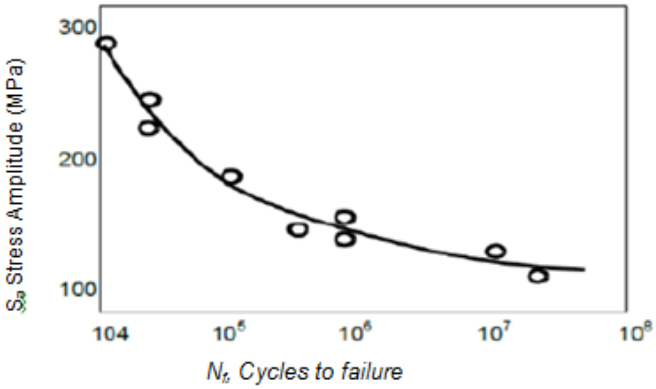

Fig (3.15): Typical S-N curve for an alloy material, log plot, σ_m=0, K_t=1

For *S-N* data that approximates a straight line on a log-linear plot, the following equations have been fitted to obtain a mathematical representation of the curve:

$$\sigma_a = C + D\log N_f \qquad (3.37)$$

In this equation C and D are fitting constants. For data approximating a straight line on a log-log plot, the corresponding equation is,

$$\sigma_a = AN_f^B \qquad (3.38)$$

This equation is often used in the following form,

$$\sigma_a = \sigma'_f \left(2N_f\right)^b \qquad (3.39)$$

The fitting constants for two forms are related by,

$$A = 2^b \sigma'_f, \; B=b \qquad (3.40)$$

Constants for equation (3.38, 39) for ductile steels extracted from Ref. [36] are given in Table (3.1), these constants are used in Chapter 8 for calculations of the number of cycles to failure.

Table (3.1): Constant for S-N curves of CS material from test at zero mean stress on unnotched axial specimens

Material	**Yield Strength σ_y (MPa)**	**Ultimate Strength σ_u (MPa)**	**True fracture Strength σ_{fb} (MPa)**	$\sigma_a = \sigma'_f (2N_f)^b = AN_f$		
				σ'_f	**A**	**b=B**
CS Normalized	228	415	776	1020	927	-0.138
CS Hot rolled	322	557	990	1089	1006	-0.115

Fatigue curves provided in Ref.[4] have been used in this thesis directly. These curves were developed from a fairly extensive database of experimental results with single amplitude push-pull and bending tests on polished specimens. The main proportion of results relate to rupture, but it had been found that results for technical crack initiation are within the scatter band of those for rupture, for the mainly small un-notched specimens rupture occurred shortly after technical crack initiation. The number of cycles to technical crack initiation was approximately 80% of those to rupture. It had been considered permissible to use all the results for cycles to rupture and for cycles to technical crack initiation in these test specimens. This has been done for the purpose of deduction of design fatigue curves till initiation of technical cracks in structures, with the usually larger dimensions Ref [33].

3.2.3.2 Notch definition, notch stress, stress concentration stress and strain parameters

Pressure vessels and heat exchangers (and most mechanical components) can have complex geometry that causes stresses to be locally elevated: for example, the junction of a tube and tubesheet, the junction of tubesheet and shells, holes, grooves, etc.

Such stress raisers are often collectively termed notches. For ductile components made of steels, alloys or other similar metals, the material can yield in a small local region without significantly compromising the strength of the component. This is due to the ability of the material to deform at the notch and shift some of the stress to adjacent regions; this behaviour is called stress redistribution. Final failure does not occur until yielding spreads over the entire cross section.

As a result of a ductile material's ability to tolerate local yielding, stress raiser effects are not usually included in applying yield criteria for static design. In other words, net section nominal stresses are used with the yield criterion, rather than local stress that include the notch effect. However, where cyclic loading may cause fatigue cracking, the stress raiser effect does need to be considered.

Results of tests with notch specimens have shown that in general not all of the total stress range is effective for the cyclic fatigue life, but only a part that depends essentially on the notch sensitivity of the material and the stress gradient.

To understand the effects of notches one must consider the parameters listed below:

A) Stress strain concentration and stress gradients

The degree of stress and strain concentration is a factor in the fatigue strength of notched parts; this is measured by the elastic stress concentration factor K_t. defined as:

$$K_t = \frac{\sigma}{S} = \frac{\varepsilon}{e} \qquad (3.41)$$

Where σ or ε is the maximum stress or strain at the notch and S or e is the nominal stress or strain. To demonstrate the idea, a classical plot of K_t verses notch dimension for a hole in a sheet is provided in Fig. (3.16), Ref [36].

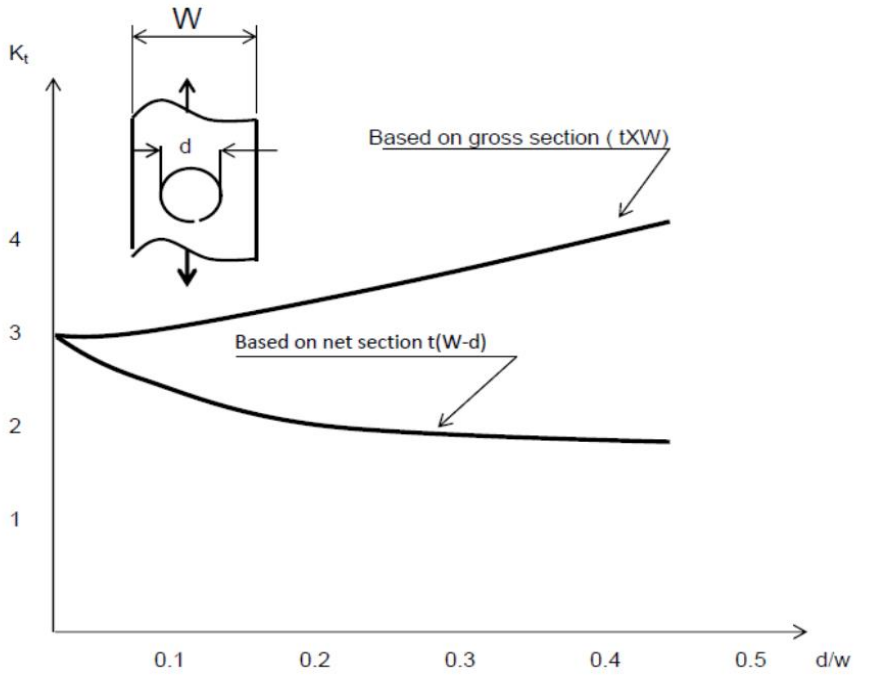

Fig (3.16): Changes of stress concentration factor with notch (hole dimensions), t is thickness

It should be noted that rapid decrease of stress with increasing distance from the notch and existence of biaxial or triaxial states of stress at a small distance from the notch are typical of stress concentrations. The stress distribution for the above geometry and its variation near a circular hole in the centre of a wide sheet in tension is given below and is shown in Fig. (3.17).

$$\frac{\sigma_X}{S} = 1.5\left(\frac{r}{X}\right)^2 - 1.5\left(\frac{r}{X}\right)^2 \qquad (3.42)$$

$$\frac{\sigma_Y}{S} = 1 + 1.5\left(\frac{r}{X}\right)^2 + 1.5\left(\frac{r}{X}\right)^2 \qquad (3.43)$$

where,

S= nominal stress= load/ area

σ_Y = axial stress

σ_X = transverse stress

X = distance from centre hole

r = radius of hole

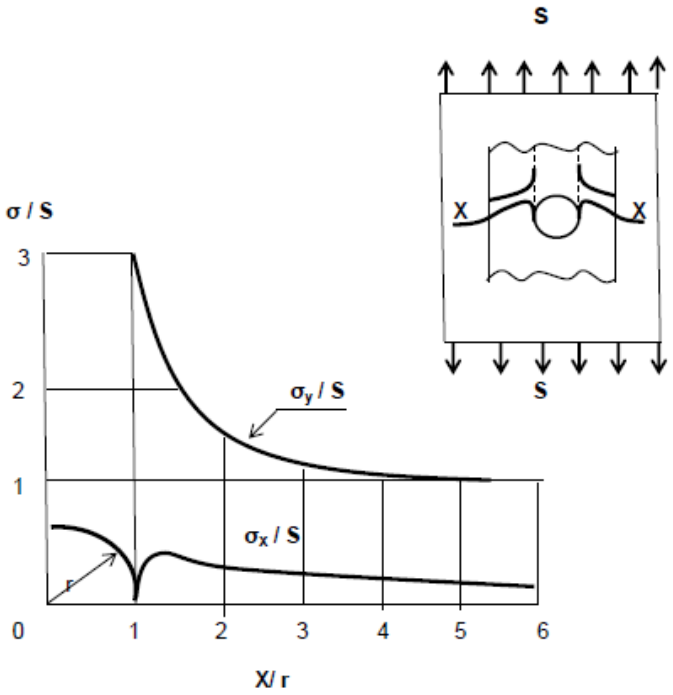

Fig (3.17): Stress concentration near a circular hole, Ref [36].

As can be seen from Fig. (3.17), a rapid increase in stress occurs close to the hole. At a sufficient distance away from the notch (circular hole) the stress pattern return to its uniform distribution. It is therefore mandatory to study such stress gradients (i.e. stress concentrations) and relate their effect to the fatigue life of a component.

Elastic stress concentration factors can be obtained from theory of elasticity, numerical solutions or experimental measurements. The most common and flexible numerical method is the finite element method. A model with relatively fine mesh in the areas of steep stress gradients is required.

Various experimental measurement techniques have been used to measure stress concentration factors, including brittle coatings, photo elasticity, thermo elasticity and strain gauges.

Details for dealing with stress concentration factors are provided in EN 13445 Part3, clause 18.

B) Stress-based approach (Mean stress effects and residual stresses)

(B.1) Mean Stress

The S-N curves provided in Ref. [4] are based on zero mean stress fatigue tests. This means before use of these curves, the effect of mean stress on stress range must be taken into account. Mean stress, σ_m, is defined as the average of the maximum and minimum stress values. Stress range, $\Delta\sigma = \sigma_{\max} - \sigma_{\min}$, is the difference between the maximum and the minimum values. These definitions are illustrated in Fig. (3.18).

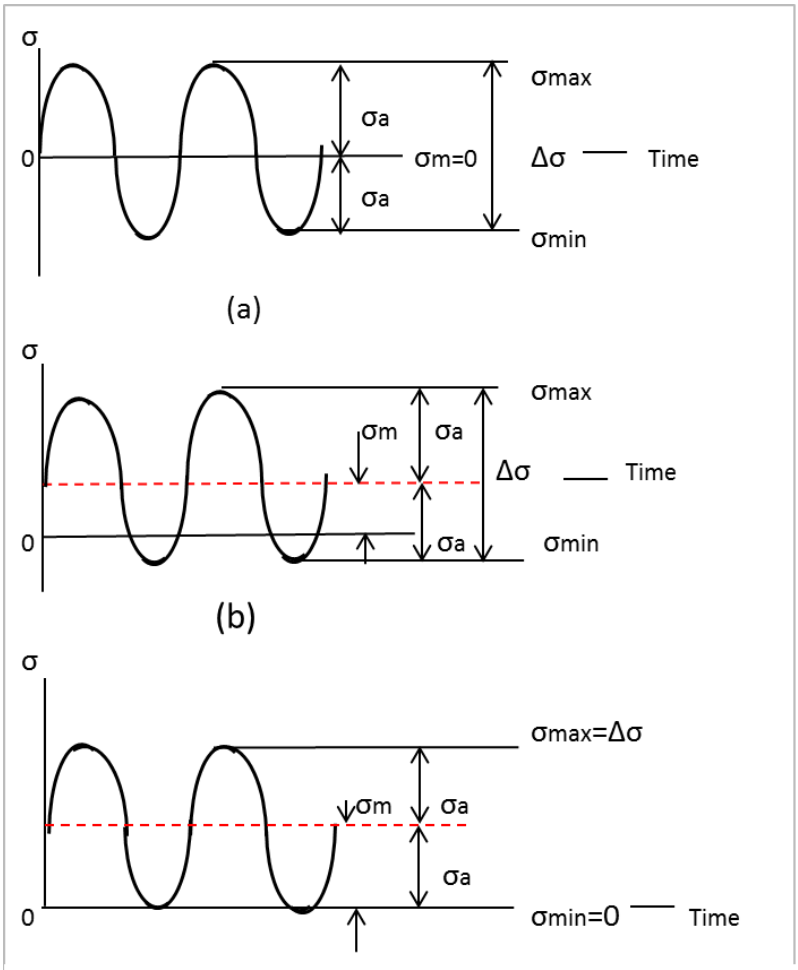

Fig (3.18): Various mean stresses, (a) complete reverse loading, σm=0, (b) loading with non-zero mean stress, (c) zero to tension stress σmin=0

S-N curves that include data for various mean stresses are widely available for commonly used metals. One procedure used for developing data on mean stress effects is to select several values of mean stress, running tests at various amplitudes for each of these. The results can be plotted as a family of S-N curves, each for a different mean stress.

As alternative means of presenting the same information is a *constant–life diagram.* This is done by taking points from the S-N curves at various values of life in cycles and then plotting combinations of stress amplitude and mean stress that produce each of these lives.

Development of *normalized amplitude-mean diagrams* is another widely used procedure; this provides an opportunity to fit a single curve that gives an equation representing the data. For values of stress amplitude approaching zero, the mean stress should approach the ultimate strength of the material (σ_u), so that a line or curve representing such data should pass through the point $(\sigma_m, \sigma_a / \sigma_{ar}) = (\sigma_u, 0)$.

To illustrate the above approach Figures (3.19-21) are provided. These figures illustrate *constant life diagrams* and *normalized amplitude-mean diagrams* for a typical alloy material. The equation of the straight line used in figure (3.21) is:

$$\left[\frac{\sigma_a}{\sigma_{ar}} + \frac{\sigma_m}{\sigma_u} = 1\right] \qquad (3.44)$$

This equation was developed by Smith from an early proposal by Goodman; the equation is called the modified Goodman equation. A variety of other equations have been proposed to more closely fit the data of this type. One of the earliest to be employed was the Gerber Parabola,

$$\left[\frac{\sigma_a}{\sigma_{ar}} + \left(\frac{\sigma_m}{\sigma_u}\right)^2 = 1\right] \qquad (3.45)$$

The Gerber equation is limited to tensile mean stresses, as it incorrectly predicts harmful effects of compressive mean stresses.

Improvement to the modified Goodman equation was proposed by Morrow by replacing σ_u by either the corrected true fracture strength σ_{fB} from tension test or by the constant σ'_f from unnotched axial S-N curve for $\sigma_m = 0$. The corresponding equations are:

$$\left[\frac{\sigma_a}{\sigma_{ar}} + \frac{\sigma_m}{\sigma_{fB}} = 1\right] \qquad (3.46)$$

$$\left[\frac{\sigma_a}{\sigma_{ar}} + \frac{\sigma_m}{\sigma'_f} = 1\right] \qquad (3.47)$$

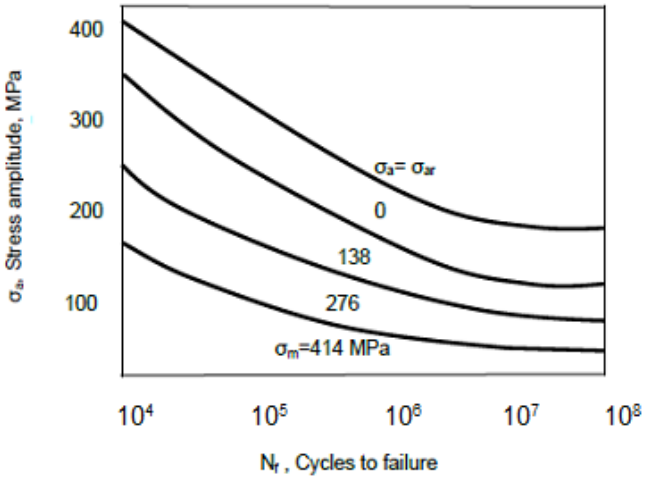

Fig (3.19): Typical axial loading S-N curves at various mean stresses for unnotched specimens of an alloy, Ref [36]

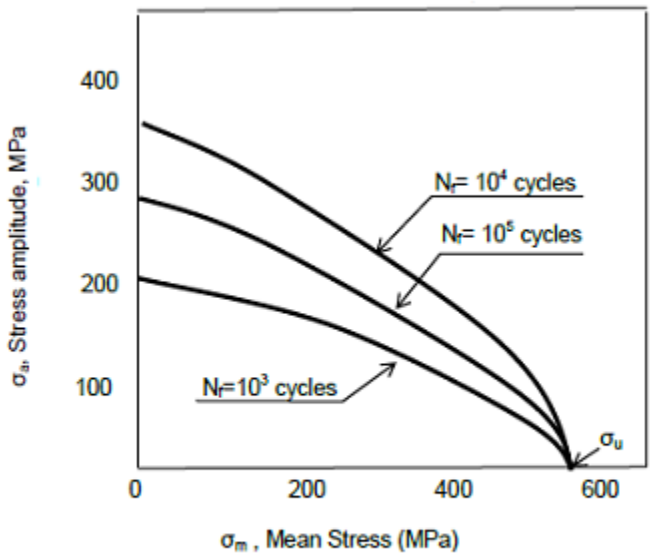

Fig.(3.20): Typical constant- life diagram of an alloy (K_t=1.0) taken from S-N curves of Fig (3.19), Ref [36].

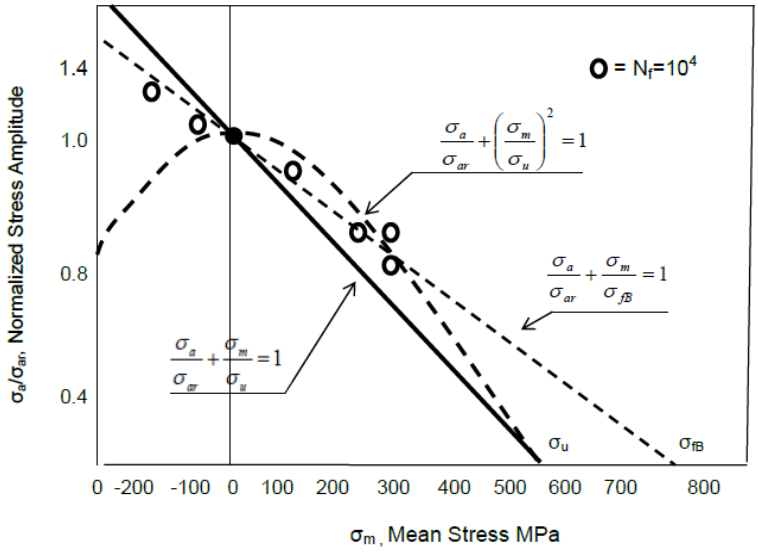

Fig (3.21): Typical normalized amplitude- mean diagram for an alloy based on Fig (3.20), Ref [36].

(B.2) Residual stress effects

Residual stresses are stresses that remain after the original cause of the stresses (external forces, heat gradient) has been removed. They remain in the component, even without external cause. Residual stresses occur for a variety of reasons, including inelastic (plastic) deformations, temperature gradients (during base metal heat treatment) or structural changes (phase transformation) during manufacturing of base metal.

Heat from welding may cause localized expansion, which is taken up during welding by either the molten metal or the placement of parts being welded. When the finished weldment cools, some areas cool and contract more than others, leaving residual stresses. Presented base metal S-N curves and fatigue weld class of weld details in Ref [1, 4] are corrected for effects of residual stresses.

C) Strain Based Approach

The strain-based approach to fatigue considers the plastic deformation that may occur in localized region where fatigue crack begin, as at stress raisers, i.e., tubesheet to shell junction. This procedure permits detailed consideration of fatigue situations where local yielding is involved; this is often the case for ductile metals.

The strain-based approach differs significantly from stress-based approach, this is because the stress-based approach is based on nominal (average) or structural stresses, rather than local stresses and strains, and it employs elastic stress concentration factors and empirical modifications. Use of the cyclic stress-strain curve is a main feature of the strain-based approach; i.e. use of a strain versus life curve, instead of a nominal stress versus life (S-N) curve. The method permits a more accurate estimation of mean stress effects by employing the local mean stress at the notch, rather than mean nominal stress. The methods are similar in that neither includes specific analysis of crack growth.

Among various equations for presenting strain life curve, Coffin-Manson, Morrow and modified Morrow relations have been used in the past. These equations are based on empirical relations. The mean stress effect is neglected in the Coffin-Manson relation but is considered by Morrow. In the modified Morrow equation, the first (elastic) term is the same, but the mean stress dependence has been removed from the second (plastic strain) term. This has the effect of reducing the estimated effect of mean stress at relatively short lives. It should be noted that the Coffin-Mason equation corresponds to curves labeled "*total*": *total* curves are log-scale plot of strain amplitude (ε_a) versus (N_f) for various steels. These curves cover result of several tests, elastic, plastic, and total strain data point versus life.

The Smith, Watson, and Topper (SWT) equation uses the strain-life curve and if the plastic strains are small, it is often used. It assumes that the life for any situation of mean stress depends on the product of $\sigma_{\max}\varepsilon_a = h''(N_f)$ **.** These equations are provided below: Ref. (36) provides details of these equations.

Coffin, $$\varepsilon_a = \frac{\sigma'_f}{E}\left(2N_f\right)^b + \varepsilon'_f\left(2N_f\right)^c \qquad (3.48)$$

Morrow, $\varepsilon_a = \frac{\sigma'_f}{E}(1-\frac{\sigma_m}{\sigma'_f})(2N_f)^b + \varepsilon'_f(1-\frac{\sigma_m}{\sigma'_f})^{c/b}(2N_f)^c$ (3.49)

Modified Morrow, $\varepsilon_a = \frac{\sigma'_f}{E}(1-\frac{\sigma_m}{\sigma'_f})(2N_f)^b + \varepsilon'_f(2N_f)^c$ (3.50)

Smith, Watson, Top – (SWT),

$$\sigma_{\max}\varepsilon_a = \frac{(\sigma'_f)^2}{E}(2N_f)^{2b} + \sigma'_f\varepsilon'_f(2N_f)^{b+c} \quad (3.51)$$

$$\varepsilon_a = \frac{\sigma_a}{E} + (\frac{\sigma_a}{H'})^{\frac{1}{n'}} \quad (3.52)$$

$\sigma'_f, b, \varepsilon'_f, c, H', n'$ are material properties

3.3 Summary

Design by analysis methods presented in Chapter 3 can be used to improve over design by formula procedures, in this way optimized thickness for various pressurized components including tube sheet of heat exchangers can be found.

Fatigue failure mode can be investigated through various procedures out lined in chapter **3**, cyclic analysis method provides detail information in regard to various issues associated with cyclic plasticity or ratcheting failure modes.

4. Code DBA Procedures

This chapter introduces the design by analysis codes and standards and provides details and requirements embedded in the standards in regard to the ductile, incremental and fatigue failure modes.

4.1 Ductile Failure under Static Load

EN 13445-3 Annex B sub-clause B.8.2 provides the rules for checking against gross plastic deformation. In this design check, the analysis used is based on:

- A linear elastic ideal-plastic constitutive law.
- Tresca's yield condition with associated flow rules.
- First- order theory.
- Proportional increase of actions.
- Stress-free initial state.
- Limitation of the maximum value of principal structural strains.

Assuming these conditions, the required analysis is limit analysis with proportional loading. However, in a structure exhibiting geometric weakening, EN13445 specifies use of large deformation theory and the evaluated collapse load is treated as a lower bound on the limit load for design purposes.

Taking a C2-Hydrogenation reactor as an example, in a specific petrochemical plant, Behseta and Schindler [37] showed that the direct route led to a thinner tubesheet than those required by design by rule procedures (ASME VIII Division1 and EN 13445-3 Clause 13 and Annex J).

Admissibility of a design is evaluated by checking both the carrying capacity of the model with reduced yield strength and the limitation of the maximum absolute value of principal structural strain by 5%, since either can individually dictate the limitation point.

ASME III and ASME VIII Div. 2 also contain guidelines for design based on limit analysis, The allowable load is established by applying design factors to the limit load such that the onset of gross plastic deformations (plastic collapse) will not occur. The allowable load (P_a) is defined as,

$$P_a = (\frac{2}{3})P_{Limit} \quad (4.1)$$

Where, P_{lim} is the limit load and (2/3=0.667) is a safety factor.

Table 5.4 of ASME Div. 2 provides load case combinations and load factors for a limit load analysis, factors of 1.5 and 1.3 are suggested depending on the design criteria, i.e.,

$$P_a = (1/1.5)P_{Limit} = (\frac{2}{3})P_{Limit} \quad (4.2a)$$

$$P_a = (1/1.3)P_{Limit} = (0.769)P_{Limit} \quad (4.2b)$$

The design factors (1.5 and 1.3) are provided for global criteria. These factors cover variation in material yield stress and loading condition. Design factor 1.5 is used for a load case that is limited to summation of internal and external maximum allowable pressure (including static head from liquid) and dead weight of the vessel. Factor 1.3 is applied to various load cases that are associated with combination of the above load case and other occasional loads such as snow load, wind load and earthquake loads. EN13445 also provides the same limits.

The following limitations apply to limit-load analysis (and equally to primary stress limits of elastic analysis 5.2.2 of ASME Div. 2).

a) The effect of strain-controlled loads resulting from prescribed non-zero displacements and temperature fields is not considered.

b) Components that experience reduction in resistance (weakening) with deformation shall be evaluated using the elastic- plastic procedure (5.2.4. of ASME Div.2).

Displacements and strains indicated by a limit analysis solution have no physical meaning. If the design specification requires a limit on such variables, the procedure in ASME Div. 2, 5.2.4 (elastic- plastic stress analysis method) shall be used to satisfy these requirements.

In ASME VIII Div. 2, the acceptability of a component using a limit load analysis is determined by satisfying the global and service criteria. The service criteria, as provided

by the user, limit the potential for unsatisfactory performance and shall be satisfied at every location in the component when subject to design load.

ASME III provides an alternative method for evaluating the gross plastic deformation or collapse state referred to as Plastic Analysis. In plastic analysis of a vessel, the designer may choose to incorporate strain hardening and/or large deformation effects. The material model specified by the designer for ASME VIII, Div. 2 plastic analysis may vary in complexity from simple bilinear hardening models to more complex curves defining the actual stress-strain curve. The inclusion of a strain hardening model means that the analysis may not demonstrate violation of equilibrium during solution, as occurs in limit analysis. In this case, protection against plastic collapse is evaluated by determining the plastic collapse load of the component. The "plastic load" is defined as the gross plastic deformation or ductile failure state.

In ASME III [3], the plastic load is determined by applying the *twice elastic slope criterion*, a graphical technique for establishing the plastic load from a load-deformation relationship obtained by plastic analysis. The load is plotted as the ordinate and the deformation parameter - deflection or strain - as the abscissa, as illustrated in the figure below. The load-deformation curve is initially linear but becomes non-linear when the limit of proportionality is reached. The plastic collapse load is defined by plotting a straight *collapse limit line* from the origin with twice the slope of the initial elastic response: that is *tan* $\phi = 2\tan(\theta)$ in Figure (4.1). The twice elastic slope load P_ϕ, corresponding to the intersection point of the load-deformation curve and the collapse limit line, is taken as the plastic collapse load in DBA (subject to a maximum strain and *triaxiality check*).

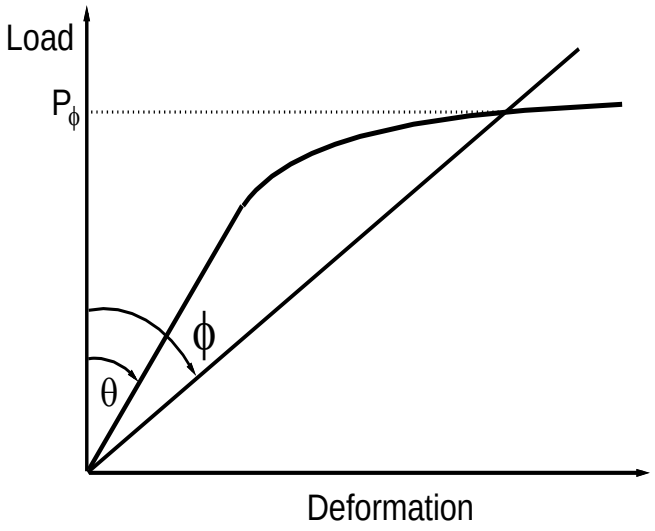

Fig. (4.1): Twice elastic slope criterion

The twice elastic slope criterion load and deformation parameters are required to characterise the plastic behaviour of the vessel, especially the formation of collapse mechanisms. The choice of type and location of the parameter is at the discretion of the designer.

Prior to 2007, the ASME VIII Div. 2 guidelines for plastic analysis were similar to those in ASME III. The 2007 ASME III Div. 2 plastic analysis procedures are significantly different to previous versions; most notably, the von Mises yield criterion is specified as the design stress basis (as opposed to the Tresca criterion used in ASME III), large deformation theory (nonlinear geometry) must be used and two *Acceptance Criteria* are specified in place of the twice elastic slope criterion. In addition, an optional true stress-strain curve that can be wholly derived from standard ASME material data is specified in Appendix 3.D. When using this model, the hardening behaviour is included up to the true ultimate stress and perfect plasticity behaviour assumed beyond this limit.

The two *Acceptance Criteria* are the *Global* and the *Service* criteria. The Global criterion requires demonstration of the point that the design does not experience overall structural instability (plastic collapse) under the specified design load cases. This is demonstrated by *convergence failure* in the analysis. The *Service criterion* provides limits on the

unsatisfactory performance under the allowable loads evaluated according to the global criterion. The effect of deformation of the component on service performance shall be evaluated at the design load combinations. This is especially important for components that experience a decrease in resistance (geometrically weaken) with deformation under applied load. In addition to designing against global plastic collapse, a local strain limit failure criterion is defined.

Inclusion of large deformation effects in elastic-plastic analysis also requires the identification of plastic-instability load; this would be beneficial as this load provides a mean for checking the correctness of calculated plastic load. The plastic instability load is an actual collapse load and not just an estimate of a plastic load. A separate definition is provided for stability load (this is not plastic-instability load). The Stability load is defined as the last converged solution of a numerical model with large deflection effects, an elastic perfectly plastic material model and Mises yield condition.

4.1.1 Alternative Definitions of Plastic Load

Various procedures have been proposed for the calculation of the plastic load. These include the:

- Twice Elastic Slope method, TES.
- Tangent Intersection Method, TI.
- Plastic Work method, PW
- Plastic Work Curvature method, PWC

The TES method is specified in ASME III for calculation of plastic load. Several workers have proposed alternative plastic collapse criteria to those currently used in the ASME procedures.

In addition to twice elastic slope(TES), two proposed methods will be further considered in these investigations, as stated above: Tangent Intersection (TI) criterion and Plastic Work Curvature (PWC) criterion.

The TI criterion is an alternative graphical construction method applied to the load deformation curve used in the TES criterion as shown in Fig.(4.2) [4].

In this method a tangent is drawn in the load-deformation diagram post yielding zone and the intersection of this tangent with the extension of the elastic line is defined as the plastic load.

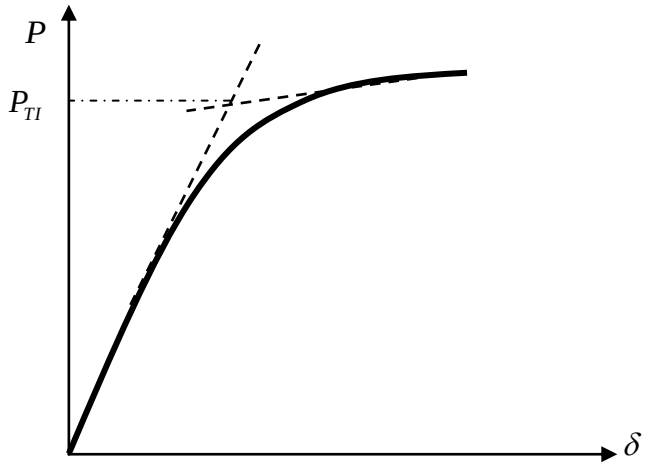

Fig (4.2): Tangent intersection criterion

The PW criterion was proposed by Muscat et. al. [29], who applied it to design by analysis of an ASME torispherical head and to a T-branch connection, The plastic work criteria assumes the proportional loading and capture the plastic response of the structure by plotting the normalized applied load, represented by the load parameter, against the corresponding cumulative plastic work.

Development of plastic failure mechanism is gradual and it is difficult to determine precisely when the plastic load is reached. In the PW method, the plastic load was defined as a load corresponding to the 5% principal plastic strain limit provided by CEN pr EN 13445-3. It was also demonstrated that the PW method, being based on the inelastic analysis, is not influenced by the elastic response of the structure.

The PW method was further developed because of the need to know the precise plastic load (and not the load associated with 5% maximum strain) in various applications. In this regard, the PW method was developed to Plastic Work Curvature method, PWC.

The PWC criterion is also based on the consideration of the dissipation of plastic energy (as a measure of internal work done on the structure) as load increases post-yield. This criterion was proposed by Mackenzie, et. al. [71] .Work by Li, et. al. [30, 70], Camilleri, et. al. [72] added to development of the method. Camilleri, et. al. [44] applied the curvature method to an ASME torispherical head.

Camilleri's work was accomplished by changing of earlier models to a shell of revolution geometry under uniform internal pressure and uniform boundary condition with a single material type (single yield value), i.e., ASME classical torispherical head under internal pressure. Linear Kinematic, Linear Isotropic and large deformation material models mainly were used on his work.

The curvature of plastic work identifies the rate of change of plastic deformation. Initially in the elastic region, plastic work is zero. In the upper stages of the elastic region, small plasticization occurs with very small curvature. Around yield the curvature starts to increase rapidly until it reaches its maximum value. The peak curvature indicates the start of gross-plastic deformation. A further increase in load reduces the curvature due to the post yielding behaviour and stress redistribution. The load corresponding to the peak curvature is defined as the plastic load. It has been proposed that gross plastic deformation occurs at a loading corresponding to about 10% of the maximum curvature, Ref (44). In other words, curvature of plastic work criteria is quite unique as the procedure depends solely on the total plastic work done on the structure. In this criterion, load, plastic work and curvature of plastic work are simultaneously and internally coupled and therefore the load causing peak curvature can be identified.

The PWC Method relies on a mechanism which identifies the maximum curvature of plastic work and relates this peak point to its corresponding load. To perform this task two interrelated plots are required, load-plastic work and plastic work- curvature of plastic work, as illustrated in Fig. (4.3). A plot of load-plastic work is firstly created; this plot provides valuable information in regard to trend and magnitude of changes in total plastic work done on the structure upon increase of the load.

To provide the second plot, i.e., plastic work-curvature of plastic work, change in slope of the load-plastic work plot is continuously tracked. These changes are presented in the form of a plot of curvature of the load-plastic work plot, which indicates the rate of stress redistribution occurring in the structure. The load correspond to the peak location on the

plot of curvature vs. plastic work identifies the greatest rate of stress redistribution but does not identify gross plastic deformation as further significant redistribution continues after this point.

A criterion of specifying gross plastic deformation at a post-peak curvature of 10% of the maximum curvature has been proposed. This large margin can be captured accurately by PWC due to its mathematical base. Introducing 10% of maximum curvature is considered as a reliable value since the load corresponding to this value is calculated accurately and is a safe indication of domination of gross plastic deformation.

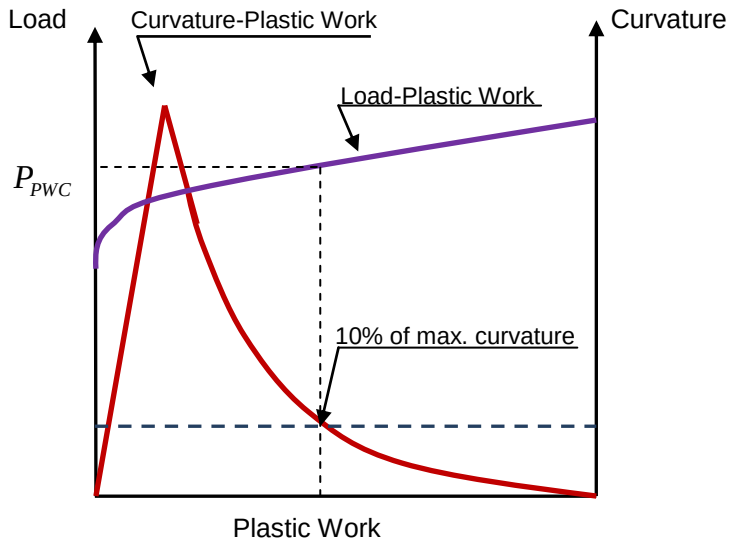

Fig (4.3): Plastic Work Criterion

4.2 Incremental Ductile Failure under Repeated Load

Incremental ductile failure under cyclic load procedures is defined in EN13445, ASME III, and ASME VIII. Guidelines for design against ratcheting based on elastic-plastic stress analyses are given in ASME VIII 5.5.7 *Ratcheting Assessment – Elastic-Plastic Stress Analysis*. This design procedure requires application, removal and re-application of the applied loadings during an elastic-plastic analysis of the vessel. An elastic-perfectly plastic material model based on the von Mises yield function and associated flow rule is specified and the effects of non-linear geometry must be included in the analysis. A

minimum of three complete repetition of the load cycle is required. Design against ratcheting is demonstrated if one of three criteria is satisfied after 3 (or if needed, more) cycles: there is no plastic action, there is an elastic core in the primary-load-bearing boundary of the component or there is no permanent change in the overall dimensions of the component. The Code shakedown limit provides a theoretical shakedown boundary as Ref. [3]:

$$\Delta\sigma_{SB} = \frac{\sigma_Y^2}{\sigma_{PM}}, if \left| \sigma_{PM} \le \frac{1}{2}\sigma_Y \right| \qquad (4.3)$$

$$\Delta\sigma_{SB} = 4(\sigma_Y - \sigma_{PM}), if \left| \sigma_{PM} > \frac{1}{2}\sigma_Y \right| \qquad (4.4)$$

These are limits given by the thermal stress ratchet criteria in NB-3222.5 of Ref. [3]. The same limits are duplicated in article (5.5.6.3) of Ref. [1], thermal stress ratcheting assessment.

4.2.1 ASME Methods of Shakedown and Ratcheting Assessment

ASME Sec.8. Div. II in Article (5.5.6) and (5.5.7) provides two different methods for ratcheting assessment, i.e., elastic "$3S_m$" method and elastic-plastic method. These methods have been described in sections [3.2.2.1]. The calculations required are presented in more detail here.

4.2.1.1 ASME Ratcheting Assessment- Elastic Method

To evaluate protection against ratcheting the following limit shall be satisfied.

A) $\Delta S_{n,K} \le S_{PS}$ (4.5)

B) The primary plus secondary equivalent stress range, $\Delta S_{n,k}$, is the equivalent stress range, derived from the highest value across the thickness of a section, of the combination of linearized general or local primary membrane stresses plus primary bending stresses plus secondary stresses $(P_L + P_b + Q)$, produced by specified operating pressure and other specified mechanical loads and by general thermal

effects. The effects of gross structural discontinuities but not of local structural discontinuities (stress concentrations) shall be included.

C) The maximum range of this equivalent stress is limited to S_{PS} . The quantity S_{PS} represents a limit on the primary plus secondary equivalent stress range and is defined in paragraph 5.5.6.1.d. In the determination of the maximum primary plus secondary equivalent stress range, it may be necessary to consider the effects of multiple cycles where the total stress range may be greater than the stress range of any of the individual cycles. In this case, the value of S_{PS} may vary with the specified cycle, or combination of cycles, being considered since the temperature extremes may be different in each case. Therefore, care shall be exercised to assure that the applicable value of S_{PS} for each cycle, or combination of cycles, is used (see paragraph 5.5.3).

D) The allowable limit on the primary plus secondary stress range, S_{PS}, is computed as the larger of the quantities below:

1) Three times the average of the *S* values (S value is 2/3 of yield) for the material from Annex 3.A at the highest and lowest temperatures during the operational cycle.

2) Two times the average of the S_Y values for the material from Annex 3.D at the highest and lowest temperatures during the operational cycle, except that the value from paragraph 5.5.6.1.d.1 shall be used when the ratio of the minimum specified yield strength to ultimate tensile strength exceeds 0.70 or the value of *S* is governed by time-dependent properties as indicated in Annex 3.A.

4.2.1.2 ASME Ratcheting Assessment Elastic-Plastic Method

Ratcheting, by definition, is plastic strain growth due to application of repeated loading. Therefore, direct investigation of the rate and magnitude of the strains growth and defining limit on the maximum strain (rather than limiting stresses to elastic criteria) has a great advantage in avoiding over conservatism. This can be achieved by studying the material post yielding behaviour subject to repeated loading.

Article 5.5.7 of ASME Sec. 8, Div. II provides procedure and gives details for ratcheting assessment according to elastic-plastic stress analysis. The ASME method relies on the

application, removal and re-application of the applied loadings. According to ASME, if protection against ratcheting is satisfied, it may be assumed that progression of the stress-strain hysteresis loop along the strain axis cannot be sustained with cycles and that the hysteresis loop will stabilize. A separate check for plastic shakedown to alternating plasticity is not required.

In addition to the above, article (5.5.7.2) of ASME suggests following steps for evaluation of protection against ratcheting using elastic-plastic analysis.

a) STEP 1 – Develop a numerical model of the component including all relevant geometry characteristics. The model used for analysis shall be selected to accurately represent the component geometry, boundary conditions, and applied loads. The tubesheet FE model presented in item (5.3) of this thesis satisfies this requirement.

b) STEP 2 – Define all relevant loads and applicable load cases. The FE model of the exchanger contains loads according to operational requirements.

c) STEP 3 – An elastic-perfectly plastic material model shall be used in the analysis. The von Mises yield function and associated flow rule should be utilized. The yield strength defining the plastic limit shall be the minimum specified yield strength at temperature from Annex 3.D. The effects of non-linear geometry shall be considered in the analysis. This material requirement also has been respected on provided calculations.

d) STEP 4 – Perform an elastic-plastic analysis for the applicable loading from STEP 2 for a number of repetitions of a loading event, or, if more than one event is applied, of two events that are selected so as to produce the highest likelihood of ratcheting. For this heat exchanger events are proportional and are in phase, i.e. pressure and temperature loads.

e) STEP 5 – The ratcheting criteria below shall be evaluated after application of a minimum of three complete repetitions of the cycle. Additional cycles may need to be applied to demonstrate convergence. If any one of the following conditions is met, the ratcheting criteria are satisfied. If the criteria shown below are not satisfied, the component configuration (i.e. thickness) shall be modified or applied loads reduced and the analysis repeated.

1) There is no plastic action (i.e. zero plastic strains incurred) in the component.

2) There is an elastic core in the primary-load-bearing boundary of the component.

3) There is no permanent change in the overall dimensions of the component.

4.2.3 Extension to ASME Method of Ratcheting Assessment

Chapter 7 of this thesis presents an extension of the ASME procedure to include a range of material models. These models are linear and multilinear isotropic hardening and linear and multi linear kinematic material hardening models.
In the analysis presented in Chapter 7, 100 half cycles (50 full range cycles) have been employed to investigate rate of the growth in plastic strains and consequently its effect on the thickness of tubesheet.

4.3 Fatigue

Annex B of EN 13445-3 provides procedure for the fatigue design check. In this design check, i.e., article B.8.5.2 states fulfilment of the requirements given in clause 18 suffices as a check against fatigue failure. It is required to show that the value of the accumulated fatigue damage index D_d for cyclic fatigue, obtained for all the cyclic load cases of pressure and temperature and other possible variable loads shall not exceed (1). Clause 18 is not incorporated in Annex B as this annex is purely based on design by analysis with inclusion of a fatigue design check.

Annex B contains all the other requirements for the direct route in design by analysis. The approach to cyclic fatigue investigation in clause 18 takes into account the fact that welded regions and unwelded base metal have different fatigue behaviour. The contrasting behaviour of the welded and unwelded regions is taken into account by use of different design fatigue curves; these curves represent the stress range versus the allowable number of cycles.

The ASME Sec. VIII, Div. 2 Annex 3.F provides smooth bar and welded joint fatigue design curves formula similar to EN standard. The procedure in both standards is similar: first total Mises equivalent of stress range at component level in hot spot(s) of the model is calculated, and then the calculated stress range is modified by applying relevant correction factors. Both standards provide detailed formulae, tables and charts

for the correction factors. After correction, the corrected stress range is qualified to be used for extracting the allowable number of cycles from the fatigue design curves.

It should be noted that the progressive plastic deformation design check does not require shakedown to linear elastic behaviour, and therefore, alternating plasticity is a response mode to be taken into account in the fatigue design check. Because of the requirement of the progressive plastic deformation design check, confined cyclic plasticity can be assumed, with the deformation controlled by the regions remaining elastic. Models with linear-elastic constitutive laws are suggested in the standard. These models will underestimate total strain in such cases of alternating plasticity due to local structural disturbance sources, and correction of the calculated stress range is required, by means of a plasticity correction factor. If in a load cycle plastic deformation occurs, linear- elastic models also require corrections for the mean stress.

4.3.1 Brief Review of Standard S-N Curves and Fatigue Weld Class

4.3.1.1 Standard S-N Curves

4.3.1.1A EN-13445- 3 Clause 18 (Base Metal)

An extensive database of experimental results with single-amplitude push-pull and bending tests on polished specimens have been used for tabulation of design fatigue curves of clause 18 for the unwelded region. Most of the data base test results are performed up to the rupture of the specimens. In this evaluation of experimental results, the established dependence of endurance limits to ultimate strength had been conservatively taken into account.

In determination of fatigue design curves, safety factors had been applied to the mean curves of the experimental results. This has been done based on the assumption of a normal distribution of the results. For the safety factor in cycle numbers, the value 10 had been chosen, which corresponds to failure probability of 0.01%. For safety factor in stresses, the value 1.63 had been chosen in the region of endurance stresses, corresponding to the same failure probability of 0.01%. Smoothening and slight adaptation of the resulting curves reduced this safety factor in stresses in the region of endurance stresses to values between 1.5 and 1.57, and increased the failure probability

in region to approximately 0.1%, a value still considered to be reasonable in pressure vessel design Ref (35).

The design fatigue curves (Fig (4.4)) have been determined by means of test results for,

- unwelded, polished, small, perfect, tensile or bending specimens made of ferritic or austenitic steels,
- specimens subject to uniaxial constant amplitude cyclic stress states,
- tests under laboratory conditions, in air and at the ambient temperature
- tests with stress or stain control, with measured strains converted into stresses by use of unbounded linear-elastic laws.

The design fatigue curves have been fictitiously extended in the high cycle regime to allow for the incorporation of the damage contribution of sub-cycles of multi-amplitude cycles with sub-cycle stress ranges below the single –amplitude endurance limit.

Influences of various factors on cyclic fatigue not accounted for in the tests and consequently on the design fatigue curves have to be accounted for in the determination of the equivalent stress range by application of appropriate correction factors.

The fatigue curves do not include stress concentration effects and therefore, the design model has to include local structural perturbation sources. The local *total stress range* is used with the fatigue design curves.

All results in the used database are for tests with uniaxial stress states, for multiaxial stress state clause 18 of Ref.[4] allows the use of Tresca's or Mises's equivalent stress. It should be noted that it is not the range of equivalent stresses that is to be used, but the range of equivalent stress of stress differences. For the frequent case of stress cycles between two states, the equivalent stress of the difference of the two stress state is the range to be used in the investigation.

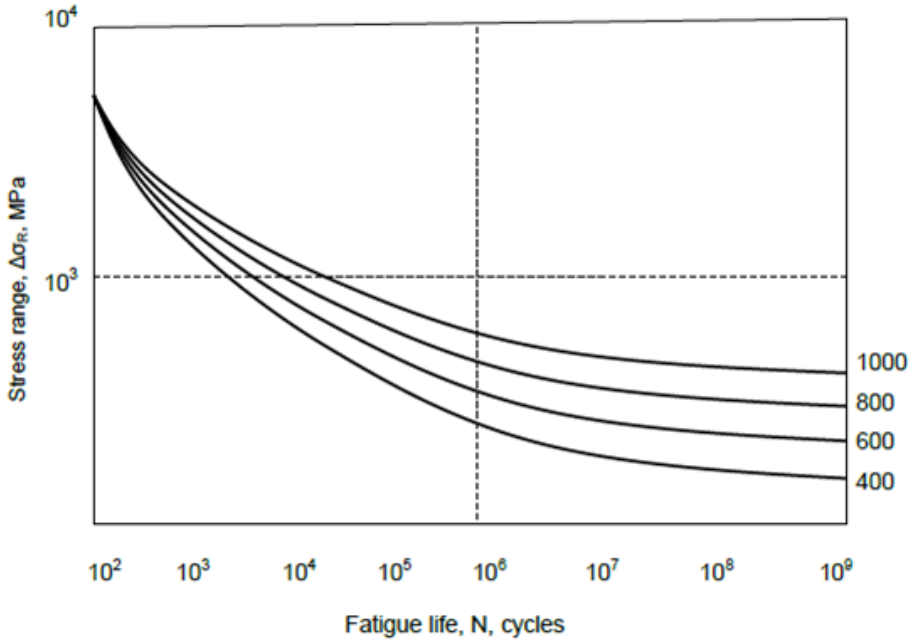

Fig (4.4): Design fatigue curve for unwelded regions for rolled and forged steels with tensile strength R_m as parameter, Ref [35].

4.3.1.1B EN-13445- 3 Clause 18 (Weld Metal)

Item (18.10.7) of EN-13445- 3 provides design fatigue curves for welded regions; these curves take into account weld details, location of hot spot, and orientation of principal stresses. Ten different design curves labelled *fatigue class* have been used: *fatigue class* is followed by a number which is equal to the value of the curve at $(2x10^6)$ allowable cycles.

The design fatigue curves were evaluated on the basis of the range of principal structural stresses in the point of crack initiation normal and parallel to the welded joint, with extrapolation of strain gauge measurements into this point of crack initiation, linear as well as quadratic extrapolation. This fact requires that, in the fatigue design check of welded regions, the very same stress ranges to be used, i.e., the ranges of principal structural stresses normal and parallel to the weld joint direction at all points of likely crack initiation (hot spot).

The Standard allows the use of stress ranges of equivalent stress differences, but then different fatigue classes are to be used. The equivalent stress does not have a direction and, therefore, the largest principal stress is used in the determination of fatigue class. Use of principal structural stress ranges as relevant stress ranges is recommended Ref. (35), as it avoids penalization in the fatigue class determination and is in the safe side in case were equivalent stress range is smaller than the maximum principal stress range.

The fatigue tests, take account of stress concentration due to surface irregularities, material inhomogeneity of the weld themselves, welding residual stresses and the mean stress resulting from applied actions. The influence of mean stress is not identifiable. It is hidden in the scatter of the test results, therefore, included in the fatigue design curve of welded regions. Alternating plasticity, temperature and thickness require correction.

Test results have shown that differences in material and material strengths, in the scope of Standard, have no statistically significant influence on the cyclic fatigue life of welded regions, in contrast to unwelded region were dependence of the fatigue life from the ultimate strength has been shown. This different behaviour is the result of the different dependencies of the crack initiation phase and the crack propagation phase. The number of cycles for crack initiation depends on the material's ultimate strength, but the number of cycles in the crack propagation phase does not. Thus, different fatigue design curve for different materials are used for unwelded regions, but for welded regions this is not required. Figure (4.5) shows the design fatigue curve for welded region, Figure (4.6) depict extrapolation details. Annex P of standard provides classification of weld details to be assessed using principal stresses.

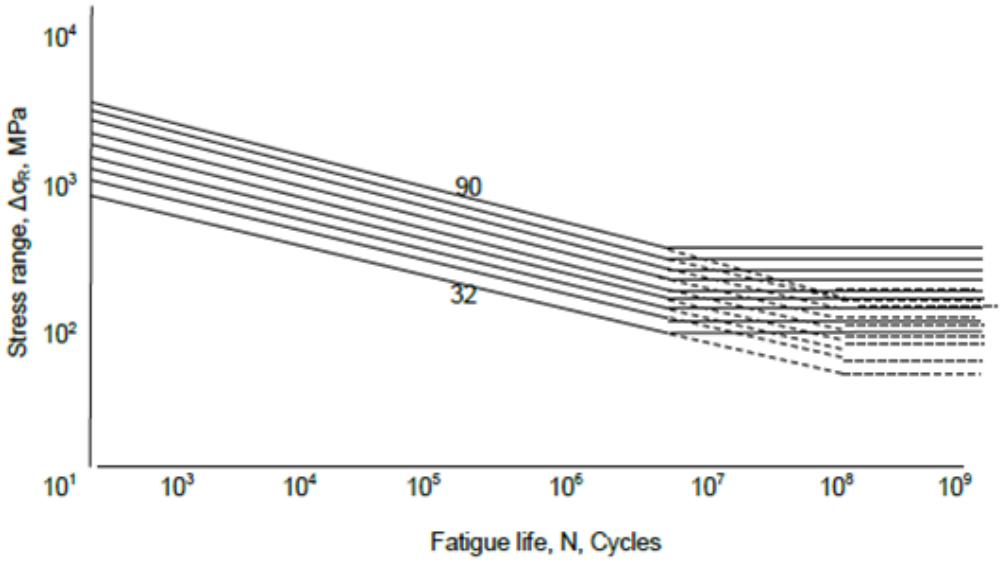

Fig (4.5): Design fatigue curves for welded region. FAT Classes (32,40,45,56,63,71,89,90), Ref [4].

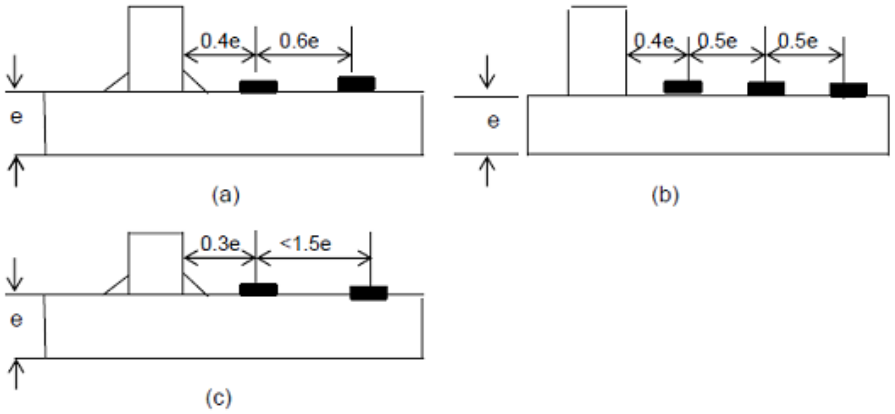

Fig (4.6): Extrapolation to obtain structural stresses from FEA or strain gauge results, Ref [4].

Notes:

(a) low bending stresses for component, gauge length ≤ 0.2e, linear extrapolation;
(b) high bending stress component, stiff elastic foundation, gauge length ≤ 0.2e, quarratic extrapolation ($Y_0=2.52Y^1-2.24Y^2+0.72Y^3$)
(c) gauge length> 0.2e, linear extrapolation

Where 'gauge length" referes to size of strain gauge or FE mesh.

4.3.1.1C ASME Sec. VIII, Div. II

Protection against failure from cyclic loading is provided in Article 5.5 of ASME VIII, Div. II. The data of the fatigue curves used in Div. II are typically presented in two forms: fatigue curves that are based on smooth bar test specimens and fatigue curves that are based on test specimens that include weld details of quality consistent with the fabrication and inspection requirements of Div. II. Design fatigue curves referenced in (5.5.3) and (5.5.4) are based on smooth bar test specimens and are adjusted for the maximum possible effect of mean stress and strain; therefore, an adjustment for mean stress effect is not required. The fatigue curves referenced in paragraph (5.5.5) are based on welded test specimens including explicit adjustments for thickness and mean stress.

Annex 3.F.1 provides fatigue curve details, details are based on testing of smooth bar polished samples. Environmental effects, size effect and mean stress corrections are included in the fatigue charts. S-N charts have a minimum design margin of 2 on stress and 20 on cycles. Other design margins are,

- 2.0 for data scatter
- 2.5 for size effect
- 4.0 for surface finish and environment
- Includes a simplified elastic plastic correction term "K_e" to correct for under predicted strains and elastic follow- up.

The design number of design cycles, N, can be computed from equation (4.6) based on stress amplitude S_a. C1 through C11 Coefficients for various materials is provided in Table (3.F.10) of Ref.[1]. S_a to be determined from part 5 of Ref [1].

$$N = 10^{X}\left(\frac{E_T}{E_{FC}}\right) \qquad (4.6)$$

Where,

$$X = \frac{C_1 + C_3\left(\frac{S_a}{C_{us}}\right) + C_5\left(\frac{S_a}{C_{us}}\right)^2 + C_7\left(\frac{S_a}{C_{us}}\right)^3 + C_9\left(\frac{S_a}{C_{us}}\right)^4 + C_{11}\left(\frac{S_a}{C_{us}}\right)^5}{1 + C_2\left(\frac{S_a}{C_{us}}\right) + C_4\left(\frac{S_a}{C_{us}}\right)^2 + C_6\left(\frac{S_a}{C_{us}}\right)^3 + C_8\left(\frac{S_a}{C_{us}}\right)^4 + C_{10}\left(\frac{S_a}{C_{us}}\right)^5}$$

Equations and parameters for welded joint design fatigue curve according to ASME VIII, Div. 2 is provided in code item 3.F.2.

In this Thesis, calculations for elastic fatigue of welded/ non-welded parts have been performed according to Ref. [4] only.

4.3.2 Fatigue Life Assessment Methods

Different approaches exist for fatigue analysis of welded joints, which can be distinguished by the parameters used for description of the fatigue life N or fatigue strength. Fig (4.7) shows the different parameters together with characteristic diagrams.

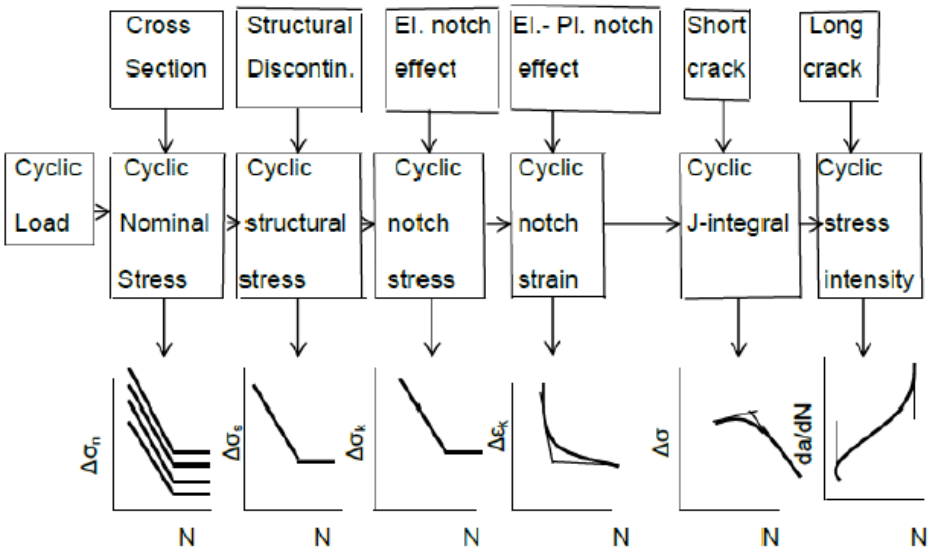

Fig (4.7): Approaches for description of the fatigue strength and life, Ref [38]

In general, the approaches can be subdivided into the following categories:

- *Nominal stress approach*, using the nominal stress range $\Delta\sigma_n$ determined by the external or internal loads and by the related cross section properties.

- *Structural or hot-spot stress approach*, using the structural stress range $\Delta\sigma_s$ at the weld to consider additionally the effect of the structural discontinuity.

- *Notch stress and notch intensity approach*, using the elastic notch stress range $\Delta\sigma_K$ or an equivalent parameter such as the stress intensity to take the notch effect of the weld toe or root into account.

- *Notch strain approach*, using the local elastic-plastic strain range $\Delta\varepsilon_K$ and/ or other parameters describing the relevant damage process in the material.

- *Crack propagation approach*, using special parameter such as ***J***-integral or the range of stress intensity ΔK to describe the increase of the crack length per cycle, i.e. the crack propagation rate da/dN.

4.3.2.1 Nominal stress approach

The fatigue assessment according to the nominal stress approach uses standard S-N curves together with detail classes of basic joints which can be found in several standards and guidelines which are mainly based on the statistical evaluation of relevant fatigue tests in 1970's, where also uniform scatter bands have been defined for the S-N curves. Later, a harmonized set of S-N curves and an associated catalogue of details was agreed upon internationally and issued by the International Institute of Welding (IIW), Ref [65].

To use above published data, calculation of nominal stresses is required. In general, nominal stresses are calculated using simple formulae, when fatigue at the welded attachment is considered, the nominal stress is calculated in the region containing the weld detail, but excluding any influence of the attachment on the stress distribution. An example of nominal stress in beam- like component using equation (4.7) is provided in Fig (4.8),

$$\sigma_n = \frac{F}{A} + \frac{M}{Z} \qquad (4.7)$$

Where:

F is axial force

A is cross section area

M is bending moment

Z is section property

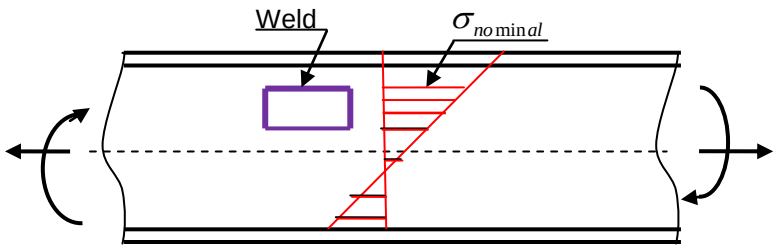

Fig (4.8): Nominal stress in a beam-like component

4.3.2.2 Structural or Hot-Spot Approach

The structural or hot- spot stress approach, sometimes also called geometric stress approach, considers the stress increase due to the structural configuration or in other words, the macro-geometry. The idea to exclude the local stress concentration due to the weld toe by using the stress or strain at a certain distance away from the weld toe is related to experimental investigation performed in 1960's by Peterson, Ref [64].

The hot-spot stress approach with the definition of reference points for the stress evaluation and extrapolation at certain distances away from the weld, which depends on the plate or shell thickness, was developed in the 1970's in a combined effort by classification societies and operators of offshore installations together with research institutes such as the International Welding Institute. The objective was the fatigue strength assessment of tubular joints.

Various codes and recommendations exist for load assumptions, for stress evaluations and extrapolations, for parametric formulae of hot-spot stress concentration factor (SCF) and for the definition of an appropriate S-N curve. This work is based on data and details as provided in Ref. [4]

Radaj [57] demonstrated that structural stress can be analyzed either by surface extrapolation or by linearization, e.g., through wall thickness, in order to exclude the local non-linear stress peak caused by the weld toe.

Figure (4.9) shows the main effect of a notch is to produce nonlinearity in stress distribution in the thickness direction, the nonlinear stress peak lies within a radius of approximately (0.3t) to (0.4t) from the notch root. A nonlinear stress peak is one reason

why a surface defect located at a notch is more dangerous than embedded defect, which is usually located in an area of lower stress, Fig. (4.10).

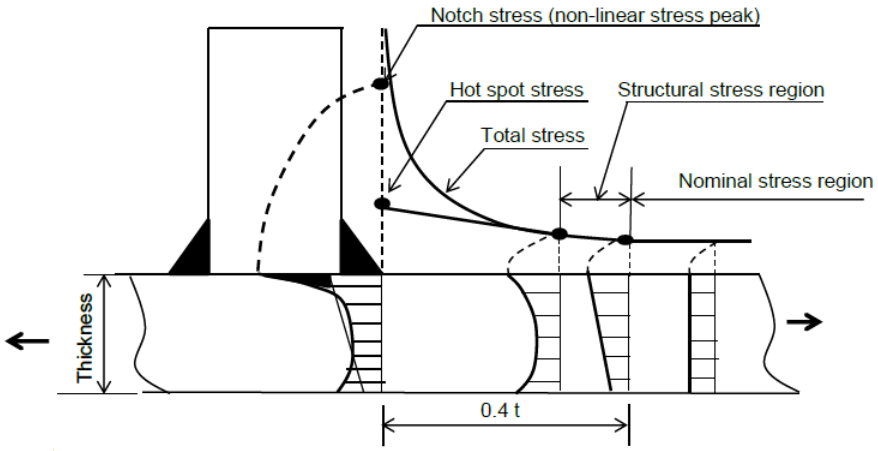

Fig (4.9): Stress distribution across the plate thickness and along the surface in the vicinity of a weld toe.

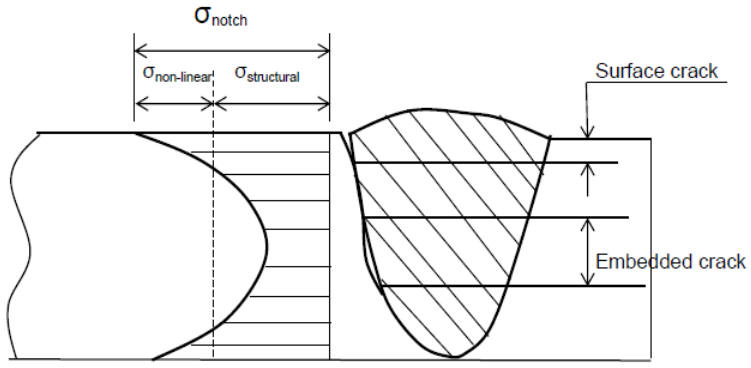

Fig (4.10): Nonlinear stress peak caused by transverse weld reinforcement.

Edge notches and small drilled holes cause similar nonlinear stress peaks, but with different orientations. The notch stress (σ_{notch}) is usually calculated by multiplying the hot spot stress by a stress concentration factor, or more precisely the theoretical notch factor, K_t. In many cases the result will exceed the yield strength of the material. Thus, elastic-plastic behavior is to be expected, and the calculated stress should be considered as a pseudo-elastic stress.

The geometry of the local notch at the weld toe varies significantly along a weld and between different welds. In spite of specified minimum requirements for the weld profile, the exact geometry is unknown. Therefore, nonlinear stress peak has a random value. A specific feature of the nominal stress approach, and also the hot spot stress approach, is that the effect of this random variable is implicitly included in the test results, and is reflected in the scatter band of the S-N curves. Therefore, nonlinear stress peaks need not be calculated when these two approaches to fatigue analysis are used. On the contrary, they must be excluded from calculated or measured nominal or hot spot stress.

4.3.2.3 Notch stress approach

The notch stress approach considers the increase in local stress at the notch formed by the weld toe or the weld root, based on theory of elasticity, i.e. without consideration of elastic-plastic material behavior. The notch stress approach allows certain effects to be considered in a refined way; in particular the weld profile can be well assessed by the notch stress approach. For example, undercuts according with different welding processes can be recorded and subsequently assesses using the notch stress approach. Furthermore, the geometry of fillet-welded joints can be optimized with respect to fatigue, taking all geometrical influence factors into account. Comprehensive investigations of welds under biaxial constant and variable amplitude loading show that in-phase loading can be treated well by conventional hypotheses. Also, the effects of multi-axial loading and residual stresses have successfully been investigated, Ref [66].

4.3.2.4 Notch Strain Approach

The notch strain-based approach was developed in early 1960's in response to the need to analyze fatigue problems of nuclear reactors to specifically deal with cyclic thermal stresses; this method has been applied to many other components since that time. Approach considers the local elastic-plastic stress and strain in the notch. Procedure permits detailed consideration of fatigue situations where local yielding is involved.

Local yielding is often the case for ductile metals in pressure vessel applications at locations of structural discontinuities, this specific feature demands an improved procedure which can deal with localized plastification more accurately For this reason

the strain-based approach can be considered to replace the existing stress-based approach.

The classical stress- based approach emphasizes on nominal (average) stresses, rather than local stresses and strains, and it employs elastic stress concentration factors and empirical modifications thereof. The more advanced stress approach provided in Ref [4] relies on extrapolation of stresses from regions close to hot spot in order to capture part of non-linear stress distribution in the geometrical discontinuities. It can be argued that in spite of the much improvement to nominal stress approach, the true stress distribution cannot be captured.

Employment of a cyclic stress –strain curve is a unique feature of the strain approach, as is the use of a strain versus life curve, instead of nominal stress versus life (S-N) curve. As a result of the more detailed analysis of local yielding, the strain-based method gives improved estimates for intermediate and especially short fatigue lives.

The elements of the approach, which has been applied to notches at the base material, include the computation of the local stress and strain taking into account the elastic support effect of surrounding material and the cyclic material behavior, i.e., the stress-strain relation as well as the crack initiation life. The approach has been applied also to welded joints to predict the crack initiation life particularly for load cycle numbers less than 10^5, where local plasticity effects are more pronounced.

To predict notch strains during plastic deformation under cyclic loading, few closed-form solutions exist. An approach of this type is related to Seeger, which is based on the “classical” elements used in connection with base metal, i.e. stress-strain relation by Romberg and Osgood. Local plasticity effect on stress strain concentration factors during plastic deformation at notch by Neuber’s rule, stress- strain path approximated according to Masing and strain S-N curve according to Manson, Coffin and Morrow. In this Thesis, numerical analysis using a kinematic hardening material model has been used, Ref [36].

5. Design of Hydrogenation Reactor Tubesheets

Tube sheets of heat exchangers have been designed according to ASME [2] classical roots for many years. This ASME procedure is based on DBF approach and relies on reduced modulus of elasticity and Poison ratio, curves (evaluated experimentally) provided by ASME account for perforation and various pitch.

Use of linear FEA through Appendix 5 application has also been adapted in industry. Various designers have tried to simplify the geometric modelling either by eliminating the perforation or by introducing beams to replace the tubes. Very few attempts have been made to reduce the tube sheet thickness through use of inelastic analysis. Behseta, et al. [56], applied inelastic analysis to a geometrically complex model to show the amount of reduction which can be achieved through application of direct route. Investigation of the gross plastic deformation failure mode relies on the study of the material's post yielding behaviour, structural behaviour of the considered model and loading mechanism. These observations can be done according to the experimental measurements and/or analytical calculations, Save [39].

From an experimental point of view, very limited information is available on the tubesheet geometry. The available data is limited to the clamped edge circular flat plates with various diameters to thickness ratios; Gerdeen [40] and O'Donnell [41] have reported some experimental data with regards to the perforated clamped edge plates with various pitch configurations.

The dominating factor, staying action of the tubes, has been omitted from the measurements due to the difficulties on building a realistic specimen and due to the further complications involving on the location for strain measurements. It is clear that tubesheets with inclusion of the tubes will not bend or behave the same way as untubed circular clamped plates do, even with taking account of the perforation.

Under uniform loading, a maximum deformation of a perforated flat plate (without tubes) occurs at the centre of the plate and this results to the end reaction in form of the bending as well as shearing stresses.

In contrast to this notion, the staying action of tubes will eliminate any considerable deformation away from the untubed portions of the plate as the behaviour is switched to rigid body motion, i.e., all parts have uniform and similar displacement. The plate rim,

although very small in size, will be subjected to shearing and bending. For clamped edge plates this deformation is additionally affected and is dominated by displacement and bending of the attached shells. It should be further noted that in practice the bending of 3 outer tube rows also has been observed.

5.1 Load Definitions

For the purpose of analytical calculations, the following classical definitions are applied consistently throughout this Thesis.

The first yield load, this is a load for which the material of the tubesheet at the location to the shell attachment first yields (the most highly stressed point), this can be determined from elastic analysis. Because only one point of the structure (of infinitesimal volume) is at yield, the surrounding elastic material restrains the tube sheet from plastic deformation as a whole. Although this yield point does not necessarily correspond to the proportional limit on a load deflection curve, ANSYS [18] always take the same value for these different definitions.

The limit load, limit load has been calculated and reported for various cases according to the following definition.

The classical definition of a limit load according to limit analysis is an idealized, mathematical one. The load for which deformation increases without limit while the action is held constant is called limit load, in an analytical model:

a. Strain- displacement relations are those of small displacement theory.

b. Material response is linear elastic- perfectly plastic.

c. Internal stresses and applied forces are related by the usual equations of the equilibrium written for the undeformed geometry.

Both first yield point and limit load are proportional to material yield strength.

Plastic Load, at plastic load, significant plastic deformation occurs for structure as a whole, i.e., the plastic region has grown to sufficient extent that the surrounding elastic region no longer prevents overall plastic deformation from occurring. The plastic load depends not only on the yield strength but also the material strain hardening behaviour.

Geometric strengthening, the geometric strengthening has been defined as a sharp rise in the load- deformation diagram post yielding (as oppose to geometric weakening which shows the decrease on the diagram). CS material poses the geometric strengthening behaviour after their first yield load. Fig (5.1) shows the intended definition.

Instability Load, in here this load is defined as a load corresponding to a solution under large deflection algorithm with elastic-perfect plastic material model. This load is calculated for the purpose of comparison only, comparisons between loads calculated from various material hardening with large deflection algorithm and this bench mark load.

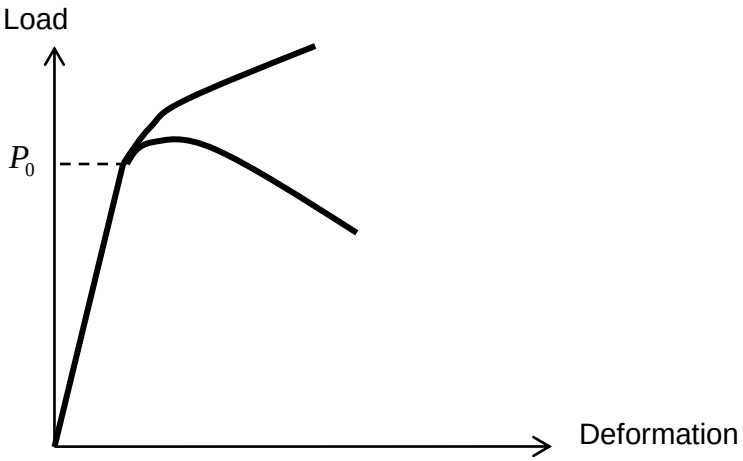

Fig (5.1): Geometric strengthening and weakening

Large deflection, large deflection here means the activations of procedure which accounts the secondary displacement derivatives in stress-deformation relationships, and is written for deformed geometry, the stiffness change due to change of elements shape or change in orientation of the elements are accounted for. This should not be taken as large magnitude of deformation for tubesheet geometry.

It should be noted that material cyclic stress-strain curves under some conditions are used, in this work due to relatively low metal temperature (108 degree C maximum) and limited cycles due to dominantly steady-state operation of unit (start-up and shout downs only) the monotonic stress-strain curves were used. Additionally, in Chapter 8 of this thesis a cyclic stress-strain curve is used for purpose of fatigue assessment.

The steady state through thickness temperature distribution in the vessel was evaluated by a preliminary thermal analysis. The skin temperatures of 50^{o}C and 108 ^{o}C were taken from the equipment data sheet. The analysis indicated an approximately linear temperature distribution through the thickness of the vessel components, applied as nodal temperatures in the ratcheting assessment.

5.2 Reactor Geometry, Material Parameters and Reactor Data Sheet

The reactor tubesheet considered is the largest and heaviest heat exchanger in an Olefin plant, a chemical reactor with 3200 tubes. Olefin plants are among the largest plant in a petrochemical complex.

Dimensions, properties, and basic material information, are given in references [37, 54] and summarized below:

- Design fluid temperature on tube side= -4/190 °C
- Design fluid temperature on shell side= -4/145 °C
- Design pressure shell side = 1 MPa
- Design pressure tube side = 4 MPa
- Shell side mean wall temperature = 50 °C
- Tube sheet mean wall temperature = 100 °C

A sketch of the area of interest local to the tube sheet/ channel connection with manufactured dimensions and uncorroded thickness using the classical ASME design by formula approach [1,2] is given in Fig. (5.2). Tube to tubesheet weld detail is extracted from reactor datasheet and is provided in Fig. (5.3), details, type of attachments and basis for establishing the allowable loads for the tube to tubesheet joints and weld detail are according to requirements provided in appendix A of Ref.[2],

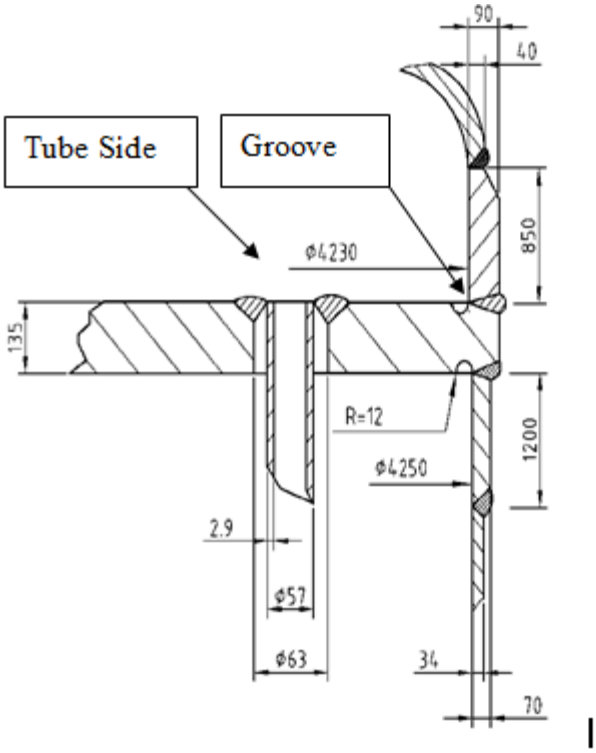

Figure (5.2): Tube sheet configuration and basic dimensions.

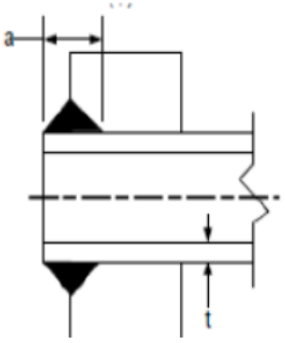

Fig (5.3): ASME tube to tubesheet weld detail, a is equal to 1.4t.

The material physical properties and material stress data are given in Table (5.1), values are reported at the calculation temperature. S_m is the allowable stress based on Table 5A of reference [6].

Table (5.1): Mechanical properties data at calculated temperature

Material	Elastic Modulus (MPa)	$R_{P/tcalc}$ (MPa)	Cold Yield $R_{P0.2/25°C}$ (MPa)	Hot Yield $R_{P0.2/tcalc}$ (MPa)	S_m (MPa)	$1.5S_m$ (MPa)	t_{calc} (°C)
Upper Shell SA 537 Cl2	193053	485	360	317	229.6	344.4	190
Lower Shell SA 516 Gr 70	195337	482.3	260	232	134.7	232	145
Tubesheet SA 266 Cl2	194173	482.3	250	217.5	144.7	217.12	167.5
Tubes SA 334 Gr1	194173	379	205	181.5	120.6	181	167.5

Calculation temperatures are:

a. Fluid design temperature for shell material of channel side
b. Fluid design temperature for shell material of shell side
c. Average design temperature for shell and tube sides for tubesheet and tubes.

5.3 Finite Element Modeling

All Finite Element Analysis presented was performed using the ANSYS program.

In the design configuration considered here, the standard tube sheet thickness of 135mm calculated according to the classical ASME DBF method and shown in Figure (5.2) is reduced to 100 mm; this thickness was chosen as it is within the range of standard plate sizes available from plate manufacturers and can be purchased without special order. The FEA model, illustrated in Figure (5.4), is similar to that used in Reference [37].

To minimise computing requirements, a symmetrical segment of vessel is modelled. The tube sheet, shell and head are modelled using 8 node isoparametric elements, 8 node isoparametric elements were used for computational efficiency. In small deformation analysis, Solid 45 and in large deformation analysis Solid 185 elements were used. The Solid 185 element is formulated to capture higher order strain terms, however this type of element must be used with care as volume and shear locking may be encountered. The locking mechanism at elements level can result in solution divergence. A groove

has been tabulated at the junction of the tubesheet to shells to reduce the effect of intersecting geometries; Fig (5.6) shows this feature. The structural effect of the remaining tubes is modelled using 12 link elements for each tube hole in the tubesheet with total axial stiffness equivalent to that of a single 3D tube. The outer four rows of tubes are modelled using 3D solid elements, as shown in Fig (5.5).

In fixed tube sheet exchangers grooves are normally placed at the junction of the tube sheet to the adjoining shells for two main objectives. One objective is from a computational point of view and other from structural point of a view. By introducing grooves one can bypass the singularities, which will be created at the intersection point. In this way the transition from one geometry to the other one (tube sheet to shell) will be smooth and sharp corners will be avoided, sharp corners produces high stresses, possibly even singularities, and more realistic stresses can be captured by modelling the radii.

The structural objective of grooves is to reduce the high surface stresses. By the introduction of grooves, the allowable number of cycle loads will be increased at the weld toe and at the base materials.

The multilinear kinematic hardening and nonlinear isotropic hardening options are not appropriate for the link elements in large strain analysis. For large deformation analysis, these elements were replaced by simple supports applied to the tube sheet locations in the gravity direction. This is appropriate as in these regions tube sheet displacement is limited.

The model consists of 42,482 elements and 82,238 nodes, symmetry boundary conditions are applied on the cut surfaces of the modelled segment as shown in Figure (5.7). Pressure loading is applied to the tube sheet, including the internal pressure in the tubes themselves, this is illustrated in Figure (5.8).Also, and end action effect is applied to last row of the channel side shell.

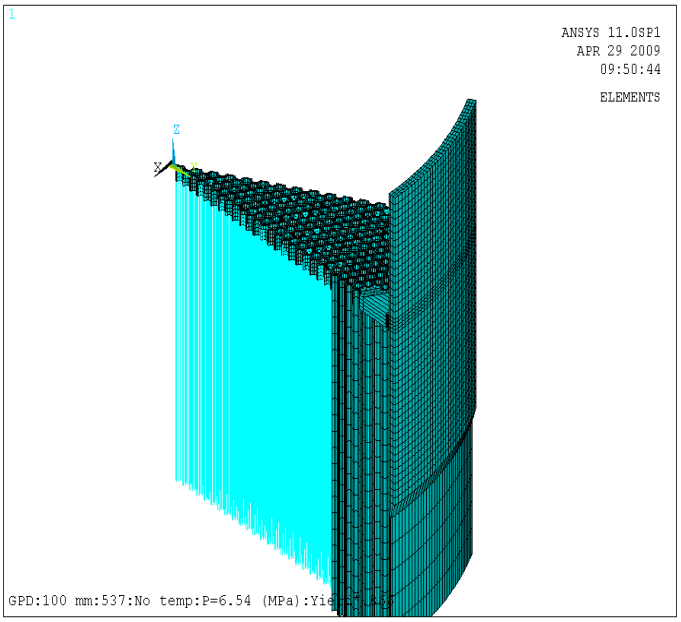

Figure (5.4): Finite element model.

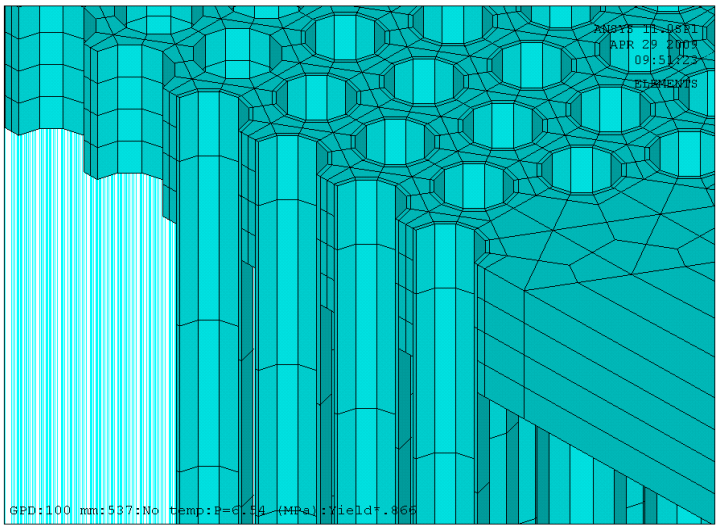

Fig (5.5): Zoomed view of outer tube modelling.

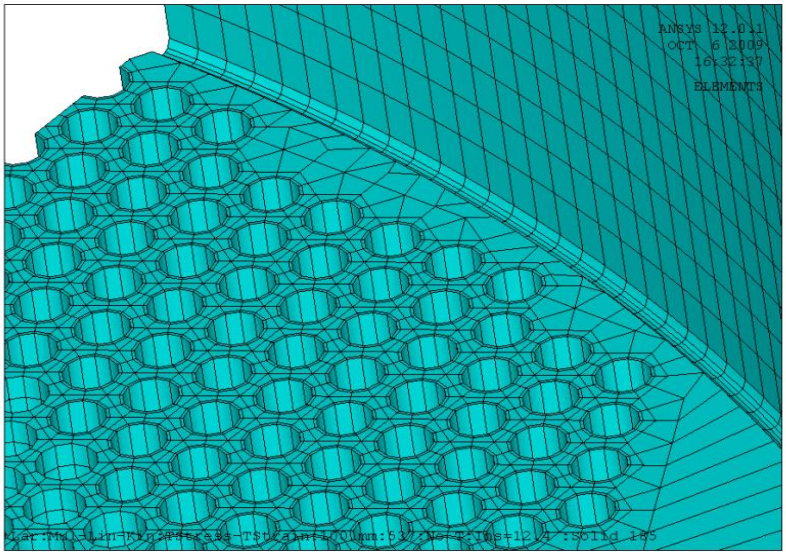

Fig(5.6): Radius location at the junction of tube sheet and shell.

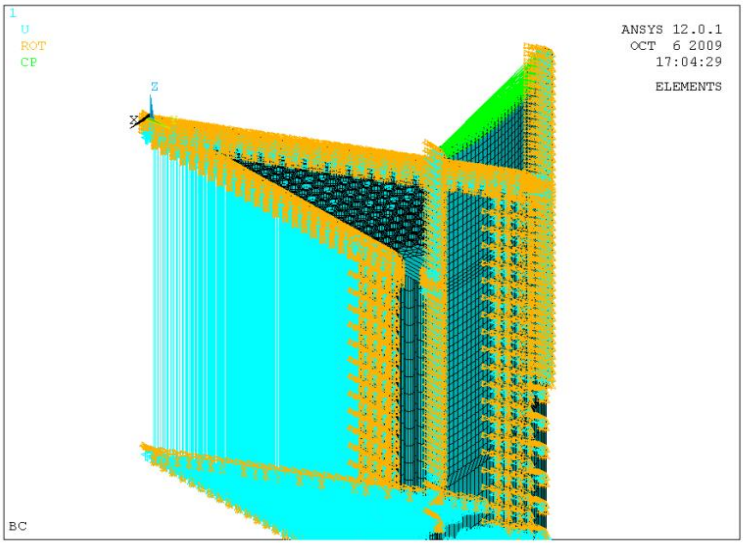

(A)

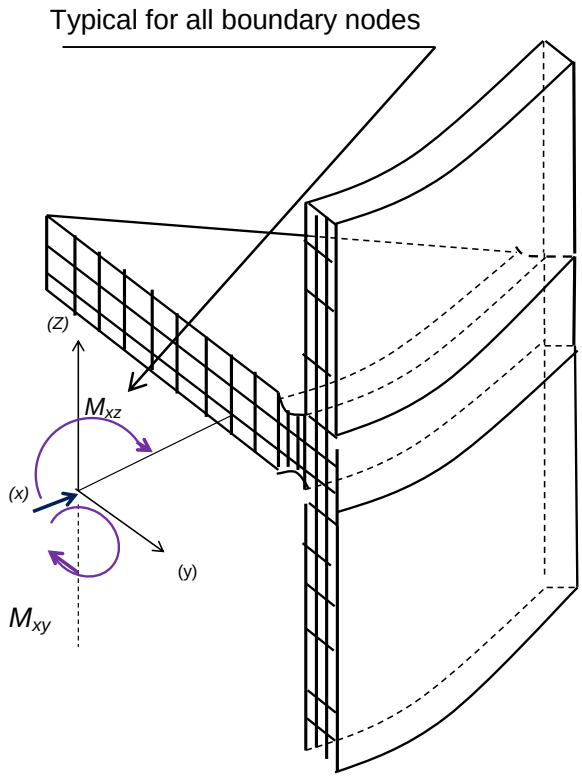

(B)

Fig(5.7): Displacement boundary condition, (A) Ansys model, (B) Schematic representation(M_{xz} is in plane bending, M_{XY} is torsion)

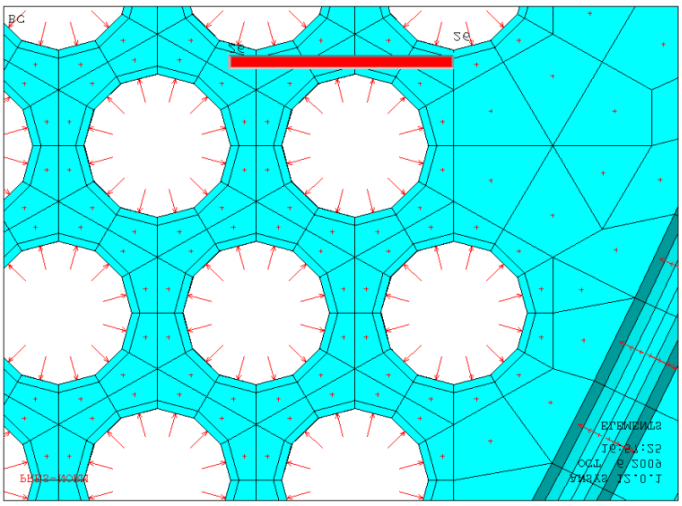

Fig (5.8): Pressure loading.

5.4 Material Model

This specific exchanger and nearly all other similar types are operated in base-load mode, with little fluctuation on the design pressure and design temperature except for full shutdowns. Based on the exchanger operating mode, bilinear isotropic, multilinear isotropic, non-linear isotropic, bilinear kinematic and multilinear kinematic rules have been used on the present investigation; these hardening rules are available in the ANSYS [18] program.

Bilinear isotropic work hardening is based on the assumption of isotropic work hardening, with one straight line representing the elastic behaviour and a second straight line representing the post-yield behaviour. Multilinear isotopic work hardening fits a multilinear approximation to the elastic-plastic stress strain curve.

Linear kinematic hardening uses the Prager [52] rule with a simple representation of the linear dependency between yield surface movement and increments of plastic strain. The multilinear hardening parameter is formulated according to the Besseling [42] model, also termed a sub- layer model, and the material response is represented by multiple layers of perfectly plastic material. Detailed explanation of these material models are presented later on in this work.

In the bilinear hardening analyses, a post-yield tangent modulus of 10% of the elastic modulus has been assumed. 10% strain hardening has previously been used in references [29], [44], [45].

The principal strains in these analyses is limited to 5% throughout; this is the limit specified by Ref [4] ; this limit on strains is much less than the rupture strains of the materials, and is adopted in here.

For material models whose solution continues to converge at the corresponding load level, the solution is terminated when 5% strain is reached. The multilinear hardening curves used in this work were derived from the true stress-strain curve procedure outlined in Annex 3.D of ASME [1].

Ref [1] additionally requires the local failure criteria to be satisfied for a component; this should be demonstrated by showing that the equivalent of principal strain is smaller than the triaxial strain. Section 5.4.1 below provides various details in regard various hardening models.

5.4.1 Material Hardening Models

Investigation and understanding of the material post yielding behaviour require constitutive models, in many of these models the plastic modulus calculation is coupled with the (kinematic) hardening rule through the yield surface consistency condition; these models are referred to as *coupled models*. In other class of models, the plastic modulus might be indirectly influenced by the hardening (kinematic) rule but its calculation is not coupled to the hardening (kinematic) rule through consistency condition, these models are referred to as *uncoupled models*.

Prager Ref.[52] proposed the first coupled model. Since that time his proposed model has been subject of continuous improvements to cover various applications and to match experimental results more closely. Models proposed by Armstrong and Frederick (1966), Chaboche (1986, 1991, 1994), Guionnet (1992), Ohno and Wang (1993) and many others belong to this class. The models proposed by Mroz (1967), Dafalias and Popov (1976), Drucker and Palgen (1981), Tseng and Lee (1983) and many others belong to the uncoupled class.

In general, the yield surface can change in shape (distortion of yield surface), size (isotropic hardening) and/or centre location (kinematic hardening) as a consequence of plastic deformation. There are mainly three common hardening rules: isotropic hardening, kinematic hardening and mixed hardening. In the following, a brief description of these rules is presented.

5.4.2 Isotropic Hardening

One of the basic hardening rules used to describe yield surface changes is isotropic hardening. The isotropic hardening rule postulates that the yield surface expands uniformly about the origin of stress space while the location of its centre remains unchanged during plastic flow. Fig (5.9) depicts this behaviour.

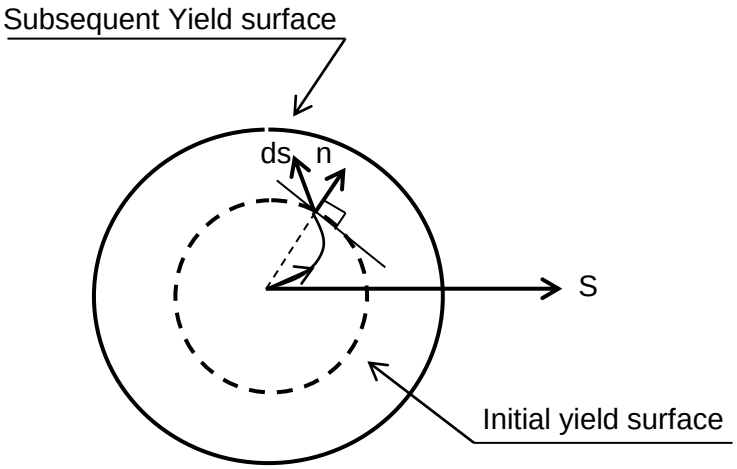

Fig (5.9): Initial and subsequent yield surfaces in isotropic hardening

The isotopic hardening model is simple to use but it applies mainly to monotonic loading without stress reversal. In this type of modelling loading surface expands uniformly (or isotropically) and remain self-similar with increasing plastic deformation and therefore cannot account for the Buschinger effect exhibited by most structural materials. Size of the yield surface depends upon plastic strain history, i.e.

$$F(\sigma_{i,j}) = K^2(\varepsilon_p) \tag{5.1}$$

For Mises, $F(\sigma_{i,j}) = J_2 = \frac{1}{2} S_{i,j} S_{i,j} = K^2(\varepsilon_p)$ (5.2)

Also, effective stress is, $\sigma_e = \sqrt{3J_2}$, then,

$$F(\sigma_{i,j}, K) = \frac{3}{2} S_{i,j} S_{i,j} - \sigma_0^2(\varepsilon_P) \tag{5.3}$$

σ_0 is material yield stress

5.4.3 Linear Kinematic Hardening Rule

The kinematic hardening rule dictates the evolution of the yield surface during a plastic loading increment by translation in stress space only, this rule was introduced by Prager (52). According to this model, the simulation of plastic response of material is linearly related with plastic strain. The equation proposed by Prager to describe the evolution of the back-stress is $\dot{\alpha}_{i,j} = c\left(\dot{\varepsilon}\right)^p_{i,j}$ **,** where **c** is a constant derived from a simple monotonic uniaxial curve and $\left(\dot{\varepsilon}\right)^p_{i,j}$ is the rate of effective plastic strain. Fig. (5.10) depicts this rule.

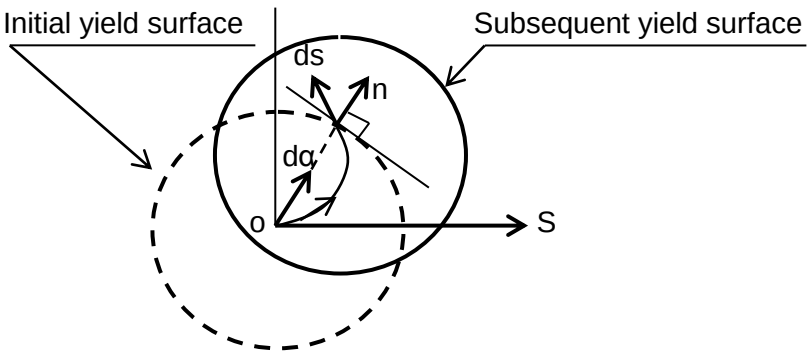

Fig (5.10): Prager- linear kinematic hardening rule

The key to a subsequent yield surface based on a kinematic hardening rule is the determination of the coordinates of the centre, $\alpha_{i,j}$, Prager rule assumes a linear dependencies of $d\alpha_{i,j}$ on $d\varepsilon_{i,j}^{P}$. It should be further noted that Prager's hardening rule is equivalent to the assumption that the vector $d\alpha_{i,j}$ moves in the direction parallel to the normal vector **n** at the current stress state on the yield surface in stress space.

5.4.4 Multilinear Kinematic Rule

Improvement to the Prager model (linear kinematic hardening) was proposed by Besseling. He derived a stress-strain relation for inelastic deformation based on a mathematical rather than physical model of the deformation process of an actual material. He assumed an element of a volume is considered to be composed of various portions, which can be represented by sub elements, all subject to the same total strain, but with different elastic limit.

In his model the uniaxial stress-strain response is represented by several linear segments, as shown in Figure (5.11), In case of uniaxial loading stress, **σ** is calculated for strain **ε,** i.e.,

$$t_1 = \frac{E - E_{T1}}{E}; t_2 = \frac{E - E_{T2}}{E}; t_3 = \frac{E - E_{T3}}{E}; t_4 = \frac{E - E_{T4}}{E}$$

This model can produce smooth shape of stress-strain response when a large number of linear segments are used; however, it fails to produce ratcheting under uniaxial loading. In case of multiaxial loading the model under predicts ratcheting. (Bari and Hassan [47]).

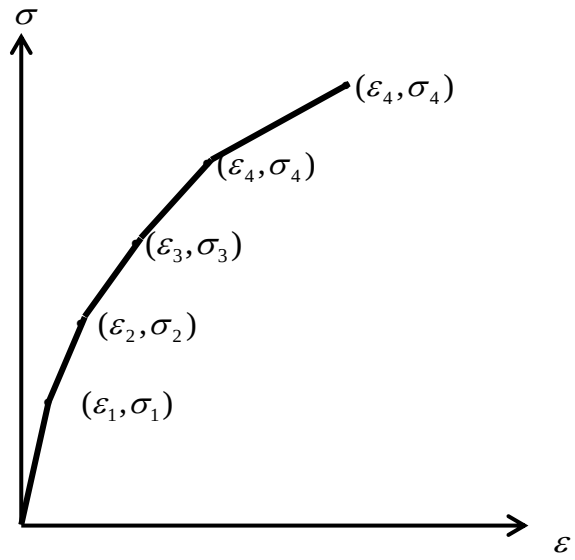

Fig (5.11): Multilinear kinematic hardening rule (Besseling)

The Mraz multisurface model is advancement to Besseling multilayer model, where each surface represents a constant work hardening modulus in the stress space. . Figure (5.12) depicts the Mraz surfaces. On the bases of Mraz's multisurface rule, a major modification has been made by replacing the nest of surfaces by two surfaces only; an inner yield surface and an outer bounding surface Ref [61,62]; Figure (5.13) depicts the idea.

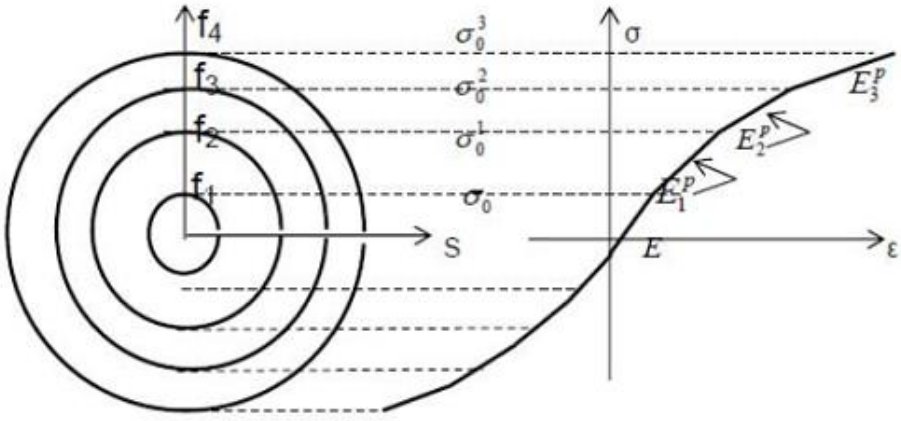

Fig (5.12): Mraz multisurface-multilinear kinematic hardening rule

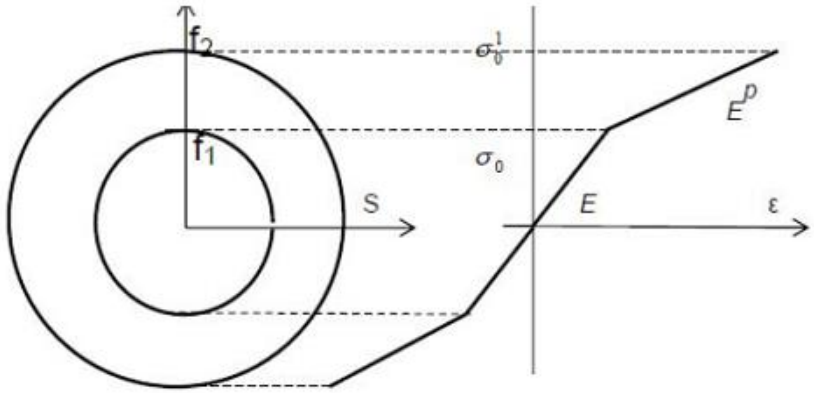

Fig (5.13): Popov Two surfaces -multilinear kinematic hardening rule

5.4.5 Non-linear Kinematic Rules

5.4.5.1 Armstrong and Frederick

Proposed by Armstrong and Frederick (1966), this model simulates the multiaxial Buschinger effect (movement of the yield surface in the stress space). Armstrong and Frederick model is based on the assumption that the most recent part of the strain history of a material dictates the mechanical behaviour. The kinematic hardening rule was purposed by following expression,

$$\dot{\alpha}_{i,j} = \frac{2}{3} C_1 (\dot{\varepsilon})^P_{i,j} - C_2 \alpha_{i,j} \dot{P} \qquad (5.4)$$

Where the first term is Prager equation and second term added by (AF), in above

$\dot{P}$ is accumulated plastic strain given by,

$$\dot{p} = \sqrt{\frac{2}{3} (\dot{\varepsilon})^P_{i,j} (\dot{\varepsilon})^P_{i,j}} \qquad (5.5)$$

The constants C_1 and C_2 are determined from uniaxial tests.

Among others, the Armstrong and Frederick (AF) hardening model has been experimentally evaluated by Hassan, T. el. Ref. [47]. He has concluded that, for uniaxial

loading, the AF rule basically provides an exponential α_x trace (Fig. 5.14a), which always starts with a modulus given by equation $H = C \mp \gamma\alpha_X$ and stabilizes to a value of $\frac{C}{\gamma}$ after traversing some amount of plastic strains.

In the above equation the negative sign is used for forward loading curve and the positive sign for reverse loading curve. Fig (5.14) extracted from Ref. [47] provides AF model's simulation of the stable hysteresis loop.

It is apparent from the figure that, experimental stress-strain curve is not necessarily exponential in nature and the attempt to simulate it by a single exponential equation does not yield a good fit. Increasing the value of C would improve the simulation during the initial nonlinear part, but simulation for the rest of the curve would suffer. Another observation that was made by Hassan was another limitation of AF model, its inability to produce constant plastic modulus exhibited by experiments for a high strain range, for which this model always stabilizes to zero plastic modulus.

Hassan additionally noted that:

(1) For a uniaxial stress cycle with mean stress, the "recall" term in the AF kinematic hardening rule produces change in shapes between forward and reverse loading paths. Therefore, the loop does not close and results in ratcheting (Fig. 5.14a).

(2) The stress-strain loop produced by this model deviates significantly from experiment and the ratcheting strain is also over predicted, as demonstrated in (Fig. 5.14b).

(3) For continued cycles between two fixed stress levels, this model simulates the same ratcheting loops for all cycles and thus, produces a constant ratcheting rate (strain accumulation per cycle) which is evident from (Fig. 5.14c).

Conceptually, the AF model has been applied in representing cyclic plasticity response of material, but is not robust enough to predict the ratcheting responses of materials.

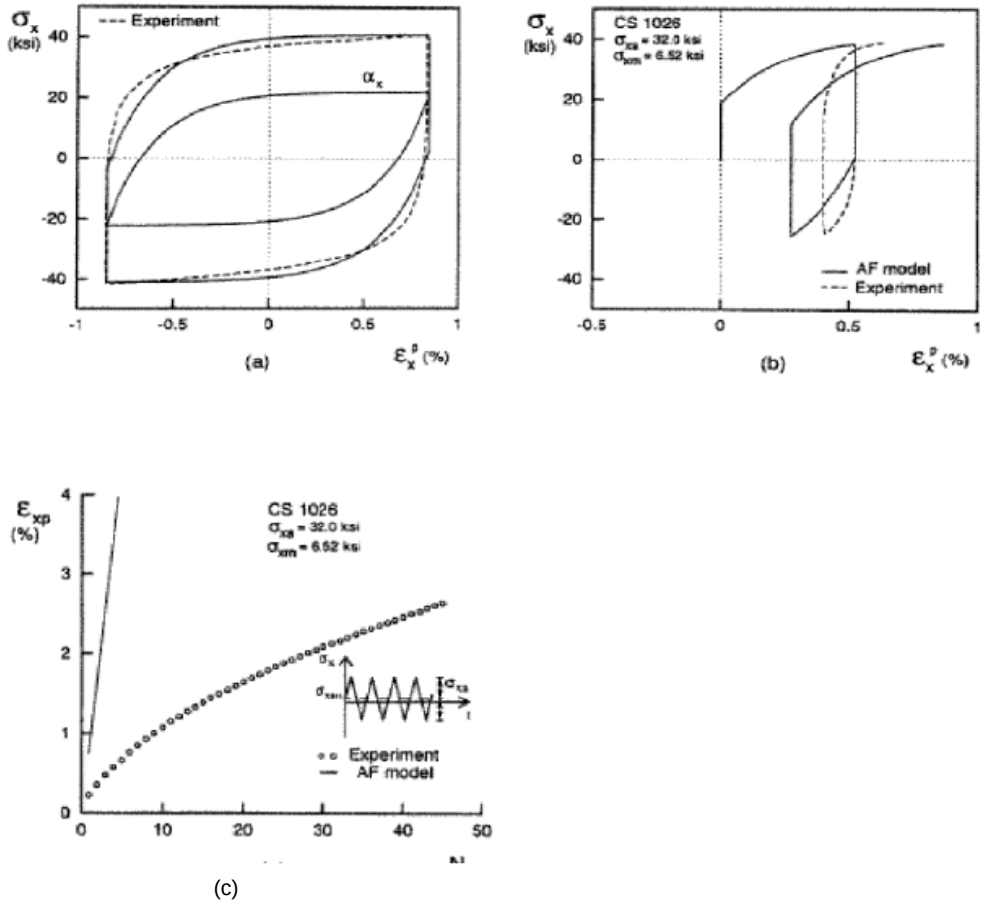

Fig (5.14): From Ref [47], predictions from Armstrong and Frederick model (AF) for (a) strain-controlled hysteresis loop, (b) stress-controlled hysteresis loop, (c) axial strain at positive stress peaks for uniaxial cycles.

5.4.5.2 Chaboche Model

Proposed by Chaboche and his co-workers (1979, 1991), this model is based on a decomposition of non-linear kinematic hardening rule proposed by Armstrong and Frederick. This decomposition is mainly significant in better describing the three critical segments of a stable hysteresis curve.

These segments are:

1. The initial modulus when yielding starts.
2. The nonlinear transition of the hysteresis curve after yielding starts until the curve become linear again.
3. The linear segment of the curve in the range of higher strain.

To improve the ratcheting prediction in the hysteresis loop, Chaboche.et al. (1979), initially proposed three decompositions of the kinematic hardening rule, corresponding to the above three segments of the hysteresis curve. Using this decomposition, the ratcheting prediction improved as compared to the (**AF**) model. It was some time later that it was found purposed model tends to greatly over-predict ratcheting in the case of normal monotonic and reverse cyclic condition. To overcome these pitfalls, Chaboche (1991) introduced a fourth decomposition of the kinematic hardening rule based on a threshold. This fourth rule simulates a constant linear hardening with in a threshold value and becomes nonlinear beyond this value. With the use of this fourth decomposition, the over-prediction of ratcheting is reduced and there is an improvement in the hysteresis curve. This is because, within the threshold, the recall term is ignored and linear hardening occurs as it did without the fourth rule. Beyond the threshold the recall term makes the hardening non-linear again and reduces the ratcheting at a higher rate to avoid over-prediction. Chaboche model was not used in this work because sufficient material data was not available.

5.5 Critical Locations

High stress/ strain zones (critical locations) in the above model have been subject of extensive study, Ref. (37). It has been shown that the junction of tubesheet to shell at the groove location is the most critical section of the model. The elastic analysis of the tubesheet has revealed the fact that nodes 67831, 17951, 4381 and 67925 are among highest stressed nodes and therefore information extracted from theses nodes have been used on the subsequent sections of this work, Figures below shows these nodal locations. It should be further noted that, above nodes (and other similar ones) are located at the junction of the channel side shell to the tube sheet and at the connections

of outer row of tubes to the tube sheet. These nodes are located on the regions with largest bending. Tube sheet bends as a result of the response of the upper shell to the action of tube side pressure. Outer rows of the tubes, following tube sheet movement, are also exposed to the large bending.

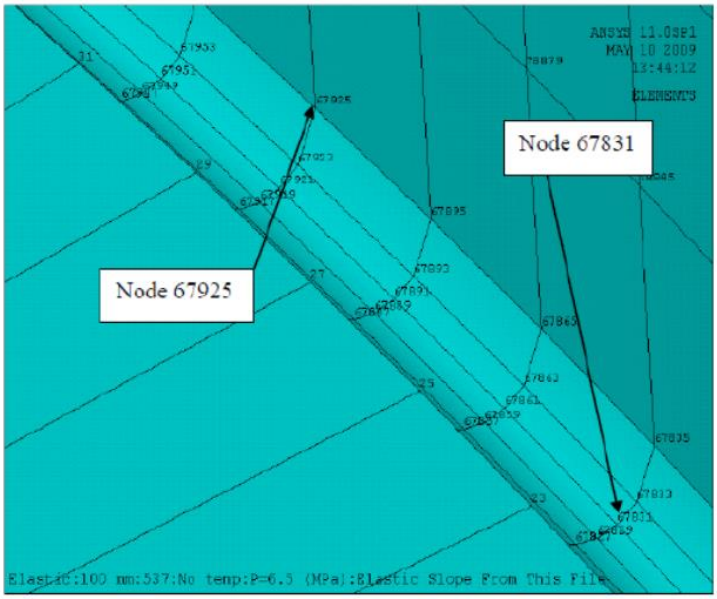

Fig (5.15): Location of nodes 67831 and 67925 (tubesheet to shell junctions)

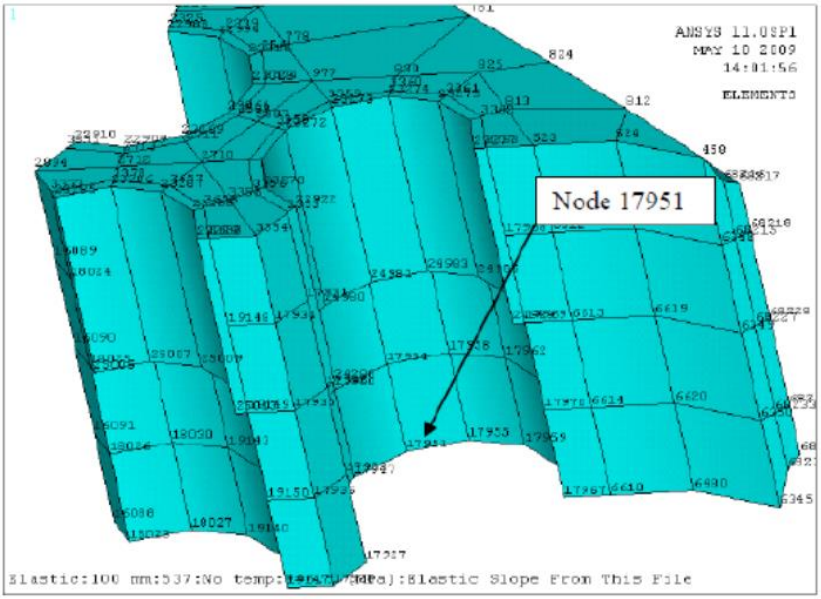

Fig (5.16): Location of nodes 17951 (bottom of tubesheet)

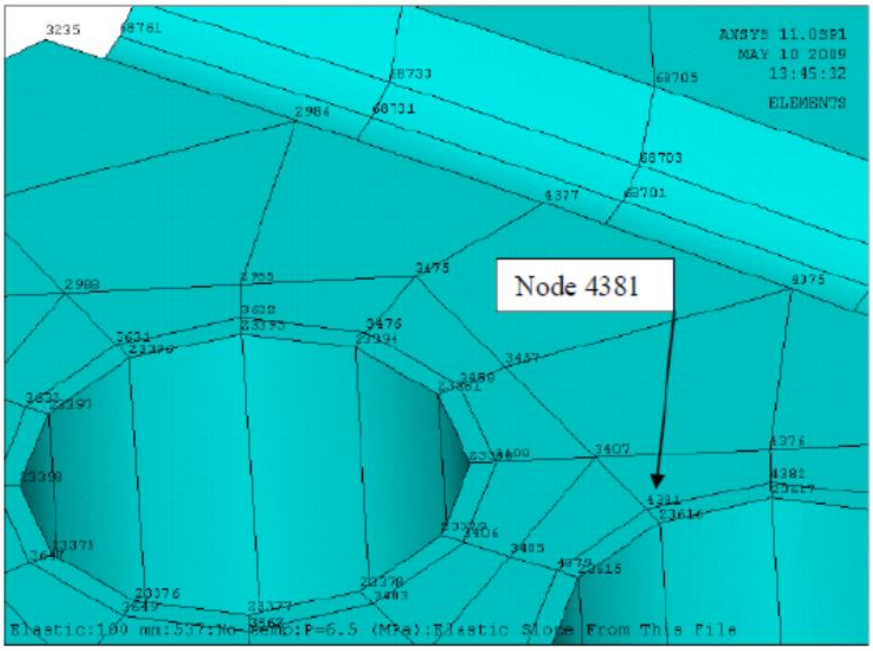

Fig (5.17): Location of nodes 4381 (tubesheet)

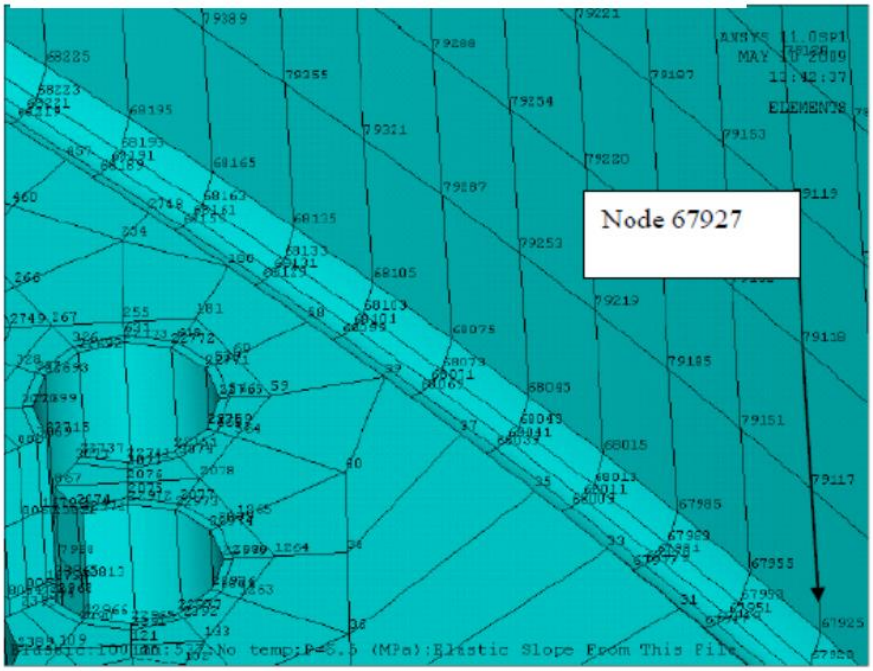

Fig (5.18): Location of nodes 67925 (junction of tubesheet with channel side shell)

5.6 Summary

The heat exchanger FEA model has been carried out through usage of existing symmetry on the geometry and on the loads. It has been discussed that the zones located between intersections of the channel side shell and the tube sheet and, the zone between tube sheet and the last outer rows of the tubes are among the highest stress parts. To further investigate the details associated with this work, nodes with highest stress values have been identified in these zones.

6. Static Ductile Failure

This chapter investigates application of the Plastic Work Curvature, PWC, and method to determine the plastic load of the tubesheet structure. This is the first investigation of the PWC method for a stiff structure of such complexity. The 3D fixed tubesheet exchanger model consists of a perforated tubesheet, tubes, channel side shell and tube side shell. This creates intersecting geometries with complex stress distributions, resulting in highly varying membrane and bending stress distributions and high local stress concentrations.

The applied loading is internal pressure including the effect of the closed head. The action of pressure on the head brings the shell on the shell-side of the heat exchanger under uniform tension. This load is transferred to the lower intersecting geometry, i.e., the junction zone.

Conservatism requires investigation of a load case which considers the effect of the pressure on the channel side once there is no pressure on the shell side (shell side pressure is 1 MPa); this load case covers the largest possible pressure difference. Moreover, under temperature load case, since the difference between the tube side and shell side temperature is not considerable no expansion joint on the shell side shell is required. Exchanger data sheet reflect this point.

The tubesheet to shell intersection zone is additionally restrained by the action of a bending load imposed to the section as a result of the bending of channel side shell. This combined loading effect is localized since it occurs only at the intersection of tubesheet to shell. The plastic work associated with this zone is large enough to dominate the global plastic work with a large proportion of structure remaining elastic during entire loading history.

The investigation also includes the effect of temperature dependent yield stress on the formation of the plastic failure mechanism, which has not been investigated in previous applications of the PWC. Small and large deformation theories are investigated through various hardening models. The material models considered (described in Chapter 5) are bilinear and multilinear kinematic hardening, bilinear and multilinear isotropic hardening and the first application of the PWC to a non-linear isotropic hardening material model.

The development of the plastic load mechanism is investigated through application of four types of analysis:

1. Linear elastic analysis, which determines the location of the first yield and other high stress regions of the heat exchanger.
2. Limit load analysis (elastic-perfectly plastic material model and small deformation theory) to identify the exchanger limit load.
3. Instability analysis through elastic-perfectly plastic material model and large deformation mechanism to identify instability load (this load is not buckling load).
4. Elastic-Plastic analysis through various hardening models and by considering large and small deformation mechanism. The plastic load is calculated using three methods:
    a. PWC
    b. Twice Elastic Slope TES method
    c. Tangent Intersection TI method

Graphs and details provided in subsequent sections of this chapter have been prepared based on ANSYS outputs for 4 nodes located at high stress regions; location of theses nodes and their significance are depicted in the Figures (5.15-18) and are explained in section 5.5.

6.1 Small Deformation Analysis

Linear elastic analysis of the heat exchanger model was carried out to observe the high stress regions of the exchanger, calculations were performed at load of 11.7 MPa. Figure (6.1) shows the Von Mises elastic stress distribution in the most highly stressed locations.

Exchanger limit load is 11.7 MPa, this is the load associated with the last converged solution. Figures (6.2) and (6.3) show the Mises stress and Mises strain distribution in the exchanger at limit load.

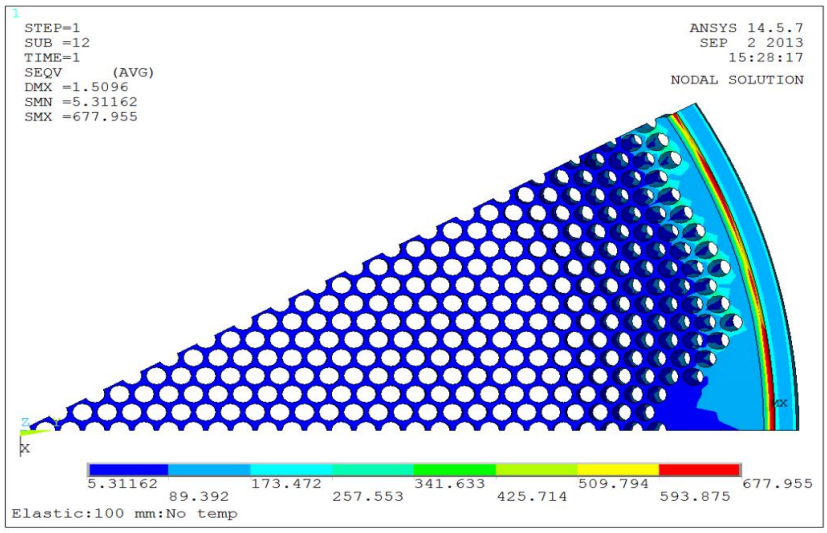

Fig (6.1): Elastic Analysis, Mises equivalent of stresses at P= 11.769 MPa, no temp.

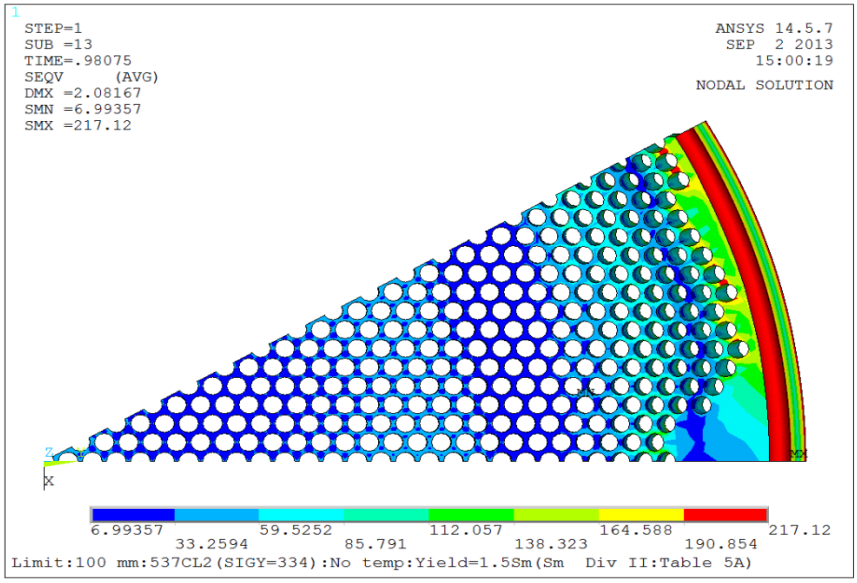

Fig (6.2): Limit Analysis, $\sigma_{(Mises)eq}$ at P= 11.7 MPa, no temp., $\sigma_{(yield)}$= 217 MPa

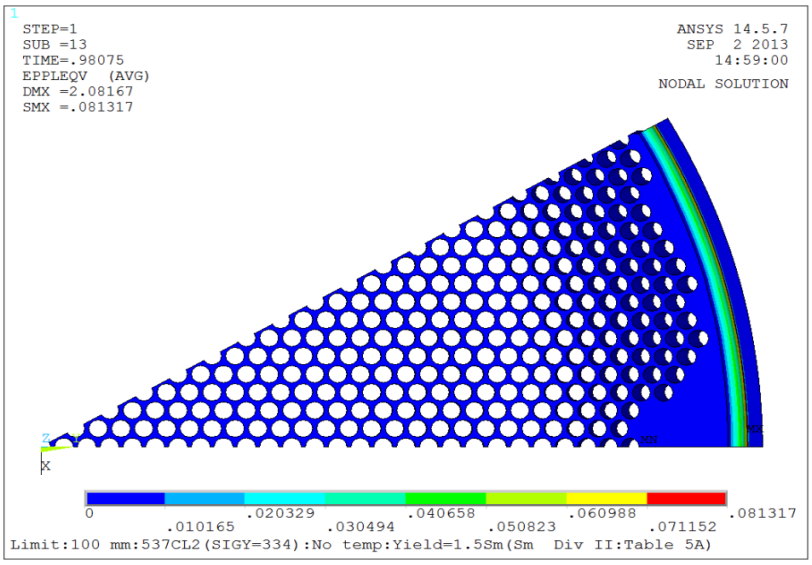

Fig (6.3): Limit Analysis, $\varepsilon_{(Mises)eq}$ at P= 11.7 MPa, no temp, $\sigma_{(yield)}$= 217 MPa

6.1.1 Linear Isotropic Hardening

The load-plastic work plot for small deformation linear isotropic material analysis is shown in Figure (6.4). Immediately post yield, the plastic deformation is highly localized, as shown in Figure (6.5), and the load-plastic work curve correspondingly exhibits a steep slope. However, as the load increases the plastic deformation becomes more extensive and increasingly higher increments of plastic work occur for similar load increments.

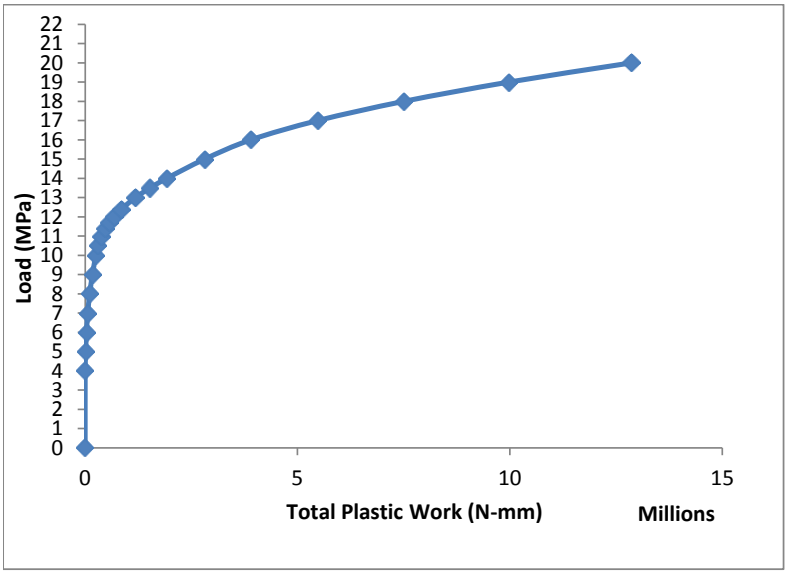

Fig (6.4): Load- total plastic work diagram for small deformation theory,linear isotropic hardening: E_t=0.1E

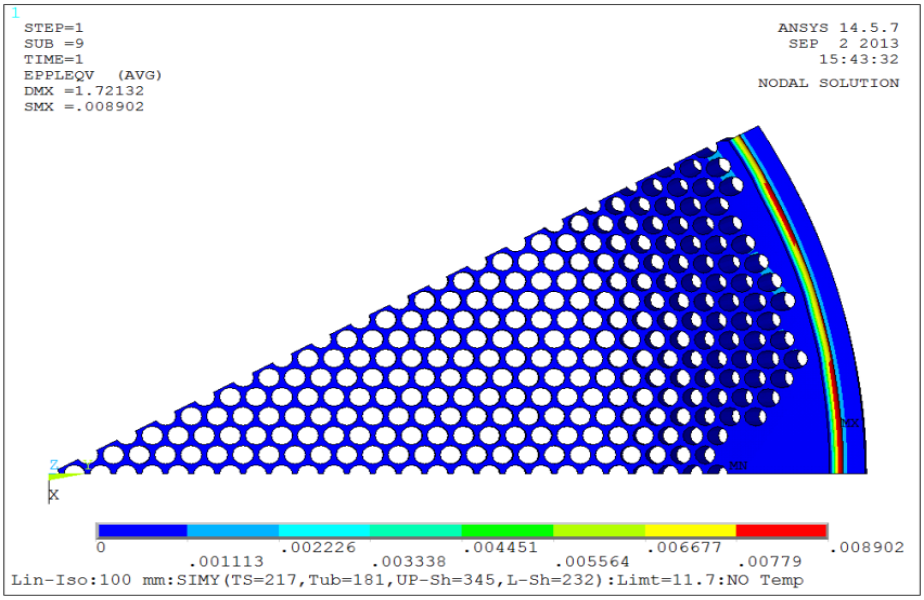

Fig (6.5): Linear Isotropic, $\varepsilon_{(Mises)eq}$ at P_{limit}= 11.7 MPa, no temp, $\sigma_{(1\text{-}yield)}$= 217 MPa

At higher load levels, the slope of the load-plastic work plot tends towards a constant slope. This indicates that a ductile failure mechanism has formed in which the plastic dissipation is mostly localized in distinct regions of the structure, in the manner of plastic hinge formation. Ductile failure occurs by a through thickness plastic deformation mechanism, as shown in Figure (6.6). However the load-plastic work plot does not exhibit a distinct feature that can be clearly identified with the state of plastic collapse (or gross plastic deformation).

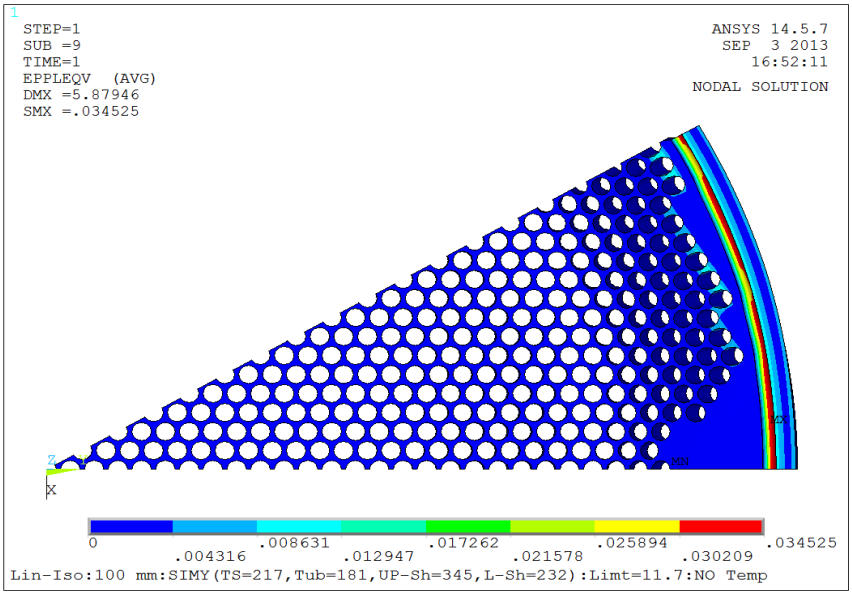

Fig (6.6): Linear Isotropic, $\varepsilon_{(Mises)eq}$ at P_{limit}=20 MPa, no temp, $\sigma_{(1\text{-}yield)}$= 217 MPa

The TES and TI criteria define the plastic load with reference to a specific local displacement (or strain) parameter at a specific location in the vessel. Here, four of the most highly loaded points in the vessel as shown in Figures (5.15-18) are considered. Node 67831 is located in the groove between the tubesheet and channel side shell, Node 67925 is located at the junction between the groove and the shell, Node 17951 is at the bottom surface of the most highly stressed outer tube sheet hole and Node 4381 is at the top side of the same hole.

Figure (6.7) shows TES and TI constructions for groove Node 67831, in this figure and in all other subsequent load-deformation plots the load is pressure and deformation is total

displacement. The characteristic load-deformation curve exhibits the expected linear response up to the load at which first yield occurs 11.7 MPa.

The steep load-deformation curve indicates that the structure is relatively stiff. This is due to the geometry of the welded junction between the tube sheet and shells plus the additional stiffening due to the staying action of the tubes at the vicinity of the junction. The displacement magnitude is relatively small even at high load levels. This type of behavior is associated with the high local strain (the 5% EN13445 Code defined strain limit was observed at load of 20 MPa). The small deformation theory linear isotropic material model solution will continue to converge regardless of the magnitude of the strain/loading.

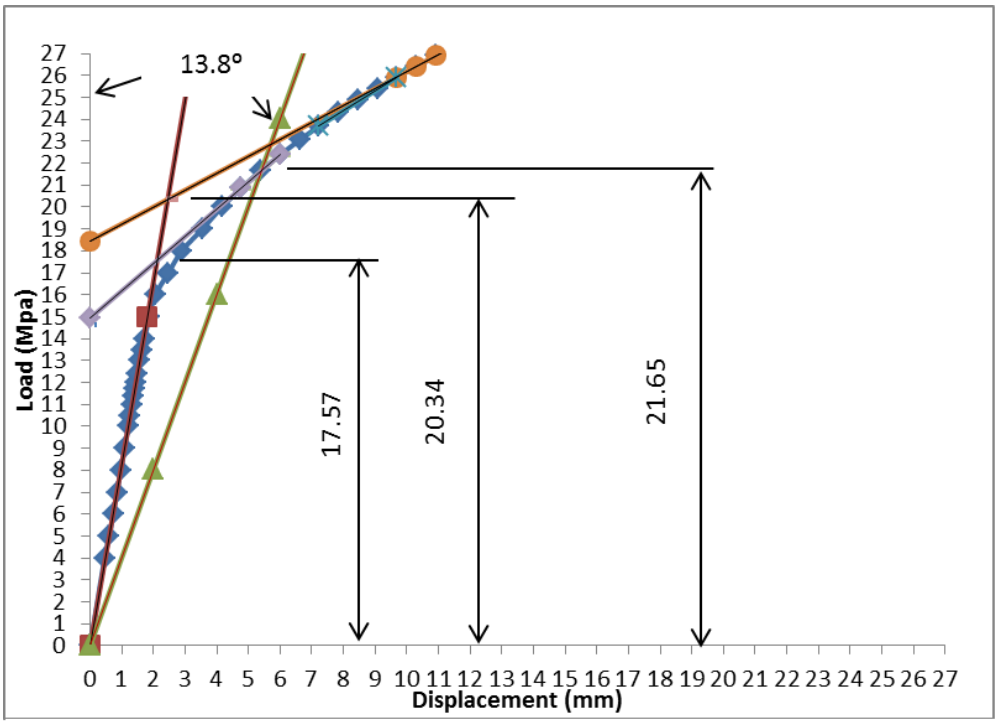

Fig (6.7): Groove Node 67831 deformation parameter TI and TES construction for small deformation theory, linear isotropic hardening: Et=0.1E.

Immediately post yield, the curve maintains the initial linear form due to the highly localized nature of the plastic deformation region: the structural response is dominated by the mainly elastic deformation of the vessel. However, as load continues to increase

the effect of the plastic deformation becomes more evident and the load-deformation curve becomes non-linear.

For twice elastic slope method, intersection of a line having a slope equal to twice of elastic slope (elastic slope is 7°, slope of intersecting line is 13.79°) with the load deformation diagram shows the load of 21.65 MPa, by definition this is the plastic load.

The TES graphical construction shown in Figure (6.7) clearly defines the plastic load for this *criterion of plastic collapse*. However, the plastic load evaluated by the TI criterion is subjective. The TI construction requires a tangent to be drawn from the high plastic deformation part of the curve (after its knee region) to the load axis. At high load levels the characteristic load-deformation plot tends towards a constant slope but it is not truly constant. This requires the designer to subjectively select the location on the curve from which the tangent is drawn. The construction shown in Figure (6.7) identifies two possible tangent lines that may be viewed as bounds on the actual tangent. Thus two different values for plastic load are identified, i.e., 17.57 and 20.34 MPa. Additional tangents can also be drawn between these bounds.

Figure (6.8) shows TES and TI constructions for the displacement parameter located at the junction between the groove and the shell, Node 67925. The characteristic load-deformation curve is similar to that for the near-by groove Node 67831displacement parameter; however there are numerical differences in the calculated TES and TI plastic loads. The TES plastic load is 21.2 MPa, compared to 21.65 MPa for the groove displacement parameter. The subjective TI plastic load bounds lay between 15.2 MPa and 17.4 MPa, compared to 17.57 MPa and 20.34 MPa for the groove location. This shows that the calculated plastic load is highly sensitive to the selected deformation parameter location.

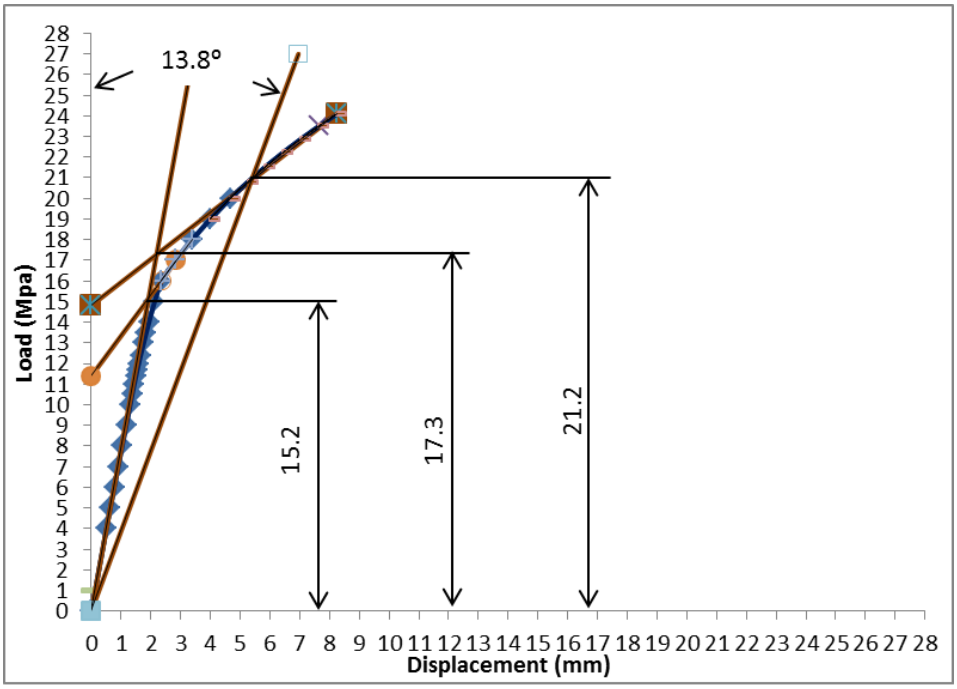

Fig (6.8): Groove-shell junction Node 67925 deformation parameter TI and TES constructions for small deformation theory, linear isotropic hardening: E_t =0.1E.

The TES and TI constructions for the displacement parameters located at the bottom and top of the highly stressed tube sheet hole, Nodes 17951 and 4381 respectively, are shown in Figure (6.9) and Figure (6.10). The characteristic load deformation curves are similar to those evaluated in the groove/junction region but the numerical values for plastic load are different between all four locations. These results demonstrate the dependence of both the TES and TI criteria on the selection of deformation parameter.

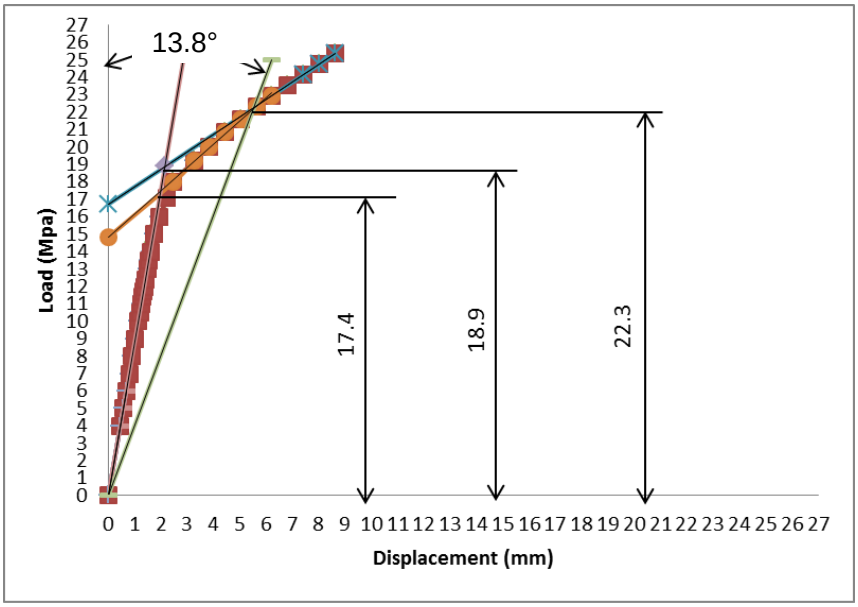

Fig (6.9): Outer-row hole bottom surface Node 17951 deformation parameter TI and TES constructions for small deformation theory, linear isotropic hardening: E_t=0.1E.

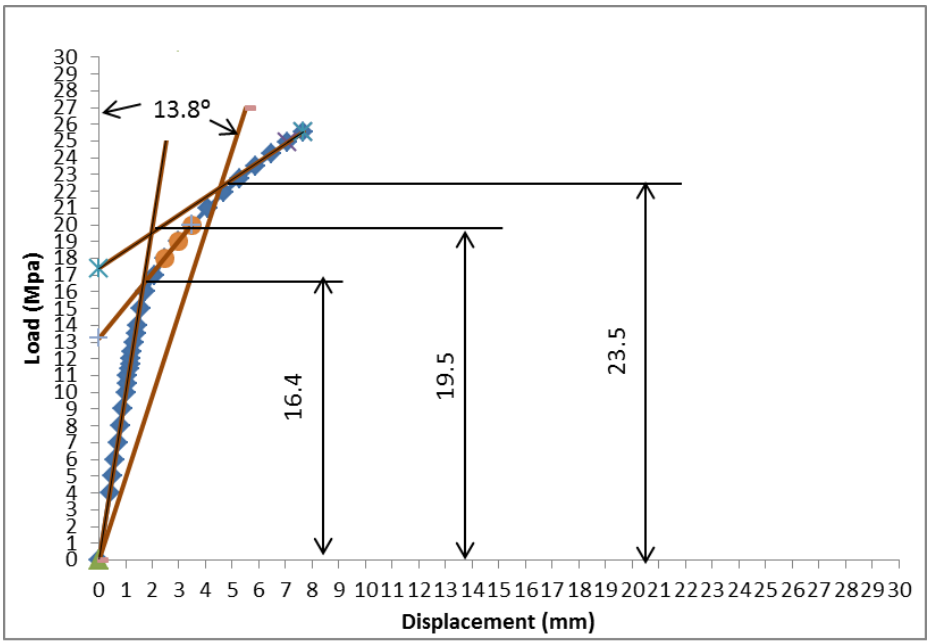

Fig (6.10): Outer-row hole top surface Node 4381 deformation parameter TI and TES constructions for small deformation theory, linear isotropic hardening: E_t=0.1E

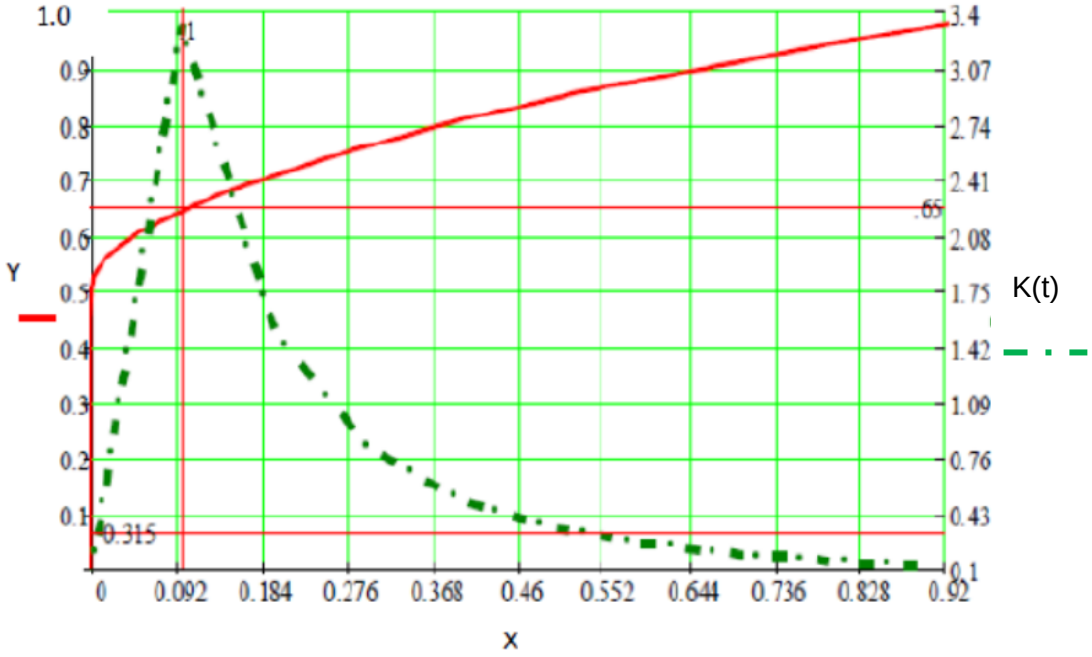

Fig (6.11): Global load-plastic work and load-plastic work curvature plots for small deformation theory, linear isotropic hardening (E_t=0.1E). X=normalized plastic work, Y=normalized load and K(t)=curvature.

The load-plastic work plot for small deformation linear isotropic analysis of Figure 6.4 is shown in normalized form as the red curve in Figure 6.11. The x-axis, X, is the plastic work normalised with respect to max plastic work. The right hand y-axis, Y, is the load normalised with respect to max pressure. The slope of the load-plastic work curve characterizes the rate of change of plastic deformation in the structure as the applied load is increased. The rate of change of slope, and the associated curvature, characterizes how rapidly the degree of plastic deformation is changing with increasing load. This is directly related to the degree of post yield elastic-plastic stress redistribution in the structure. The curvature of the load-plastic work curve with increasing plastic dissipation is shown as a second curve in green, with curvature value K(t) on the right hand y-axis.

In the elastic region the curvature is zero. When first yield occurs in the highly stressed junction region of the heat exchanger, plastic stress redistribution begins and the slope of the load-plastic work curve is non-linear. As the load increases, the plastic zone grows

through elastic-plastic stress redistribution. This corresponds to an increase in curvature as the plastic deformation mechanism develops. The maximum stress redistribution occurs at the load corresponding to the maximum curvature. At this stage plastic deformation within the plastic zones of the hinge-type failure mechanism begins to dominate the structural response. Thereafter, the curvature and associated rate of stress redistribution begins to decrease until the gross plastic deformation mechanism is fully formed, after which the stress distribution becomes almost constant with increasing load and the curvature tends towards zero. By this stage, the structure has reached a state of gross plastic deformation and the corresponding load is designated the plastic load. In general, some redistribution occurs even at very high load levels and a state of zero curvature is not achieved. In the PWC, the plastic load is defined as the load corresponding to 10% of the maximum curvature.

In the small deformation theory, linear isotropic hardening analysis, Figure 6.6, the maximum value of curvature occurs shortly after first yield. The maximum curvature value of 3.35 occurs at normalised plastic work value 0.092. The normalised load corresponding to this degree of plastic work from the load-plastic work curve is 0.65, which in turn corresponds to an applied load of 12.8 MPa. The curvature thereafter decreases with increasing load and reaches 10% of the maximum value at normalised plastic work value 0.552. The normalised load corresponding to this degree of plastic work from the load-plastic work curve is 0.87 (approx), which in turn corresponds to an applied load of 17.1 MPa .

Table 6.2 summarised the plastic pressures calculated on the basis of the four different deformation parameters (nodal displacement) investigated. Conservatism required that the deformation parameter giving the lowest plastic pressure must be used in design. Table 6.1 summarises the plastic load evaluated by limit analysis and the TI, TES and PWC criteria.

Table (6.1): TI and TES values for plastic pressure for the four deformation parameters considered.

Criterion	Plastic Pressure (MPa)			
	Displacement parameter location			
	Groove Node 67831	**Groove-shell junction** Node 67925	**Hole bottom surface** Node 17951	**Hole top surface** Node 4381
TI	17.5 to 20.3	15.2 to 17.3	17.4 to 18.9	16.4 to 19.5
TES	21.65	21.2	22.3	23.5

Table (6.2): Small deformation theory, linear isotropic hardening (E_t=0.1E) plastic loads.

Criterion	Plastic Pressure (MPa)
Limit Analysis	11.8
TI	15.2
TES	21.2
PWC (10% max)	17.1

6.1.2 Multilinear isotropic hardening

This material option uses multilinear curve instead of a bilinear curve**,** Figures (6.12) to (6.14) give plots related to the Load- Plastic Work and Load-Deformation mechanism under multilinear isotropic material model for nodes 67831 and 67925. Plots related to nodes 1795 and 4381 are omitted as they show similar behaviour with some numerical differences. Plot of Load- Curvature of plastic work is given in figure (6.15). Table (6.3, 4) summarizes the plastic loads at various locations.

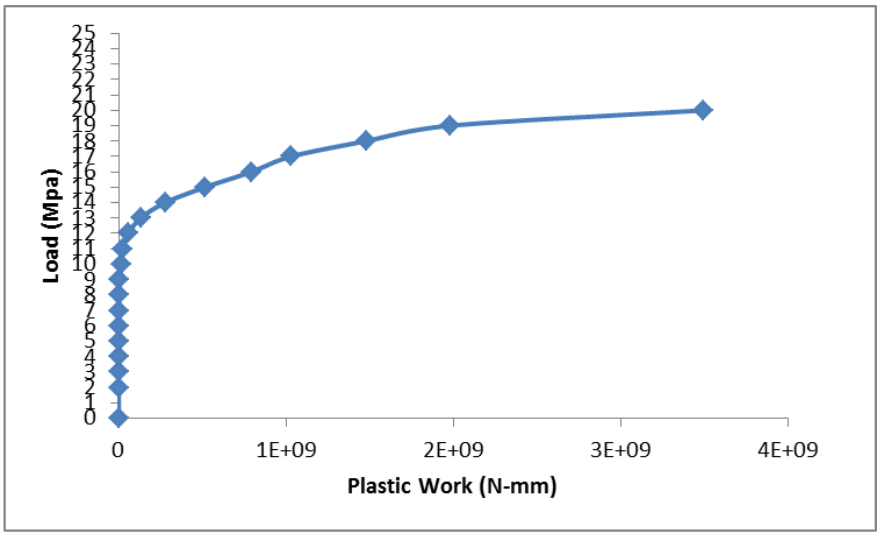

Fig (6.12): Load-total plastic work diagram for small deformation theory and multiliner isotropic hardening:

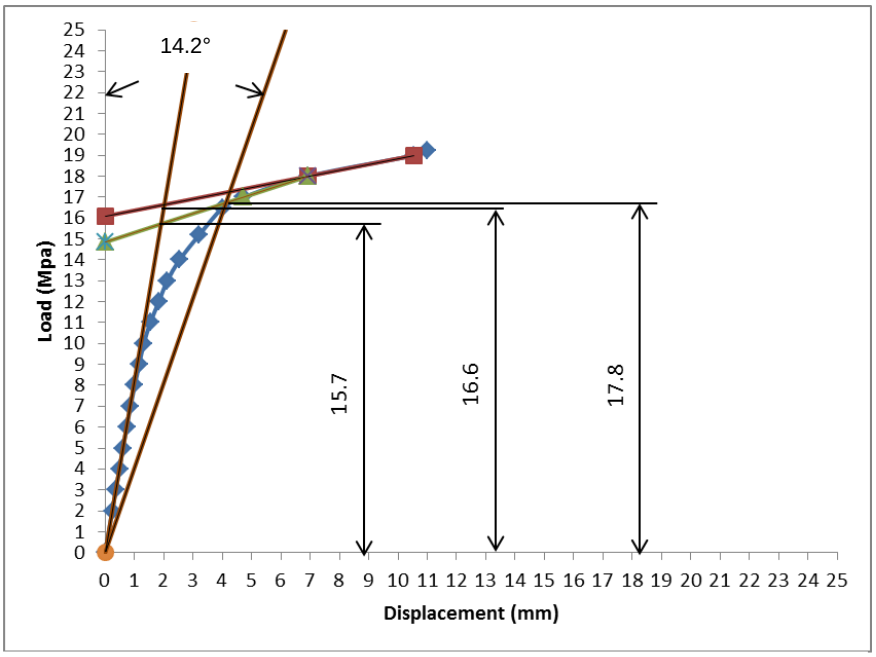

Fig (6.13): Groove Node 67831 deformation parameter TI and TES constructions for small deformation theory, multilinear linear isotropic hardening: E_t =0.1E.

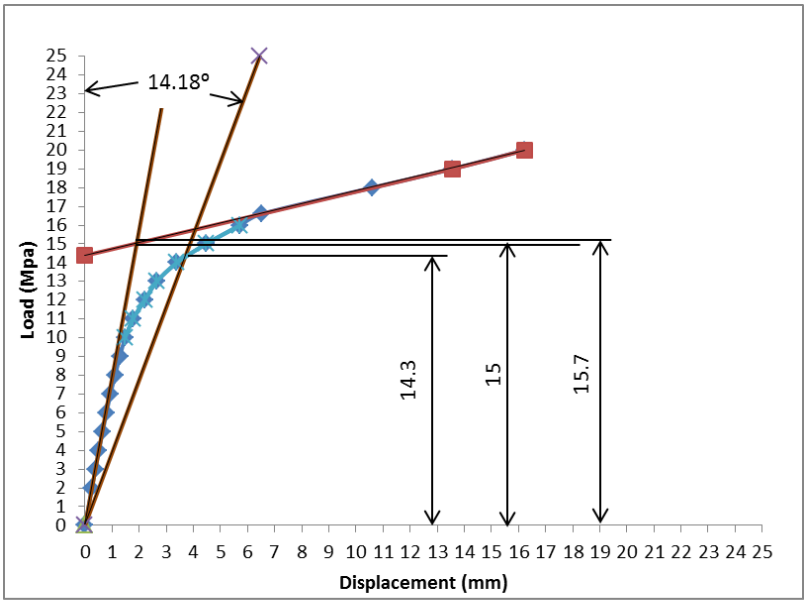

Fig (6.14): Groove- shell junction Node 67925 deformation parameter TI and TES construction for small deformation theory, multilinear isotropic hardening.

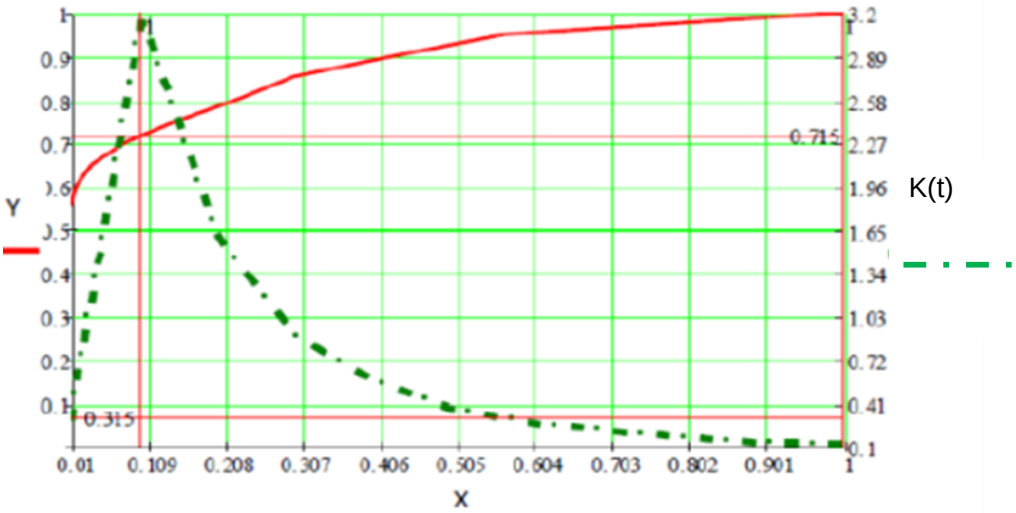

Fig (6.15): Global load-plastic work and load-plastic work curvature plots for small deformation theory, multilinear isotropic hardening. X= normalized plastic work, Y= normalized load and K(t)= curvature.

Table (6.3):TI and TES values for plastic pressure for the four deformation parameters considered.

Criterion	**Plastic Pressure (MPa)**			
	Displacement parameter location			
	Groove Node 67831	**Groove-shell junction** Node 67925	**Hole bottom surface** Node 17951	**Hole top surface** Node 4381
TI	15.7 to 16.6	15.7 to 15	15.38 to 15.46	15.6 to 15.3
TES	17.8	14.3	16.3	15.2

Table 6.4 summarises the plastic load evaluated by limit analysis and the TI, TES and PWC criteria.

Table (6.4): Small deformation theory, multilinear isotropic hardening plastic load

Criterion	Plastic Pressure (MPa)
Limit Analysis	11.8
TI	15
TES	14.3
PWC (10% max)	17.6

Load plastic work diagram for multilinear isotropic case as it is shown in Figure (6.12) indicates relatively the same type of structural behaviour in comparison with the same plot for the case of linear isotropic hardening, however, following observation can be noted:

- After first yield the slope of the curve remain unchanged for a few larger successive loads, this was also observed for the case of linear isotropic; however, the longer trend can be noted for this case. Constant slope post first yield point means that

structural response to load increase remains largely elastic and that localized yielding has a minor effect, this is as a result of stress redistribution mechanism.

- At a load larger than first yield load the relation between load and plastic work become highly nonlinear, this is related to the formation of gross plastic deformation mechanism. The knee portion of the curve manifest occurrence of this mechanism and that a local plastic hinge is formed. The degree of non-linearity between load and plastic work is higher than the case of linear isotropic; this can be observed by comparing the shape of the knee portion of the relevant curves.
- Immediately after knee portion, the curve changes its characteristic by possessing a constant slope. This change revals the fact that the structure is experiencing gross structural deformation and ductile failure mechanism is in place, actual failure occurs on somewhat larger load. Loss of equilibrium can mathematically be observed by noting that the solution does not converge.
- Details related to the above behaviour can easily be observed in the curvature plot as curvature is the measure of change of slope; in this case it identifies how fast the mechanism of gross plastic deformation is occurring.

In regards to load associated with TI method it should be noted that since load deformation diagram of multilinear isotropic case shows smoother gradient in comparison to linear isotropic case a better possibility of drawing tangent to the post yielding portion of the curve can be obtained. Still it is difficult to draw a single tangent however difference between tangents are much smaller.

The Twice Elastic Slope method (TES) also produces different plastic load values for different nodes, this is so as the method has high dependency to the shape of the load deformation plots. The Plastic load calculated according to TES method for node 67925 is close to the value of the plastic load calculated according to the curvature method.

The Plastic Work Curvature method, being mathematical rather than graphical, produces a single plastic load value for structure. This is a unique feature of the method as it relies on total plastic work done on the structure rather than local deformation parameter.

6.1.3 Bilinear Kinematic Hardening

This material option uses a linear kinematic curve**.** Figures (6.16) to (6.18) give plots related to the Load- Plastic Work and Load-Deformation mechanism under this material model. A plot of the Load- Curvature of plastic work is given in figure (6.19). Table (6.5, 6) summarizes the plastic loads at various locations.

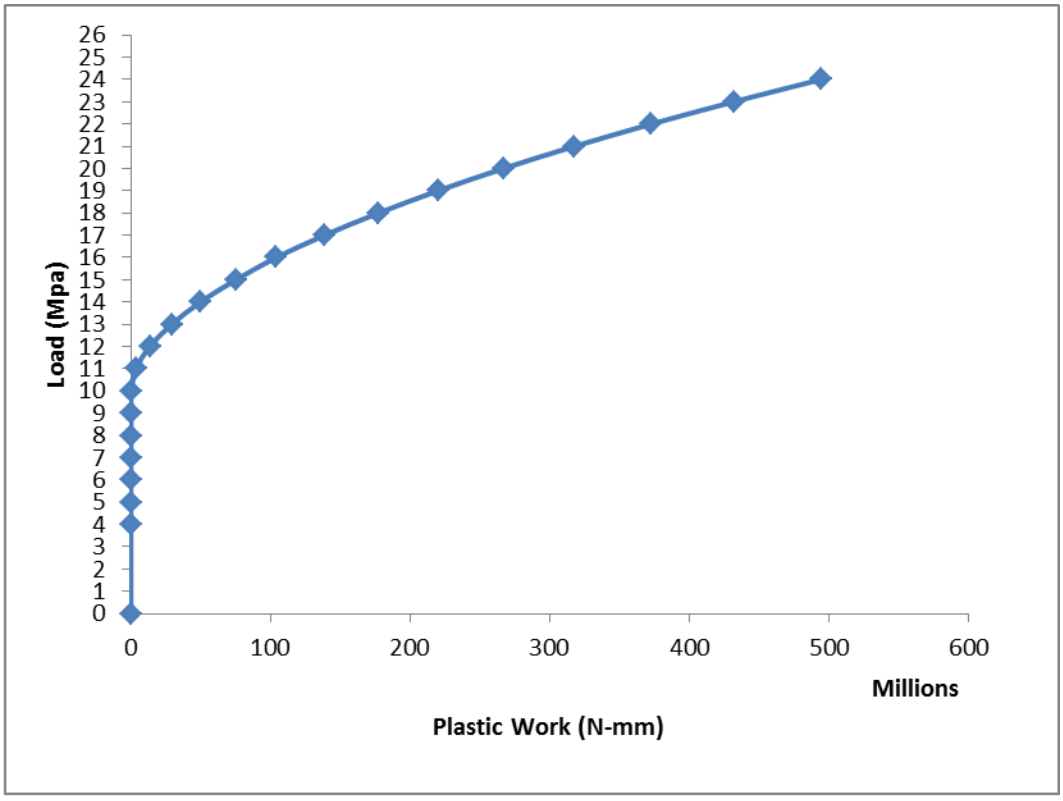

Fig (6.16): Load-total plastic work diagram for small deformation theory and linear kinematic hardening: E_t=0.1E.

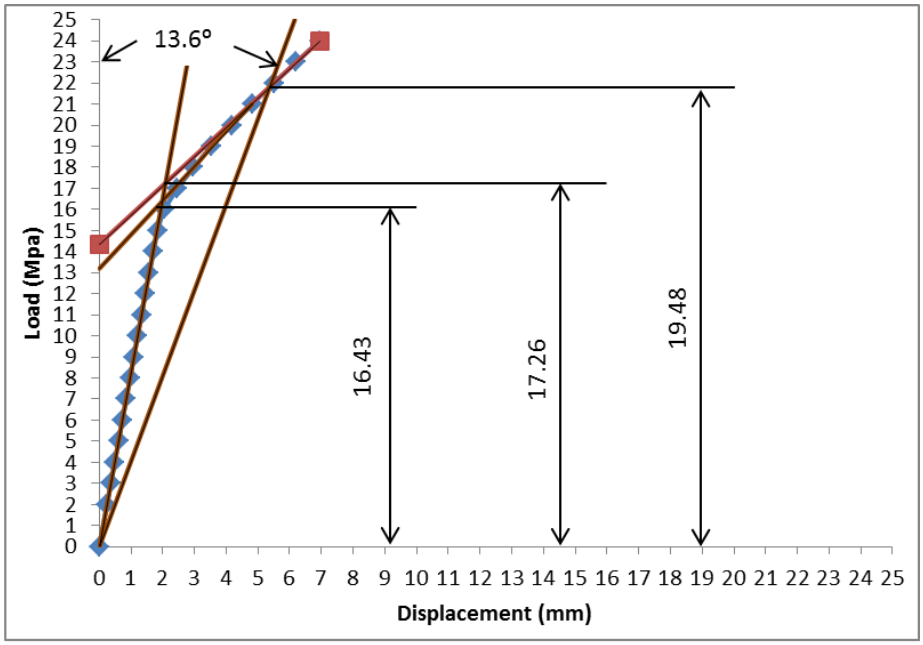

Fig (6.17): Groove Node 67831 deformation parameter TI and TES constructions for small deformation theory, linear kinematic hardening: E_t =0.1E.

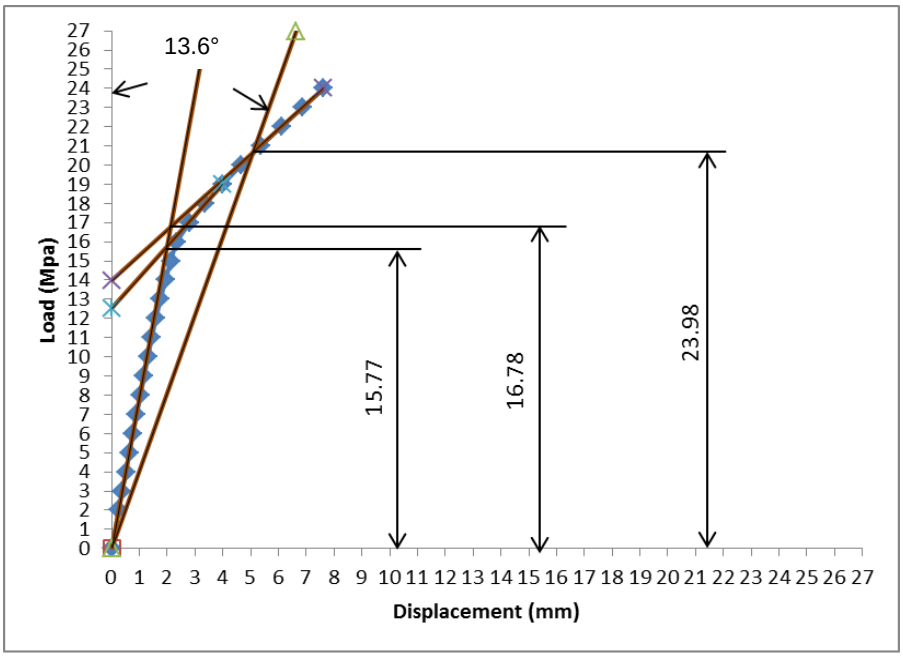

Fig (6.18): Groove Node 67925 deformation parameter TI and TES constructions for small deformation theory, linear kinematic hardening: E_t =0.1E.

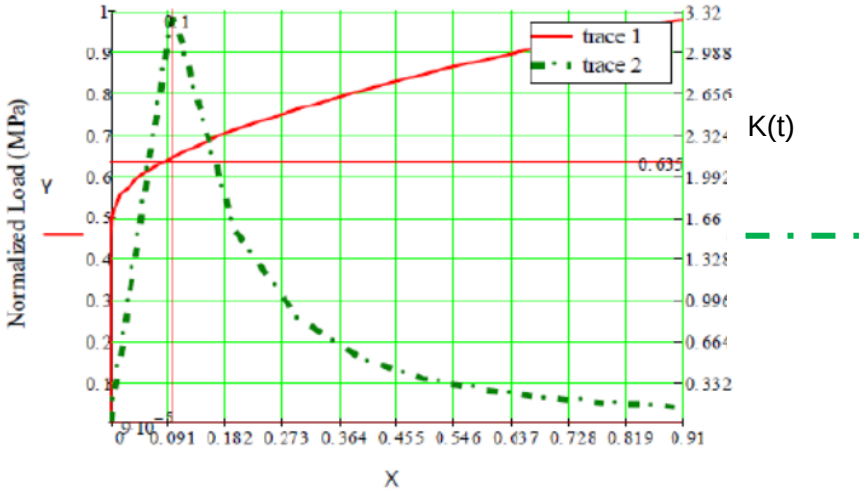

Fig (6.19): Global load-plastic work and load-plastic work curvature plots for small deformation theory, linear kinematic hardening (Et=0.1E). X=normalized plastic work, Y=normalized load and K(t)=curvature.

Table (6.5): TI and TES values for plastic pressure for the four deformation parameters considered.

Criterion	**Plastic Pressure (MPa)**			
	Displacement parameter location			
	Groove Node 67831	**Groove-shell junction** Node 67925	**Hole bottom surface** Node 17951	**Hole top surface** Node 4381
TI	16.4 to 17.2	15.7 to 16.7	16.2 to17.4	16.3 to 17.2
TES	19.48	23.98	28.14	22.6

Table (6.6) summarises the plastic load evaluated by limit analysis and the TI, TES and PWC criteria.

Table (6.6): Small deformation theory, linear kinematic hardening (E_t=0.1E) plastic load

Criterion	Plastic Pressure (MPa)
Limit Analysis	11.8
TI	15.7
TES	19.48
PWC (10% max)	17

For this material model, the rise in the load-deformation diagram is similar to linear isotropic hardening, this is so as this model also converges continuously regardless of the load magnitude. For this reason, it is not possible to draw a single tangent line on the post yielding portion of the curve. The twice elastic slope method also gives very large value of plastic load in comparison to TI or PWC methods. Curvature method provides most accurate value of plastic load since it is based on the total plastic work done on the structure.

6.1.4 Multilinear Kinematic Hardening

This material option in Reference [18] is presented by multiple layers of perfectly plastic material; the total response is obtained by weighted average behaviour of all the layers. Individual weights are derived from the uniaxial stress-strain curve.

The Figures (6.20) to Figure (6.22) give plots of Load-Plastic Work and Load-Deformation mechanism under multilinear kinematic material model. Plot of Load-Curvature of Plastic Work is given in figure (6.23). Table (6.7, 8) summarizes the plastic loads at various locations.

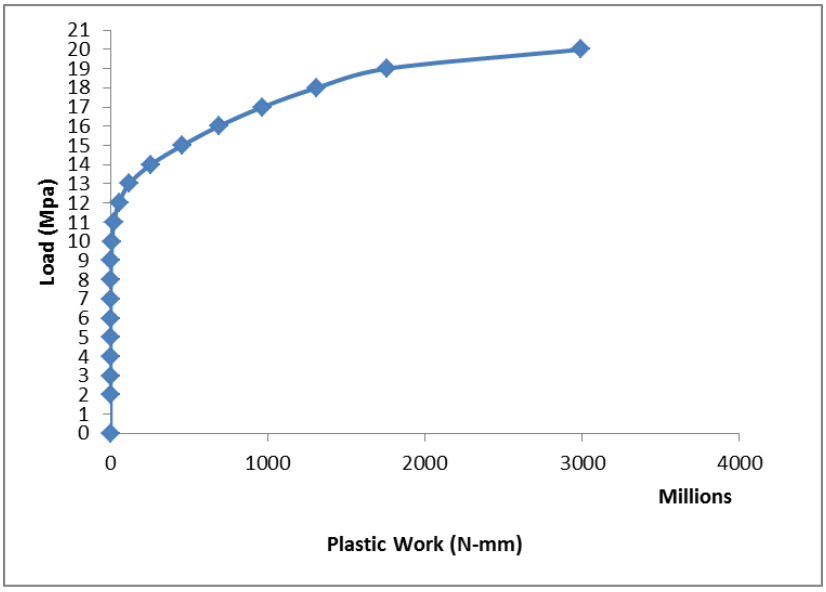

Fig (6.20): Load-total plastic work diagram for small deformation theory and multilinear kinematic hardening:

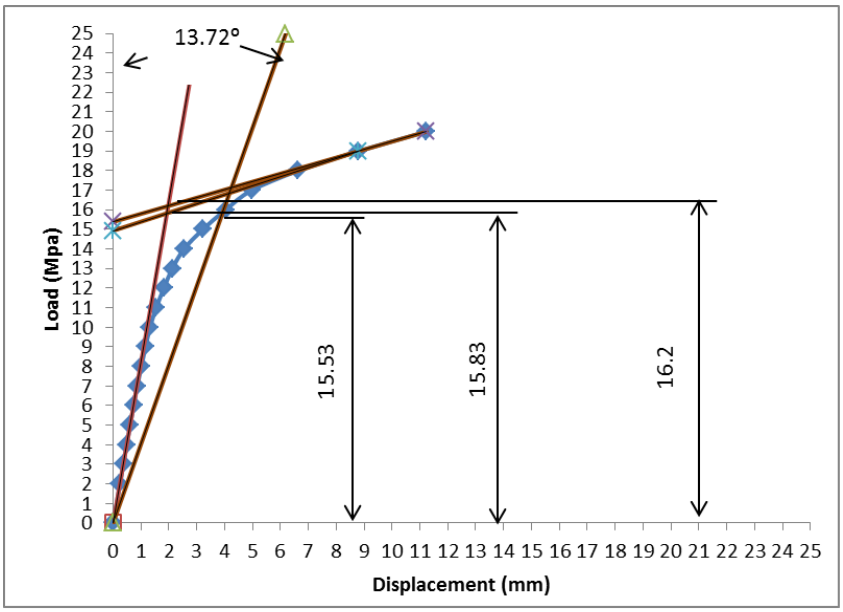

Fig (6.21): Groove Node 67831 deformation parameter TI and TES constructions for small deformation theory, multilinear kinematic hardening:

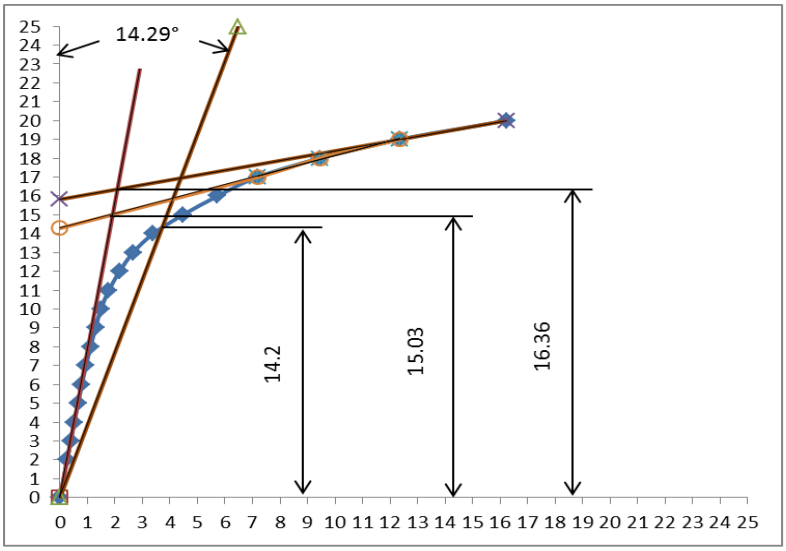

Fig (6.22): Groove Node 67925 deformation parameter TI and TES constructions for small deformation theory, multilinear kinematic

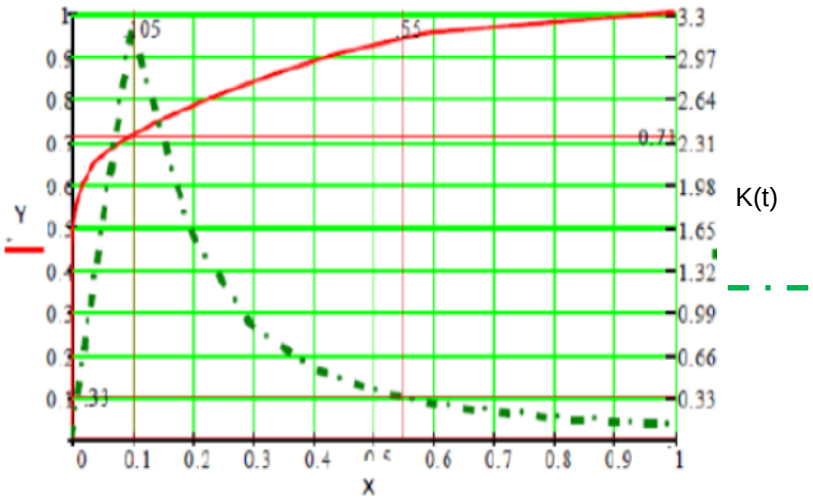

Fig (6.23): Global load-plastic work and load-plastic work curvature plots for small deformation theory, multilinear kinematic hardening X=normalized plastic work, Y=normalized load and K(t)=curvature.

Table (6.7):TI and TES values for plastic pressure for the four deformation parameters considered.

Criterion	Plastic Pressure (MPa)			
	Displacement parameter location			
	Groove Node 67831	**Groove-shell junction** Node 67925	**Hole bottom surface** Node 17951	**Hole top surface** Node 4381
TI	15.83 to 16.2	15 to 16.36	16.3 to 15.74	15.9
TES	15.53	14.2	15.52	15.93

Table (6.8) summarises the plastic load evaluated by limit analysis and the TI, TES and PWC criteria.

Table (6.8): Small deformation theory, multilinear kinematic hardening plastic load

Criterion	Plastic Pressure (MPa)
Limit Analysis	11.8
TI	15
TES	14.2
PWC (10% max)	18.5

Referring to figures (6.21) to (6.23) it can be observed that for this type of material hardening it is still not possible to draw single tangent line on post yielding portion of the load-displacement diagram. This is so as load deformation diagram indicates small changes in slope for part of the curve after its knee portion. Magnitude of deformation is small even for higher level of loads.

For this type of material model it can also be observed that magnitude of plastic load associated with twice of elastic slope is smaller than the lowest of the plastic load

reported according to tangent intersection method. This is in contrast to the linear kinematic hardening model. For the case of the linear kinematic model, it is shown that the larger value of plastic load is related to twice of elastic method; this is a consequence of the shape of the load deformation diagram. For this specific material model and for the node 67925; the TES method gave the same result as curvature method.

The curvature method gives distinct value of plastic load (18.5 MPa), this value relies on magnitude of total plastic work done on the structure and is independent of local parameter such as load-displacement form.

6.2 Large deformation

6.2.1 Bilinear Isotropic Material Hardening

Figure (6.24) provides change of plastic workaccording to change of the load for linear isotropic material with 10% tangent modulus. Figures (6.25) to (6.26) provide plastic loads calculated according to twice elastic slope and tangent intersection methods for nodes 67831 and 67925, plots for nodes 4381 and 17951 are omitted as they show similar behaviours. Nodes are the same nodes as the case of calculation under small deformation scenario. Plot of Load- Curvature of plastic work is given in figure (6.27). Table (6.9, 10) summarizes the magnitude of plastic loads at various locations.

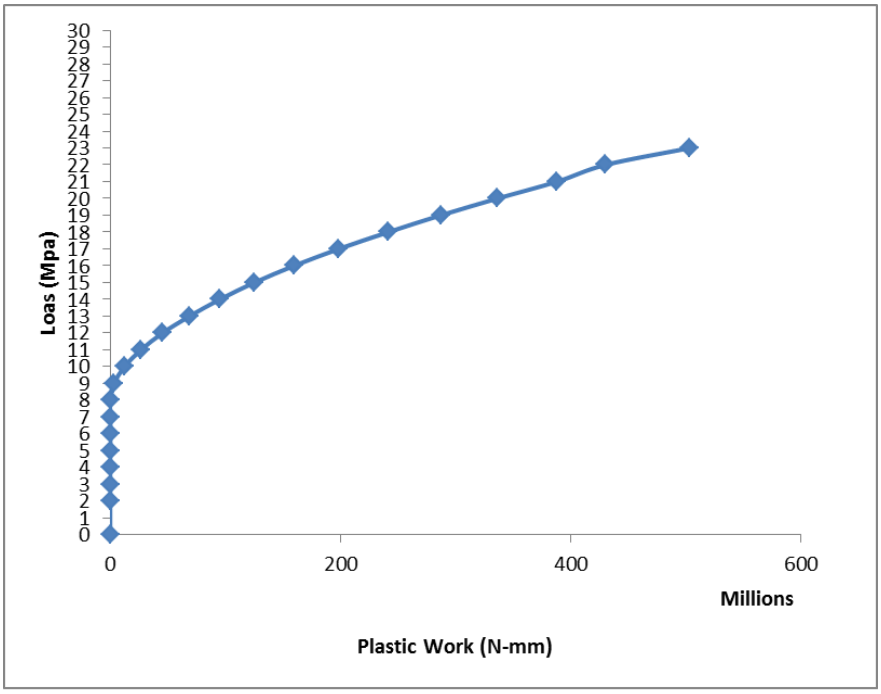

Fig (6.24): Load-total plastic work diagram for large deformation theory and linear isotropic hardening: E_t=0.1E.

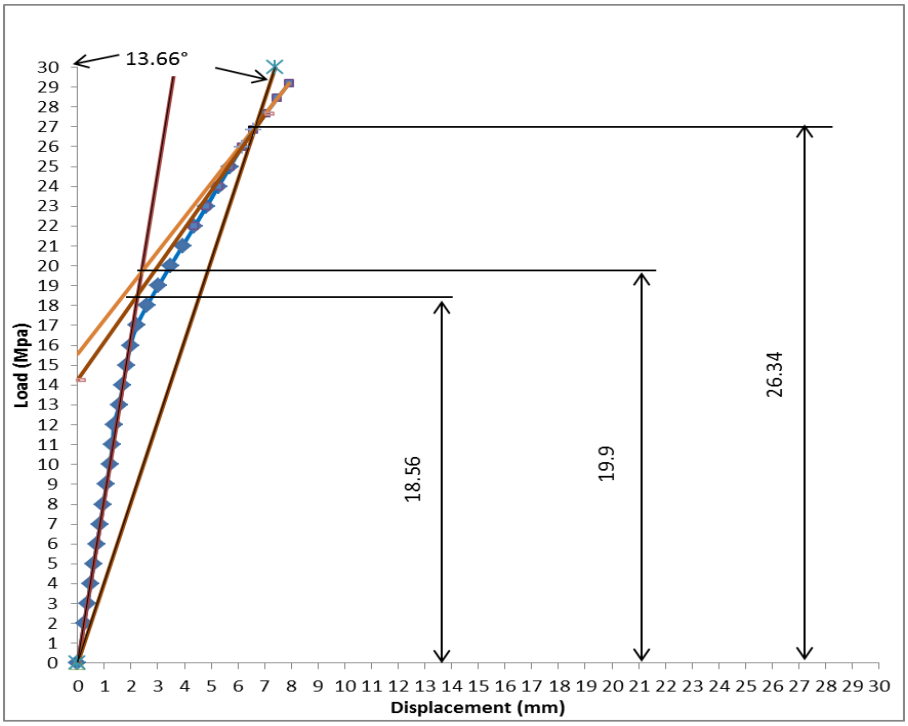

Fig (6.25): Groove Node 67831 deformation parameter TI and TES constructions for large deformation theory, linear isotropic hardening: E_t =0.1E.

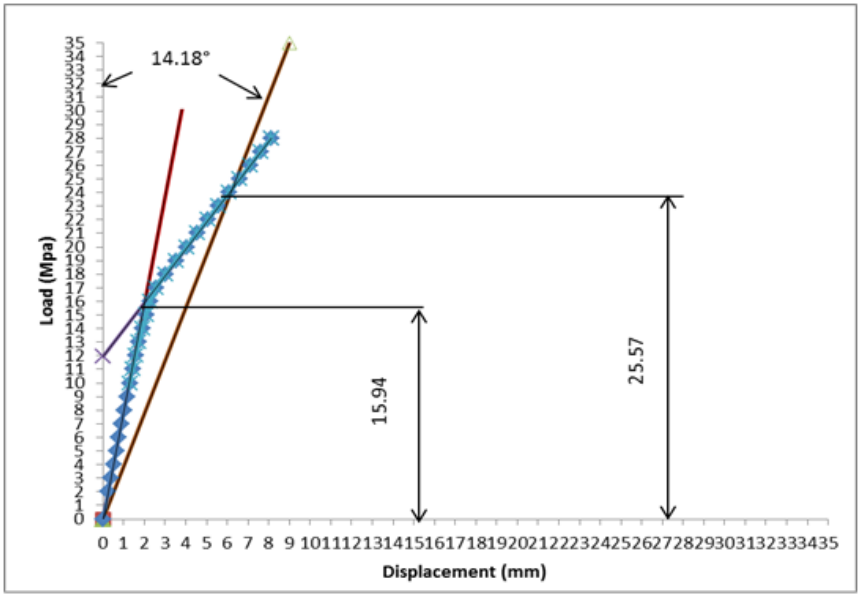

Fig (6.26): Groove-shell junction Node 67925 deformation parameter TI and TES construction for large deformation theory, linear isotropic hardening, E_t=0.1E.

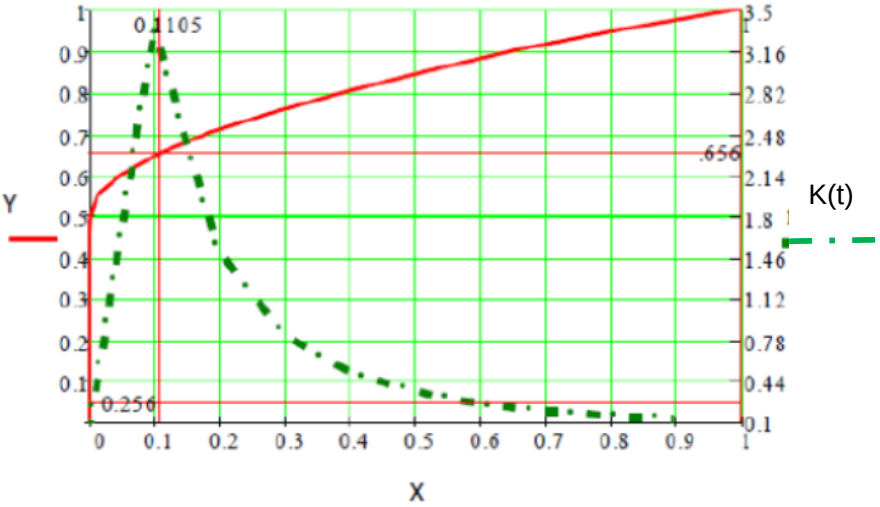

Fig (6.27): Global load-plastic work and load-plastic work curvature plots for large deformation theory, linear isotropic hardening (E_t=0.1E). X=normalized plastic work, Y=normalized load and K(t)=curvature.

Table (6.9):TI and TES values for plastic pressure for the four deformation parameters considered.

Criterion	Plastic Pressure (MPa)			
	Displacement parameter location			
	Groove Node 67831	**Groove-shell junction** Node 67925	**Hole bottom surface** Node 17951	**Hole top surface** Node 4381
TI	18.5 to 19.9	15.94	19 to 21.2	19.4 to 20.7
TES	26.34	25.57	25.97	29.4

Table (6.10) summarises the plastic load evaluated by limit analysis and the TI, TES and PWC criteria.

Table (6.10): Large deformation theory, linear isotropic hardening plastic loads

Criterion	Plastic Pressure (MPa)
Limit Analysis	11.8
TI	15.94
TES	25.57
PWC (10% max)	17.4

Large deflection formulation is associated with two main criteria; these criteria are large magnitudes of deformation with large strain and existence of a nonlinear relationship between stresses and strains. These features demand for the equilibrium equation to be written on the deformed structure. In this way the secondary strain terms are captured. These additional strain terms take part in strain compatibility equations and consequently will affect the structure behaviour.

Coupling of this material model with large deflection theory reveals the fact that the magnitudes of deformations at the specified locations are not significant and

consequently the equilibrium equations for deformed and undeformed structure provides relatively similar results in spite of existence of secondary terms in large deformation formulation. However, plots of Figures (6.25 and 6.26) show somewhat different structural behaviour. When these plots are compared with a similar hardening scenario with the small deformation formulation, structural strengthening can be observed. Load-deformation plots for all of the considered nodes show a similar behaviour.

This structural strengthening is due to the specific constructional features of fixed tubesheet exchangers; these constructional features provide constraints at or close to the tubesheet to shell junction in a way that secondary strains occure in these specified locations. Mathematically, these secondary strains can be approximated by use of large deflection formulation.

The shape of the load-deformation diagrams for all considered locations are close to the case of small deformation with linear isotropic hardening, however, the actual magnitude of plastic loads are higher for all of the considered nodes.

It should be noted that the twice elastic slope method produces an unrealistically large plastic load; this can be observed in the load-deformation diagram. Intersection of a line with slope equal twice of elastic slope occurs at an elevated load. The Tangent Intersection method gives smaller values in comparison with the twice elastic slope; however, the reported plastic loads are larger than loads calculated through curvature method. Dependency of these methods to shape of load- deformation diagram is the main source of error.

The plastic load calculated through the curvature method and according to large deformation analysis reports a larger plastic load compared to the same case under small deformation theory, however, the difference is small (about 3%). This small difference shows that although secondary strains are the cause of increase in plastic load they have a minor effect on this structure, this conclusion is in contrast to the result of applying large deflection formulation to a standard geometry; i.e., perforated clamped edge circular plate, as normally activation of secondary strains produces much larger plastic load for this classical case. The TI and TWS methods being based on the local deformation parameters give larger plastic load values.

Comparing plots of load- plastic work under large and small deflection Figures (6.4) and (6.24) reveals the fact that the most of strain energy is transferred to plastic work at relatively higher loads, however, the peak curvature as it take place at the lower portion of the diagram manifest the activation of a failure mechanism characterised by gross plastic deformation. Magnitude of plastic load as expected is not affected by prolonged transformation of load to plastic work with consequence of ductile failure.

6.2.2 Multilinear Isotropic Material Hardening

Figure (6.28) gives the load-plastic work plot, plots (6.29) and (6.30) provides load-deformation diagram for considered nodes. Figure (6.31) provides the plastic load calculated according to curvature of plastic work method. Table (6.11, 12) encompasses the results of calculation according to multilinear isotropic material model with large deflection scenario.

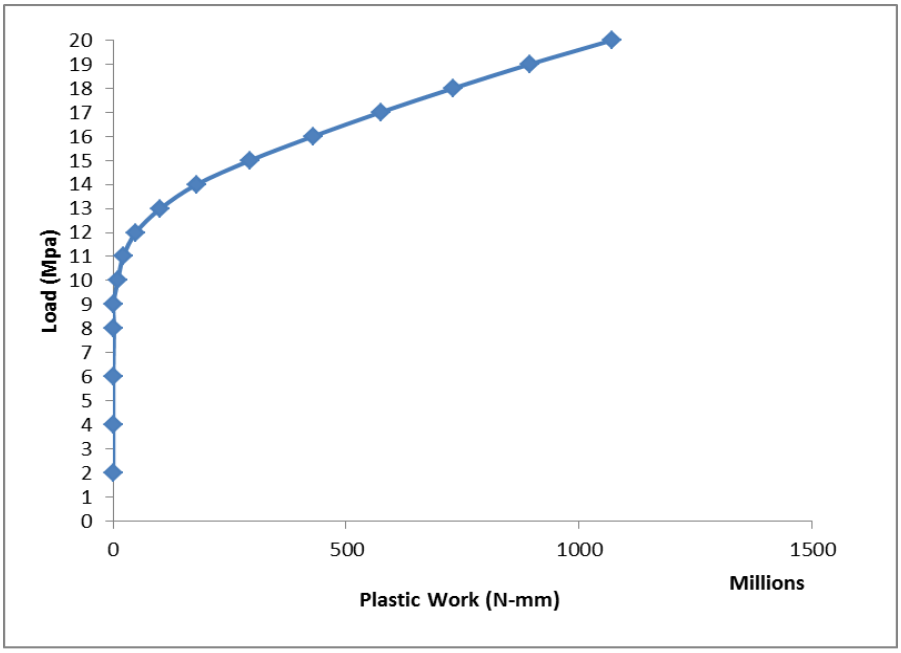

Fig (6.28): Load-total plastic work diagram for large deformation theory and multilinear isotropic hardening:

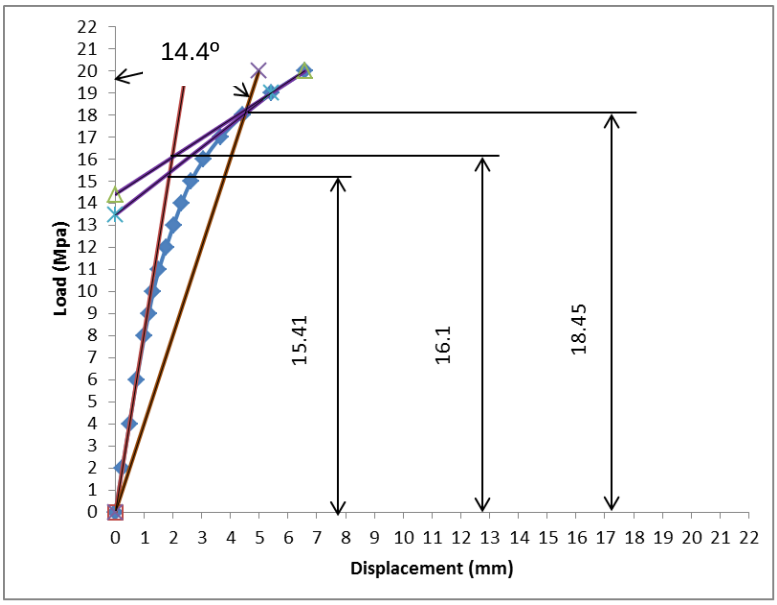

Fig (6.29): Groove Node 67831 deformation parameter TI and TES constructions for large deformation theory, multilinear isotropic hardening:

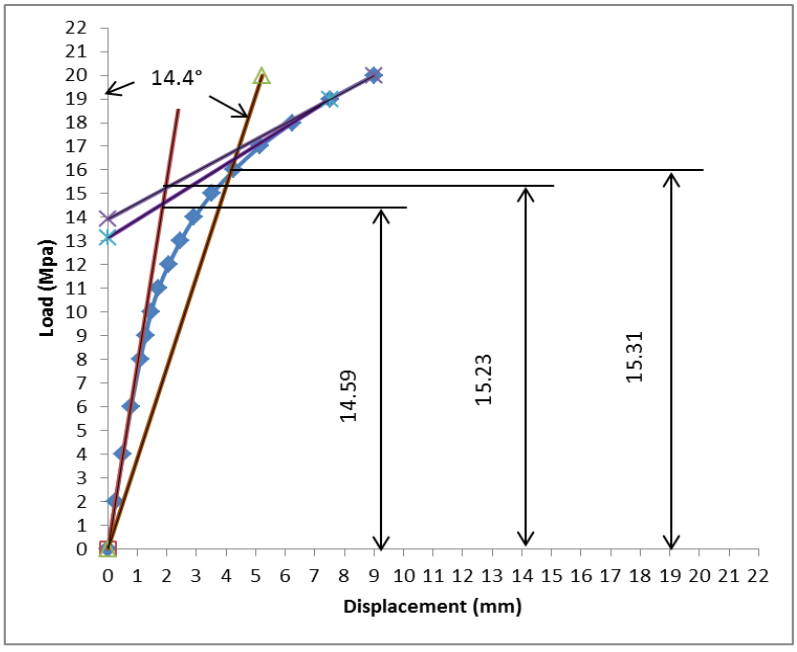

Fig (6.30): Groove Node 67925 deformation parameter TI and TES constructions for large deformation theory, multilinear isotropic hardening.

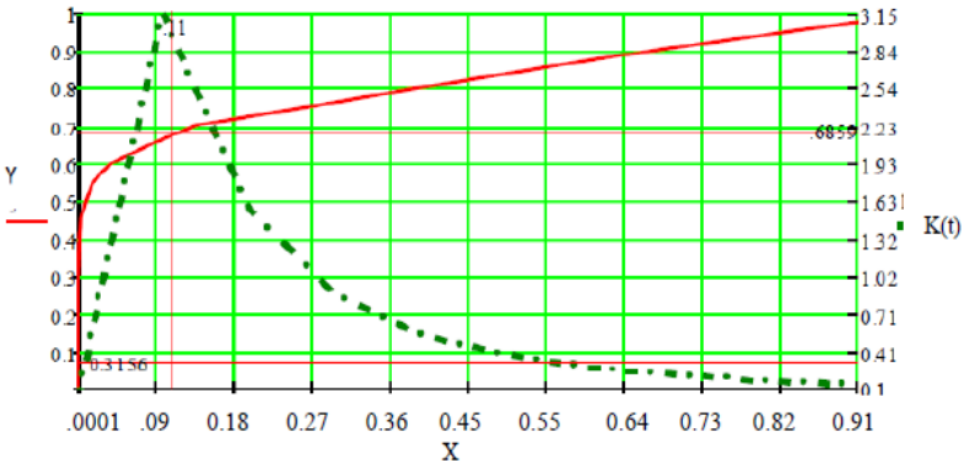

Fig (6.31): Global load-plastic work and load-plastic work curvature plots for large deformation theory, multilinear isotropic hardening . X=normalized plastic work, Y=normalized load and K(t)=curvature.

Table (6.11):TI and TES values for plastic pressure for the four deformation parameters considered.

Criterion	**Plastic Pressure (MPa)**			
	Displacement parameter location			
	Groove Node 67831	**Groove-shell junction** Node 67925	**Hole bottom surface** Node 17951	**Hole top surface** Node 4381
TI	15.41 to 16.1	15.23 to 14.59	15.18 to 15.81	15.37 to 16.1
TES	18.45	15.31	17.12	17

Table (6.12) summarises the plastic load evaluated by limit analysis and the TI, TES and PWC criteria.

Table (6.12): Large deformation theory, multilinear isotropic hardening plastic load

Criterion	Plastic Pressure (MPa)
Limit Analysis	11.8
TI	15.18
TES	15.31
PWC (10% max)	17.4

Referring to Figure (6.28) it is noted that above 20 MPa no convergence could be obtained, this is the limiting factor on load-deformation diagram. Referring to Figures (6.29) and (6.30), it can be observed that the structural strengthening of material is occurring under this material scenario. Rise of load-deformation diagram is sharp and for this reason line drawn with slope equal to twice of elastic slope intersect with the load-deformation diagram at a high load, i.e., TWS method is not suitable for large deflection formulation within frame of this work.

The Tangent Intersection method has produced in average a plastic load of magnitude of 15.5 (MPa) for all considered nodes. For this material model, it is not possible to draw a single tangent line due to the shape of the load-deformation diagram; this is in the specified range of the calculated load.

The PW curvature method gives load of 13.6 MPa at maximum curvature, 10% of maximum curvature corresponds to 17.4 MPa, this can be judged by reviewing the curvature diagram showing that after tip point still large margin is left before arriving to the zero curvature and therefore ductile collapse of the system.

6.2.3 Non-linear Isotropic Material Hardening

Figure (6.32) gives load-plastic work plot, figures (6.33), (6.34) provides load-deformation diagram for the considered nodes. Figure (6.35) provides a plastic load calculated according to curvature of plastic work method. Table (6.13-14) encompasses

the results of calculation according to nonlinear isotropic material model with large deformations.

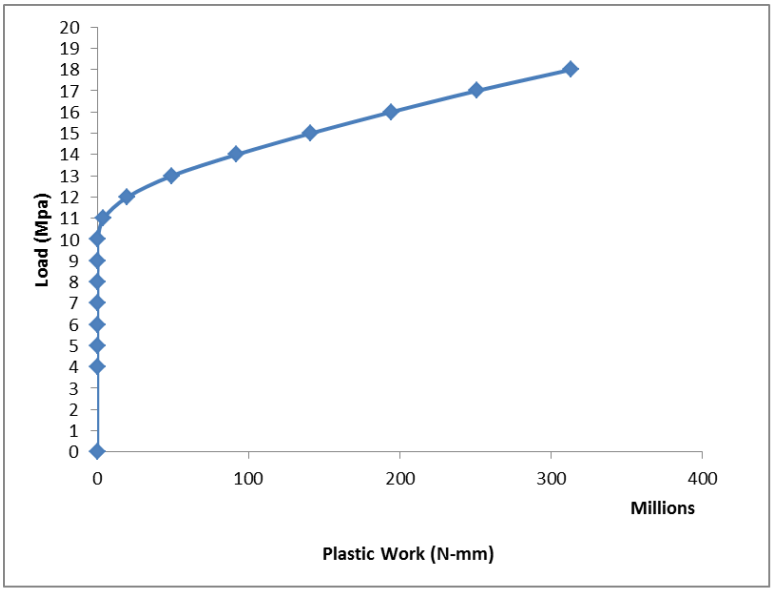

Fig (6.32): Load-total plastic work diagram for large deformation theory and nonlinear isotropic hardening:

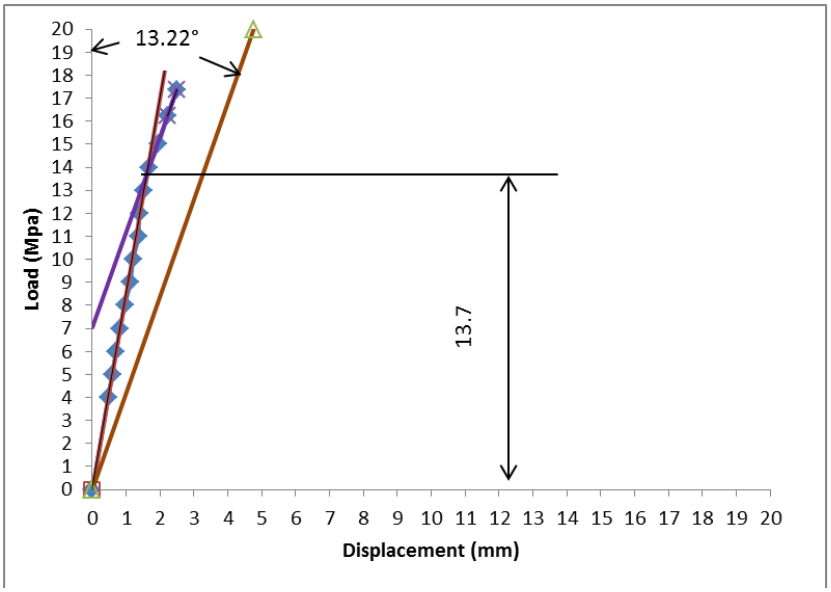

Fig (6.33): Groove Node 67831 deformation parameter TI and TES constructions for large deformation theory, nonlinear isotropic hardening.

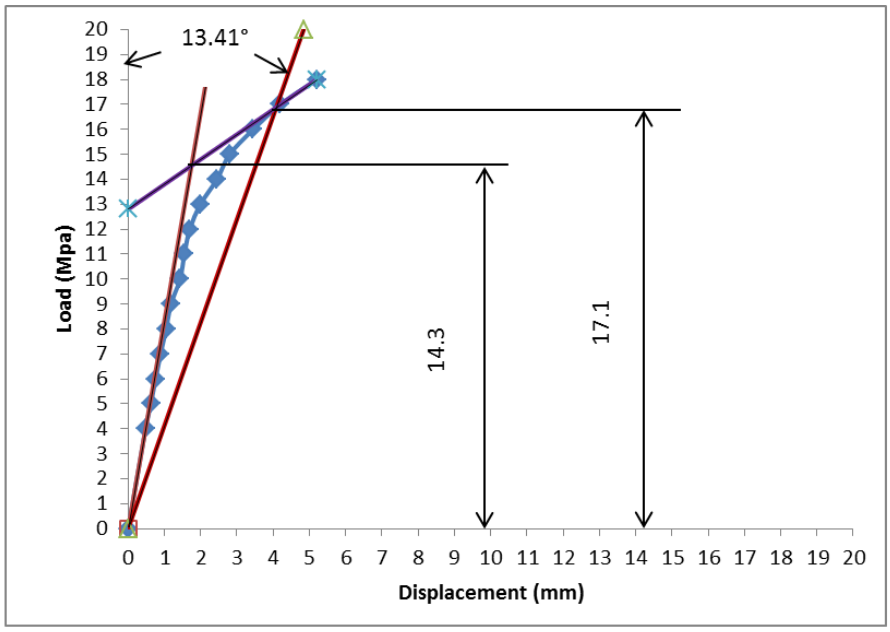

Fig (6.34): Groove Node 67925 deformation parameter TI and TES constructions for large deformation theory, nonlinear isotropic hardening.

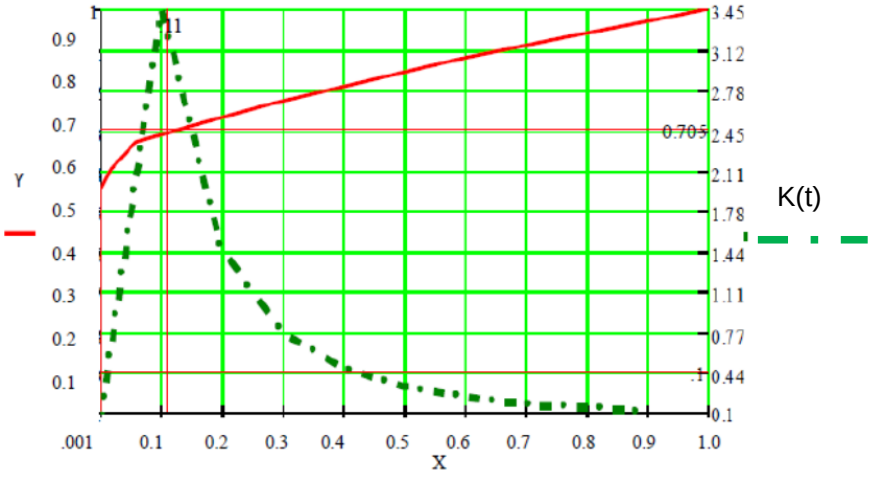

Fig (6.35): Global load-plastic work and load-plastic work curvature plots for large deformation theory, nonlinear isotropic hardening X=normalized plastic work, Y=normalized load and K(t)=curvature.

Table (6.13):TI and TES values for plastic pressure for the four deformation parameters considered.

Criterion	**Plastic Pressure (MPa)**			
	Displacement parameter location			
	Groove Node 67831	**Groove-shell junction** Node 67925	**Hole bottom surface** Node 17951	**Hole top surface** Node 4381
TI	13.7	14.3	13.94	13.7
TES	(1)	17.1	(1)	(1)

Notes: (1) No intersection

Table (6.14): Large deformation theory, nonlinear isotropic hardening plastic loads

Criterion	**Plastic Pressure (MPa)**
Limit Analysis	11.8
TI	13.7
TES	17.1
PWC (10%max)	14.9

Figure (6.32) shows that at 19 MPa no convergence could be obtained, this is the limiting factor on load-deformation diagram, identification of yield point is also difficult with this material model. Figures (6.33- 34) show very large structural stiffening under this material model. The rise of load-deformation diagram is quite sharp and for this reason the line drawn with slope equal to twice of elastic slope does not intersect with the load-deformation diagram. The form of the load-deformation diagram suggests that the sharp raise of the diagram is due to structural hardening, this is actually an indication of high geometrical constrains.

To compare above with case of clamped edge perforated flat plate as a model for a fixed tubesheet, under large deformation analysis a flat plate subject to a large pressure

displaces itself from neutral condition considerably. Such a displacement activates membrane forces which then superpose their effects on the bending criteria of the plate. Here, as it is shown, the behaviour of tubesheet does not depict the formation of membrane forces due to deflection criteria.

The non-linear isotropic material model is based on Voce [46] formulation which uses an exponential term to describe the post yielding behaviour; identification of yielding point is difficult with this material model for this specific geometry. Voce formulation produced a few data points after an apparent yield point, these data points where crucial on the results noted on the above.

The twice elastic slope did not intersect the load deformation diagram for 3 nodes. For the 4^{th} node intersection was barely obtained, the point of intersection occurred just below termination load. The Tangent Intersection method produced smaller values.

The curvature method gives load of 12.9 MPa at maximum curvature, 10% of maximum curvature is 14.9 MPa, this value can be judged by reviewing the curvature diagram showing that after tip point on the diagram still large margin is left before arriving to the zero curvature.

6.2.4 Bilinear Kinematic Material Hardening

Figure (6.36) is the Load-Total Plastic Work diagram for the bilinear kinematic material hardening material model. Plots (6.37, 38) give details related to load- deformation mechanism under linear kinematic material model. Plot of Load- Curvature of plastic work is given in figure (6.39). Table (6.15, 16) summarize the magnitude of plastic loads at various locations.

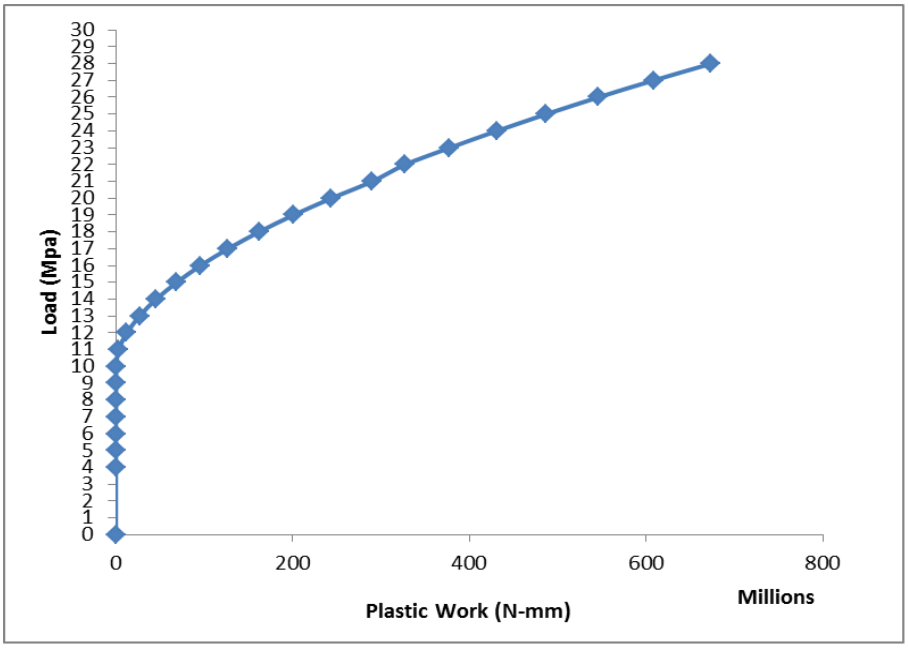

Fig (6.36): Load-total plastic work diagram for large deformation theory and linear kinematic hardening: E_t=0.1E.

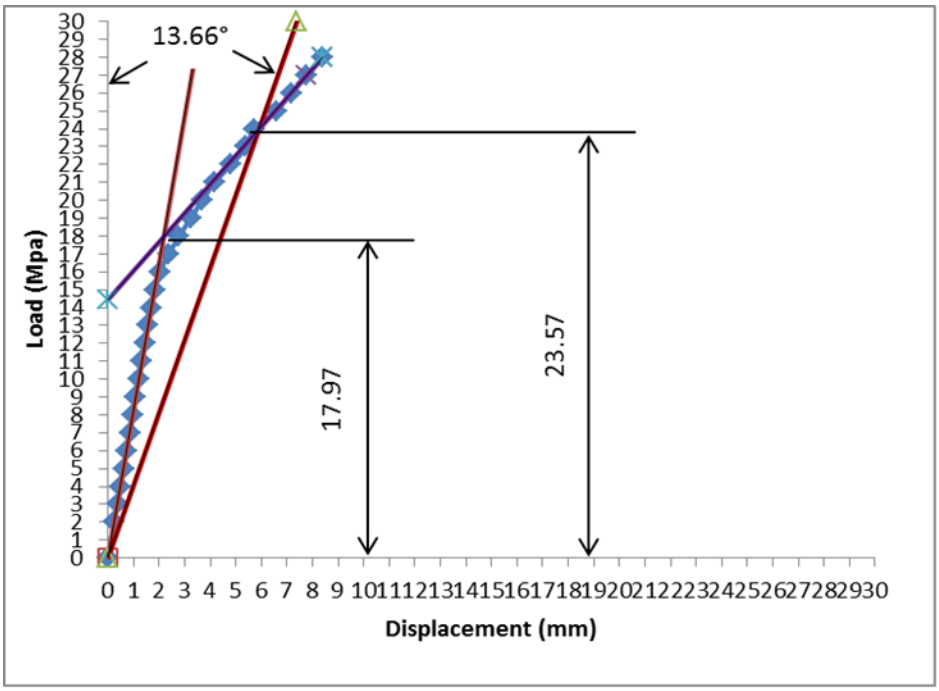

Fig (6.37): Groove Node 67831 deformation parameter TI and TES constructions for large deformation, linear kinematic hardening: E_t=0.1E.

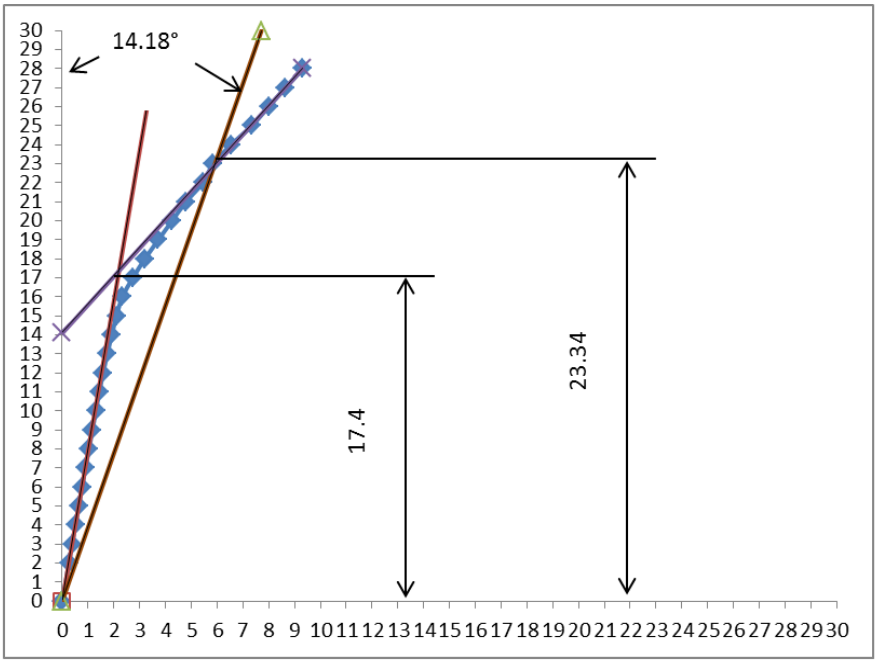

Fig (6.38): Groove Node 67925 deformation parameter TI and TES constructions for large deformation theory, linear kinematic hardening: E_t =0.1E.

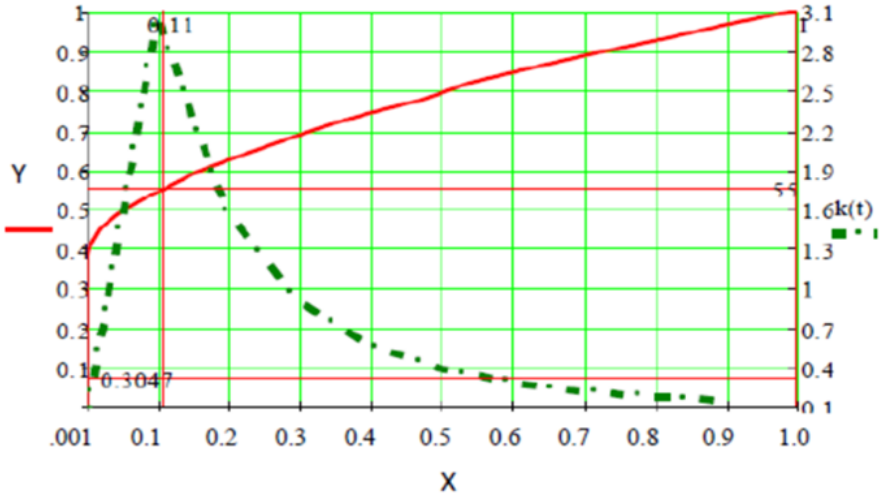

Fig (6.39): Global load-plastic work and load-plastic work curvature plots for large deformation theory, linear kinematic hardening (Et=0.1E). X =normalized plastic work, Y= normalized load and K(t)= curvature

Table (6.15):TI and TES values for plastic pressure for the four deformation parameters considered.

Criterion	Plastic Pressure (MPa)			
	Displacement parameter location			
	Groove Node 67831	**Groove-shell junction** Node 67925	**Hole bottom surface** Node 17951	**Hole top surface** Node 4381
TI	23.57	23.34	25.97	17.66
TES	17.97	17.4	18.29	17.66

Table (6.16) summarises the plastic load evaluated by limit analysis and the TI, TES and PWC criteria.

Table (6.16): Large deformation theory, linear Kinematic hardening (E_t=0.1E), plastic loads.

Criterion	Plastic Pressure (MPa)
Limit Analysis	11.8
TI	17.6
TES	17.7
PWC(10%max)	22.68

6.2.5 Multilinear Kinematic Material Hardening

Figure (6.40) provides magnitude plastic work according to the PW curvature method. Displacements data have not been collected for this case.

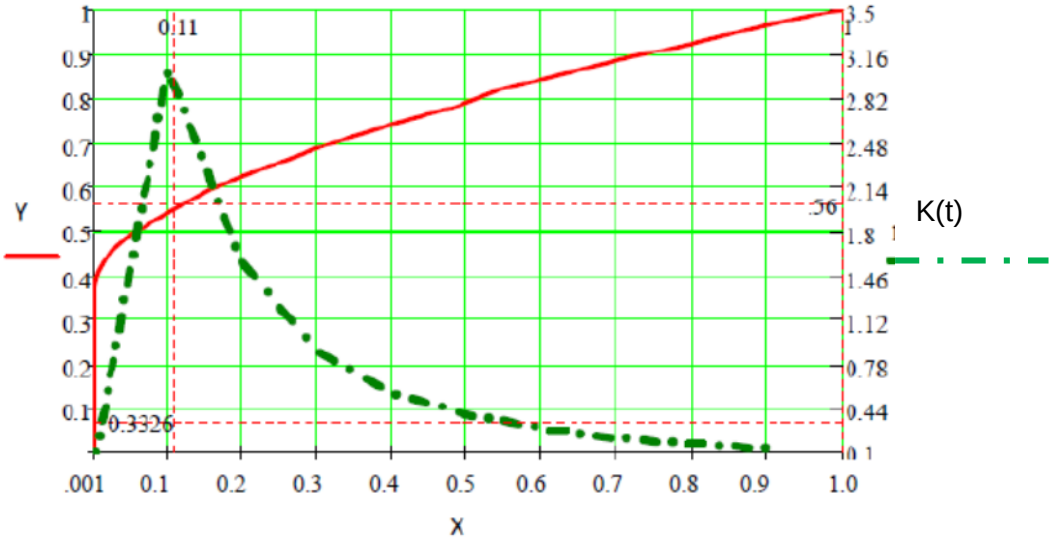

Fig (6.40): Global load-plastic work and load-plastic work curvature plots for large deformation theory, multilinear kinematic hardening, X=normalized plastic work, Y=normalized load and K(t)= curvature

6.3 Results

6.3.1 Small Deformation

Table (6.17) provides values of plastic loads calculated according to various material hardening models.

Table (6.17): Plastic load values under various hardening rules.

Procedure			Isotropic		Kinematic	
			Linear	Multilinear	Linear	Multilinear
			E_t= 0.1E	True stress -strain	E_t= 0.1E	True stress -strain
Max. curvature of plastic work (PWC)			12.8	14.3	12.7	14.2
10% of Max. curvature of plastic work			17.1	17.6	17	18.5
Limit Load			11.7	11.7	11.7	11.7
Tangent Inters. (TI)	**4381**	**Hole top surface**	17.95	15.45	16.75	15.93
	17951	**Hole bottom surface**	18.15	15.42	16.8	16.02
	67831	**Groove**	18.9	16.15	16.8	16
	67925	**Groove-shell junction**	16.25	15.35	16.2	15.68
Twice elastic slope (TWS)	**4381**	**Hole top surface**	23.5	15.2	22.6	15.93
	17951	**Hole bottom surface**	22.3	16.3	28.14	15.52
	67831	**Groove**	21.65	17.8	19.48	15.53
	67925	**Groove-shell junction**	21.2	14.3	23.98	14.25

Note: Plastic loads given for TI method is an averaged value.

6.3.2 Large Deformation

Table (6.18) provides results of calculations according to large deflection formulation under various material hardening models. In this table, plastic load calculated according to large deformation theory through PWC criterion are compared with the numerical instability load of the vessel, in here instability load is defined as large deflection algorithm and elastic- perfect plastic material model (this is not buckling load).

Table (6.18) gives plastic load values under various hardening rules with large deformation.

Procedure			**Isotropic**			**Kinematic**	
			Linear	**Multilinear**	**Non-linear**	**Linear**	**Multilinear**
			E_t= 0.1E	**True stress -strain**	**Voce**	**E_t= 0.1E**	**`True stress -strain**
Max. curv. of plastic work (PWC)			13.2	13.6	12.92	14.85	15.12
10% of Max. curv. of plastic work			17.4	17.1	15.01	22.86	21.6
Instability load			12.4	12.4	12.4	12.4	12.4
Tan. Intersection (TI)	**4381**	**Hole top surface**	19.4	15.37	13.7	17.66	(4)
	17951	**Hole-bottom surface**	19	15.48	13.94	25.97	(4)
	67831	**Groove**	18.5	15.41	13.7	23.57	(4)
	67925	**Groove-shell junction**	15.94	14.59	14.3	23.34	(4)
Twice elastic slope (TWS)	**4381**	**Hole top surface**	29.4	17.01	(3)	17.66	(4)
	17951	Hole-bottom	25.97	17.12	(3)	18.29	(4)
	67831	**Groove**	26.34	18.45	(3)	17.97	(4)
	67925	**Groove-shell junction**	25.57	15.31	17.1	17.4	(4)

Notes:

(1) Nodes 4381, 17951, 67831, 67925 are located in higher stress zones.
(2) Plastic loads given for TI method is lowest value.
(3) No intersection
(4) Data have not been collected

6.4 Discussion of Results

Different types of analyses and different plastic load criteria were considered in the investigation resulted in a wide range of calculated plastic pressures. Values ranged from limit pressure of 11.7 MPa to numerical instability pressures in excess of twice this figure. In the case of the small deformation bilinear hardening analysis, numerical instability did not occur for the load range considered; the analysis was terminated when the plastic strain exceeded 15%.

The TES and TI plastic pressures require specification of a deformation parameter to define a characteristic load-deformation curve. In the analyses presented here, the displacement vector (sum) of a highly loaded node in the groove between the tube sheet and shell was used as the deformation parameter; this parameter resulted in high values of TES plastic load due to the stiff nature of the tube sheet and constrained nature of the plastic zone.

It should be further noted that, the choice of deformation parameter is not arbitrary; in general the proper choice is the one that satisfies the requirement of product of the load parameter and deformation parameters to represent work. In past, various choices of load deformation parameters have been suggest for various mechanical systems, for example for a cantilever beam under end force proper deformation parameter is displacement below the load, for the same beam under end moment the proper deformation choice is angle of rotation. In pressure vessel applications, the radial deflection of a cylindrical shell under pressure has been suggested as proper deformation parameter. Choice of deformation for closed vessel has been suggested to be taken as volume of pressurized fluid, in pressure vessel head this choice is deflection in knuckle region and for a nozzle is axial deflection of nozzle.

In this work, it has been found that the choice of vector of nodal displacement (sum) is a good indicator of plastic load. The exchanger is subject to combination of pressure and axial load due to head enclosure, existence of tubesheet and lower shell prevents free radial deformation of upper shell and these rule out the choice of radial deformation. It is not practical to account for vessel volume changes as the process media is gas with compressibility features. The axial displacement also is not a good choice as the junction is subject to bending as well. It is believed that, the choice of displacement vector (sum)

is an appropriate one and plots presented as load-deformation are capable of capturing plastic work adequately.

The TES criterion does not capture the nature of the plastic collapse mechanism in this situation properly and is not therefore suitable as the basis for design against gross plastic deformation. The main reason for this is the shape of the load-deformation diagram, in all considered cases the diagrams showed structural strengthening, the magnitudes of the displacements for very stiff tubesheet to shell junction is small (few millimeters) and this is the actual cause of sharpness in load-deformation plots. This point is even more severe with the case of large deflection. As for some cases (non-linear isotropic) no value was obtained.

The TI criterion is dependent on where the tangent is drawn to the plastic deformation portion of the load deformation curve. In this configuration, the curve exhibits a steady slope at high load levels and taking the tangent from this region results in relatively high values of TI plastic load. Range of the values was obtained with no clear identification of what specific value to choose, conservatism would require use of the lowest.

Extensive plastic deformation occurs in the grooved region at the edge of the tube sheet at significantly lower pressures and it is possible that a gross plastic deformation mechanism forms in the structure prior to the steady state plasticity exhibited at higher pressures.

The ASME VIII Div. 2 Global Criterion of structural instability indicated by convergence failure is not appropriate for the small deformation bilinear analyses presented (as the code requires use of large deformation theory). These models continue to converge at very high load levels and solution is terminated by defining a limiting strain for the FE solver.

The tubesheet as a flat plate is an ineffective pressure container because of its shape. It has zero curvature and responds to pressure by bending, large deformations must develop before membrane action can aid in the support of pressure, as in the case of the curved shells. This principle is not happening for the tube sheet as the presence of the tubes and their staying action prevent any type of bending away from a small annular ring. The membrane forces which increase the load capacity of the plate are small and ineffective. Here, it is proposed that the reason for the calculated higher plastic load is a

material hardening effect and not the involvement of membrane forces. The tubesheet junction experiences structural strengthening, i.e., the rise in the load-deformation diagram, however, this strengthening is formed due to activation of hardening mechanism.

In the large deformation analyses, numerical instability occurs at high load levels, in excess of twice the limit load. In these cases a Service Criterion must be applied in order to define a plastic load suitable for design. Direct use of plastic collapse load is not appropriate as at this higher load the deformations and strains are very high. High level of deformation could cause weld distortion at the junction of tubes to tube sheet, or can create movements of the tubes that are limited by presence of the baffles. The PWC criterion is an appropriate Service Criterion with respect to preventing excessive plastic deformation.

The PWC maximum curvature indicates that considerable stress redistribution has occurred in the structure but the state corresponding to gross plastic deformation in limit analysis has not yet been achieved. At higher loads, the amount of stress redistribution decreases and a gross plastic deformation mechanism is established. It has previously been suggested that reduction in curvature to 10% of the maximum is a suitable indication of gross plastic deformation. It is proposed here that the *maximum PWC* is a suitable indicator of the plastic pressure of the vessel. This is a conservative interpretation but results in a plastic load for design purposes that is higher than the limit load due to the effect of work hardening on the development of a plastic failure mechanism.

For the present FEA model, data sheet thickness of 136mm reported according to the classical ASME method has been reduced to 100 mm for purpose of the plastic load calculation. It has been shown that the 100mm thickness can withstand the pressure of 12.8 MPa (from large deformation analysis) according to true stress strain material data. This pressure is almost 3 times higher than the datasheet design pressure indicating that the thickness could perhaps be further reduced using this method; however design safety factors and other design checks must be applied. One additional observation is noted here; as tube sheet is supported by numerous tubes the effect of the tubing is to prevent excessive relative transverse deformation of different sections of the tubesheet,

in fact tubes are making these sections relatively rigid. However the sections of the tubesheet without tubes and the sections of the tubesheet located at the outer tubes rows do experience bending. The magnitude of the plastic load therefore will have a high dependency on the behavior of these critical regions.

The results indicate that PWC method gives robust value for allowable load is recommended for the tube sheet design.

7. Progressive Plastic Deformation

Application of the progressive plastic deformation design check has been the subject of various studies. Works presented by many researchers have aimed to apply various methods of shakedown analysis to mechanical components subject to cyclic loads. Apart from classical elastic shakedown methods, few attempts have been made to apply the cyclic method of shakedown analysis to tubesheet.

In this section of this thesis the shakedown-ratchet response of the tubesheet of a reactor is studied extensively. The response of the tubesheet to cyclic load under reduced thickness has been calculated through use of elastic, elastic-perfect plastic, linear and multiliner isotropic and linear and multilinear kinematic material models. These material models are explained in chapter 5. Cyclic calculations are performed in later part of this chapter. In addition, the existence of an elastic core in the “hot spot” location is investigated.

7.1 Extension to ASME Method of Ratcheting Assessment

To investigate the response of the exchanger to various material models, calculations and details are presented in the subsequent sections for the elastic "$3S_m$"method, and for cyclic method through use of elastic perfect plastic material model according to ASME recommendation.

Further analysis has been performed using various strain hardening elastic-plastic material models. In this way, the post yield behaviour of the exchanger subject to cyclic loads arising from start-up and shutdown conditions is evaluated more appropriately. To demonstrate the existence of elastic core additional calculations have been performed and results presented.

7.2 Reactor Design Parameters

As it is noted in Chapter 1, heat exchanger tube sheets are a significant expense in power and process plants. The cost of a tube sheet is dependent on the basic thickness required to satisfy safety and functional considerations, not only in terms of material cost but also the added manufacturing costs associated with forming, machining, drilling, welding and NDT. These costs can be minimized by reducing the tube sheet thickness at the design stage through use of the inelastic design route.

In this Thesis, the tubesheet data sheet thickness of 136 mm calculated according to conventional elastic analysis methods has been reduced to 100 mm. The plastic load under this reduced thickness was calculated and reported for monotonically increasing load (pressure). In this chapter, two design pressures are considered: 7.8 and 8.53 MPa, corresponding to the limit load and instability load calculated in chapter 6 after applying safety factor of 1.5 (the limit and instability loads are reported in Tables (6.17,18) of chapter 6 as 11.7 and 12.4 MPa). These design pressure values are treated as operating pressure and used in ratcheting assessment of the vessel. These loads are significantly higher than the data sheet design pressure of 4 MPa reported in section 5.2.

The objective of study in this part of the thesis is to investigate the cyclic elastic-plastic response of the tube sheet under reduced thickness subject to the above increased operating pressures. In this reactor, the cycles are defined as start-up and shut downs. Fluctuations around these operating conditions are considered separately in chapter 8.

As previously noted in chapter 2, reactor tube sheets under combined pressure and temperature loads are subject to a complex stress distributions in the outer rows of the tubes and at the junction between the tube sheet and the shell. Recalling ASME Div. II, App. 5 definition of stresses, the stress in these regions exhibits characteristics of primary stress due to the equilibrium requirements and secondary stress due to the through thickness temperature gradient and self- constraint at the stiff junction. Moreover, although pressure is mainly responsible for general and local primary stress, it also contributes to the secondary stresses at the junction. By definition secondary stresses are required to satisfy the continuity of the stress field at the structure discontinuity.

The vessel is intended to operate under steady state condition; however, it is also subject to repeated loading cycles due to deviation from standard operating modes, process upsets, etc. The largest stress range cycle occurs from start up to full shutdown, and causes largest variation in stress magnitude, effect of these cases are investigated in Chapter 8 of this thesis.

Reinhardt *et al* [48] have previously presented a ratcheting analysis and assessment of a tube-sheet subject to rapid transient thermal loading in which the perforated region of the tube-sheet was replaced by an equivalent solid plate with anisotropic yield properties. His approach is not applicable to this case as this reactor is not subject to rapid transient thermal load. Here, a full 3-D model of the tubes, tube-sheet and shells is used. The FEA model and other geometric data are given in Chapter 5.

It should be noted that material cyclic stress-strain curves is normally used for cases related to high cycle fatigue, i.e., when the cycles are in order of several millions, for this exchanger more appropriate equation is equation of monotonic loading curve, this is due to relatively low metal temperature (108 ˚C maximum) and limited cycles due to dominantly steady-state operation of unit (start-up and shut downs mainly). The anticipated number of scheduled start-up and shut-down operations during the life of the plant is expected to be in the region of 50 full cycles.

The steady state through thickness temperature distribution in the vessel was evaluated by a preliminary thermal analysis. This was done through use of ANSYS thermal elements. The geometry of the model used in thermal analysis is identical to that used in mechanical module. Material thermal property, i.e., identical material conduction coefficients ($K_{XX,}$ K_{YY}, and K_{zz}) have been used for purpose of temperature distribution calculations.

In thermal analysis, thermal boundary conditions (i.e. heat transfer coefficients), are inputs to the analysis. This exchanger operates at the steady state-steady flow condition with tube sheet skin temperatures of 50 ˚C and 108 ˚C. Installation of an expansion joint in shell side shell to compensate for differential expansion between tube bundle and shell side shell was not required as they have small temperature difference, data sheet of this exchanger shows this.

The exchanger is not subject to any type of transient heat input Therefore, in this case the thermal analysis was simplified as the surfaces temperature on hot side face and on the cold side face are known (as defined in the exchanger data sheet) and consequently there was no requirement to calculate these coefficients. The shell side shell, channel side shell and tubes temperature was taken from data sheet, Ref. [54].

Thermal conduction calculations show smooth gradient of temperature in the tube sheet, which is expected as the skin temperatures are low and their values are close to each other. The calculated temperature distribution is shown in Figure (7.1). The results of the thermal analysis were used to define temperatures in the ratcheting assessment.

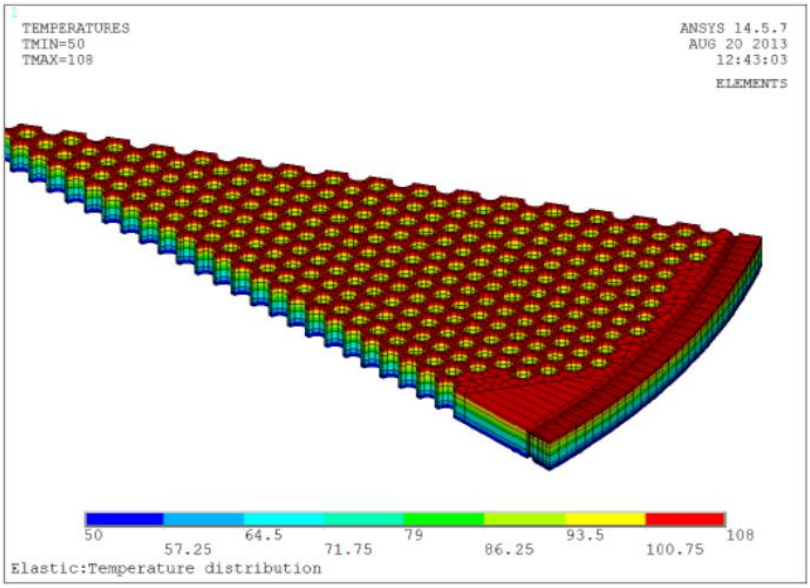

(A)

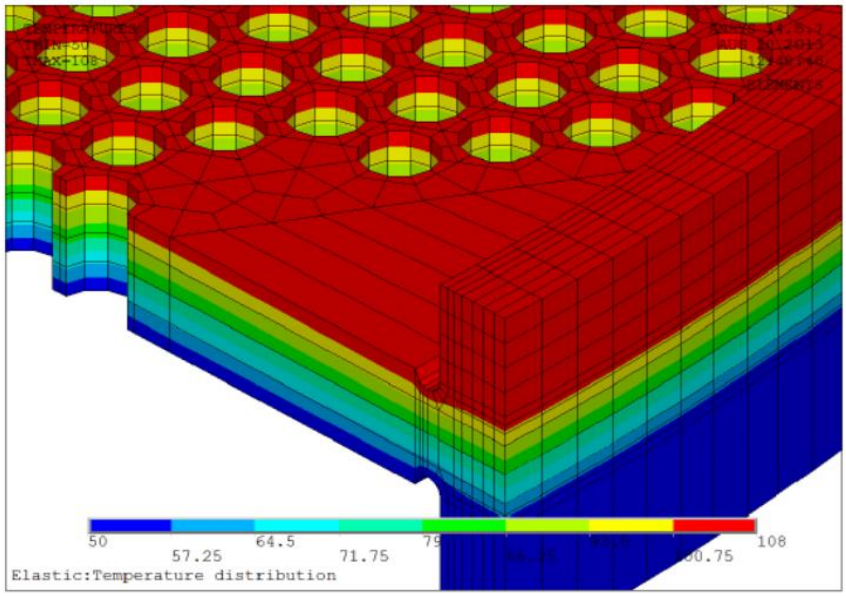

(B)

Fig (7.1): Tubesheet temperature distribution (°C) used in ratcheting analysis

7.3 Elastic Finite Element Analysis and Stress Classifications

Elastic finite element analysis was performed for the calculated temperature distribution for two design pressures: 7.8 MPa and 8.53 MPa. Stress linearization was then carried out to identify the higher stress regions at which ratcheting are to be checked.

Figures (5.4 to 5.6) show the model geometry. Displacement boundary conditions are provided in Figure (5.7) and in Figure (5.8). Pressure is applied to the appropriate faces of relevant elements forming tubesheet, channel and 3-D tubes geometry. Fig (7.2- 4) provide pressure boundary conditions.

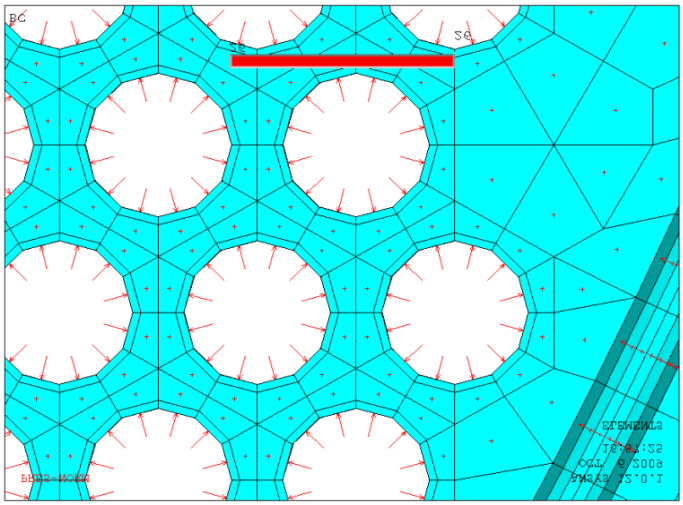

Fig (7.2): Pressure loading inside the tubes

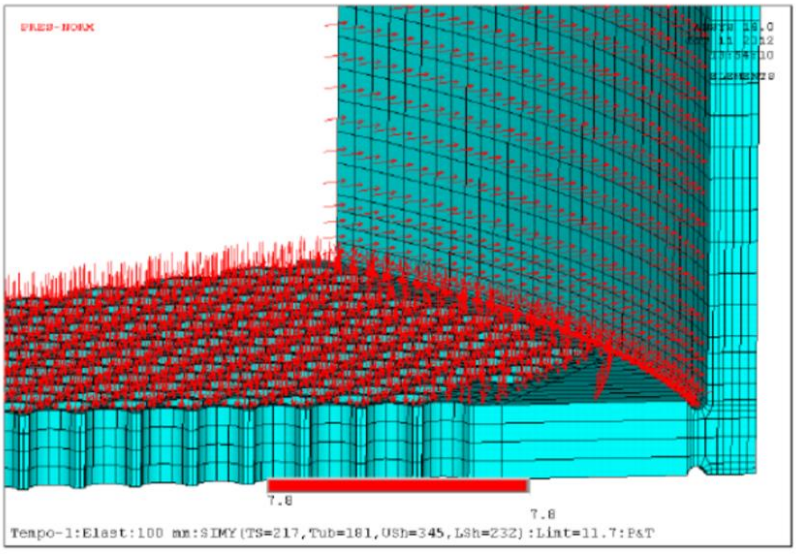

(a)

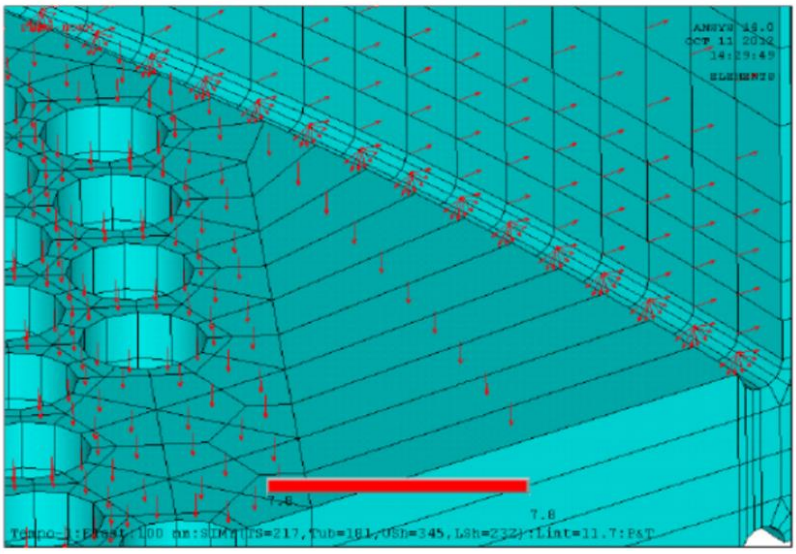

(b)

Fig (7.3): Pressure load on the (a) tubesheet and channel side shell, (b) on the tubesheet groove

The effect of the end head action is provided as a longitudinal distributed nodal force, which is applied to the top nodal rows of the elements forming the channel side geometry. Temperature is assigned to elements nodes according to Figures (7.1.A,B) above.

The stress results of the elastic analyses are component stresses at the various nodes. These stresses are not suitable for direct comparison with Code allowable limits due to the fact that elastic design rules of the Code are based on the thin shell theory concepts and require identification of membrane and bending stresses. The Code defines the stress distribution in terms of membrane, bending and peak stress, Membrane and bending stress are categorised as primary (general or local) or secondary stress, with different allowable values defined for different combinations of these stresses. This has created some difficulties on placing stresses under above categories for geometries not included in Table (5.6) of Ref. (1). As an example, for a nozzle opening in spherical shell under internal pressure, in spite of significant bending in the shell close to nozzle, only membrane stresses are classified as primary and bending stresses are placed under the secondary classification. This was done since only the circumferential (hoop) and longitudinal (membrane-meridional) stresses in the nozzle are required to satisfy the law of equilibrium with internal pressure. In this specific case it is essential that the bending stresses are considered under the correct category.

In design by analysis using 2D or 3D continuum elements, the calculated stress results (in the form of stress components) must be post-processed to extract equivalent membrane and bending stress distributions for Code assessment. In general, and for the case of tubesheet to shell junction in particular; due to the thickness of intersecting members, the stresses have non-linear through thickness characteristics and the assumption of plain sections remaining plain implicit in linearization procedures may not be valid.

Bending stresses may require linearization as they can have non-linear distribution at structural discontinuities. This is because by definition they are variable component of normal stresses and the variation may not be linear across the section thickness. Membrane stresses are uniform over the cross section, however, in the case of a discontinuity, their magnitude will change as cross section dimensions changes. In this case they assume local characteristics and are classified as local membrane.

Linearization has been carried out by identifying stress classification lines for evaluation of failure modes of plastic collapse and ratcheting. Stress classification lines are typically located at gross structural discontinuities. Ref. [1] puts some restrictions in regard to the stress classification lines characteristics, these restrictions are:

- Stress classification lines should be oriented normal to contour lines of the stress component of highest magnitude. As an alternative, classification lines can be placed normal to the mid-surface of the cross section. This latter requirement has been respected for all of the classification lines provided in the following sections.

- Longitudinal and circumferential component stress distributions on the stress classification line should be monotonically increasing or decreasing, except for the effect of stress concentration or thermal stresses. This can be observed in the following linearization plots.

- For pressure loading the through- thickness stress should be equal to the compressive pressure on the applied surface, and approximately zero on the other surface defining the stress classification line. When the stress classification line is not perpendicular to the surface this requirement will not be satisfied.

- The shear stress distribution should be parabolic and/or the stress should be low relative to circumferential and meridional stresses. Depending on the type of loading, shear stress should be approximately zero on both surfaces defined by the stress classification lines. When shear stresses are small, their orientation is not important. If they are distributed linearly, the shear stress is likely to be significant.

It should be noted that above conditions on shear stresses are meant to check the normality of stress classification line to the middle surface.

Linearization of stresses on the following parts has been obtained through use of the post processor of the ANSYS program. ANSYS has a capability of defining a path between identified nodes and a path operation is used to linearize the non-linear stress distribution along the path line. ANSYS uses Ref. [17] for the linearization process.

Ref. [17] makes reference to beam bending stress- a uniaxial stress- and attempts to define an equivalent linear stress distribution on the classification line. The procedure depicted in Figure (7.4) shows a typical stress distribution.

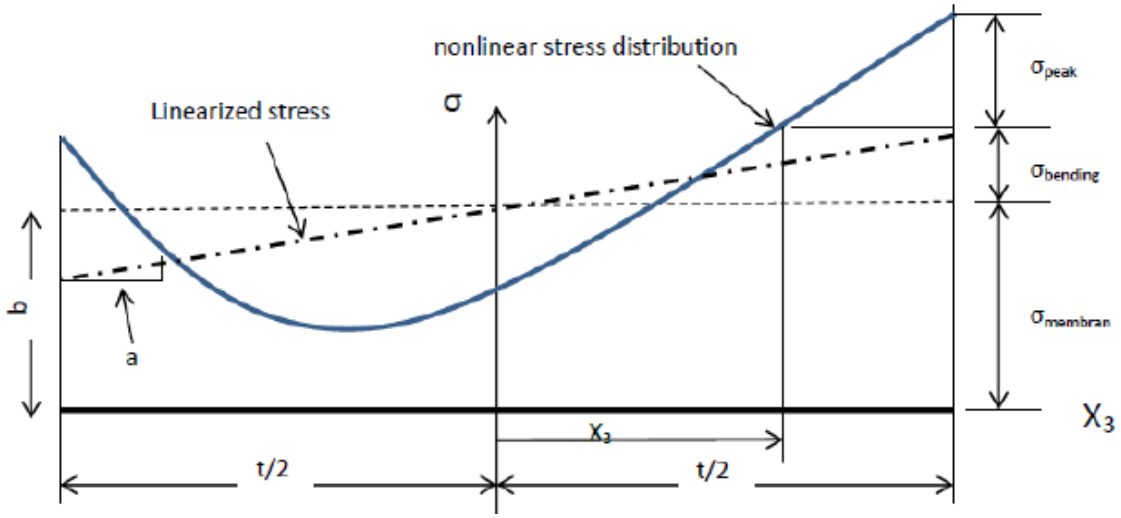

Fig (7.4): Typical stress distribution

The worst case of stress classification line(s) for ratcheting assessment was identified as a path through the junction between the tube sheet and channel side shell of the exchanger. This region is the most highly stressed part of the reactor, since tubesheet bending is additionally influenced by the upper shell action.

The stress distribution away from junction is linear; at the junction stress distribution has an additional nonlinear part. The stresses characteristics are primary membrane and primary bending away from the junction and local membrane and secondary bending and peak stress types at the junction. Due to intersecting geometries, a significant rise of the nonlinear part of the stress distribution at the junction occurs. This rise in stress dominates the magnitude of the total stress. The closeness of the outer tube limit zone to the groove radius location brings some local variation to this high stress region.

To understand how stresses are distributed at the junction, interpretations of stress paths are required. Stresses reported by paths above and below and away from junction are discussed first, and then the paths bounding the junction zone should be considered

for additional investigation. Figures (7.5) through (7.9) provide details with regard to tubesheet loading and considered stress zones, Fig (7.6) shows highest stress distribution zone is located at the junction of tubesheet to channel side shell. This high stress region is created as a result of dissimilar behaviours of tubesheet and channel side shell under pressure and temperature loading.

Temperature imposes larger displacement in comparison to pressure but stresses due to pressure have larger values. It should be noted that the values of thermal stresses are strongly affected by degree of the flexibility of various parts. Tubesheet movement is greatly affected by the movement of the tubes and attached shells. Tubes move up under temperature and few rows of them, close to the imperforated region, will bend as a result of the interaction of movement coming from the shells.

Under temperature loading only, tubesheet moves up uniformly except in the rim area close to and at the grooves. At these locations restriction come from adjoining shells. Under pressure loading only, tubesheet moves down (as a rigid body) except at the rim, the rim portion is dominated by rotation of the upper shell, which pushes the tubesheet in this region up. Rim of the tubesheet, which is extended below the upper shell, rotates slightly down due to the bending action enforced by the upper shell movement.

Upper shell extends itself in radial and axial directions. This displacement influences the tubesheet movement at and close to most of the regions. The lower shell with much lower pressure brings extra stiffness to the region, and it acts as a peripheral support for tubesheet, preventing adjoining tubesheet axial displacement in the region of attachment. Consequence of above actions is creation of high stress zone at the junction of tubesheet with upper shell, stress details regarding to this zone are provided in Fig (7.10-18).

Detail explanation of stresses magnitudes is provided in the below sections, schematic location of various path is provided in Fig (7.9).

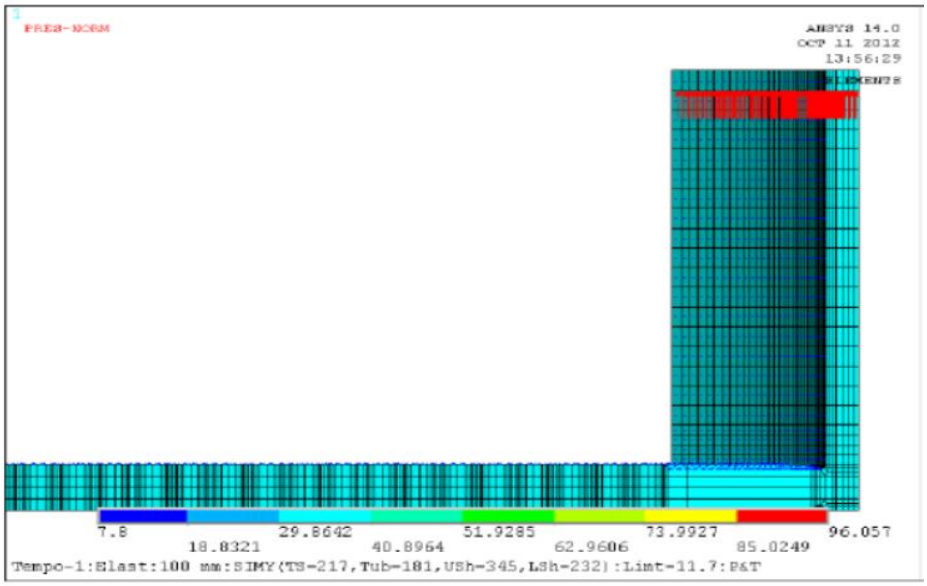

(7.5): End effect load

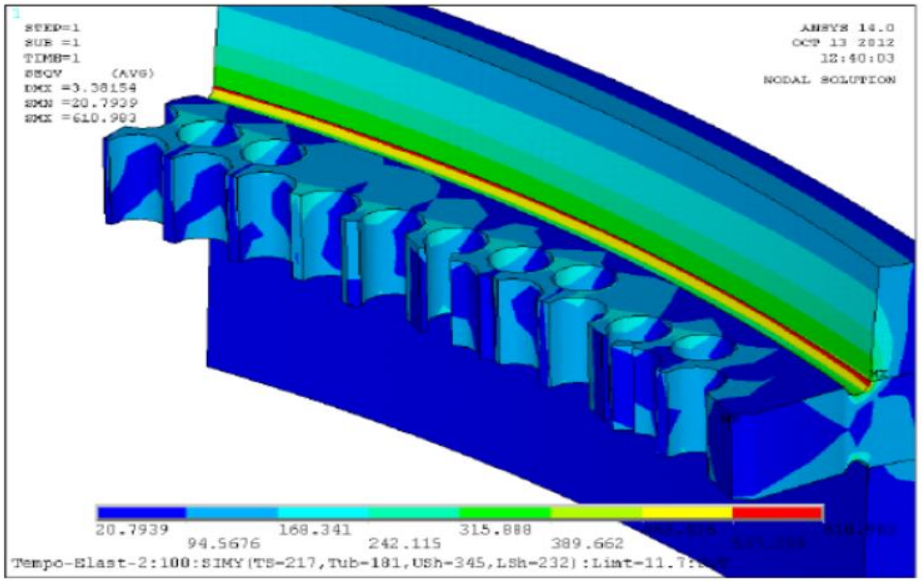

(7.6): High stress zone at the junction of tubesheet- channel side shell

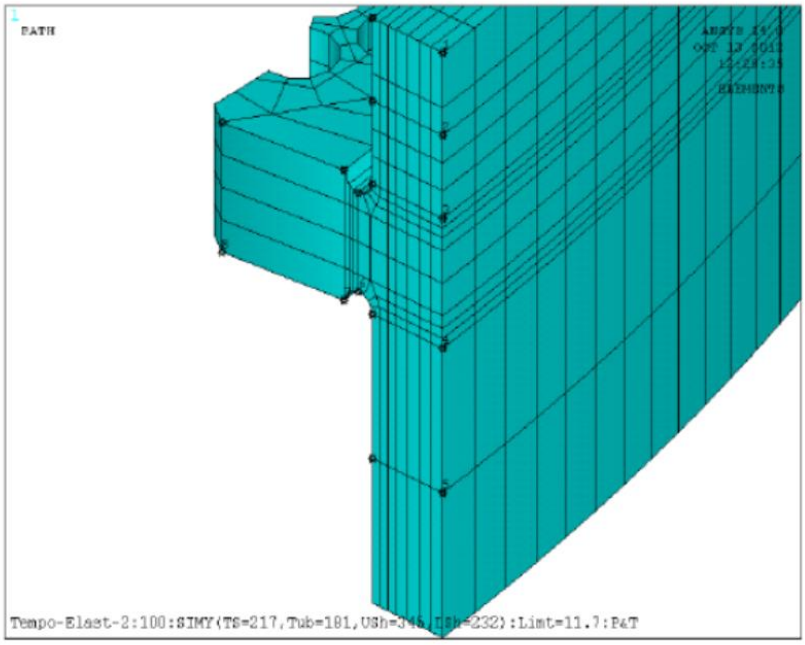

(7.7): Locations of path lines

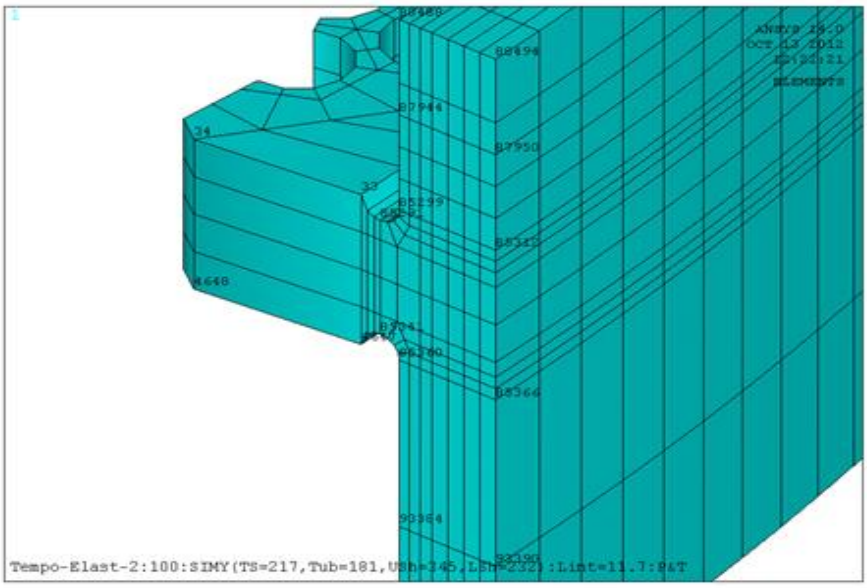

(7.8): Path nodes

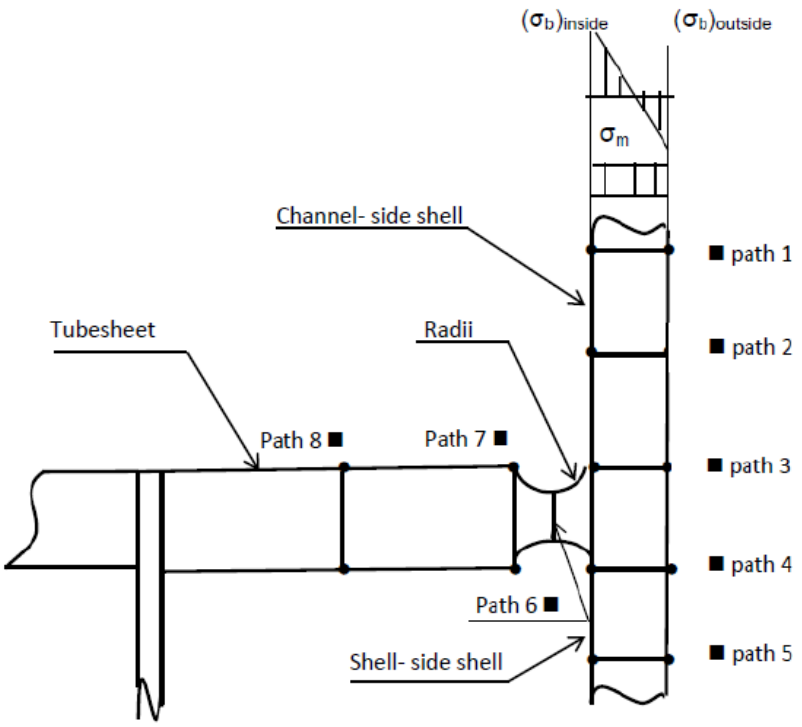

Fig (7.9): Paths model and schematic locations

Path 1 and 2 Fig (7.10-11), these paths are located above junction zone, close to the intersecting zone. Recalling ASME definition of general membrane and bending stresses, the membrane and bending stresses in theses paths are classified as the general primary type. It can be observed from Fig (7.10-11) that, across the thickness the membrane stresses have a uniform distribution and bending stresses have a characteristic linear distribution. These paths have been used to determine the changes in stresses in general and observe the trend of changes in membrane, bending and peak stresses in particular. The magnitude of membrane stresses do not (and should not) change from path 1 to path 2 and within each path, for both paths ($\sigma_m = 96$ MPa), this is so as membrane stresses do not require linearization since they are averaged across the thickness. Bending stress however shows differently, it has an increase from path 1 ($\sigma_m + \sigma_b = 132$ MPa) to path 2 ($\sigma_m + \sigma_b = 230$ MPa). This increase in membrane plus bending stress is associated with a pressure effect on the tube side (which acts on a

larger area for path 2 location in comparison with path 1) and that the path 2 is closer to the junction line, junction zone behaviour is dominated by a coupling. This coupling action is related to bending and comes in one way from channel side shell behaviour under pressure loading and in other way from tubesheet bending at its rim due to the pressure application.

Additionally, path 2 shows some non-linearity in bending distribution at the location close to the outside surface. This means that the linearization procedure has not been able to linearize bending stresses fully. Existence of some peak stresses can also be observed, this indicates that the actual stress distribution at this location has a degree of non-linearity in comparison with path1 stress distribution. Non linearity in stress distribution is a result of its closeness to the discontinuity region.

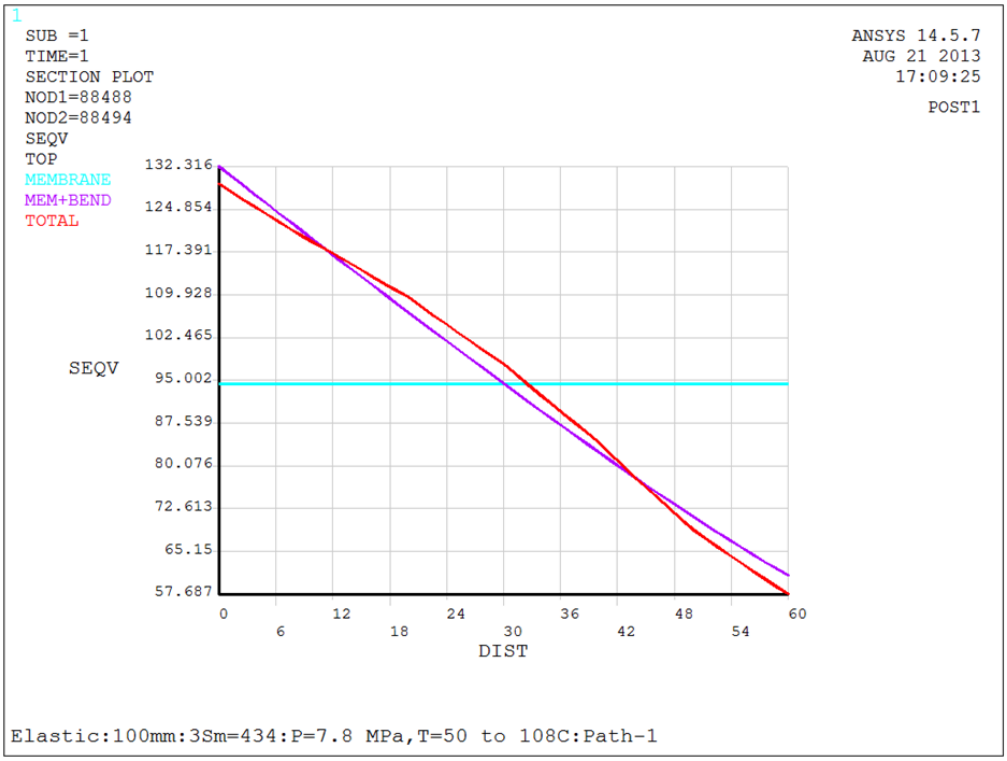

Fig (7.10): Mises equivalent of linearized stresses for path 1 from node 88488 to 88494

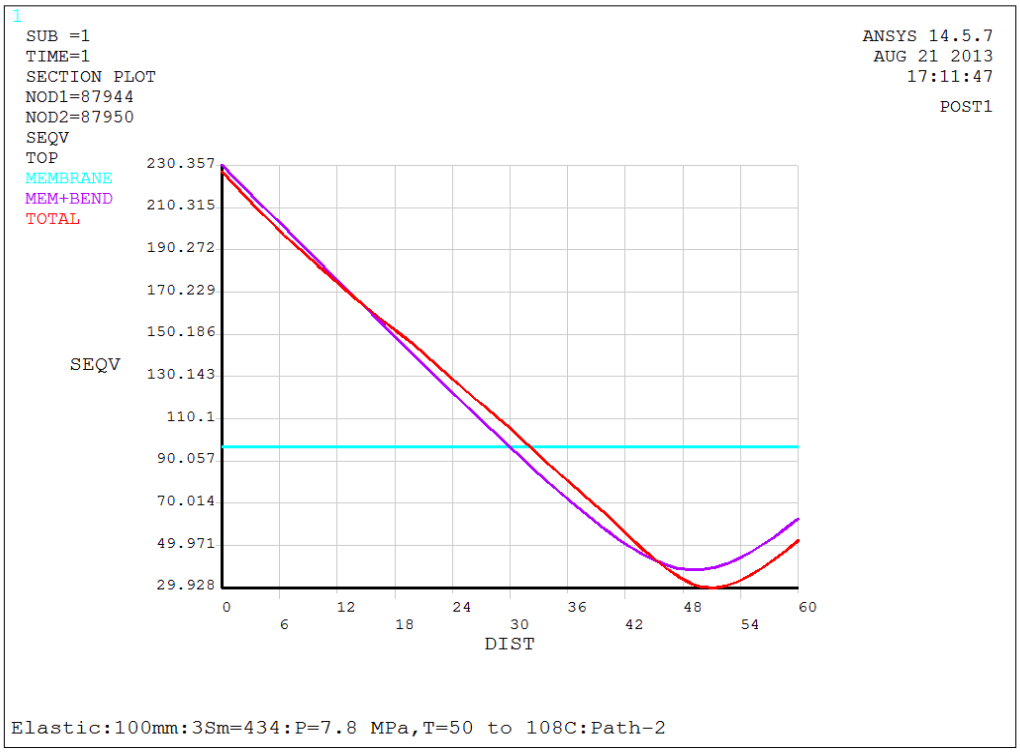

Fig (7.11): Linearized stresses for path 2 from node 87944 to 87950

Path 5, Fig (7.12), is located at the shell side below the tube sheet. Across this path constant membrane stress of ($\sigma_m = 67$ MPa) can be observed and bending stress has a small magnitude ($\sigma_m + \sigma_b = 68$ MPa). The bending stresses are affected by the junction geometry and do not have a linear distribution. Path 5 is not exposed to a significant pressure; transmitted bending due to action of junction zone is much smaller for this path. Additionally, formation of very small peak stresses can be observed.

It should be recalled that, the lower shell material is different from the tube sheet material, the lower shell actually plays no significant role in bending behaviour of the tubesheet apart from acting as a support for tubesheet at its outer rim. The lower shell for this exchanger is exposed to much lower pressure.

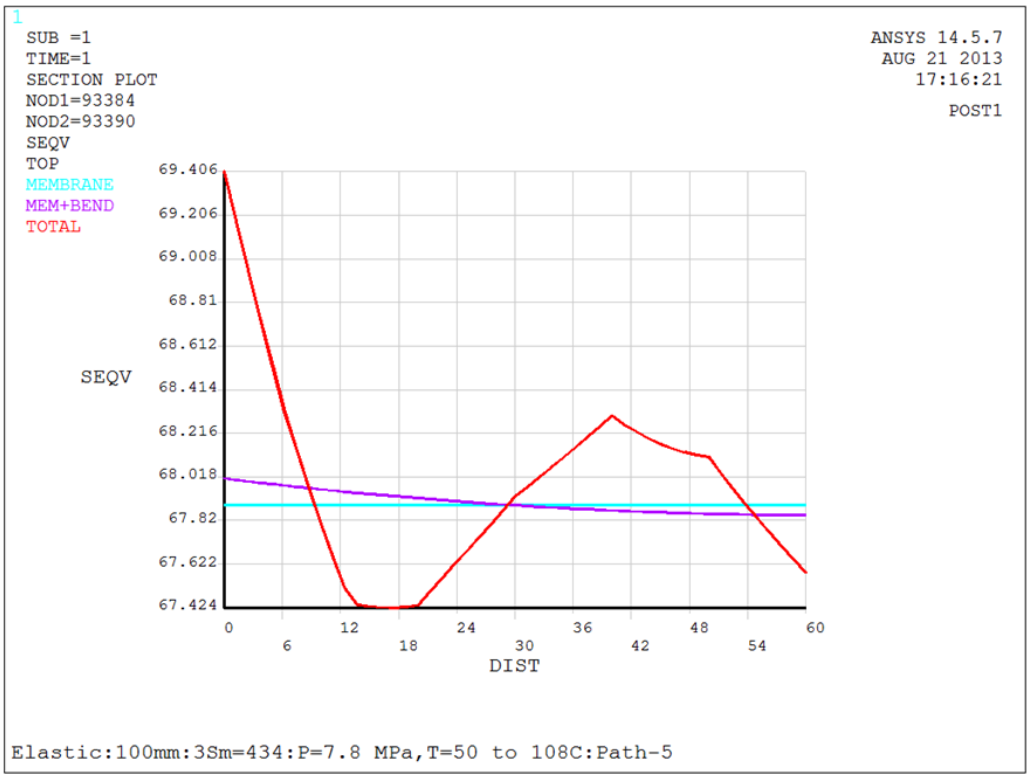

Fig (7.12): Mises equivalent of linearized stresses for path 5 from node 93384 to 93390

Path 8, Fig (7.13), is located away from junction zone on tubesheet side. For this path the membrane stress is ($\sigma_m = 34$ MPa) and bending stress has larger value in comparison to path5, ($\sigma_m + \sigma_b = 93$ MPa). These values are much smaller than the channel side shell membrane and bending stresses, this is so as the tubesheet is much thicker (100mm) than channel side shell (60 mm), furthermore, stresses at this location are also affected by tubes staying action.

For path 5, load causing the membrane stress is perpendicular to the thickness, i.e., it is an in-plane force, generated by internal reaction due to the junction zone behaviour. It is not generated directly by pressure; rather it is a consequence of pressure application on the junction zone and requirement of compatibility.

Bending behaviour in this location comes both from junction zone bending and tubesheet rim bending; it also receives some minor effect from bending of the tubes close to this path. There exists no peak stresses at this path, as it is away from junction; lack of peak stress means the stress distribution at this location is linear.

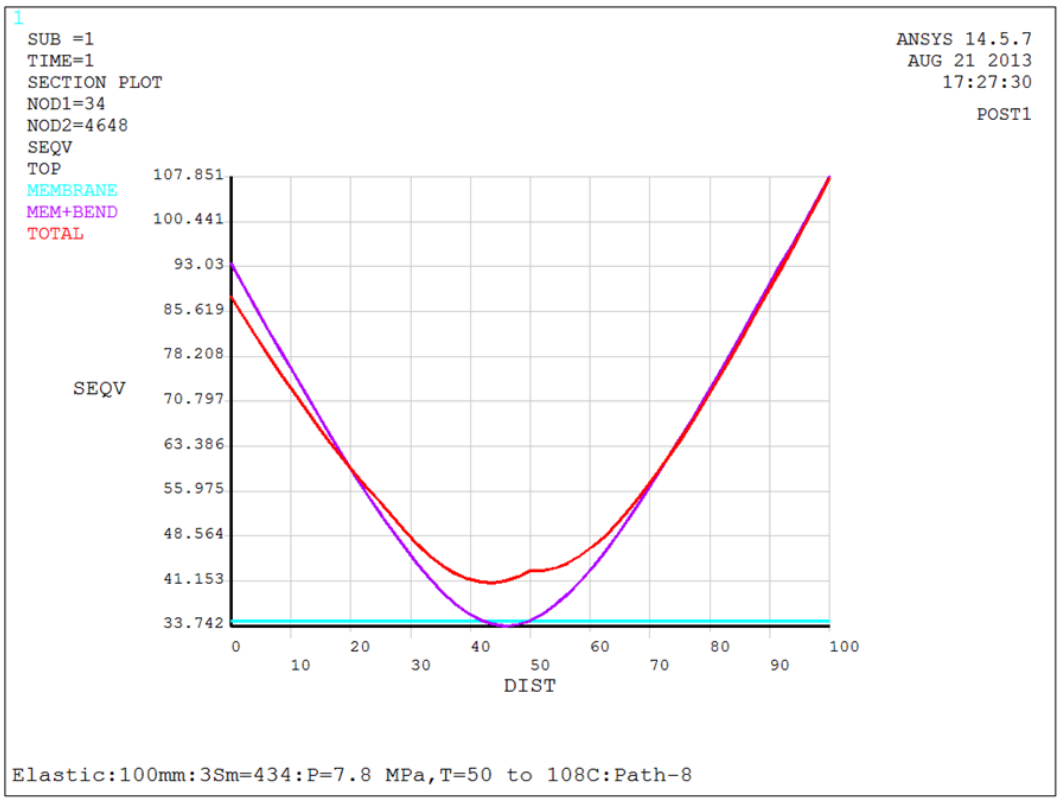

Fig (7.13) Mises equivalent of linearized stresses for path 8 from node 34 to 4648

Paths 3, 4, 6 and 7, Fig (7.14-17), are junction zone paths. They encompass the junction zone geometry and therefore their study provides adequate information on how the stresses are formed at the junction zone.

The membrane stresses of paths 3 and 4 (path 3 is directly above path 4 at upper face of the tubesheet) are 87 and 97 MPa with uniform distribution. The differences in magnitude are due to different material properties and the fact that these paths are not subject to the same in-plane force. The requirement on equilibrium of forces and compatibility of strains at either side of the junction of the tubesheet with attaching shells are causes of difference between in - plane forces. This will result in different membrane stress; however, the difference is small.

However, bending stresses are quite different, In path 3, the bending plus membrane stress is ($\sigma_m + \sigma_b = 315$ MPa) at the inside node, while for path 4 their magnitude is ($\sigma_m + \sigma_b = 97$ MPa). This difference comes from the fact that localized bending has

much larger value at the bottom of the channel shell in comparison with the lower shell. This is so as action of pressure on the channel side shell dominates the bending behaviour of the junction. Existence of very large peak stress ($\sigma_{total} = 498$ MPa) indicates that highly nonlinear stress distribution is formed in path 3 location. Path 3 is located at the edge of the junction of radii and channel side shell with a consequence of largest total stress in the system.

Path 7, being in tubesheet side of the radii, has membrane stress ($\sigma_m = 51$ MPa) and ($\sigma_m + \sigma_b = 147$ MPa). Both of these values are larger than the values noted for path 8. This is due to the location of this path, which is at the edge of the groove. The tubesheet rim bending as a result of pressure is larger at this path location (due to existence of the rim area), the membrane force for this path is dictated by compatibility condition and equilibrium requirement.

Path 6 is at the bottom of the radii. This path has membrane stress ($\sigma_m = 56$ MPa) and membrane plus bending stress is ($\sigma_m + \sigma_b = 230$ MPa).The membrane stress shows an increase in comparison with its value in path 7 since tubesheet is thinner at this section. Peak stresses at this location is also high, this is an indication of larger degree of nonlinearity in stress distribution in comparison to Path 7.

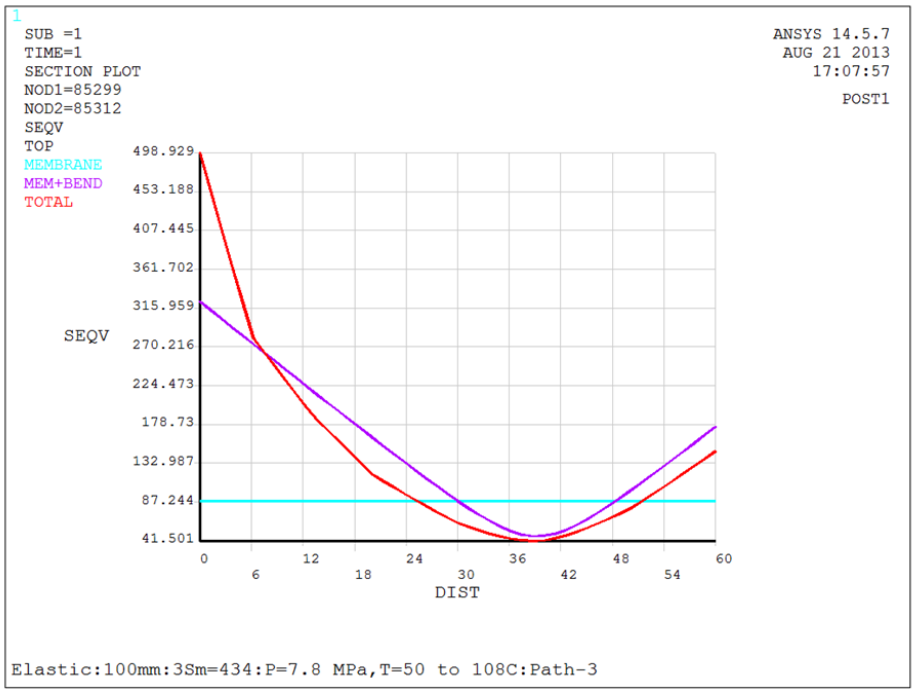

Fig (7.14) Mises equivalent of linearized stresses for path 3 from node 85299 to 85312

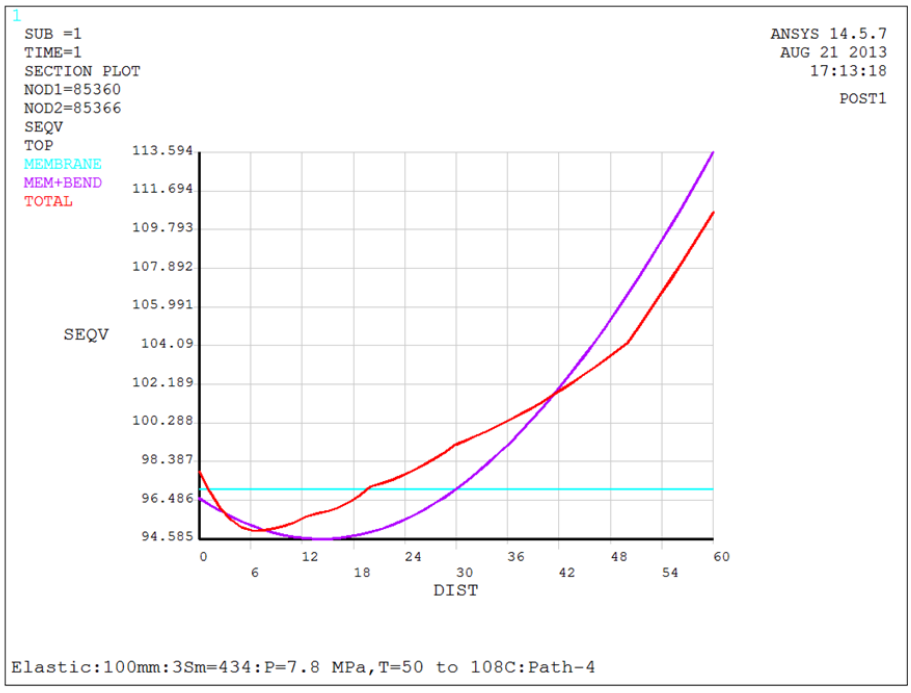

Fig (7.15) Mises equivalent of linearized stresses for path 4 from node 85360 to 85366

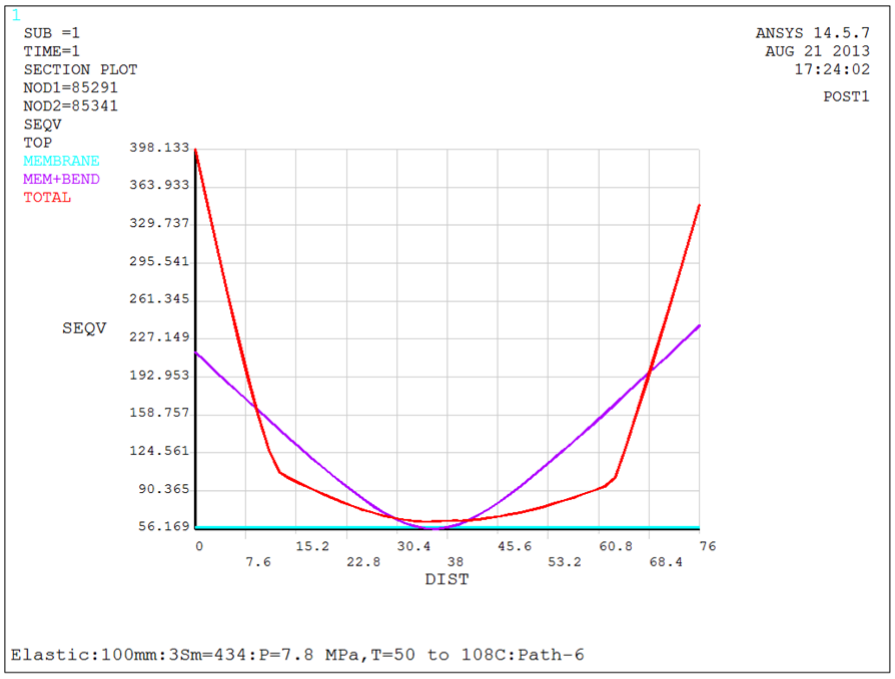

Fig (7.16) Mises equivalent of linearized stresses for path 6 from node 85291 to 85341

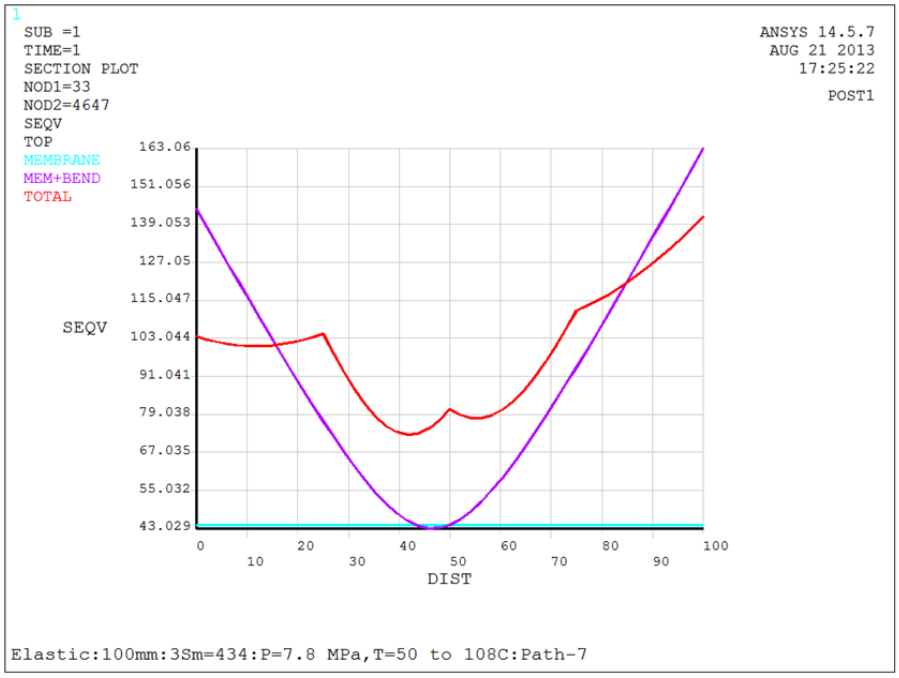

Fig (7.17) Mises equivalent of linearized stresses for path 7 from node 33 to 4467

Path 3, being located at the junction of tubesheet to channel side shell, depicts detail information in regard to the state of stress at this junction zone. Linearized equivalent

stress plots for pressure 7.8MPa and 8.53MPa are shown in Figure (7.18a) and Figure (7.18b) respectively. The nonlinear component of stress through thickness is by default listed as a peak stress by the ANSYS linearization post-processor. Peak stress is associated with local stress concentration effects and is not included in ratcheting assessment, therefore, the combined membrane and bending stresses only should be considered.

Non-linear through thickness stress distributions may also arise in thick components and at global structural discontinuities, due to structural equilibrium and compatibility requirements, and in such cases they are associated with primary and primary plus secondary stress. However, in this assessment since the solid elements (and not shell elements) have been employed the nonlinear component of stress is treated wholly as peak stress. The stress linearization plots of Figure (7.18) show that there is a high peak stress at the groove around the inside surface of the vessel. The effect of peak stress is observed through thickness to around 10% of the length of the stress classification line.

The maximum linearized membrane plus bending equivalent stress was found to be 323.6 MPa for p=7.8 MPa and 353.2 MPa for p= 8.53 MPa. The $3S_m$ limit for tube sheet material is 434 MPa. Therefore, the elastic analysis ratcheting criterion is satisfied for both pressure considered indicating that shakedown has occurred. Further, the presence of significant peak stress indicates that vessel experience plastic shakedown for the loads considered, rather than elastic shakedown.

Lists of stresses associated with various paths as discussed above are provided in Tables (7.1) and (7.2).

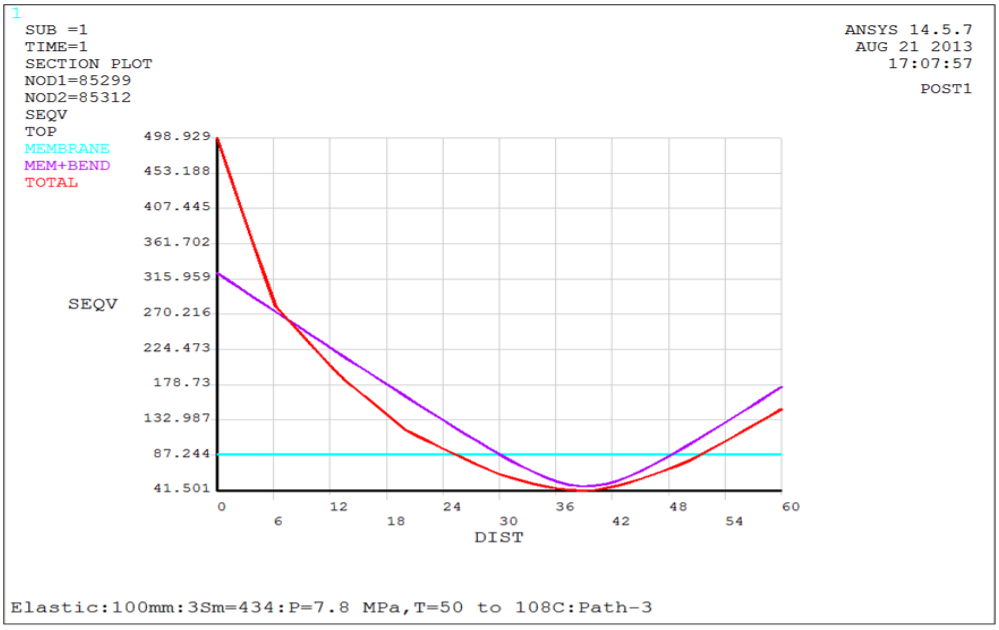

(a)

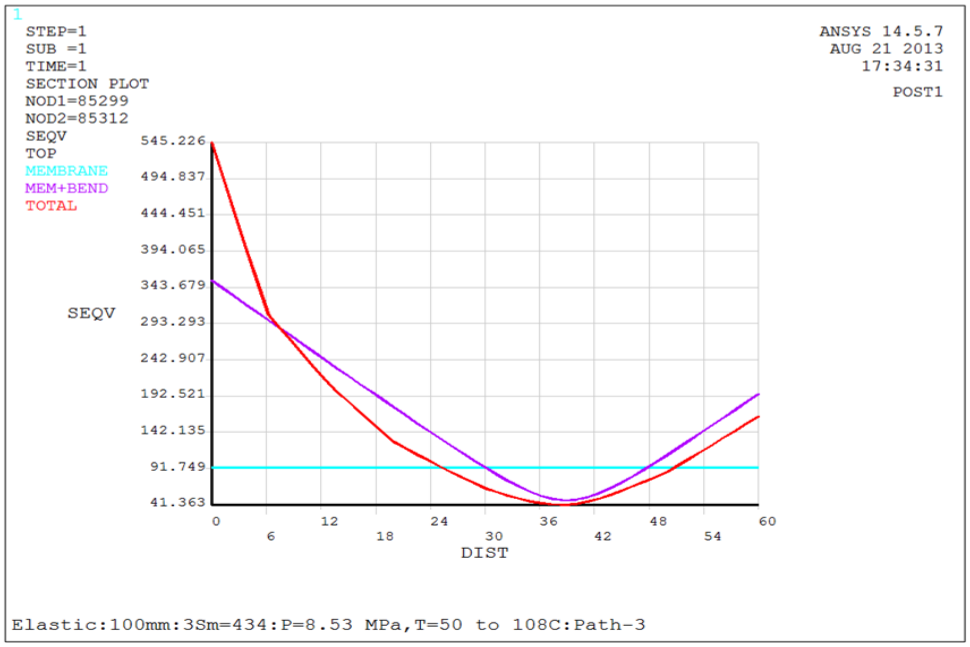

(b)

Fig (7.18): Total and linearized Mises equivalent of stress distribution along stress classification path 3, (a) P= 7.8 MPa, (b) P= 8.53 MPa. Path 3 is between nodes 85299 and 85312.
Note: The blue line is membrane stress, purple line is membrane plus bending for top layer and read line is total stress, stresses are plotted across thickness of 60 mm.

Table (7.1): Membrane, bending and total stresses for path 1 to 8, P=7.8 MPa

Path	**From**	**To**	**Through thickness location**	σ_m	$\sigma_m + \sigma_b$	σ_{total}
1	88488	88494	channel above junction	95	147.2	145
2	87944	87950	channel above junction	100	230.3	228
3	85229	85312	channel radii junction	87.2	315.9	498.9
4	85360	85366	shell-radii junction	97.2	113.5	110
5	93384	93390	shell below junction	67.96	68.1	69.57
6	85291	85341	bottom of channel side radii to top of shell side radii	56.2	210.3	398.6
7	33	4647	tubesheet top radii to bottom radii	51.3	167.3	144.05
8	34	4648	tubesheet close to radii	31.5	86	103.1

Table (7.2): Linearized stresses for path 3 between nodes 85299& 85312

Pressure (MPa)	σ_m	σ_b	$\sigma_m + \sigma_b$	σ_{peak}	σ_{total}
7.8	88.51	245	323.6	180.8	498.9
8.53	93.16	269.8	353.2	197.4	545.2

7.4 Cyclic analysis- Elastic Perfect Plastic

The reactor response to full start up and shout down conditions is considered in this Section. The pressure and temperature loads are proportionally cycled from their ambient conditions (start-up) to their operating magnitudes and from their operating values back to the ambient state (shut down), Fig. (7.19, 20) depict the load cycles.

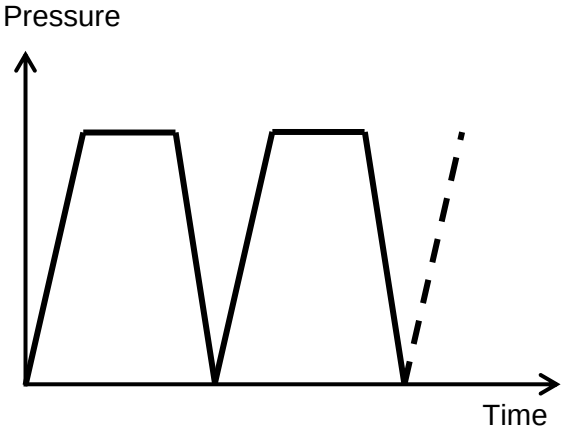

Fig (7.19): Pressure load

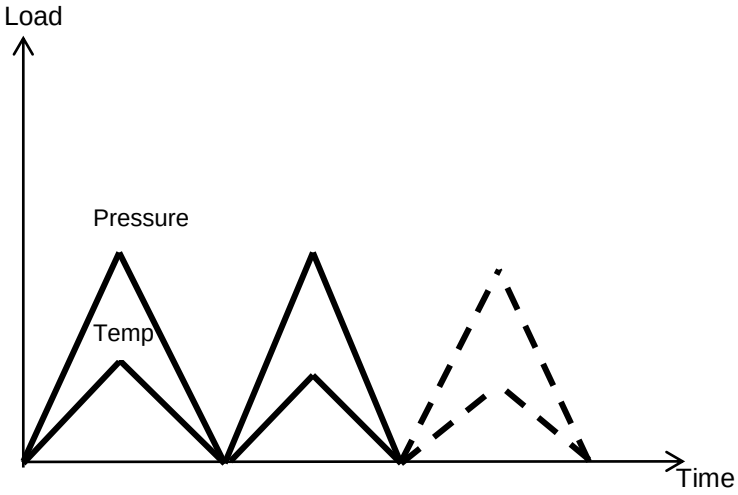

Fig (7.20): Loads Cycles

Following plots have been provided for node 86616; this node is located at a high stress region just below the junction of tubesheet to channel side shell. Fig (7.21) shows this node location.

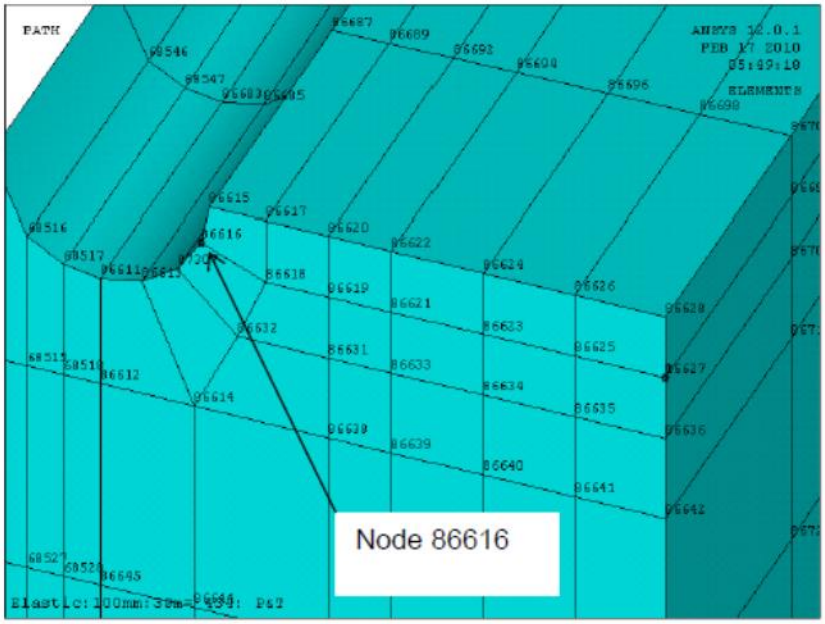

Fig (7.21): Location of node 86616

Small deformation theory and elastic-perfectly plastic analysis was applied for a sufficient number of cycles to capture the cyclic-plasticity response, typically up to 100. For 10 full cycles (20 half cycles) of the applied temperature distribution and pressure of 7.8 MPa, the von Mises equivalent plastic strain accumulation is shown in Fig (7.22a). The analysis was repeated for 3 full cycles of the applied temperature distribution and P= 8.53 MPa. The equivalent plastic strain accumulation is shown in Fig. (7.22b).

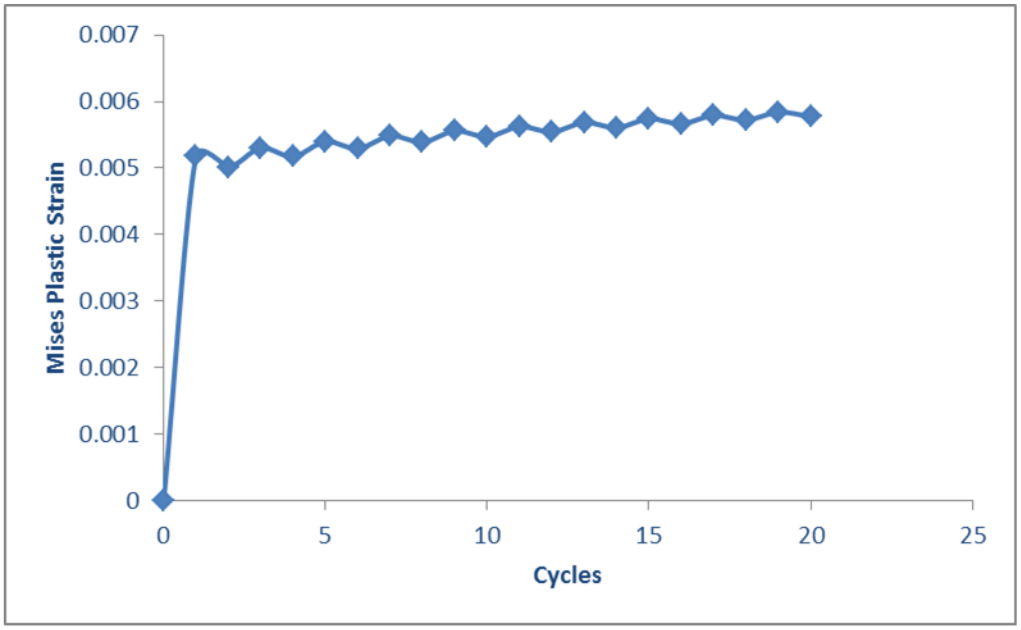

(A)

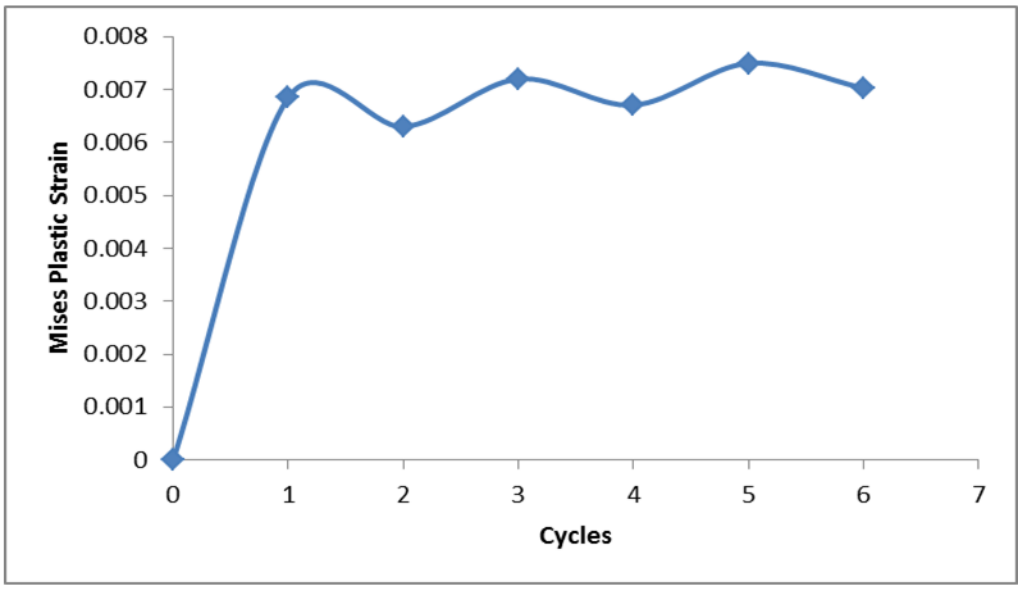

(B)

Fig (7.22): Small deformation theory with elastic-perfect plastic under applied temperature distribution and (a) P= 7.8 MPa, 20 half cycles and (b) P=8.53 MPa, 6 half cycles . Node 86616

Figure (7.22) shows that the vessel experiences incremental growth in plastic strain, i.e. ratcheting, for up to the 10 cycles modelled. The strain increments are very small, as would be the total plastic strain accumulation over the 50 full cycle life of the component

and the design can be accepted as fit for purpose on that basis. However, the underlying ratcheting failure mechanism differs from the plastic shakedown mechanism implicit in the elastic analysis and stress categorization analysis. This suggests that the nonlinearity stress identified in the stress linearization procedure is not wholly peak stress.

7.5 Cyclic analysis-Linear, Multilinear Isotropic and Linear Kinematic Hardening

The post yield cyclic behaviour simulated in a finite element analysis is dependent on the material model used in the analysis. In the static analysis of the heat-exchanger presented here both isotropic and kinematic models were considered.

Material models in form of linear, multilinear isotropic hardening and linear kinematic hardenings are not suitable in ratcheting analysis as use of these models always result in adaptation to a shakedown response; this is due to the expanding yield surface for case of isotropic hardening, and due to unbounded stress-strain curve (0.1% continuous slope) for linear kinematic case. Plots indicating shakedown under these types of material modelling are provided below. It should be added that, for above material models, usually after the first cycle under pure load control or after several cycles under displacement control shakedown occurs. Figures (7.23) through (7.28) illustrate this feature. The adaptation to shakedown mode for multilinear case occurred after a few cycles.

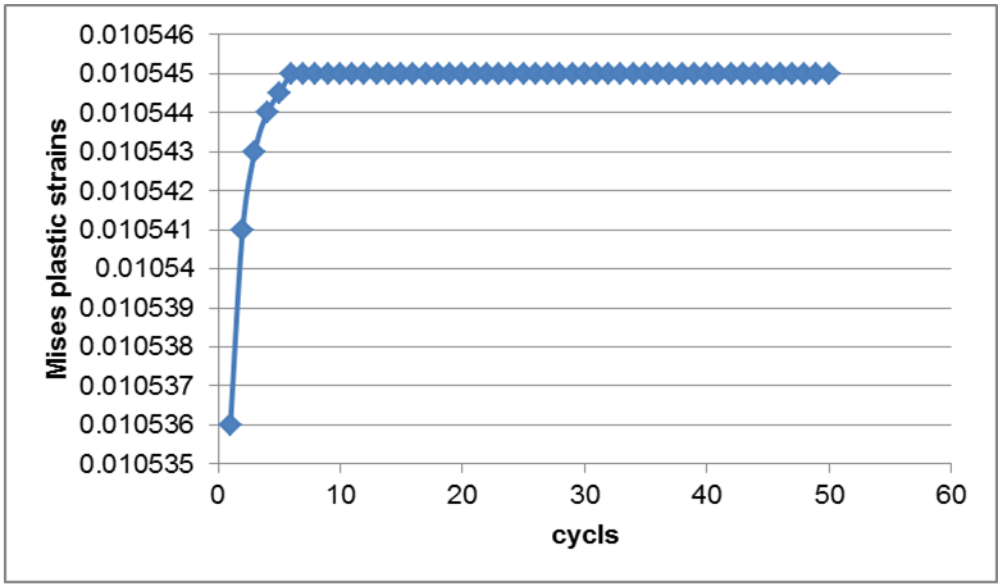

Fig (7.23): Mises plastic strain, 50 full cycles, linear isotropic, slope=0.1, node 86616.

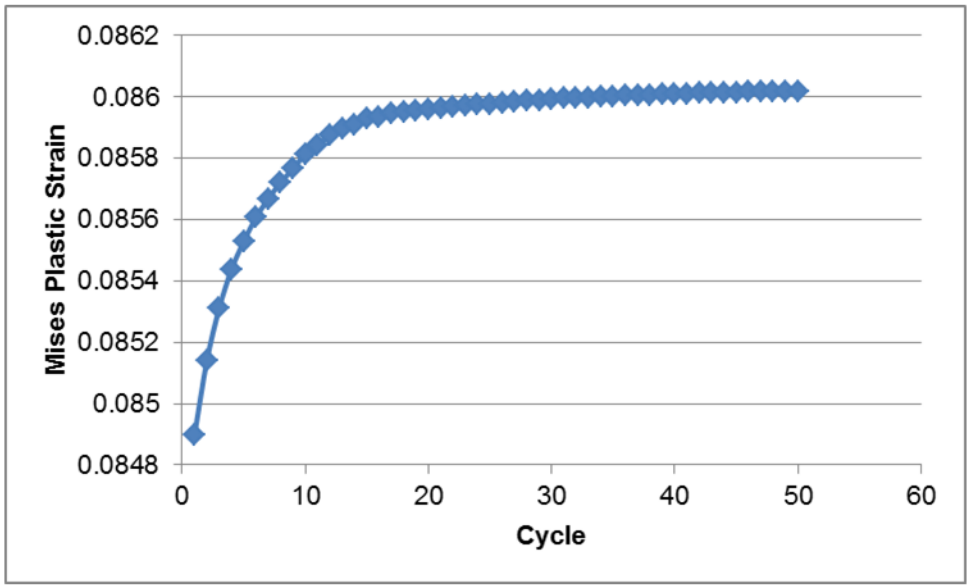

Fig (7.24): Mises plastic strain, 50 full cycles, multilinear isotropic, node 86616

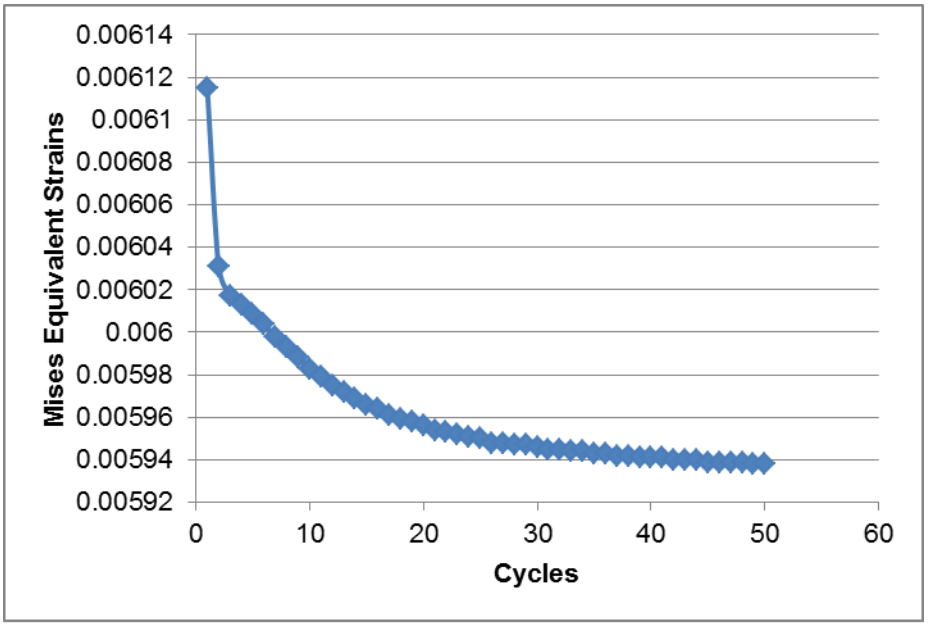

Fig (7.25): Mises plastic strain, 50 full cycles, linear kinematic, slope=0.1, node 86616

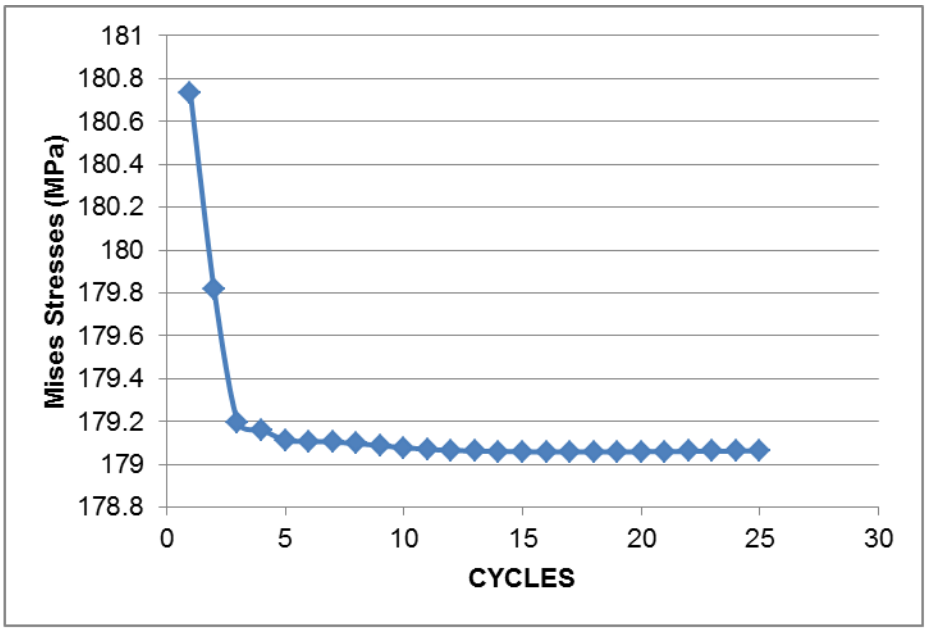

Fig (7.26): Mises residual stress, 50 full cycles, linear kinematic, node 86616

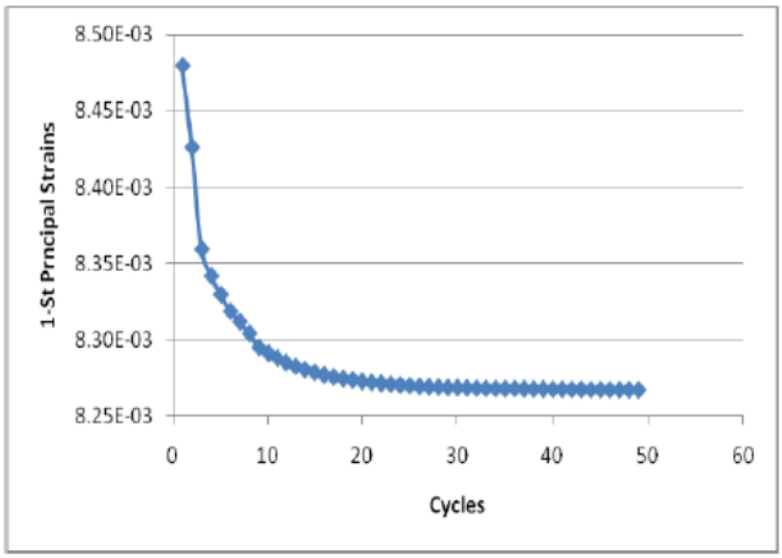

Fig (7.27): 1-St principal plastic strain, linear kinematic, slope= 0.1, 50 full cycles, node 86616

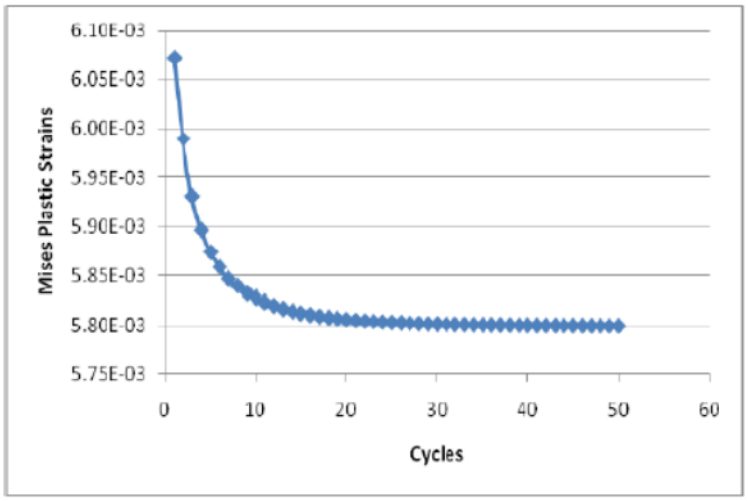

Fig (7.28): Mises residual plastic strain, linear kinematic, slope= 0.1, 50 full cycles, node 86616

7.7 Cyclic Analysis- Multilinear Kinematic Hardening

The effect of material strain hardening on the cyclic response was investigated by performing elastic-plastic analysis using the ASME strain hardening material model. The equivalent strain accumulation for the applied temperature and P=7.8MPa is shown in Figure (7.29). In this analysis, the vessel exhibits plastic strain accumulation during the first 5 full cycles, after which the behaviour shakes down to alternating plastic strain without further strain accumulation. A similar response was observed for a cyclic pressure of 8.53MPa.

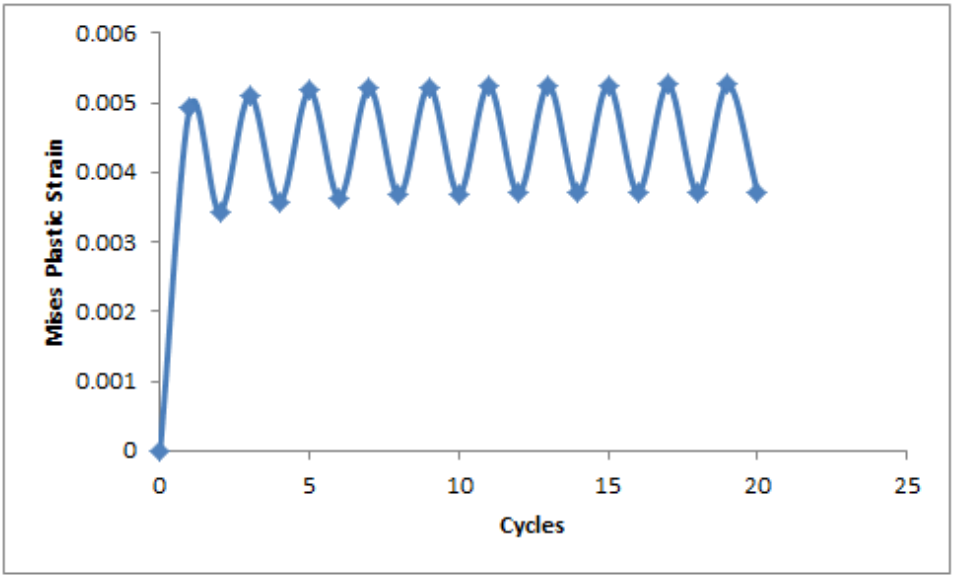

Fig (7.9): Small deformation theory, strain hardening response under applied temperature distribution. P=7.8 MPa. Node 86616

Permanent deformation of the component is, obviously, correspondingly small. Figure (7.30A) shows the deformation of the highest loaded point in the vessel, at the junction between the tube-sheet and the channel side shell, given by elastic-perfectly plastic analysis. The permanent deformation is seen to increase for the first 10 full cycles and continues to increase in subsequent cycles. Figure (7.30B) shows the deformation of the

same point given by strain hardening analysis. Deformation increases for the first 6 cycles but thereafter no further permanent deformation occurs.

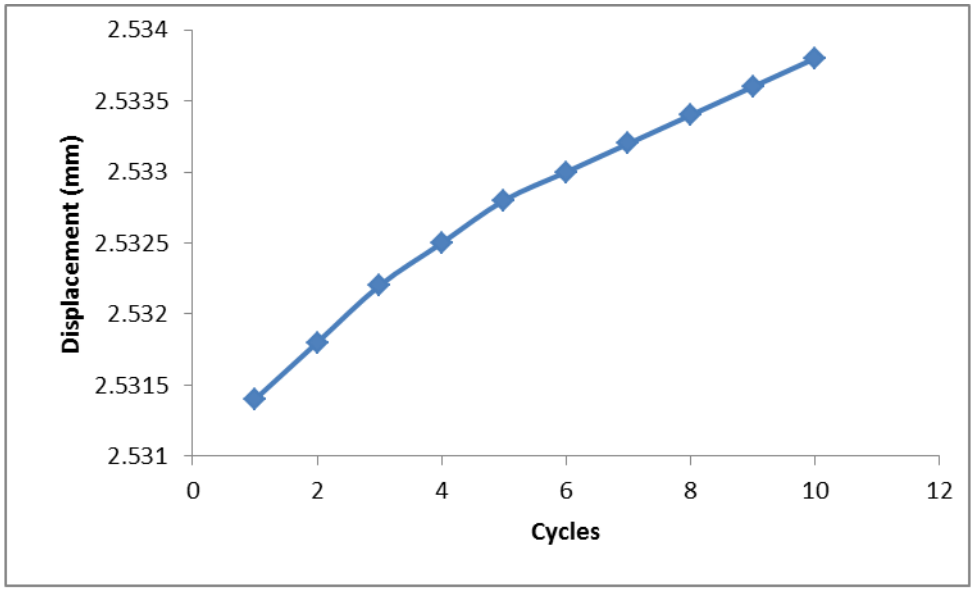

(A)

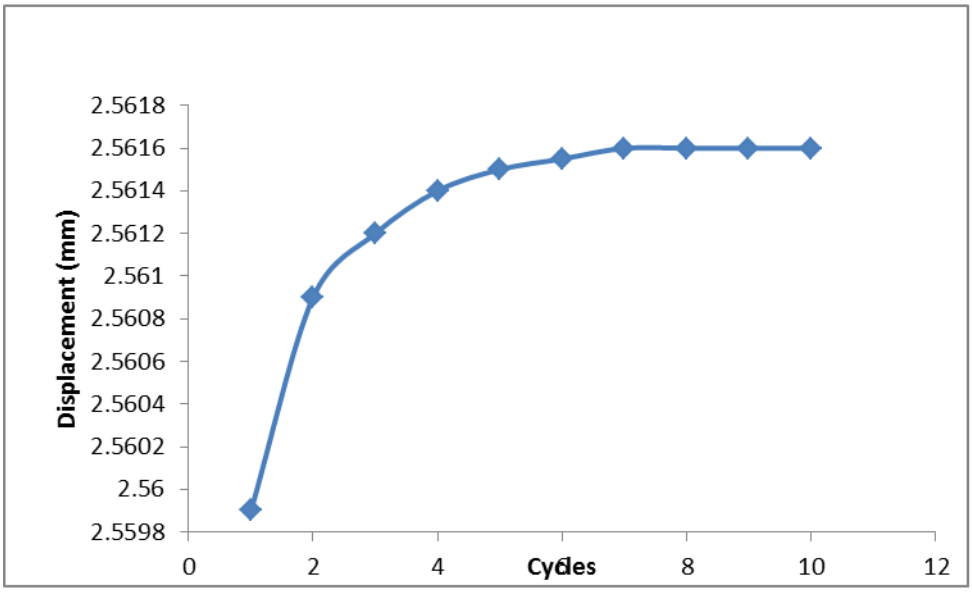

(B)

Fig (7.30): Deformation of high stress point at intersection etween tubesheet and chanellside shell (A) elastic -perfect plastic, (B) strain hardening

7.7 Elastic Core Calculations

The elastic core method as suggested by Kalnins [32] can be a simple way to assess shakedown. According to Kalnins, a structure cannot experience incremental collapse as long as a continuous elastic core in the structure that exists throughout the load cycle supports the applied loads. The elastic core method is mostly suitable for parts that experience occurrence of plastic cycling in a localized region.

Figure (7.31) below indicates location of through thickness nodes for linear kinematic, existence of elastic core is demonstrated in the following figures (7.32, 33). Plots are thickness vs. plastic strains.

Very high strain gradient at the edge of the elements located at the junction of tube sheet to channel side shell intersection can be observed. The finer mesh may indicate higher value, however, in this case the interest is to show the existence of the elastic core where the stress distribution is almost constant and the mesh in this region is appropriate.

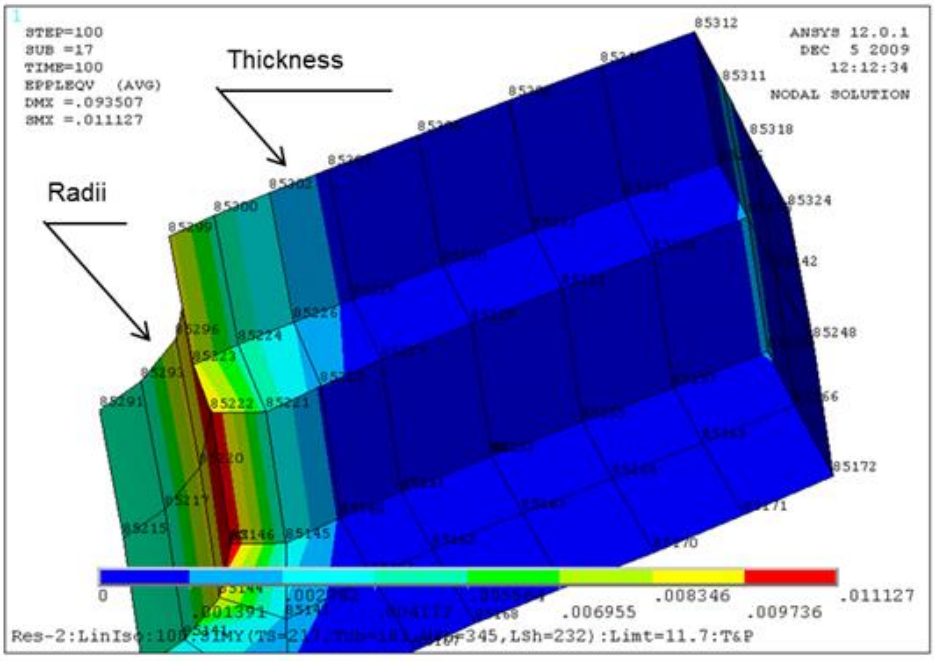

Fig (7.31): Through thickness nodes locations

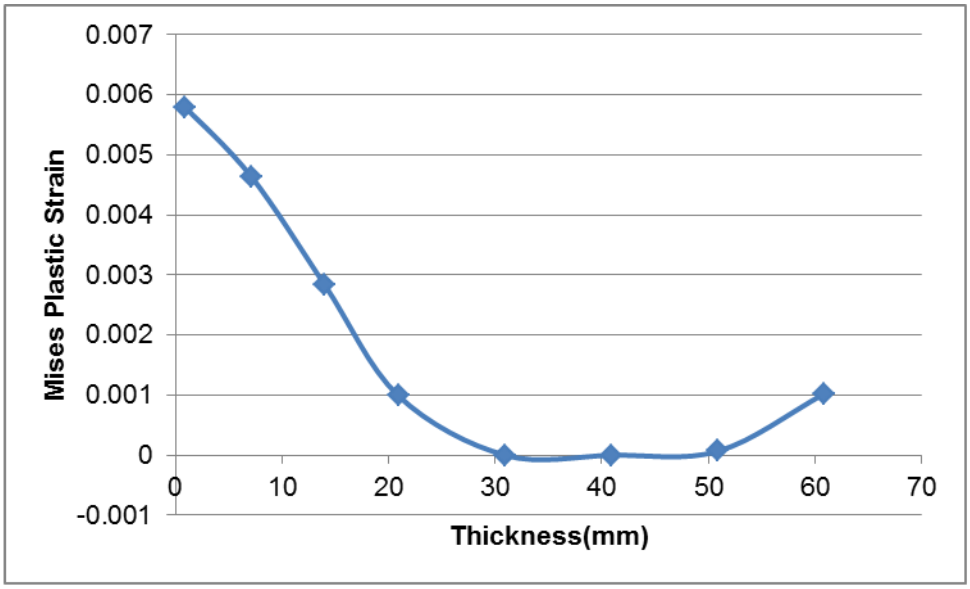

Fig (7.32): Elastic core, 50 cycles, linear kinematic

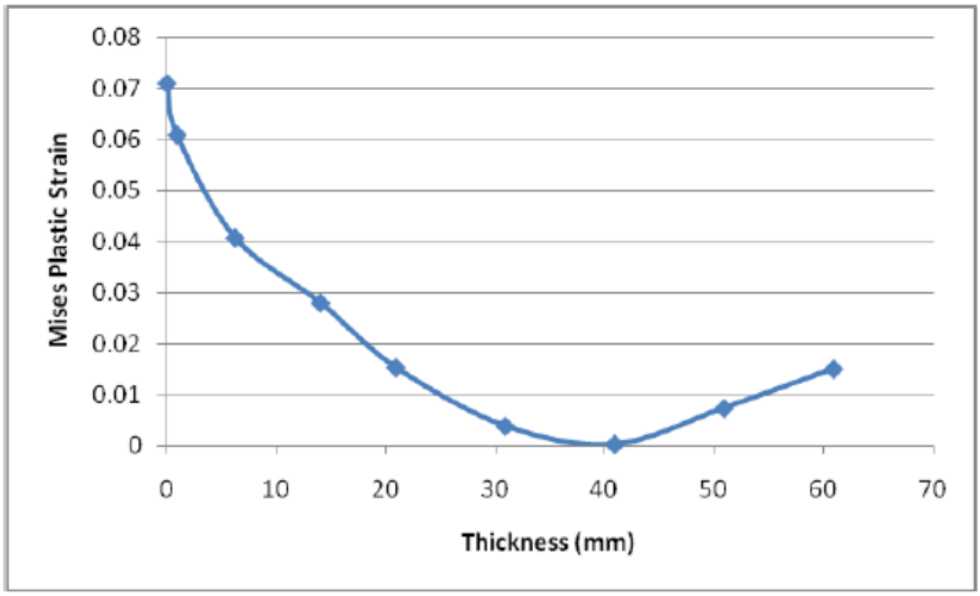

Fig (7.33): Elastic core, 50 cycles, multilinear kinematic

7.8 Results

Tubesheet response of a fixed tubesheet heat exchanger under reduced thickness has been calculated, tubesheet is subject to cyclic load arising from start-up and shutdown conditions and analysed using various material hardening models. The material models considered are elastic, elastic-perfectly plastic and linear and multilinear hardening. The results of these analyses are summarised in Table 7.3.

Table (7.3): Results of calculations according to various material model

Material Model	Classification	ASME criteria	Notes
Elastic	Plastic shakedown	Satisfied $3S_m$	Significant peak stress
Elastic-perfect plastic	Ratcheting	Small rate of plastic strain growth	Results after 50 cycles
Linear& Multilinear Isotropic	Shakedown	-	Shakedown always occurs with these models
Linear Kinematic	Shakedown	-	After few cycles
Multilinear Kinematic	Plastic shakedown	-	Shakedown to alternating plasticity after 5 full cycles

Referring to table (7.3) the following conclusions can be stated:

- In the ASME elastic route (with stress linearization), the nonlinear part of stress distribution is always treated as peak stress. In reality, part of this peak stress is secondary membrane plus bending. These stresses come to existence due to the equilibrium and compatibility requirements at the junction.

As ratcheting assessment should not include peak stress, only combined membrane and bending stresses should be considered. In this case, it is concluded that the actual magnitude of combined membrane and bending is larger than the values reported by the post possessor. This conclusion indicates that usage of $3S_m$ method can be non-conservative in practice.

- The ASME elastic-perfect plastic material model incorrectly predicted ratcheting behaviour for the tubesheet model. If ASME guidelines are followed, a tubesheet of thicker section would be required. More detailed analysis indicates that this is not justified.

- The multilinear kinematic hardening material model used in this work indicates shakedown to cyclic plasticity. As the magnitude of plastic strains is small, adapting the design to this kind of material model will result to thinner section.

- The linear kinematic hardening and linear-multilinear isotropic hardening material models incorrectly predict shakedown as they are not capable of predicting the actual and correct behaviour of the tubesheet. These rules should not, therefore, be used in direct route design by analysis ratcheting checks.

7.9 Conclusion

Calculations based on elastic analysis have been performed through study of combined membrane and bending stresses at the vicinity of the junction of tubesheet to channel side shell under pressure, temperature and reaction due to end head effect. This junction zone is exposed to large bending and membrane stresses in comparison with other parts of the exchanger. Stresses have been linearized near and at the vicinity of the junction to observe and eliminate the magnitude of the peak stresses and the remaining portion of stresses have been verified against the Code $3S_m$ limit. Identification of linearized stresses for application of the elastic shakedown theorem is a mandatory requirement; elastic shakedown relies on magnitude of linearized stresses only and therefore is sensitive to correct identification of secondary stresses.

Linearization of stresses at the junction of tubesheet to channel side shell shows the existence of large local peak stresses. It is noted that, procedure for linearization of solid

elements treats any remaining stresses which are not classified as membrane or bending stresses as peak stress. In this case, not all of what is classified as peak stress is entirely peak stress. Investigation of the effect of localized peak stresses has been carried out in Chapter 8 of this Thesis in the form of fatigue study.

Cyclic calculations have been performed by changing material model to elastic-perfectly plastic model. To observe and trace the growth of local strains, 100 half cycles of loads have been imposed to the geometry. The growth of local plastic strain is observed by presenting plot of number of cycles against Mises plastic strains, in this regard ratcheting type behavior has been noted.

Elastic and elastic- perfectly plastic material models are recommended by ASME. To extend the ASME procedure, calculations have been carried out by considering linear and multilinear isotropic and linear and multilinear kinematic hardening for various numbers of cycles. For multilinear kinematic hardening, 100 half cycles is considered and based on the plot of number of cycles against Mises plastic strain it has been observed that after initial ratcheting the cycle will stabilize with small amount of plastic strain. This has revealed the fact that use of elastic- perfectly plastic material as it is suggested by ASME predicts the tubesheet response to cyclic loading incorrectly. Moreover, to comply with additional ASME requirement existence of elastic core has been proved, this has been done for the case of Multilinear kinematic material model, plots showing variation of through thickness plastic strains are provided.

8. Fatigue Failure

Fixed tubesheet exchangers are normally designed for steady state steady flow operation. However, startup, shutdowns, shifts from operating mode, upsets and emergency shutdowns will expose this type of equipment to cyclic loads. It is therefore essential to ensure that the equipment can tolerate these changes in operating load without fatigue failure occurring. This Chapter considers determination of the fatigue life of a fixed tube-sheet exchange with reduced tube-sheet thickness using three different procedures:

1. Stress Life.
2. Local Strain.
3. Experimental Equations.

To deal with fatigue issue, the various operating modes of the heat exchange are defined. For purpose of this study, two cyclic sets are defined. Each cyclic set covers four different load cases.

8.1 Exchanger Operating Modes

The fatigue life of the fixed tubesheet and their junctions depends on the changes in action parameters (pressure and temperature). Small but continuous fluctuations, large periodic changes, partial or full scheduled and unscheduled shutdowns can substantially affect the useful life of this type of equipment. These operating modes and their consequences on fatigue life depend on how the units and plant is operated; i.e., proper operational management from this prospective can lead to a prolonged fatigue life by eliminating the number of periodic or non-periodic cycles which these exchangers can be exposed to.

Setting up a common load-unload mechanism in the form of the periodic and non-periodic spectral data for design purposes can be difficult to achieve, however, some collected data or standard recommendations can be employed. Designing a tube sheet to shell junction and its attachment weld for the above fluctuating actions requires special attention. Following suggested procedures as given in the various standards

[Refs. (1,4)] can lead to over conservative values of the required component dimensions, resulting in considerable increase in equipment cost.

According to the data sheet of the reactor Ref., [54] the reactor operating mode is based on a steady state steady flow parameter. However, due to the process upsets or process needs, the reactor sometimes shifts to different pressure/ temperature states. This is accomplished through proportional loading, i.e., the exchanger is not subject to different gradients of temperature under constant pressure load, rather the pressure and temperature both changes slowly and simultaneously.

The tubesheet and other vital parts of the reactors are protected by continuous monitoring of the critical flow parameters. These upsets are mostly corrected by automatic action on operating parameters, i.e., regulating flow, pressure and/or temperature via adjustment of control valves actions, etc. If these situations are not corrected, then shutdown logic will be activated and the unit will trip to the full stop position.

Table (8.1) and Fig (8.1) extracted from equipment data sheet specify various operating modes. If these modes are exceeded, activation of the shutdown logics occurs. The exchanger is brought back to its standard operating mode once it is shifted to any of the upset modes. Table (8.1) also provides pressure and temperature associated with various operating modes.

Table (8.1): Operating modes parameters

Operating Modes		1 Standard Operation	2 Short term upset	3 Short term upset	4 Short term Max.
Tube Side	Pressure (MPa)	4	4	4	4
	Temperature (°C)	190	190	190	203
Shell Side	Pressure (MPa)	1	-1	0.55	1
	Temperature (°C)	145	65	115	145

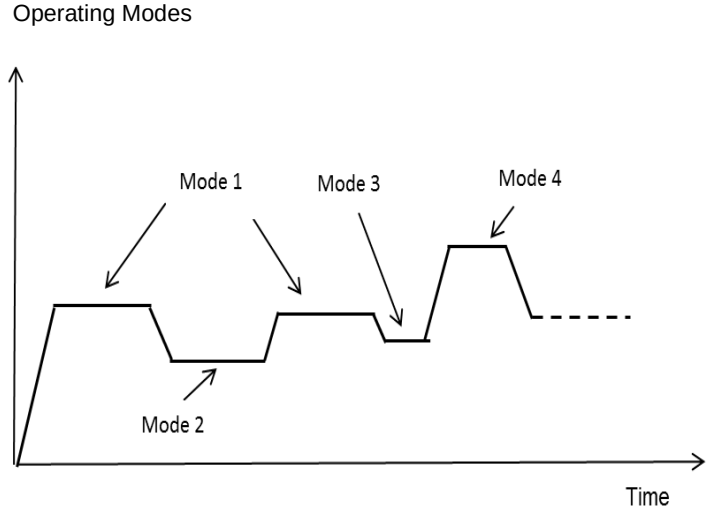

Fig (8.1): Operating modes of heat exchanger

8.2 Estimation of Number of Operating Cycles

To estimate fatigue life of the exchanger, calculation of the stress ranges associated with the various load cases arising from various operating modes must be performed. These calculations require identification of the number of operating cycles. In here, each operating mode is associated with a load case. The numbers of operating cycles is estimated according to the following operating modes:

I. Cyclic- Set 1

This cyclic set contains 4 different load cases; these load cases are standard operating mode (load case-1) and upset modes (load cases 2, 3, 4). Upset load cases are the cause of shutdowns if not corrected. The numbers of cycles associated with Cyclic-Set-1 are,

I.1) standard operating cycles (Load case-1). These are full range cycles and are associated with scheduled startup and shutdown of the reactor, i.e., from steady-state, steady- flow to full stop and vice versa. The specified design occurrences are 500 cycles during 20 years of operation.

I.2) Upset to shut down. These are upset conditions which will cause shutdown since they cannot be corrected (Load cases- 2, 3, 4). The estimated occurrences are 500 cycles during 20 years of the operation.

II. Cyclic Set-2

This set is all the load cases associated with cyclic-set 1 plus additional cycles accounting for correction of upset condition; i.e., cycles shifting the reactor from upset conditions to stand operating mode. 500 cycles are associated with these shifts for each load case. Although various operation scenarios are possible, the above definitions of cycles are considered as conservative estimates and are investigated in this Chapter. Table (8.2) provides process data for various load cases associated with the various operating modes.

Table (8.2): Assumed cyclic operation of exchanger

Cyclic count for operating modes	**Load Cases**	**LC1 Standard mode**		**LC2 Upset 1**		**LC3 Upset 2**		**LC4 Upset max**	
	Item	Shell	Tube	Shell	Tube	Shell	Tube	Shell	Tube
	P (MPa)	1	4	-1	4	0.55	4	1	4
	T (°C)	145	190	65	190	115	190	145	203
Cycle- set 1		from standard to zero 500 cycles		from upset 1 to zero 500 cycles		from upset 2 to zero 500 cycles		from Max. to zero 500 cycles	
Cycle- set 2		cyclic set 1 and following sub cycles: from standard to upset 1 and back 500 cycles from standard to upset 2 and back 500 cycles							

8.3 Stress Life Evaluation

The *stress life fatigue evaluation* approach adopted is defined in Clause 18 of EN-13445-3. Clause 18 provides a procedure which relies on the calculation of elastic stress range and direct application of an S-N curve subject to application of several correction factors, to match the actual design parameters to the parameters used in determination of the S-N curve.

Clause 18 of EN-13445-3 provides different procedures for calculation of the number of allowable cycles at the base metal and at the weldment. To estimate the allowable number of cycles at the junction, i.e. the weld between the tubesheet and channel side

shell, the standard requires identification of the non-linear part of the elastic stress distribution. This means the calculated stress range has to be extrapolated to the junction. Extrapolation of the calculated stress range to the junction zone is performed through use of a second order polynomial. After this step, the modified stress range, which now contains the magnitude of nonlinear part of stress distribution, is used to calculate number of cycles. The calculated number of cycles is then corrected according to the defined fatigue weld class. Various fatigue weld classes are provided in the standard. The applicable weld class is selected to provide a close match between the Code detail and actual tube to tubesheet junction weld.

The fatigue life of a fixed tubesheet exchanger as calculated by the stress approach is controlled by the magnitude of the peak stresses at the tubesheet to shell junction. For the purpose of stress range calculation, the stress approach has been set based on calculation of von Mises equivalent stresses range at the component level. The isolation of peak stresses from total stress is therefore of prime importance and is one of the main objectives of this design route.

Fatigue analysis based on the elastic method requires identification of total stresses as a base for calculation of stress range. Total stress is the combined membrane, bending and peak stress, where the peak stresses is considered to be the nonlinear component of the total elastic stress distribution. Peak stresses occur at local discontinuities and at the surface of thick components: in this case, at the intersection of the tubesheet and channel side shell at the groove line.

Structural stress range calculations have been carried out for the specified operating loads, using elastic material model. The location of the nodes with the highest von Mises stress values are shown in Fig. (8.2). As show in Fig. (8.2), this node is located at the junction of tubesheet to channel shell and is exposed to highest magnitude of stress under load case one.

Figures (8.3, 4) give nodes locations and Mises equivalent of stresses (MPa) for load case one (LC-1).

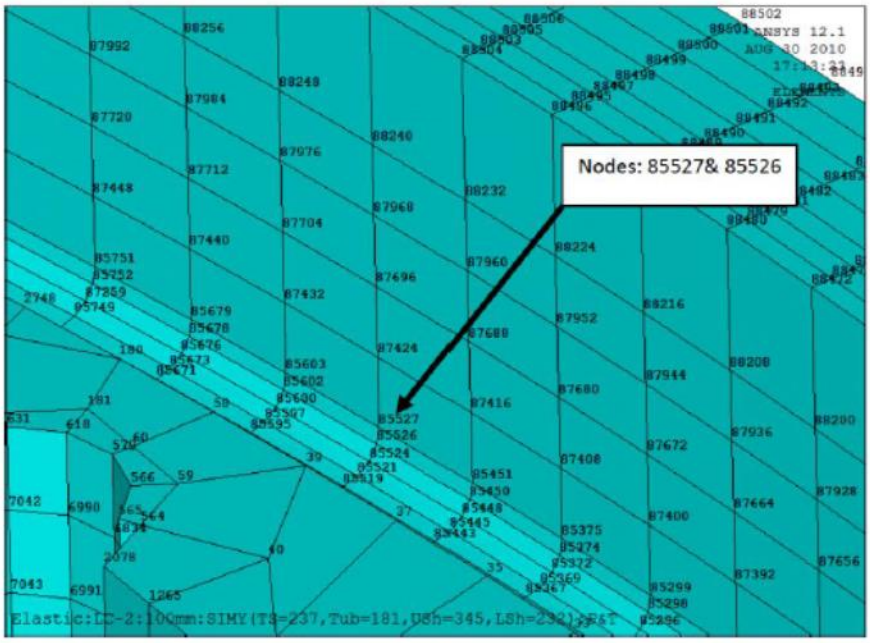

Fig (8.2): Nodes 85526 and 85527 locations

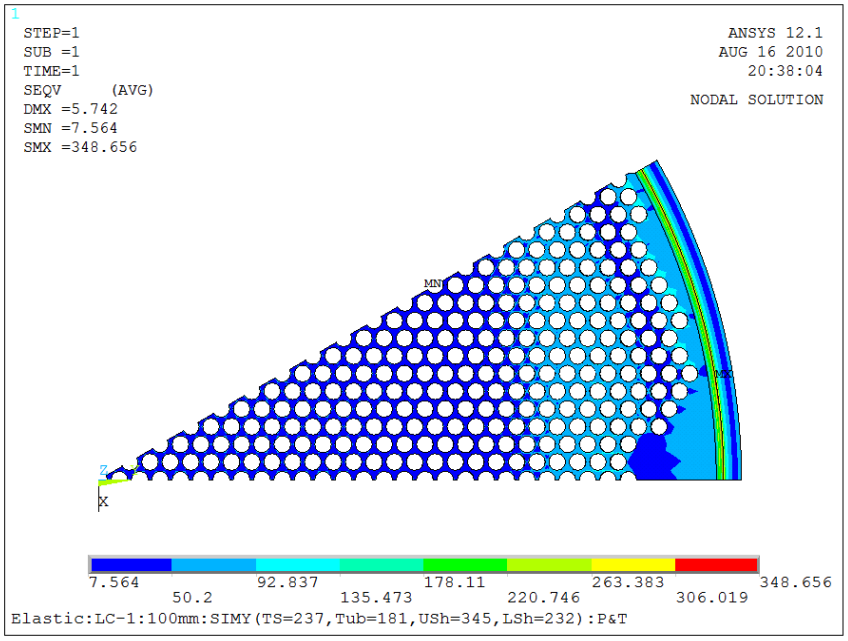

Fig (8.3): Operating load case 1, Mises equivalent of total stresses (MPa), elastic analysis.

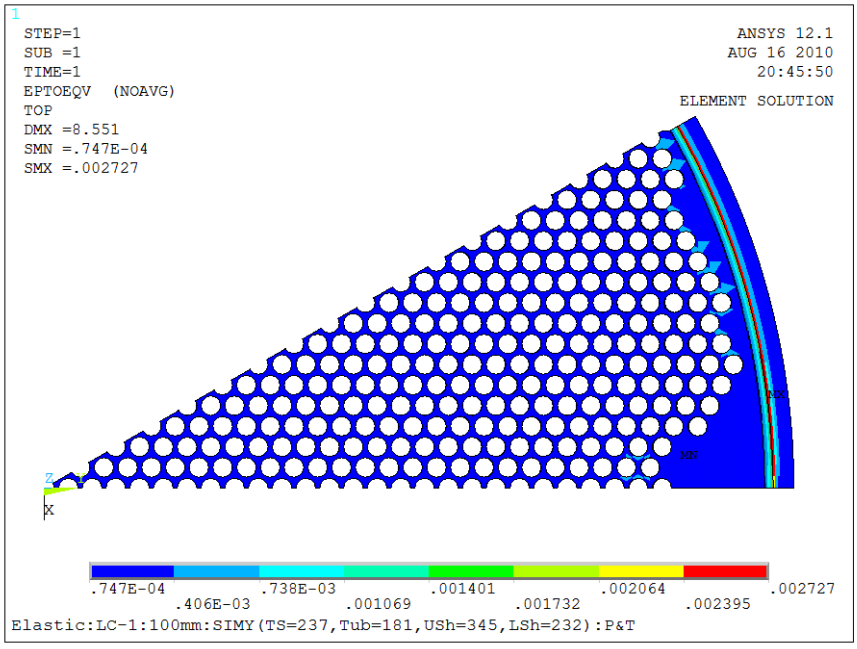

Fig (8.4): Operating load case 1, Mises equivalent of total strains, elastic analysis.

.

Table (8.3) gives von Mises equivalent stress and strain values at node 85527, as evaluated by the elastic FEA.

Table (8.3): Mises equivalent of total stress and total strain[1] at node 85527[2] for various load cases.

Parameters	Material Model	Load case 1	Load case 2	Load case 3	Load Case 4
$[\sigma_{eq}]_{Mises}$	Elastic	348.6	345.8	376.26	328.5
$[\varepsilon_{eq}]_{Mises}$	Elastic	.002727	.002712	.002839	.002663

Notes:

(1) Total strain (mechanical+ thermal)

(2) Node 85527 is located at the weld line of tubesheet to channel side shell

Table (8.4) covers Mises equivalent of stress ranges (MPa) associated with cyclic set 1,i.e., LC1 to LC4. The load cases associated with these stress ranges are defined in Table (8.2). Ranges are provided for nodes 85526 and 85527; these nodes are in the high stress zone, located in base metal and in the weld line at intersection of radii and channel side shell.

Table (8.4): Range of Mises equivalent of total stresses for cyclic set-1 (MPa)

Cycles-Set1	Location	Node	Load case 1	Load case 2	Load case 3	Load Case 4
$[\Delta\sigma_{eq}]_{Mises}$	Radii -(base metal)	85526	308.3	299.5	328	293.3
	Weld line (shell-tubesheet)	85527	348.66	345.8	376.26	328.5

To perform the fatigue calculations, the stress ranges provided in Table (8.4) are rearranged in a diagram that presents them as a reservoir (in sense of stress).

8.4 Reservoir Cycle Counting

Figures (8.5, 6) provide various operating cycles of the exchanger according to information of Table (8.2), these figures depict reservoir modeling of the stress ranges per Table (8.4). Operating set 2 is depicted in Figure (8.7)

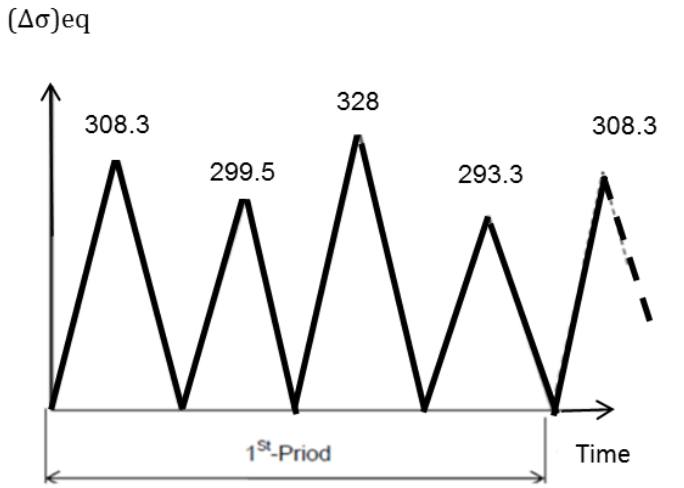

Fig (8.5): Reservoir presentation of stress ranges associated with node 85526 (base metal) for cyclic set-1 operating mode, 500 cycles

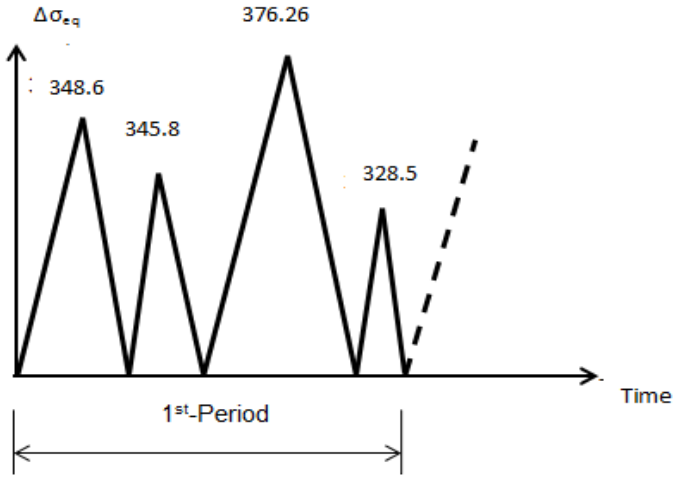

Fig (8.6): Reservoir Presentation of stress ranges associated with node 85527 (weld location) for cyclic set-1 operating mode, 500 cycles.

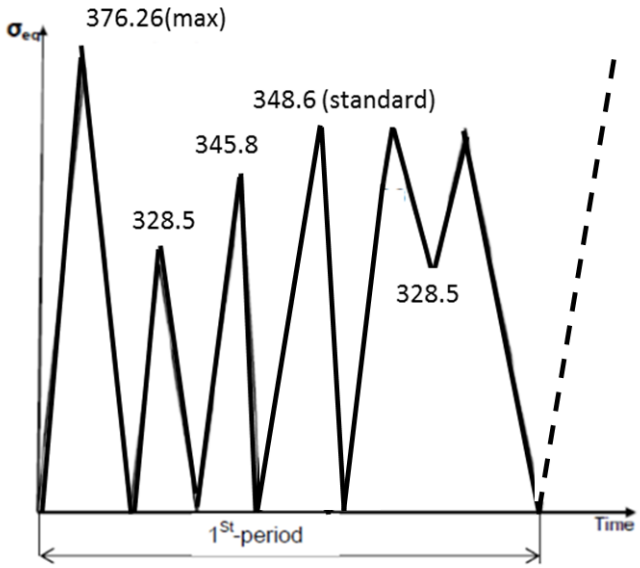

Fig (8.7): Reservoir presentation of stress ranges associated with node 85527 (weld location) for cyclic set-2 operating mode, 500 cycles.

8.5 Allowable Number of Cycles According to Structural Stress Method

Details in regard to calculated allowable number of cycles for base metal and for the Weldment are provided below. Calculations for these regions are different from each other as a different S-N curve must be used. In addition, some corrections applicable to base metal are not required for a weld. Calculations are carried out for set-1 operating cycles, set-1 is defined in table (8.2)

8.5.1 Base Metal and Weldment Nodes

The locations of the nodes used in the calculations are shown in Fig (8.2), node 85527 is at the weld zone and node 85526 is in the base metal zone. These nodes are surface nodes and have highest stress ranges.

8.5.2 Weld between Tubesheet and Upper Shell

Here the procedure for calculation of allowable number of cycles in a weld is taken from Ref [4]. Fig (8.8) shows the node locations used in extrapolation of stresses ranges.

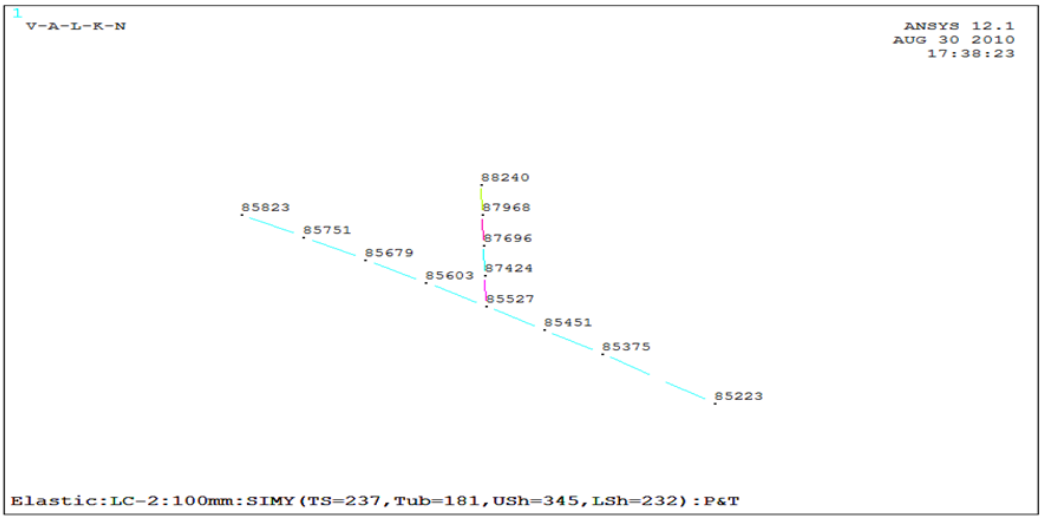

Fig (8.8): Nodes locations used for extrapolation of the stresses

8.5.3 Allowable Cycles for Cyclic Set-1 Operating Mode

8.5.3.1 Base Metal

The allowable number of cycles is extracted from the S-N curve. The S-N curve for CS material is provided by EN-13445, Ref. [4] and is depicted in Fig (4.4). This S-N curve is for polished specimens of 25 mm thickness tested under push-pull test (zero mean stress) at 25 ˚ C; details as provided below are according to Ref [4]. Fatigue life is calculated by considering a "corrected" von Mises equivalent stress range. The required correction factors are *plasticity correction factor*, *effective stress concentration factor*, *thickness correction factor*, and *mean stress correction factor*, *temperature correction factor.*

Corrections are applied to stress ranges given in Table (8.4) for node 85526 before their further use. Node 85526 is considered as a node in base metal and is located slightly below weld line of tubesheet to channel side weld.

The procedure for calculation of the allowable number of cycles is to *estimate* the number of cycles first and then correction factors are calculated based on this estimate. The calculated overall correction factor is applied to the stress range

afterwards. The corrected stress range is used to calculate the allowable number of cycles through the fatigue curve equation. The result of this later calculation is matched to the initial assumption and the procedure is repeated until matching between estimated and calculated cycles occurs. Table (8.5) provides a flow chart of this procedure,

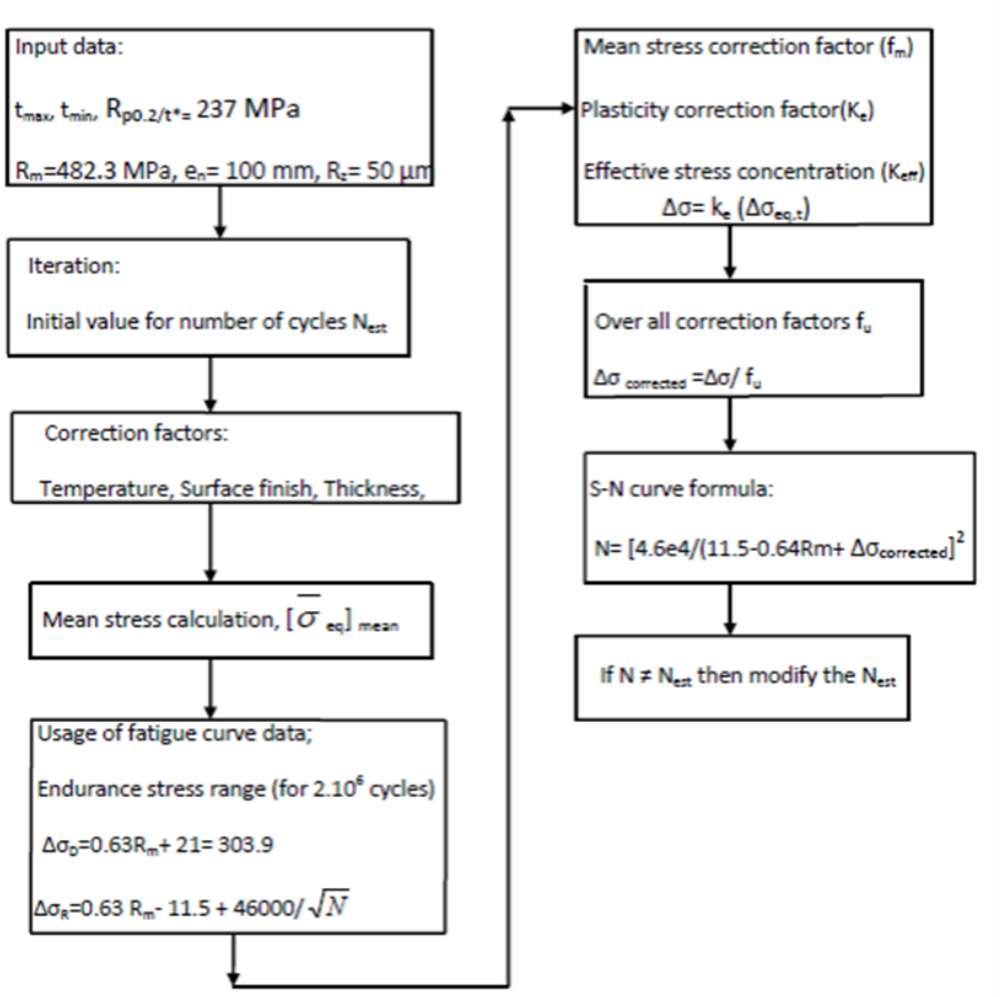

Table (8.5): Procedure for calculation of allowable number of cycles for unwelded region

Details of allowable number of cycles for cycle set-1 are provided in below.

Number of cycles is assumed as a start point, assumed cycles are 10000. Appendix A provides details related to calculation of various correction factors. Based on Appendix A calculations, the combined or overall correction factor, Ref [4], is;

$$f_u = (f_s)(f_e)(f_m)(f_t)K_{eff}$$

$$f_u = (0.81)(0.8913)(0.9225)(0.9552)(1.0)$$

$$f_u = 0.64$$

$$\Delta\sigma_{corrected} = \frac{\Delta\sigma}{f_u} = 308.3 / 0.6329 = 487.13 \quad \text{MPa}$$

Entering equation of the S-N curve with this value, the calculated cycle is,

$$N = [\frac{4.6e4}{(11.5 - 0.64R_m + \Delta\sigma_{corrected})}]^2$$

N= [4.6e4/ (11.5-0.64Rm+ $\Delta\sigma_{corrected}$)]^2

N= 58 640.9 cycle,

The estimated cycle of 10000 is now increased and a number of trials performed to arrive at the matching case. With N= 32000 cycle the LC1 case matches according to the parameters

f_t= 0.9552

f_s= 0.762

f_e= 0.865

f_m= 0.894, $\Delta\sigma_R$= 549.5

K_{eff}=1

f_u =0.562$\Delta\sigma_{corrected}$= $\frac{\Delta\sigma}{f_u}$ = (308.308/0.562)= 548.57

N= [4.6e4/ (11.5-0.64Rm+ $\Delta\sigma_{corrected}$] ^{2}

N= [4.6e4/ (11.5-0.64(482.3) + 548.57] ^{2}, N=33000 cycles, OK

Table (8.5) provides number of cycles calculated for various load cases based on the above procedure.

Table (8.5): Number of cycles for various load cases (cyclic set-1 node 85526, base metal)

Load Cases	LC-1	LC-2	LC-3	LC-4
Cycles	32000	41500	31000	42000

8.5.3.2 Weld

The number of correction factors needed for calculating the allowable number of cycles for a weld is different to that of a base metal. In the fatigue curves (fatigue class) for welds, the correction factors account for stress concentration due to surface irregularities, material inhomogeneity of the weld, welding residual stresses, mean stress resulting from applied loads are considered.

For the welded region, the formulae for thickness correction factor and temperature correction factor remain the same; however, the plasticity correction factor should be applied to principal stresses Ref. [35].

To capture the nonlinear part of stress distribution, stresses are extrapolated to the weld line; this is done by considering directions normal and parallel to the weld line. These directions are marked with arrows on the procedure described below, where (→) means parallel and **(↑)** means perpendicular. Details of calculations are provided in Appendix A. From (A.2),

$(\Delta\sigma_{eq\uparrow})_{\text{corrected}} = (\Delta\sigma_{eq\uparrow})_{\text{Base}}/f_w = 246.8/(0.675) = 365.3$

$(\Delta\sigma_{eq\rightarrow})_{\text{corrected}} = (\Delta\sigma_{eq\rightarrow})_{\text{Base}}/f_w = 344.3/(0.675) = 510.07$

A) Allowable number of cycles

Recall (B.1), fatigue design curve data (see A.2.2.1);

$N = C_1/ (\Delta\sigma_R)^3 = [5.0e11/ (365.3)^3]$

N= 10257 for direction (↑)

Also,

$N = C_1/ (\Delta\sigma_R)^3 = [1.02e12/ (510.7)^3]$

N= 7689 for direction (→)

Allow able number of cycles associated with cyclic set-1 is provided in Table (8.6).

(8.6): Allowable number of cycles for various cases associated with cyclic set-1 for welded region

Load Cases	**LC-1**	**LC-2**	**LC-3**	**LC-4**
Allowable Cycles	7689	7998	6613	8853

Note: Above results are based on full penetration welds made from one side without backing strip for direction perpendicular to weld (FTC=80) and for direction parallel to the weld (FTC=63).

8.6 Number of Allowable Cycles for Cyclic Operation Set-2

Another possible mode of operation is operating set-2, defined in Table (8.2). From the definition of this operating mode, cyclic set-2 is the same as cyclic set-1 plus additional 500 cyclic shift from standard operating mode (LC1) to upset modes of 1 and 2 (LC2, LC3) and back to standard mode. Load cases stress ranges associated with these cycles and allowable number of cycles following above procedure is given below.

8.6.1 Stress Ranges

According to the definition of cyclic set-2, Table (8.4) is used identically for this set. This table provides Mises equivalent of total stress at the base metal (node 85526) and at the Weldment (node 85527) for various load cases. These load cases participate in setting up the various cyclic operating modes, i.e., cyclic set-1 and set-2. For cyclic set-2, Table

(8.4) is represented by Table (8.7), since the $\Delta\boldsymbol{\sigma}_{\mathbf{eq}}$ of table (8.4) should be replaced by $\boldsymbol{\sigma}_{\mathbf{eq}}$. This is necessary as not all ranges associated with cyclic set 2 are between the designated load cases and zero state. Details of calculated stress ranges through use of reservoir method are provided in Fig. (A.3, 6), these ranges are obtained by draining each trough.

Table (8.7): Mises equivalent of stresses for cyclic set- 2[1]

Cyclic set-2	**Node**	**LC1**	**LC2**	**LC3**	**LC4**
$\boldsymbol{\sigma}_{\mathbf{eq, Mises}}$	85526	308.3	299.5	328	293.3
	85527	348.66	345.8	376.26	328.5

Note: $\Delta\sigma_{eq}$ of table (8.4) is replaced by $\sigma_{eq, Mises}$ in this table.

Details of calculated stress ranges through use of the reservoir method are provided in Appendix A.3, these ranges are obtained by draining each trough.

8.6.2 Stress range values for LC-5 and LC-6

The Mises equivalent of stress ranges associated with LC-5 and LC-6 are very small.

$\Delta\sigma_{eq5}$ is stress range between 348.6 and 345.8 MPa (component base), as it can be seen the variation of stress range for this case is very small therefore. No attempt has been made to calculate the difference of the component, i.e., it is assumed $\Delta\sigma_{eq5}$= 348.6-345.8=2.8 MPa. Also, $\Delta\sigma_{eq6}$ is stress range between 348.6 and 328.5 MPa (component base) , although the difference in equivalent stresses are larger than the case associate with the $\Delta\sigma_{eq5}$, however, for this case also the same route is take, i.e.,

$\Delta\sigma_{eq6}$= 348.6-325.8=22.8 MPa.

Table (8.8) provides the stress ranges for cyclic set-2 of operating modes. Appendix (A.3) depict the stress ranges.

Table (8.8): Stress ranges for cyclic set-2

Action	**LC1 to Zero**	**LC2 to Zero**	**LC3 to Zero**	**LC4 to Zero**	**LC1 to LC2**	**LC1 to LC4**
Designation[(1)]	$\Delta\sigma_4$	$\Delta\sigma_3$	$\Delta\sigma_1$	$\Delta\sigma_2$	$\Delta\sigma_5$	$\Delta\sigma_6$
Stress range (MPa)	348.8 (Standard)	345	376.3	328.5	2.8	22.8

Note: Period of cyclic set-2 is 500 times.

8.6.3 Allowable Number of Cycles for Cyclic Set-2

The allowable number of cycles will not change in comparison with cyclic set 1, as the stress ranges are similar. Addition of two upset conditions (from LC1 to LC2) and from (LC1 to LC4) also will not affect the result, since in both cases $\Delta\sigma_{eq} \leq \Delta\sigma_{D,}$ which means allowable number of cycles are infinity for both cases. Table (8.9) provides allowable number of cycles associated with various stress ranges.

Table (8.9): Allowable number of cycles for operating mode set-2

Cycle Action	**LC1 to Zero**	**LC2 to Zero**	**LC3 to Zero**	**LC4 to Zero**	**LC1 to LC2**	**LC1 to LC4**
Stress range	$\Delta\sigma_4$= 348.8	$\Delta\sigma_3$= 345	$\Delta\sigma_1$= 376.3	$\Delta\sigma_2$= 328.5	$\Delta\sigma_5$= 2.8	$\Delta\sigma_6$= 22.8
Allowable Cycles	7689	7998	6613	8853	∞	∞

8.7 Fatigue Damage Accumulation

Fatigue Damage accumulation is calculated through evaluation of the fatigue damage index. An important step in determination of the fatigue damage index is to deduce from multi-amplitude stress history a sequence of single–amplitude stress cycles, that, applied separately without interaction, result in the same fatigue damage (index) as the original stress history.

For determination of the cumulative fatigue damage index (***FI***), Miner's rule is often used. Miner's rule states that the cumulative fatigue damage index of a sequence of groups of constant amplitude stress cycles, of equal relevant characteristics, is given by,

$$FI = \frac{n_1}{N_1} + \frac{n_2}{N_2} + ... + \frac{n_i}{N_i} \qquad (8.1)$$

where n_i is the number of single cycles in group *i*, and N_i is the number of allowed cycles corresponding to the parameters of these stress cycles in group *i*. This rule takes no account of the effect of the order of occurrences of the constant amplitude cycles, but it is very simple, and it is considered to render fair approximation in usual cases, i.e., cases with strongly alternating individual stress cycles without any especially pronounced cycle order. Clause 18 of Ref.(4) specifies the Miner rule and Reservoir Cycle Counting Method to be used in this regard.

8.7.1 Fatigue Damage Index

Referring to tables (8.5,6 &8), the fatigue damage indexes for cyclic set 1 and 2 are similar:

A. Base metal

$FI = (500/32000) + (500/41500) + (500/31000) + (500/42000) = .07 <$ 1, OK

B. Weld

$FI = (500/7689) + (500/7998) + (500/6613) + (500/8853) = .26 <$ 1, OK

8.8 Inelastic Fatigue Calculation According to the Local Strain Approach

On early days of investigations into fatigue problems; emphasis was on stresses well below the yield strengths of the used material. In this part of the high cycle fatigue regime, a one-to-one relationship exists between stress and strain. Therefore, stresses were considered to be the relevant response parameter in design with material strength parameters being determined in tensile tests.

This representation of fatigue curves hides the fact that it is not the range of stress cycles, but the range or amplitude of the *strain cycles* that is the essential physical cause of failure damage. The strain-based approach to fatigue considers the plastic deformation that may occur in localized regions (hotspots) where fatigue cracks begin; this approach allows detail consideration of fatigue situations where local yielding is involved.

It should be noted that the strain-based approach differs significantly from the stress-based approach. The strain-based approach relies on a cyclic stress-strain curve and aims for calculation of local strains and local stresses. In the stress based approach, nominal (average) or structural stresses are calculated first, and then calculated values are modified through application of empirical elastic stress concentration factor. This means no attempt is made to calculate local stresses and strains. Use of cyclic stress-strain curve is a unique feature of the strain-based approach, while direct use of nominal stress versus life (S-N) curve is unique feature of the stress based approach.

A strain versus fatigue life curve is a plot of strain amplitude versus cycles to failure. Such a curve is employed in the strain-based approach for a life estimates in a manner analogous to the use of the S-N curve in the stress–based approach.

To calculate the number of allowable cycles based on the local strain approach, two methods have been used here. These methods are use of a multilinear kinematic model to identify a stable strain cycle with subsequent conversion of strains to stresses and use of experimental coefficients and formulas expressing material post yielding behaviour.

8.8.1 Strain Range Calculation Using Inelastic Material Model

ASME Sec VIII, Div. II item 5.5.4 provides a procedure for performing fatigue assessment according to elastic-plastic stress analysis method. In this clause the ASME Code requires calculation of the effective strain range by performing cyclic analysis through a plasticity algorithm with a kinematic hardening constitutive law. Use of a cyclic stress- strain material model, as provided in 3.D.4 of Annex 3.D, is suggested. However other cyclic stress- strain curves may be used that are known to be either more accurate for the application or lead to more conservative results.

Annex 3.D, item 3.D.3 also provides a stress-strain material model to be used in calculations when strain hardening characteristics are considered. Comparing two equations of Annex 3.D with each other has revealed the fact that both models have a common base in a Ramberg Osgood type of formulation. Existence of additional terms on equation 3.D.3 suggests that this equation traces the stress-strain behavior of a material more closely and therefore its use should produce a more conservative result. This finding has been investigated further through the following calculations.

To arrive to stable cyclic strain range, both of the above material models were used in conjunction with a multilinear kinematic hardening constitutive law. In this regard, the exchanger was forced to experience 10 full range cycles under two different load cases.

The first load case considers a pressure of 11.7 MPa. This is the exchanger limit pressure reported in chapter 6. In the second load case pressure was reduced to 4.0 MPa (data sheet pressure), temperature distribution was included in both of these load cases. Figures (8.9, 10) depict variation in Mises equivalent of plastic strains after exchanger exposer to 10 full range cycles. Table (8.10) gives the various strain ranges. Figure (8.11,12) shows the Mises equivalent of strain/ stress under datasheet pressure of 4.0 MPa, these values have been used for calculation of number of allowable cycles.

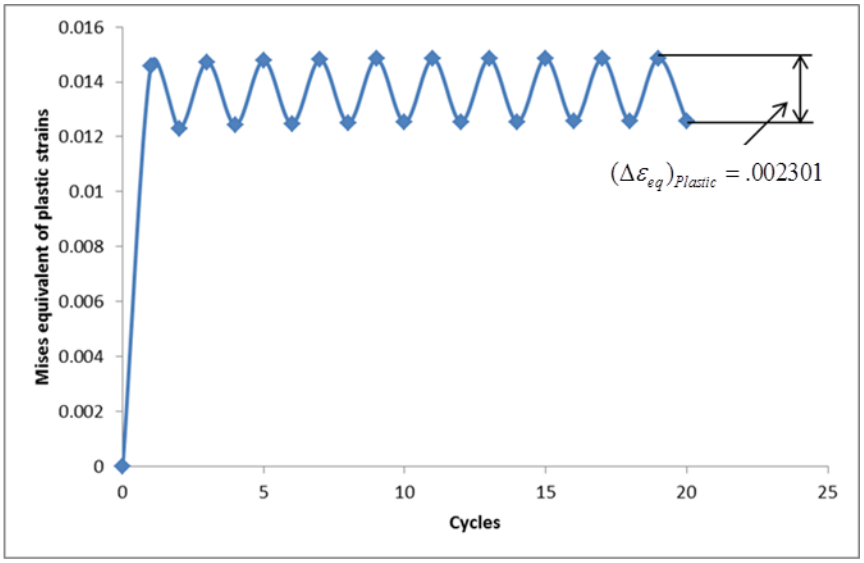

Fig (8.9): Range of Mises equivalent of plastic strains after 20 half cycles, P=11.7 (MPa) and temperature distribution. Cyclic stress strain curve (ASME 3.D.4), node 85527.

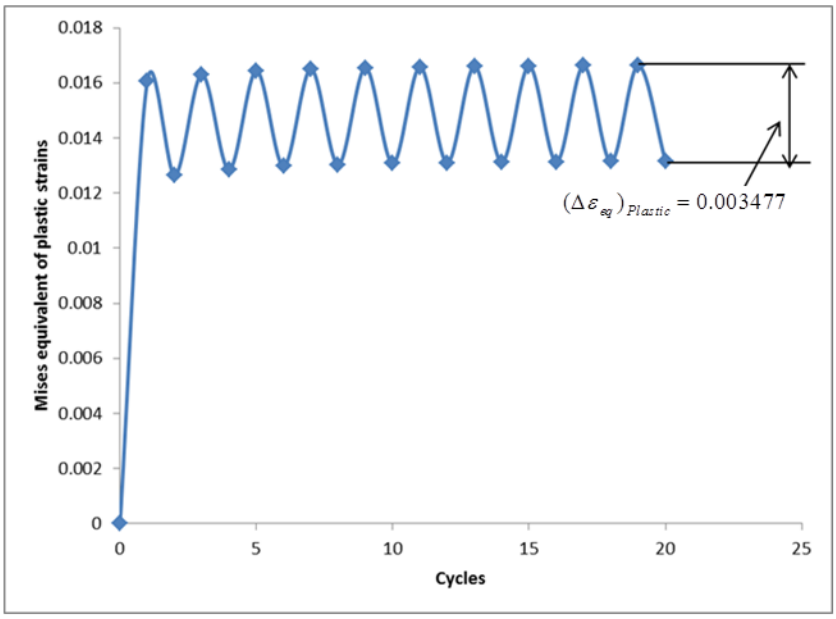

Fig (8.10): Range of Mises equivalent of plastic strains after 20 half cycles, P=11.7 (MPa) and temperature distribution. Non-Cyclic stress strain curve (ASME 3.D.3), node 85527.

Table (8.10): Ranges of Mises equivalent of Plastic and residual strains after 20 half cycles

Material Model	Pressure (MPa)	$[\Delta\varepsilon_{pl}]_{eq}$	Residual Strain
Non-Cyclic ASME 3.D.3	4.0	0.941E-3	-
Cyclic ASME 3.D.4	4.0	0.358E-3	-
Non-Cyclic ASME 3.D.3	11.7	.003477	.013801
Cyclic ASME 3.D.4	11.7	.002301	.013801

Use of non-cyclic strain stress curve produces a much larger strain range in comparison with cyclic stress strain curve and therefore it is more conservative, as a larger plastic strain range will result in a lower allowable number of cycles. Both of the ASME material models are based on Ramberg Osgood formulation, however, additional term existed on non-cyclic equation provides more accurate estimation of material performance post yielding.

The residual strain field under the non-cyclic material model is slightly larger than the residual strain field calculated by the cyclic material model. Both models produce close results under data sheet pressure (P=4.0 MPa). This is because the load is not large enough to produce significant plastic strains.

Figures (8.11, 12) provide plots of Mises equivalent stresses and strains for standard operating condition (LC-1). The material model is multilinear kinematic hardening. For definition of standard operating mode see Table (8.1).

The mechanical strain range is converted to stresses through use of the elastic stress-strain relationship. This allows the use of the S-N curves. It is also noted that addition of isothermal thermal strain to the summation of elastic and plastic strains will not affect the

magnitude of converted equivalent stresses, as individual terms will cancel each other out.

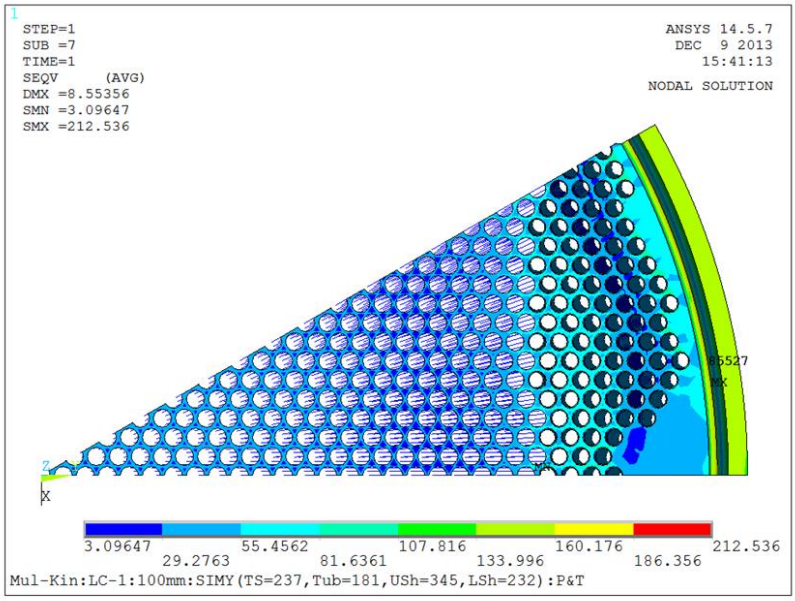

Fig (8.11): Operating load cases 1, Mises equivalent of total stresses, multilinear kinematic hardening.Node 85527

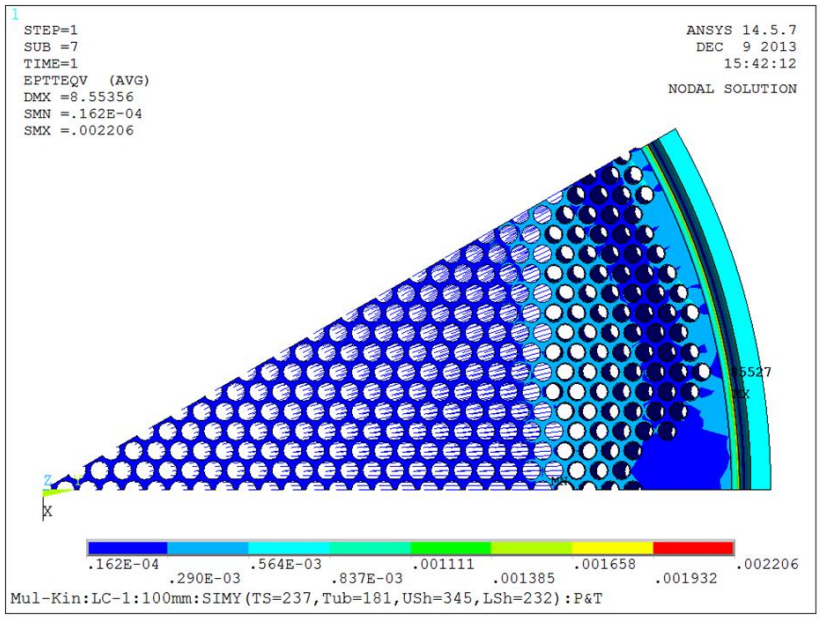

Fig (8.12): Operating load cases 1, Mises equivalent of total strain, multilinear kinematic hardening.Node 85527

A summary of the total mechanical strains (elastic and plastic) and thermal strain for node number 85527 is provided in Tables (8.6,7).

Table (8.11): Total mechanical strain at node 85527x (1E-3)

Node	ε_{xx}	ε_{yy}	ε_{zz}	ε_{xy}	ε_{yz}	ε_{xz}
85527	-0.1826	-0.4565	1.9064	0.1595	1.3088	-0.0608

Table (8.12): Total thermal strain at node 85527x (1E-3)

Node	$\varepsilon_{xx,Th}$	$\varepsilon_{yy,Th}$	$\varepsilon_{zz,Th}$
85527	0.21447	0.21477	0.21477

The mechanical elastic stress- strain relations of equation (8.2) was used to convert mechanical total strains to stresses, where $\sigma_{xx}, \varepsilon_{xx}$, etc. are stress and strain components in designated directions.

$$\begin{vmatrix} \sigma_{xx} \\ \sigma_{yy} \\ \sigma_{zz} \\ \tau_{xy} \\ \tau_{xz} \\ \tau_{yz} \end{vmatrix} = E/(1+\nu)(1-2\nu) \begin{vmatrix} (1-v) & v & v & 0 & 0 & 0 \\ v & (1-v) & v & 0 & 0 & 0 \\ v & v & (1-v) & 0 & 0 & 0 \\ 0 & 0 & 0 & (1-2v)/2 & 0 & 0 \\ 0 & 0 & 0 & 0 & (1-2v)/2 & 0 \\ 0 & 0 & 0 & 0 & 0 & (1-2v)/2 \end{vmatrix} \begin{vmatrix} \varepsilon_{xx} \\ \varepsilon_{yy} \\ \varepsilon_{zz} \\ \gamma_{XY} \\ \gamma_{Xz} \\ \gamma_{yz} \end{vmatrix} \quad (8.2)$$

$$\begin{vmatrix} \sigma_{xx} \\ \sigma_{yy} \\ \sigma_{zz} \\ \tau_{xy} \\ \tau_{xz} \\ \tau_{yz} \end{vmatrix} = \frac{194177}{(1+.3)(1-.6)} \begin{vmatrix} 0.7 & 0.3 & 0.3 & 0 & 0 & 0 \\ 0 & 0.7 & 0.3 & 0 & 0 & 0 \\ 0 & 0 & 0.7 & 0 & 0 & 0 \\ 0 & 0 & 0 & 0.2 & 0 & 0 \\ 0 & 0 & 0 & 0 & 0.2 & 0 \\ 0 & 0 & 0 & 0 & 0 & 0.2 \end{vmatrix} \begin{vmatrix} \text{-0.1826e-3} \\ \text{-0.4565e-3} \\ \text{1.9064e-3} \\ \text{0.15195e-3} \\ \text{-0.0608e-3} \\ \text{1.309e-3} \end{vmatrix}$$

$$\begin{vmatrix} \sigma_{xx} \\ \sigma_{yy} \\ \sigma_{zz} \\ \tau_{xy} \\ \tau_{xz} \\ \tau_{yz} \end{vmatrix} = \begin{vmatrix} 114.7 \\ 73.78 \\ 426.7 \\ 11.34 \\ -4.54 \\ 97.76 \end{vmatrix}$$

$$(\sigma_{i,j})_{Mises} = \begin{vmatrix} 114.7 & 11.34 & -4.54 \\ 11.34 & 73.8 & 97.76 \\ -4.54 & 97.76 & 426.7 \end{vmatrix}$$

$$(\sigma_{i,j})_{Mises} = 375.36$$

It is noted that the stress range calculated previously (Table (8.3) for the same operating load, i.e., LC1 (standard operating mode) using elastic material model for node 85527, was reported as $\Delta\sigma_{i,j} = 348.66$. The difference between the two cases arises from inclusion of plastic strains.

Following the same procedure, the results of calculations for number of allowable cycles for a multilinear material model is provided in Table (8.13).

Table (8.13): Allowable number of cycles

Material Mode;	**Elastic**	**Mul.-Lin.**
Allowable Cycles	Weld→ 7698	Weld→ 7754

Similar calculations can be carried out for the base metal, however, the allowable number of cycles for the base metal is much higher than the weld material and therefore additional calculations have been omitted.

8.9 Strain range calculation using experimentally determined coefficients (experimentally determined strain versus fatigue life curve)

The allowable number of cycles calculated through use of the experimentally determined material coefficients is presented below.

8.9.1 Strain Based Approach

Table (8.15) gives the allowable number of cycles based on the consideration of Mises equivalent of total strains. The magnitude of the total strains is taken from Fig. (8.12). Details of the equations are provided in section 3.2.3.2.C. Material data is given in Table (8.14). Following calculations have been performed for node 85527 (junction of radii to shell, weld location), with $(\Delta\sigma)_{eq}$= 212.54 MPa and $(\varepsilon_{total})_{eq}$=.0022, Fig. (8.11,12).

Mean stress in this load case is an average value (component base) between zero and stress calculated from LC1 under multilinear hardening formulation (212.54 MPa), i.e., σ_{mean}= 99 MPa. Tubesheet material has relatively the same material properties as material type 2 in table (8.14), using material parameters of item 2 in table (8.14) the number of allowable cycle is:

$$Morrow, \varepsilon_a = \frac{\sigma'_f}{E}(1-\frac{\sigma_m}{\sigma'_f})(2N_f)^b + \varepsilon'_f(1-\frac{\sigma_m}{\sigma'_f})^{c/b}(2N_f)^c$$

σ_m= 99 MPa

$$\varepsilon_a = (\frac{1090}{203000})(1-\frac{99}{1089})(2N_f)^{-0.115} + 0.912(1-\frac{99}{1089})^{\frac{-0.606}{-0.115}}(2N_f)^{-0.606}$$

$$\varepsilon_a = (.00488)(2N_f)^{-0.115} + (0.551)(2N_f)^{-0.606}$$

$N_f = 21275$ cycles

Note 21275 cycles produces the same magnitude of total strains, i.e., $\varepsilon_a = 0.0022$

Table (8.15) gives allowable number of cycles for node 85527 located at the junction of tubesheet to shell according to various formulations.

Table (8.14): Cyclic stress-strain and strain-life constants for CS material

Material		**Tensile properties**		**Strain- life curve**				**Cyclic stress-strain curve**		
CS		σ_y (MPa)	σ_u MPa	σ'_f (MPa)	b	ε'_f	c	$E(10^3)$ (MPa)	H'	n'
1	normalized SAE-1015	228	415	1020	-0.138	0.439	-0.153	207	1349	0.282
2	hot-rolled Man-Ten	322	557	1089	-0.115	0.92	-0.606	203	1096	0.187

Table (8.15): Allowable number of cycles according to strain models

Equation(1)	Coffin	Morrow	Modified Morrow	SWT
Number of Cycles	97500	21275	79000	24950

Notes:

(1) Experimental coefficients

8.9.2 Stress based approach

Table (8.16) shows the number of cycles to failure according to various stress-life formulations, as discussed in Chapter 3.2.3.2, Equations (3.48, 49, 50, and 51). Calculations are performed for node 85526 located at radii with stresses calculated through elastic law (table (8.4) load case 1). Following material data:

(Tubesheet material), $\sigma'_f = 1089, b = -0.115$

For node 85526, at LC-1,

$\Delta\sigma_{eq} = 308.29$ MPa

$\sigma_a = \left(\overline{\sigma}_{eq}\right)_{mean} = 218.27$ MPa

It is noted that above material properties are close but are not identical to the tubesheet and shell material.

$\sigma_a = \sigma'_f \left(2N_f\right)^b = 1089\left(2N_f\right)^{-0.115}$ MPa

Recall, Morrow equation, $\frac{\sigma_a}{\sigma_{ar}} + \frac{\sigma_m}{\sigma'_f} = 1$, and rearrange to below equation and note σ_a is half the range which is the variation about mean (see Fig. (3.18), then:

$$\sigma_{ar} = \frac{\sigma_a}{1 - \frac{\sigma_m}{\sigma'_f}} = \frac{218.2}{1 - \frac{218.27}{1089}} = 273$$

$\sigma_{ar} = 273$ MPa

$$N_f = \frac{1}{2}\left(\frac{\sigma_{ar}}{\sigma'_f}\right)^{\frac{1}{b}} = \frac{1}{2}\left(\frac{273}{1089}\right)^{1/-0.115} = 83924$$ Cycles

Table (8.16): Number of cycles to failure according to various stress models

Stress Model		**Cycles to Failure (N_f)**
Modified Goodman	$\frac{\sigma_a}{\sigma_{ar}} + \frac{\sigma_m}{\sigma_u} = 1$	7820
Gerber Parabola	$\frac{\sigma_a}{\sigma_{ar}} + (\frac{\sigma_m}{\sigma_u})^2 = 1$	138320
Morrow	$\frac{\sigma_a}{\sigma_{ar}} + \frac{\sigma_m}{\sigma'_f} = 1$	84000

8.10 Results

Table (8.17) shows the allowable number of cycles for node 85527 (weld location) for various load cases under elastic and multilinear kinematic hardening calculations. Table (8.18) provides number of allowable cycles for LC1 at node 85526 and 85526 location calculated through various formulations.

Table (8.17): Allowable number of cycles for node 85527 (weld line)

Load Case	Elastic	Mul.-Lin
1	7689	7754
2	7978	8009
3	6612	5876
4	8852	9591

Table (8.18): Allowable number of cycles for LC-1

Location	Radii (Node 85526)	Weld (node 85527)
Elastic	32000	7689[1]
Elastic-Plastic Multilinear Kinematic	-	7754[1]
Goodman	7820[2]	-
Gerber	138320[2]	
Morrow	84000[2]	
Coffin	-	97500[2]
Morrow (Strain)	-	21275 [2]
Modified Marrow	-	79000[2]
SWT	-	24950[2]

Notes:
(1) Datasheet material data, table (5.1)
(2) Material properties from item 2, table (8.14)

8.11 Discussion of Results

It has been demonstrated that the weld between the tubesheet and upper shell is the most critical portion of the reactor from a stress range and fatigue point of the view. Result of calculations shows that allowable number of cycles for this weld is far less than allowable number of cycles of the “neighboring” base material; therefore any stress regime responsible for crack initiation will most probably start in this region.

The region parallel to the weld line is the weakest region of the reactor and therefore limits the allowable number of the cycles. High quality welding and comprehensive NDT is essential in this critical region.

Conversion of total strains to the single stresses through use of the multilinear kinematic material model law gives a close result to classical elastic (stress) approach. As no plastic correction is required for local strain approach, this approach is advised.

Considering all of the mean stress equations given, neither the Goodman nor Gerber equations are very accurate, with the former often being overly conservative, and later often non conservative.

The Morrow equation, in comparison to other stress/stain based equations, gives closer results once it is compared to the results of calculations according to the multilinear kinematic hardening procedure and S-N curve approach. Use of the exact Strain-Life constants should produce a closer value.

The results of the comprehensive fatigue evaluation presented in this chapter show that under reduced thickness, tubesheet of the reactor will satisfy design fatigue requirements. Therefore, it can safely be concluded that tube sheet thickness of this reactors can be reduced substantially without provoking any failure mechanisms considered in this work.

9. Conclusions

The plastic load calculated according to the Plastic Work Curvature criterion is not dependent on the local parameters, as it is based on the total plastic work done on the structure. This criterion has a mathematical base rather than experimental one and therefore more accurately predicts the plastic load related to the gross plastic deformation failure mode. In comparison with other methods, the procedure is unique and has been successfully applied to very complex tube sheet geometry of fixed tubesheet heat exchangers.

This method can be applied to the various material hardening models with large or small deformation constitutes laws. Accuracy embedded in the procedure suggests that the curvature method can be applied to various pressurized geometries with confidence.

This method was applied to a very large and complex fixed tubesheet exchanger in order to reduce the tubesheet thickness; this was done through comprehensive calculations. It was highlighted that considerable reduction on tubesheet thickness can be obtained by adapting the curvature procedure. Adoption of the method for design purpose after applying a safety factor is recommended.

Further checks on admissibility of tubesheet thickness to additional design requirements have been performed by investigating the susceptibility of the tubesheet geometry to failure modes associated with incremental collapse and fatigue mechanisms.

With regards to the check for incremental collapse and identification of shakedown load, two different approaches have been used; elastic and inelastic.

In elastic stress analysis, through thickness stress linearization procedure has been carried to categorize stress components. According to this procedure, the non-linear component of through thickness stress distribution is assumed to be peak stress. Isolation of peak stresses from membrane and bending stresses has indicated that the tube-sheet configuration exhibits shakedown under the cyclic temperature and pressures.

The presence of significant peak stress has also revealed the fact that the likely failure mechanism is low cycle fatigue associated with the steady state cyclic plastic strain range. This result indicates that the stress categorization procedure used in the elastic

analysis may not be appropriate. In this case, it is not conservative to assume that the non-linear component of through thickness stress is wholly peak stress and therefore can be disregarded in elastic shakedown analysis.

The result of the inelastic analysis indicates that in fact what is reported as the peak stress in elastic analysis is in part secondary in nature and should not be wholly excluded from the elastic ratcheting assessment.

Inelastic analysis based on an elastic-perfectly plastic material model indicates that the configuration experiences a different failure mechanism, incremental plastic straining or ratcheting. The cyclic plastic strain increments are small and would not give rise to a global plastic failure mechanism over the required 50 cycle life of the vessel by a considerable margin, thus the vessel can be deemed to be acceptable for service. The elastic-perfectly plastic material model is not an appropriate choice of material model for fixed tubesheet exchangers, as its use will result in a thicker section.

ASME VII Div. 2 does not include a ratchet checking procedure based on non-linear analysis assuming a strain hardening material model. However, this advanced type of analysis can be more representative of the actual structural behaviour of the component (although highly dependent on the plasticity model used). The results given by the strain hardening analysis indicate that in practice the structure would shake down to steady state alternating plasticity after 6 load cycles, with no global plastic deformation thereafter.

This finding, although not appropriate for Code design, indicates that whilst the elastic design route presented here may not be strictly conservative, it is likely to be safe in practice with respect to the shakedown criterion due to the constraining effect of the material strain hardening on the growth of plastic zones.

The effect of material strain hardening on the cyclic response was investigated by performing elastic-plastic analysis using multilinear strain hardening material model. The exchanger exhibits plastic strain accumulation during the first few full cycles, after which the behaviour shakes down to alternating plastic strain without further strain accumulation.

As proven by performed design calculations, this reactor under reduced thickness will experience no damage from fatigue failure mode in spite of being exposed to the various operating modes defined.

Comparing the results of the elastic stress method (Code fatigue procedure) and local strain method has indicated that the calculated results are in agreement. The local strain approach is a superior method in comparison to classical elastic stress (hot spot) method as identification of structural stresses is not required. Further, stress interpolation to hot spots is not a determinant factor and there exist no constraint on the size of elements apart from standard FEA practice. Limitation on the size of the elements located in front of the weld toe provides a constrain on the FEA modeling. The number of required corrections in the case of the local strain approach is minimized, i.e., plasticity and local stress concentration is not required.

All calculations have been performed under reduced tubesheet thickness, therefore, it can safely be concluded that tubesheet thickness can be reduced without provoking any mechanism involving any of the above failure modes, i.e., gross plastic deformation, incremental collapse and fatigue.

As this type of the exchanger is quite common in Oil and Gas plants, and the majority of them are under similar operating conditions, it can be stated that considerable reduction in the cost of this type of equipment can be obtained through adopting the above design approach.

10. Recommendations and Future Work

Further investigation of the above work can be carried out through experimental measurements. Experiments can be carried out for a fixed edge perforated plate, with installation of tubes in outer 3 rows. The experimental model requires both shell side shell, channel side shell and lower and upper heads. The deflection, rotation and strain measurements at the rim should provide data for comparison with the above results.

The nonlinear kinematic hardening material model can be employed for further investigation of the incremental collapse failure mode.

The limits provided by the Bree problem is suitable for Bree geometry and stresses defined therein. The tubesheet to shell junction geometry, loads and stresses are not similar to the Bree problem and therefore attempts can be made to define the limits based on these parameters and through use of various material hardening parameters.

The fatigue local strain approach uses the strain range obtained from stabilized cycles. Conversion of these plastic strains to stress is performed through elastic procedure for purpose of use with the S-N curve. In reality stress range associated with strain range should be used through flow rule, and it should be interesting to investigate this approach.

In all of the above, the loads have been taken as proportional. The effect of rotation of principal stresses, i.e. non-proportional loading on all of the design checks performed above can also be investigated

In this work thermal stresses are treated as isotropic, exceptionally, some tubesheets could be as thick as 400 mm with different cladding material, effect of these exceptional parameters can be investigated also.

References

[1] ASME, Boiler and Pressure Vessel Code Section VIII, Div. 2, American Society for Mechanical Engineers, New York, 2007.

[2] ASME, Boiler and Pressure Vessel Code Section VIII, Div. 1, American Society for Mechanical Engineers, New York, 2007

[3] ASME, Boiler and Pressure Vessel Code Section III, American Society for Mechanical Engineers, New York, 2007

[4] EN 13445, “European Standard for Unfired Pressure Vessels- Part 3: Design”, European committee for Standardization (CEN), 2002.

[5] Timoshenko, S., Woinowsky- Krieger, S.,” Theory of plates and shells”, McGraw-Hill, 1959.

[6] ASME, ASME Boiler and Pressure Vessel Code Section II, Part D. the American Society of Mechanical Engineers, New York, NY, 2007.

[7] Gardner, K.A., “Heat Exchanger Tube sheet Design- Part 2: Fixed Tube sheets”, J. Applied Mechanics, Transaction of ASME, 74 (1952), 215-231.

[8] Gardner, K.A., “Heat Exchanger Tube sheet Design- Part 3: U- Tube and Bayonet Tube Sheets”, J. Applied Mechanics, Transaction of ASME, 74 (1960), 25-32.

[9] Gardner, K.A.,” Tube Sheet Design: A Basis for Standardization. Proc.First Int. Conff. Pressure Vessel Technology: Part 1, Design and Analysis, pp. 621- 648. ASME New York, 1969.

[10] Pressure Vessels and Piping: Design and Analysis- A Decade of Progress. Components and Structural Dynamics.Vol.2.ASME New York, 1976.

[11] O'Donnell, W. J., Langer, B.F.," Design of Perforated Plates", J. Engineering for Industry, 84 (1962), p. 307.ff.

[12] Merjers, P.," Plates with Doubly-Periodic Pattern of Circular Holes Loaded in Plane Stress or Bending", Proc. First Intl. Conf. Pressure Vessel Technology, part I, 551-570. ASME, New York, 1969.

[13] Slot, T., O'Donnell, W.J., "Effective Elastic Constants for Thick Perforated Plates with Square and Triangular Penetration Patterns. J. Engineering for Industry 93 (1971), p. 935 ff.

[14] O' Donnell, W. J., "A Study of Perforated Plates with Square Penetration Patterns", WRC Bulletin No. 124 (1967).

[15] ASME, "Criteria of the ASME Boiler and Pressure Vessel Code for Design by Analysis in Sections III and VIII, Division 2," The American Society of Mechanical Engineers, New York, 1969. Reprinted in *Pressure Vessel Design and Analysis - A Decade of Progress*, The American Society of Mechanical Engineers, New York, 1972

[16] Kroenke, W. C., "Classification of finite element stresses according to ASME Section III stress categories", Proc. 94 th ASME Winter Annual Meeting, 1973.

[17] Kroenke, W. C., "Interpretation of finite element stresses according to ASME III", ASME Tech. Paper 75-PVP-63,1975.

[18] ANSYS Computer Program, Ver. 12, ANSYS, Inc.

[19] Gokhfeld, D.A., and Chemiavsky, O.F., 1980, " Limit Analysis of Structures at Thermal Cycling, Suthoff& Nordhoff, Alphen anden Rijn, The Netherlands.

[20] Mackenzie D, Boyle JT, "A simple method of estimating shakedown loads for complex structures" Proc. ASME PVP, Denver, 1993, 265, 89-94.

[21] Mackenzie D, Boyle JT, Hamilton R, Shi J, "Secondary stress and shakedown in axisymmetric nozzles", Proc. ASME PVP, Honolulu, 1995, 313-1, 409-413.

[22] Ponter ARS & Carter KF, "Shakedown state simulation techniques based on linear elastic solutions" Computer Methods in Applied Mechanics & Engineering, 1997, 140, 259-279.

[23] Chen HF, Ponter ARS, "Shakedown and limit analyses for 3-D structures using the Linear Matching Method," International Journal of Pressure Vessels and Piping 2001; 78:443–451.

[24] Preiss R, "On the shakedown analysis of nozzles using elasto-plastic FEA," Int. J. of Pres. Ves. & Piping, Vol. 76, pp421- 434, (1999).

[25] Muscat M , Hamilton R and Boyle JT, "Shakedown Analysis for Complex Loading using Superposition," Trans IMechE, Journal of Strain Analysis for Engineering Design, Vol. 37, No. 5, pp. 399-412, 2002.

[26] Muscat M, Mackenzie D and Hamilton R, "Evaluating shakedown by non-linear static analysis," Computers and Structures, 81, pp1727-1737, 2003.

[27] Zeman, J.L., 2002, "The European Approach to Design by Analysis," PVP Vol. 439, ASME PVP Conference, Vancouver, BC, Canada, pp.31-37.

[28] Reinhardt, W. “Distinguishing ratcheting and shakedown conditions in pressure vessels”. PVP- Vol. 458, PVP2003-1885

[29] Muscat, M., MacKenzie, D., Hamilton, R., 2003, “A Work Criterion for Plastic Collapse”, International Journal of Pressure Vessels and Piping, Vol. 80, PP 49-58.

[30] Li. Hongjun, MacKenzie, D., 2005, ” Characterising Gross Plastic Deformation in Design by Analysis”, International Journal of Pressure Vessel and Piping, Volume 82, PP 777- 786.

[31] Bree,J. “ Plastic deformation of a closed tube due to interaction of pressure stresses and cyclic thermal stresses”, Int. J. Mech. Sci., Vol. 31, No. 11/12 pp 865-892,1989.

[32] Kalnins, A., 2002, “Shakedown and Ratcheting Directives of ASME B & PV Code and their Execution,” PVP Vol. 439, ASME PVP Conference, Vancouver, BC, Canada, pp. 47-55.

[33] Niemi, E., “Stress Determination for Fatigue Analysis of Welded components”, Abington Publishing , 1995.

[34] DNV-RP-C203, “Fatigue Design of Offshore Steel Structures”, April 2010.

[35] Zeman, L., Rauscher, F., Schindler, S., “Pressure Vessel Design, The Direct Route”, 2006 Elsevier Ltd, Kidlington, Oxford, UK.

[36] Dowling, N. E., “Mechanical Behaviour of Materials”, pp 721, Pearson ,2007.

[37] Behseta, K., Schindler, S., 2006, “On the design of the tubesheet and tubesheet to shell junction of a fixed tubesheet exchangers”, International journal of pressure vessels and Piping, 83, 714-720.

[38] Radaj D, Sonsino CM.," Fatigue assessment of welded joints by local approaches", Cambridge, Abington Publishers, 1998.

[39] Save, M., " Experimental verification of plastic limit analysis of torispherical and toriconical heads", Pressure vessel piping: design and analysis, vol. 1. New York: ASME; 1972. P. 382-416.

[40] Gerdeen, J.C., 1979, " Critical evaluation of plastic behaviour data and unified definition of plastic components", WRC Bulletin, 254, pp. 1-89.

[41] O'Donnell, W.J., Interpretive Report on limit analysis of full circular plates, WRC report, May 1977.

[42] Besseling, J.F., 1958. A theory of elastic, plastic and creep deformation of an initially isotropic material. Journal of Applied Mechanics 25, 529,536

[43] Seshadri R & Kizhatil R K, "Inelastic analyses of pressure components using the "GLOSS" diagram". Proc. ASME PVP, Vol. 186, Nashville, pp105-113, (1990).

[44] Camilleri, D., MacKenzie, D., Hamilton, R., 2008, "Evaluation of Plastic Loads in Torispherical Heads Using a New Criterion of Collapse", ASME Journal of Pressure Vessel Technology, Vol.130, PP 011202-1 to 011202-8.

[45] Kalnins, A., Rana, M.D., 1996," A New Design Criterion Based on Pressure Testing of Torispherical Heads", WRC Bulletin 414, PP 1-60.

[46] Voce, E., 1955, "A practical strain- hardening function", Metallurgia.

[47] Bari, S., Hassan, T., " Anatomy of coupled constitutive models for ratcheting simulation". Int. J. Plasticity. 16, 381-409, 2000.

[48] Reinhardt W, Kizhatil R, McClellan GH, "Analysis of a tubesheet undergoing rapid transient thermal loading," ASME J Pressure Vessels. Tech, Vol. 122, pp476-481, 2000.

[49] Jawad, M. H., Farr, J. R., “Structural analysis and design of process equipment”, pp 504, John Wiley, 1989.

[50] Soler, A.I., Caldwell, S. M., Soler, S.D., “ A proposed ASME Sec. VIII, Div. 1, tube sheet design procedure”, Proceeding of the 1990 ASME PVP Conference, Nashville, Vol. 186 (H00605)

[51] Soler, A. I., Caldwell, S.M., Singh, K.P., “ Tube sheet analysis- A proposed ASME design procedure”, ASME publication H00343, Thermal/ Mechanical/ Heat Exchanger Design- Korl Gardner Memorial Session.

[52] Prager, W., 1956. “A new method of analysing stresses and strains in work hardening plastic solids”, Journal of Applied Mechanics 23, 493-496.

[53] Koiter WT, “General theorems for elastic plastic solids,” Progress in solid mechanics, Vol.1, J.N. Sneddon and R. Hill, eds., North Holland, Amsterdam, pp167-221, 1960.

[54] Hydrogenation Reactor Mechanical data sheet

[55] Ponter, A.R.S., and Chen, H., 2001,”A Minimum Theorem for Cyclic Load in Excess of Shakedown with Application to the Evaluation of a Ratchet Limit,” European Journal of Mech.A/ Solids, Vol. 20, pp. 53.

[56] Behseta K, Mackenzie D, Hamilton R, .Plastic load evaluation for a fixed tube sheet heat exchanger, submitted to Int. J. Pres. Ves. Piping,92,2012,pp 11-18.

[57] Radaj D, “Design and analysis of fatigue-resistant welded structures”, Cambridge, Abington Publishers, 1998.

[58] Nadarajah, C. , Ng, H.W.," Biaxial ratcheting and cyclic plasticity for Bree-type loading- part II: comparison between finite element analysis and theory", Journal of Pressure Vessel Technology, Vol. 118, May 1996.

[59] Updike, P.D., and Kalnins, A., 1988, "Tensile plastic instability of axisymmetric pressure vessels," ASME J. Pressure Vessel Technology, 120, pp. 6-11.

[60] TEMA, Standard of Tubular Exchanger Manufacturing Association, eight edition, 1999.

[61] Krieg, R.D., 1975, "A practical two-surface plasticity theory", ASME J Appl. Mech.,42(3), pp. 641-6.

[62] Dafalias, Y.F., Popov, E.P, "Plastic internal variables formalism of cyclic plasticity", ASME J. Applied Mech., 1976, 43(4), pp. 645-51.

[63] Otno, N., Kachi Y., "A constitutive model of cyclic plasticity for nonlinear hardening materials", ASME J. Appl. Mech., 1986, 53(2), pp. 395-403.

[64] Pikey, W.D., " Peterson's Stress Concentration Factors ", Wiley, New York, 1997.

[65] International Institute of Welding, BP 51362-VILLEPINTE, 95 942 ROISSY CH DE GAULLE Cedex, France

[66] Socie, D.F., Marquis, G..,B., " Multiaxial Fatigue", SAE international,, Warrendale, PA, 2000.

[67] TEMA, Standard of Tubular Exchanger Manufacturing Association, ninth edition, 2007.

[68] Marriott. D. L., "Evaluation of deformation or load control of stresses under inelastic condition using elastic finite element stress analysis," ASME PVP- Vol. 136, Pittsburgh, Pa., 1988.

[69] IIDA K.," Application of hot spot strain concept to fatigue life prediction", Welding in the Word, Volume 22(1984), No. 9/10, pp. 222-246.

[70] Hongjun, L., Mackenzie, D.," Characterising Plastic Collapse of Pipe Bend Structures", Pressure vessels and piping, International Journal of Pressure Vessels and Piping, 83, 2006. pp. 85-95.

[71] Mackenzie, D., Hongjun, L.," A plastic load criterion for inelastic design by analysis", Journal of Pressure Vessel Technology, 2006, Vol 128, PP 39-45.

[72] Camilleri, D., Mackenzie, D., Hamilton, R.," Material strain hardening in pressure vessel design by analysis", Proc. Imech E, Vol. 221 Part E: Journal of Process Mechanical Engineering, pp. 89-100.

[73] Okamoto, A., Nishiguchi, I., and Aoki, M.," Recent Advancement on the Draft of Alternate Stress Evaluation Criteria in Japan Based on Partial Inelastic Analysis", ASME PVP Vol. 419, pp. 17-24, Pressure Vessel and Piping Codes Standards, edited by M.D. Rana, 2001.

[74] Ponter, A.R.S., and Chen, H., 2001, "A Minimum Theorem for Cyclic Load in Excess of Shakedown with Application to the Cyclic Load in Excess of Shakedown with Application to the Evaluation of a Ratchet Limit," Eur. J. Mech. A/ Solids, Vol. 20, pp. 53

[75] Osweiller, F., and Robert, D., "New Design Rules for Fixed Tube Sheet Heat Exchangers: A Comparison of CODAP and ASME Approaches", PVP- Vol. 210-2

Appendix 1

A.1 Correction Factors for Base Metal

A.1.1 Temperature correction factor LC1

P_t= 4.0 MPa, P_s= 1.0 MPa, t_t= 190 ˚C, t_s= 145 ˚C

$t_{c,max}$= 190 ˚C

$t_{c,min.}$= 21 ˚C

t^*= 0.25 ($t_{c,max}$)+ (0.75) $t_{c,min}$ (A.1)

t^*= 0.25 (21)+ (0.75)190= 147.75 ˚C

f_t^*= 1.03- (1.5e-4) t^*-1.5(e-6)$(178.75)^2$

f_t^*= 0.9552

A.1.2 Surface correction factor

$$f_s = (F_s)^{(0.1Ln(N)-0.465))} \; for N \le 200000 \quad \text{(A.2)}$$

$$F_s = 1 - 0.056(Ln(R_Z)^{0.64} Ln(R_m) + 0.289(Ln(R_Z))^{0.53} \quad \text{(A.3)}$$

R_z= 200 μm for surface of rolled and extruded parts

R_z= 50 μm for machined surfaces

The approx. F_s given in literature for untreated surface of deep drawn components and forgings is,

$$F_s = 0.25 + 0.75(1 - (R_m / 1500))^{1.8} \quad \text{(A.4)}$$

Tubesheet face and radii are machined roughly, therefore R_z= 50 has been selected. Moreover, R_m=482.3 (see table 5.2.1) for tubesheet material.

$$F_s = 1 - 0.056(Ln(50)^{0.64} Ln(482.3) + 0.289(Ln(50))^{0.53}$$

F_s= 0.767

$$f_s = (0.767)^{(0.1Ln(10000)-0.465))} = 0.81$$

A.1.3 Thickness correction factor

$$F_e = (25/e_n)^{0.12} \qquad 25 < e_n \le 150 \qquad \text{(A.5)}$$

$e_n =$ tubesheet thickness=100

$$F_e = (25/100)^{0.12} = 0.777$$

$$f_e = 0.777^{(0.1Ln10000-0.465)}$$
$$f_e = 0.892$$

A.1.4 Mean stress correction factor

This is a very important factor in fatigue life determination,

M= 0.00035 R_m- 0.1

R_m=482.3

M= .0688

For $N = 10000$,

$$-R_{p0.2/t^*} \le [\bar{\sigma}_{eq}]_{mean} \le 0.5\frac{\Delta\sigma_R}{(1+M)} \qquad \text{(A-6)}$$

Note 1: Mean stress $(\bar{\sigma}_{eq})$ is calculated according to following,

$$\bar{\sigma}_{i,j} = [(\sigma_{i,j})_{\max} + (\sigma_{i,j})_{\min}]/2 \qquad i,j = 1,2,3 \qquad \text{(A-7)}$$

For load case 1 and for node number 85526, the von Mises equivalent of stress range from Table (8.4) is $[(\Delta\sigma)_{eq}]_{Mises} = 308.29$ MPa.

Recall LC1 is part of cyclic set 1, this is a load case which acts between standard operating mode and an ambient condition 500 times (cycles), data is provided in Table (8.2). To account for mean stresses, the averaged stresses between two operating statuses must be obtained; this requires magnitude of various stress components for

each status. Component of stresses for LC1 is provided below, the mean stress associated with this load case is,

$$\text{LC1= From } \begin{vmatrix} 103.6 & -6.41 & -24.3 \\ -6.41 & 117.43 & 110.1 \\ -24.3 & 110.12 & 348.5 \end{vmatrix} \text{ to } \begin{vmatrix} 0 & 0 & 0 \\ 0 & 0 & 0 \\ 0 & 0 & 0 \end{vmatrix}$$

$\bar{\sigma}_{1,1} = (103.6 + 0)/2 = 51.8, etc.$

$[\bar{\sigma}_{eq}]_{mean} = 218.27$ (A.8)

$\Delta\sigma_R$ is stress range from fatigue curve data; its value for assumed 10000 cycles is,

$\Delta\sigma_R = 0.63R_m - 11.5 + (46000/\sqrt{N})$ (A-9)

$\Delta\sigma_R = 0.63(482.3) - 11.5 + (46000/\sqrt{10000}) = 752.4$

Recall, $M = 0.0688$

$$-R_{p0.2/t^*} \le [\bar{\sigma}_{eq}]_{mean} \le 0.5\frac{\Delta\sigma_R}{(1+M)}$$

$$-237 \le 218.27 \le 0.5\frac{\Delta\sigma_R}{(1+M)}$$

$$-237 \le 218.27 \le 0.59(\frac{752.4}{1.0688})$$

Since $-237 \le 218.27 \le 703.96$ then, f_m is

$$f_m = [1 - \frac{M(2+M)}{(1+M)}(2\bar{\sigma}_{eq}/\Delta\sigma_R] \quad \text{(A-10)}$$

$$f_m = [1 - \frac{.069(2+.069)}{1.069}(\frac{2(218.27)}{752.4})]^{0.5}$$

$f_m = 0.925$

A.1.5 Plasticity correction factor

For LC1 node 85526, $\Delta\sigma_{eq,t} = 308.3$ MPa (see table 8.4) since

$308.3 < 2R_{p0.2/t^*} = 2(237)$, no plasticity correction factor is required, i.e.,

$\Delta\sigma = K_e(\Delta\sigma_{eq,t}) = (1.0)(308.308) = 308.308$ MPa

A.1.6 Effective stress concentration factor

$$K_{eff} = 1 + \frac{1.5(K_t - 1)}{1 + 0.5Max[1; \frac{K_t(\Delta\sigma_{eq})}{\Delta\sigma_D}]} \quad \text{(A-10)}$$

$\Delta\sigma_D =$ Endurance limit for single- amplitude stress cycles (unwelded region)

The test results for most steels indicate for single-amplitude cycles abrupt changes in slope occur at approximately 10^7 (test) cycles, this change in slope is frequently called knee point, and the corresponding stress range is called endurance limit.

Endurance limit equation is provided as:

$\Delta\sigma_D = 0.63R_m + 21 = 0.63(482.3) + 21 = 324.85$ MPa

$$K_{eff} = 1 + \frac{1.5(1-1)}{1 + 0.5(\frac{308.3}{324.85})} = 1$$

A.1.7 Overall Correction factor

$f_u = (f_s)(f_e)(f_m)(f_t)K_{eff}$

$f_u = (0.81)(0.89)(0.92)(0.95)(1.0)$

$f_u = 0.64$

A.2 Correction Factors for Weld

A.2.1 Stress Range

Table (A.1) provides range of principal stresse for cyclic set 1 between action value and ambient (zero)

Table (A.1): Range of principal stresses for cyclic set 1

Load case	Nodes locations	σ_{11}	σ_{22}	σ_{33}	Notes
LC1	87424	205.3	31	-3.0	Perpendicular to weld joint
	87636	150	23.1	-2.8	
	88240	103.4	22.9	-3.4	
	85451	401.9	92.1	28	Parallel to weld joint
	85375	402.9	91.92	28.35	
	85223	390.42	90.57	28.16	
LC2	87424	210.86	37	-3.6	Perpendicular to weld joint
	87636	180.64	29.5	-2.8	
	88240	108.8	27.2	-3.4	
	85451	403.7	98.12	28.8	Parallel to weld joint
	85375	404	97.9	28.9	
	85223	402.2	95.6	28.7	
LC3	87424	218.4	3.3	-3.4	Perpendicular to weld joint
	87636	158.7	-2.6	-5.1	
	88240	97.06	-3.3	-3.7	
	85451	423	67.4	38.8	Parallel to weld joint
	85375	420.9	69.9	40.2	
	85223	430.8	70.5	40.2	
LC4	87424	194.3	67	-3.1	Perpendicular to weld joint
	87636	134.9	-0.02	-2.3	
	88240	85.5	1.03	-2.9	
	85451	371	64.1	25.6	Parallel to weld joint
	85375	308.7	63.8	20.5	
	85223	301.8	61.4	20.1	

Taking into account the required corrections, details for the calculations for $\Delta\sigma_{eq}$ are:

- $\Delta\sigma_{eq\uparrow}$,perpendicular to hot spot

Values of Table (A.1, 2) extracted from FEA output are used for extrapolation of stresses in perpendicular direction (↑) using following equation Ref [4], see also Figure (8.8).

$$(\sigma_{11})_{Base} = 2.52(\sigma_{11})_{location-Y1} - 2.24(\sigma_{11})_{location-Y2} + 0.72(\sigma_{11})_{location-Y3} \quad \text{(A.1)}$$

$$(\Delta\sigma_{11})_{Base} = 2.52(205.3) - 2.24(150) + 0.72(103.4)$$

$(\Delta\sigma_{11})_{Base} = 244.6$

$(\Delta\sigma_{22})_{Base}=17.66$

$(\Delta\sigma_{33})_{Base}=-17.79$

$$(\Delta\sigma_{eq\uparrow})_{Base} = \sqrt{\frac{(\sigma_{11}-\sigma_{22})^2 + (\sigma_{11}-\sigma_{33})^2 + (\sigma_{22}-\sigma_{33})^2}{2}}$$

$$(\Delta\sigma_{eq\uparrow})_{Base} = \sqrt{\frac{(244.6-17.66)^2 + (244.6+17.79)^2 + (17.66+17.79)^2}{2}}$$

Table (A.2): Node distance and stress values used in extrapolation direction (↑)

Node location	**Vertical distance to base (node-85527) (mm)**	**σ_{11}**	**σ_{22}**	**σ_{33}**
				-3.0
87424	21.25	205.3	31	-3.0
87696	42.5	150	23.1	-2.8
88240	63.75	103.4	22.9	-3.4

Similarly for calculation of $(\Delta\sigma_{eq\rightarrow})_{Base}$ values of Table (A.3) are used.

Table (A.3): Node distance and stress values used in extrapolation direction (→)

Location	**Horizontal distance to base node - 85527 (mm)**	σ_{11}	σ_{22}	σ_{33}
85451	33.5	401.9	92.1	26
85375	67	402.9	91.92	26.35
85223	100.5	399.42	90.57	26.15

$\left(\Delta\sigma_{eq\rightarrow}\right)_{Base}$ =344.3 MPa

Calculated $\left(\Delta\sigma_{eq\rightarrow}\right)_{Base}$ should now be corrected by plasticity correction factor.

A.2.2 Design Fatigue Curve and Plasticity Correction Factor

A.2.2.1 Welded Region Design Fatigue Curve Data

The design fatigue curves chosen in the standard are able to take into account weld details, location of hot spots, and orientation of principal stresses. 10 different design fatigue curves, corresponding to 10 different fatigue classes, have been chosen by the code committee and labeled using fatigue class, followed by number which is equal to the value of the stress amplitude range at 2 million allowable cycles. Test results covered the range of 10000 to 10 million cycles. These curves can be described as follows:

For $\Delta\sigma_R \geq \Delta\sigma_D$ where $\Delta\sigma_R$ is stress range $\left(\Delta\sigma_{eq\rightarrow}\right)_{Base}$ and $\Delta\sigma_D$ is endurance stress range (for single amplitude stress cycle- welded region), the number of cycles (N) is given by.

$$N = (C_1 / \Delta\sigma_R)^3 \qquad \text{(A.2)}$$

For $\Delta\sigma_R \le \Delta\sigma_D$ stress cycle N is infinity.

The applicable data to junction of tubesheet to channel side shell weld is provided below,

Direction (↑), weld load as shown in Fig.(A.1), fatigue class is 63, $\Delta\sigma_D$= 46

and $\Delta\sigma_R = \left(\Delta\sigma_{eq\rightarrow}\right)_{Base}$ = 246.8> 46, then:

$$N = (C_1 / \Delta\sigma_R)^3$$

With, $C_1 = 5.0e11$

Fig (A.1): Weld load in longitudinal direction

Direction (→), weld load as shown in Fig. (A.2), fatigue class is 80, $\Delta\sigma_D$= 59

And $\Delta\sigma_R = [(\Delta\sigma_{eq})_{Base}] = 344.3 > 59, then$:

$$N = (C_1 / \Delta\sigma_R)^3$$

with C_1= 1.02E12

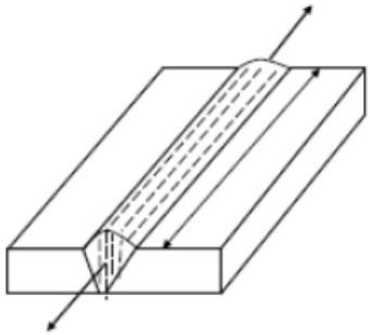

Fig (A.2): Weld load in radial direction

A.2.2.2 Plasticity Correction Factor

If $\Delta\sigma_{eq} \leq 2\sigma_{p0.2/t^*}$ no plasticity correction factor is required, i.e.,

$(\Delta\sigma_{eq\uparrow})_{Base}$=246.8 ≤ 2(237), 246.8 ≤ 474

and, $(\Delta\sigma_{eq\rightarrow})_{Base}$=344.3 ≤ 2(237), 344.3≤ 474

A.2.2.3 Overall Correction Factor

Recall, temperature correction factors, f_{t^*}= 0.955. Thickness correction factor (f_{ew}) is required to take into account the influence of the fatigue relevant thickness on the design fatigue life. Unlike its pendant for unwelded region, this factor depends only on the relevant thickness e_n, in mm and is in general specified by,

$f_{ew} = (25/ e_n)^{0.25}$ for $25< e_n< 150$

$f_{ew} = (25/ 100)^{0.25}$= 0.707

Then, total correction factor is:

f_w= (f_{t^*})(f_{ew})= (0.707)(0.955)= 0.675

$(\Delta\sigma_{eq\uparrow})_{corrected}$= $(\Delta\sigma_{eq\uparrow})_{Base}/ f_w$=246.8/(0.675)= 365.3

$(\Delta\sigma_{eq\rightarrow})_{corrected}$ =$(\Delta\sigma_{eq\rightarrow})_{Base}/ f_w$= 344.3/(0.675)= 510.07

A.3 Reservoir Counting

Details of calculated stress ranges through use of reservoir method are provided in Fig. (A.3- 6), theses ranges are obtained by draining each trough.

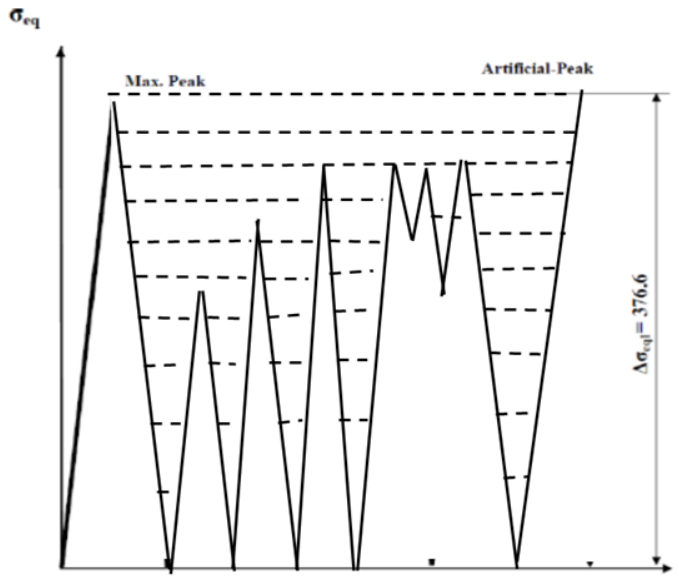

Fig (A.3): Draining through associated with σeq1,i.e.,Δσeq1=376.6-0.0=376.6 MPa

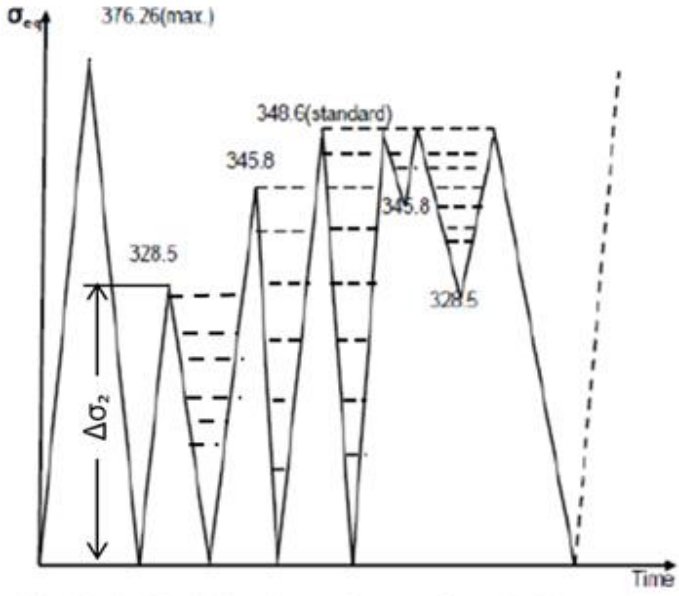

Fig (A.4): Draining through associated with σeq2,i.e.,Δσeq2=328.5-0.0=328.5 MPa

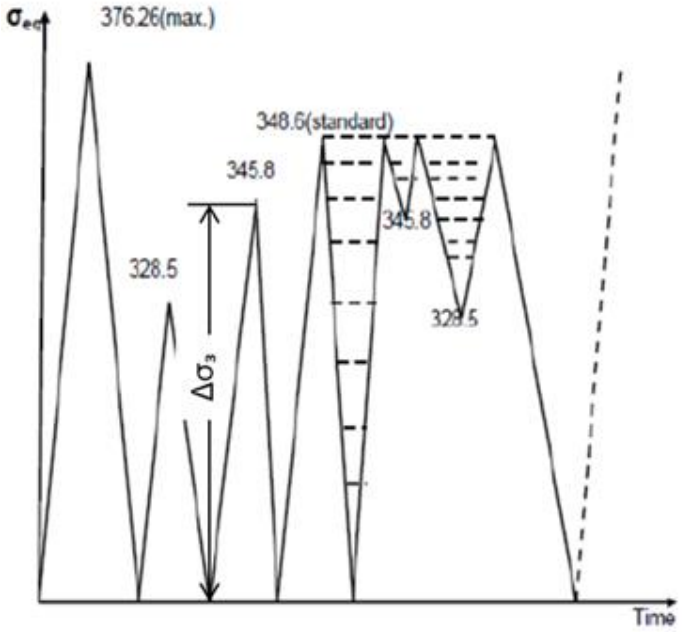

Fig (A.5): Draining through associated with σeq3,i.e.,Δσeq3=345.8-0.0=345.8 MPa

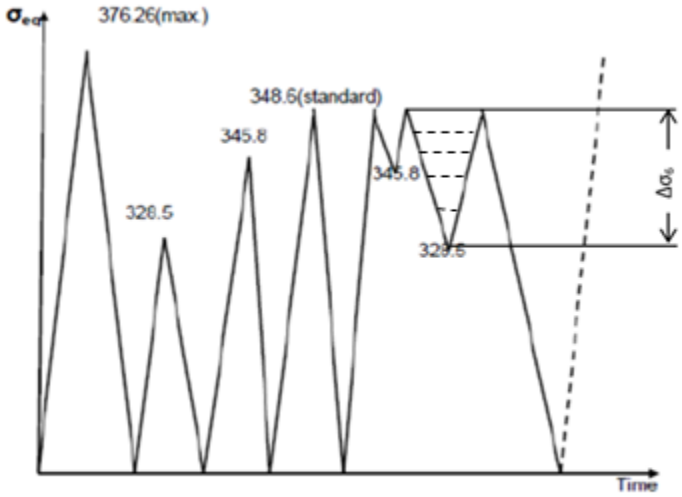

Fig (A.6): Draining through associated with σeq6,i.e.,Δσeq6 is stress range between 348.6 and 328.5 MPa (component base)